Splice Switching Small Molecules as Inducers of Apoptosis

Olivia Ines Rutherford

Thesis submitted for the degree of

Doctor of Philosophy

Date: October 2018

Academic Supervisor: Professor Glenn A. Burley

Industrial Supervisor: Dr Jacob Bush

Contents

Declaration of Authenticity

This thesis is the result of the author's original research. It has been composed by the author and has not been previously submitted for examination which has led to the award of a degree.

Signed: _____ (Olivia Ines Rutherford)

Date: October 2018

Acknowledgements

First and foremost I would like to extend a massive thank you to my PhD supervisor, Professor Glenn Burley, for giving me the opportunity to carry out this PhD under his guidance and supervision. It has been a great experience and I truly appreciate the continuous help and support you have given me during this project.

I would also like to acknowledge the University of Strathclyde, GSK and the EPSRC for providing the funding for my project and allowing me to carry out my research.

I would like to extend a special thank you to Dr Jamie Withers for taking the time to proof read my thesis. A large mug of Milo and a marmite sandwich is waiting for you!

I also owe a thank you to Helena Buchanan, Marine Hatit and Emma Campbell for helping me in the last few months with the completion of my thesis and for their friendship throughout. Also I would like to wish Emma all the best of luck with the continuation of this project. Marine did warn you that a click PhD project would have been an easier choice! It has also been a great pleasure carrying out my PhD in the Burley Lab and I have my past and present colleagues to thank for that. There has never been a dull moment to say the least (and I'll leave it at that!).

I would also like to thank my four year PhD companion Giacomo Padroni. I really appreciate all the help and advice you have given me throughout this time.

Due to the multidisciplinary nature of my PhD project, the completion of this thesis would not have been possible without input from a number of our collaborators. Therefore, I must express gratitude to Dr Jacob Bush for showing me the ropes during my secondment in GSK. To Professor Ian Eperon, Dr Cyril Dominguez and Dr Carika Weldon for introducing me to the world of RNA splicing first-hand. And also Hatice Esenkaya, Dr Zoë Waller and Elise Wright for carrying out the *in vitro* splicing assays and FRET melting assays for me. Finally, I would like to thank Dr John Parkinson for taking the time to run the RNA NMR experiments with me.

I would not have made it through the last four years without the constant and unwavering support from my friends and family, especially my Mum, Dad and Jordan. Finally, thank you Jordan for never letting me give up and for *still* falling asleep every time I talk about chemistry!

Abstract

One of the most important post-transcriptional processes that occurs during the transcription of DNA to RNA is alternative splicing. Alternative splicing is a highly regulated process that occurs during gene expression and is the basis for the large protein diversity that is achieved in eukaryotes. It allows multiple protein isoforms to be formed from one pre-mRNA sequence. Although alternative splicing is necessary to provide protein diversity, aberrant splicing can also lead to diseases such as cancer. Recently, there has been an interest in the ability of small molecules to exogenously modulate alternative splicing as therapeutics for aberrant splicing diseases. The ellipticine analogue GQC-05 has been found to have splice switching capabilities towards the apoptotic oncogene Bcl-x, however the mode of action of GQC-05 is not understood.

This thesis describes efforts made to elucidate the mode of action of GQC-05 by synthesising a library of ellipticine derivatives for testing in a range of biochemical assays to evaluate their ability to bind and stabilise Bcl-x.

The background to alternative RNA splicing and the aberrant splicing process that can lead to diseases such as cancer is introduced in Chapter 1. The importance of the oncogene Bcl-x and the current limitations in targeting it therapeutically are also presented.

Chapter 2 investigates current literature methods to prepare 9-methoxyellipticine. However it is found that these methods do not provide a modular framework in which to systematically alter the ellipticine structure.

Chapter 3 describes the development of a one-pot, sequential, palladium cross-coupling methodology to construct the backbone of the natural product ellipticine. This methodology has been further extended to synthesise a range of ellipticine analogues with modular changes throughout the structure.

Chapter 4 examines the ability of the ellipticine derivatives synthesised to stabilise a putative G-quadruplex structure within Bcl-x through the use of UV melting assays. The ligands have also been investigated for their ability to stabilise a range of competitor DNA structures with the help of FRET melting assays. The interaction of GQC-05 with the putative Bcl-x G-quadruplex has also initially been examined using NMR spectroscopy. And finally, the ellipticine derivatives have been tested in Bcl-x *in vitro* splicing assays to determine whether they are capable of exerting the same splicing modulation on Bcl-x as their parent compound GQC-05.

Abbreviations

A	Adenine/Adenosine
Ac	Acetyl
APAF1	Apoptotic protease activating factor 1
b	broad
BAD	Bcl-2-associated death promoter
BAK	Bcl-2 homologous antagonist killer
BAX	Bcl-2-associated X
Bcl-2	B-cell lymphoma 2
Bcl-xL	B-cell lymphoma-extra large
Bcl-xS	B-cell lymphoma-extra small
BH	Bcl-2 homology
Boc	*tert*-butyloxycarbonyl
BrettPhos	2-(Dicyclohexylphosphino)3,6-dimethoxy-2′,4′,6′-triisopropyl-1,1′-biphenyl
Bn	Benzyl
Bu	Butyl
C	Cytosine/Cytidine
CD	Circular dichroism
CI	Chemical ionisation
c-Kit	Mast/stem cell growth factor receptor
CMD	Concerted metalation deprotonation
c-Myc	V-Myc avian myelocytomatosis viral oncogene homolog
COSY	Homonuclear correlation spectroscopy
Cy	Cyclohexyl
CYP	Cytochrome P450
d	Doublet
dd	Doublet of doublets
dt	Doublet of triplets
DavePhos	2-Dicyclohexylphosphino-2′-(*N*,*N*-dimethylamino)biphenyl
DCM	Dichloromethane
DcpS	Scavenger mRNA-decapping enzyme
DFT	Density functional theory
DMA	Dimethylacetamide
DMAP	4-Dimethylaminopyridine
DMF	Dimethylformamide
DMPU	*N*,*N*′-Dimethylpropyleneurea

DMSO	Dimethylsulfoxide
(ds)DNA	(double stranded) Deoxyribonucleic acid
EDG	Electron donating group
e.g.	Exempli gratia
ELISA	Enzyme-linked immunosorbent assay
Equiv.	Equivalent
ESE	Exonic splicing enhancer
ESI	Electrospray Ionisation
ESS	Exonic splicing silencer
EtOH	Ethanol
EWG	Electron withdrawing group
FAM	5(6)-carboxyfluorescein
FDA	Food and Drug Administration (US)
FRET	Förster resonance energy transfer
FTIR	Fourier transform infrared
G	Guanine/Guanosine
G4	G-quadruplex
GCMS	Gas chromatography mass spectroscopy
GFP	Green fluorescent protein
GTP	Guanosine triphosphate
H-bonding	Hydrogen bonding
HIF 1-alpha	Hypoxia-inducible factor 1-alpha
HMBC	Heteronuclear multiple bond correlation
HMDS	Hexamethyldisiloxane
Hr	Hour
hnRNPs	Heterogeneous nuclear ribonucleoproteins
HSQC	Heteronuclear single quantum correlation
hTelo	Human telomere DNA
HTS	High throughput screen
IC_{50}	Half maximal inhibitory concentration
i.e	Id est
ISE	Intronic splicing enhancer
ISS	Intronic splicing silencer
HRMS	High resolution mass spectroscopy
Hz	Hertz
IR	Infrared radiation
K	Kelvin
kb	Kilobase

K_D	Equilibrium dissociation constant
KIE	Kinetic isotope effect
k-ras	Kirsten Rat Sarcoma Viral Oncogene Homologue
LCMS	Liquid chromatography mass spectroscopy
LDA	Lithium diisopropylamide
LiHMDS	Lithium bis(trimethylsilyl)amide
LNA	Locked nucleic acid
LRMS	Low resolution mass spectroscopy
m	Meta
m	Multiplet
M	Molar
MeCN	Acetonitrile
MeOH	Methanol
mg	Milligram
mins	Minutes
mL	Millilitre
mmol	Millimolar
mRNA	Messenger RNA
Ms	Mesyl
m/z	Mass to charge ratio
N/A	Not applicable
NBS	*N*-Bromosuccinimide
NHC	*N*-heterocyclic carbenes
NIS	*N*-iodosuccinimide
nOe	Nuclear Overhauser effect
NOESY	Nuclear Overhauser effect spectroscopy
NHE	Nuclease hypersensitive element
nm	nanometer
NMP	*N*-Methyl-2-pyrrolidone
NMR	Nuclear magnetic resonance
NRAS	Neuroblastoma RAS viral oncogene homologue
Ns	Nosyl
nt	Nucleotide
o	Ortho
OMM	Outer mitochondria membrane
p	Para
PAGE	Polyacrylamide gel electrophoresis
PDB	Protein data bank

Pd/C	Palladium on carbon
$Pd_2(dba)_3$	Tris(dibenzylideneacetone)dipalladium(0)
PDGFR-β	Platelet-derived growth factor receptor β
Ph	Phenyl
PLOR	Position selective labelling of RNA
PNA	Peptide nucleic acid
ppm	Parts per million
QGRS	Quadruplex forming G-rich sequences
qPCR	Quantitative polymerase chain reaction
RDS	Rate determining step
(ss)RNA	(single stranded) Ribonucleic acid
rNTP	Ribonucleoside triphosphate
RP-HPLC	Reverse phase high pressure liquid chromatography
r.t.	Room temperature
Rt	Retention time
RT-PCR	Reverse transcription polymerase chain reaction
s	Singlet
SAR	Structure activity relationship
S_E3	Substitution electrophilic trimolecular
S_EAr	Electrophilic aromatic substitution
SF1	Splicing factor 1
SMA	Spinal muscular atrophy
SMN	Survival of moto neutron
SPR	Surface plasmon resonance
SR proteins	Serine arginine proteins
SRSF1	Serine/arginine-rich splicing factor 1
snRNA	Small nuclear ribonucleic acid
snRNP	Small nuclear ribonucleic protein
t	Triplet
T	Thymine/Thymidine
TAMRA	5-carboxytetramethylrhodamine
TBAB	Tetra-*n*-butylammonium bromide
TBAHS	Tetrabutylammonium hydrogen sulfate
TCE	Trichloroethylene
TERRA	Telomeric repeat-containing RNA
Tf	Trifluoromethanesulfonate (triflate)
TFA	Trifluoroacetic acid
THF	Tetrahydrofuran

TLC	Thin layer chromatography
T_m	Melting temperature
TMS	Trimethylsilyl
TOCSY	Two-dimensional nuclear magnetic resonance spectroscopy
TRF2	Telomeric repeat-binding factor 2
tRNA	Transfer ribonucleic acid
U	Uracil/Uridine
U2AF	U2 small nuclear RNA auxiliary factor
U2AF35	U2 small nuclear RNA auxiliary factor 35
U2AF64	U2 small nuclear RNA auxiliary factor 64
UTR	Untranslated region
UV	Ultraviolet
XPhos	2-Dicyclohexylphosphino-2′,4′,6′-triisopropylbiphenyl
μM	Micromolar
μW	Microwave
Δ	Change
δ	Chemical shift
λ	Wavelength
π	Pi
σ	Sigma
%	Percentage
°C	Degrees Celsius

Chapter 1

Introduction

1.1 The Central Dogma of Molecular Biology

The Central Dogma is a concept which explains the flow of genetic information within a biological system.[1] A key feature of the Central Dogma is the transfer of information from DNA to RNA (transcription) and RNA to proteins (translation) but crucially, never from proteins to DNA or RNA. This concept is represented in Figure 1a where the blue arrows indicate processes which occur in every biological system whereas, the red dotted arrows represent processes which only occur occasionally in certain cells and organisms such as viruses and retroviruses.[2]

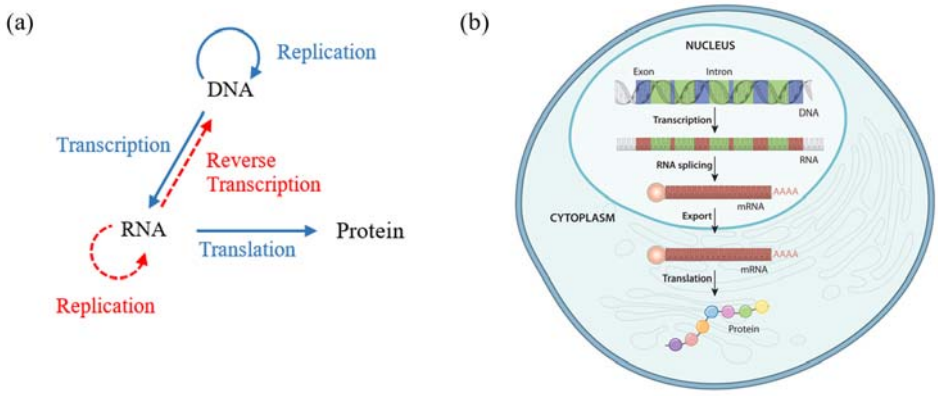

Figure 1. (a) The flow of genetic information from DNA to proteins.[1] (b) Transfer of information from the nucleus of a cell to the cytoplasm.[3]

Transcription is the first step in gene expression and involves an RNA polymerase reading the template DNA strand in the 5′ → 3′ direction and synthesising a single stranded, complementary RNA sequence from this.[4,5] As the pre-mRNA strand is being synthesized, the 5′ end of the pre-mRNA undergoes post-transcriptional processing which includes splicing, 5′ capping and 3′ polyadenylation, to convert pre-mRNA into mature mRNA.[6] Mature mRNA is then exported from the nucleus to the cytoplasm to be translated into the appropriate protein isoform (Figure 1b). Transcription and translation are highly regulated processes within both prokaryotic and eukaryotic cells, which are used to maintain cellular homeostasis and to adapt to changing environmental conditions.[3,7]

1.2 DNA and RNA Structure

Underpinning the function of nucleic acids to store and transmit genetic information is their ability to act as a template. The structure of DNA and RNA are constructed from monomers called nucleotides.[8] Nucleotides have three components: a base, a ribose sugar and a phosphate. DNA and RNA have three bases in common; guanine (**1.1**), adenine (**1.2**) and cytosine (**1.3**), while

thymine (**1.4**) is unique to DNA, whereas uracil (**1.5**) is unique to RNA (Figure 2a). In both DNA and RNA G pairs with C and A pairs with either T in DNA and U in RNA (Figure 2b).[6] The sugar and phosphate components of nucleotides form the sugar-phosphate backbone of the nucleic acid chain. Two sugar conformations can form for the furanose ring of DNA. These conformations are referred to as C2′-endo (**1.9**) and C3′-endo (**1.10**) and rapid interconversion between both of these conformations is seen at room temperature. The C3′-endo (**1.10**) sugar pucker gives rise to compact A-form DNA, while the C2′-endo (**1.9**) sugar pucker is found in B-form DNA. RNA only adopts the C3′-endo (**1.11**) conformation due to the possible steric class from the 2′-OH and 3′-O in the C2′-endo sugar pucker orientation.[9] Through Watson-Crick base pairing, DNA predominately exists as a stable double stranded duplex, whereas RNA is predominantly found in single stranded form.

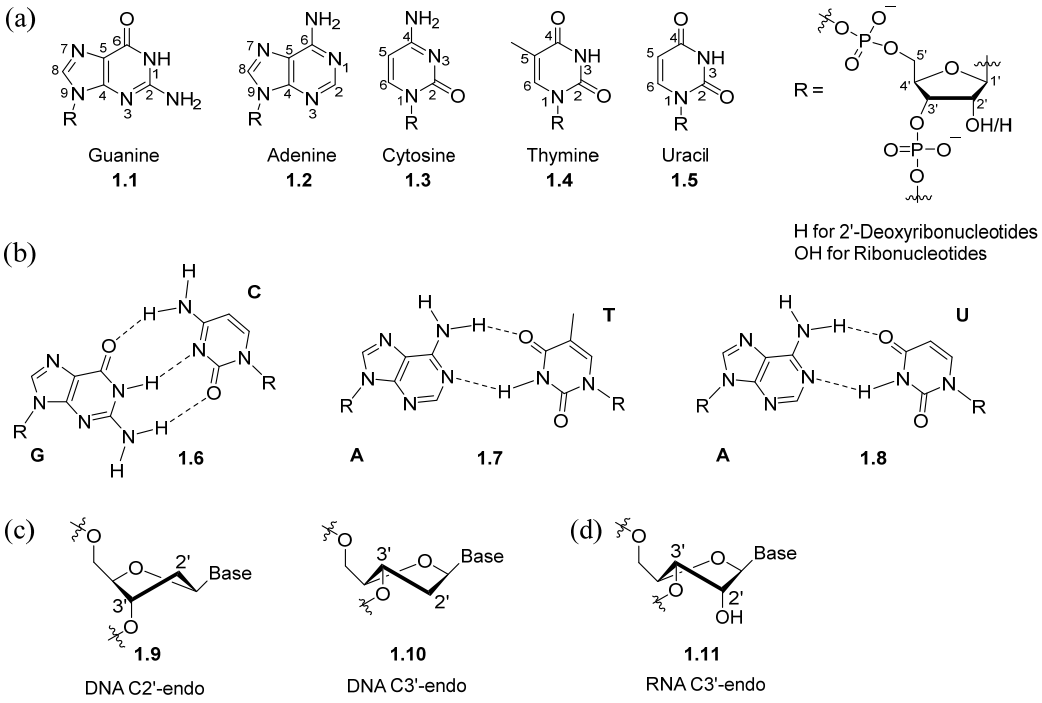

Figure 2. (a) Structures of DNA and RNA ribonucleotides, Guanine (**1.1**), Adenosine (**1.2**), Cytosine (**1.3**), Thymine (**1.4**) and Uracil (**1.5**).[8] (b) Watson-Crick base pairing, (**1.6**) G-C pair, (**1.7**) A-T pair, (**1.8**) A-U pair. H for 2′-Deoxyribonucleotides; OH for Ribonucleotides. Sugar puckers preferences for (c) DNA and (d) RNA.

The secondary structure of both DNA and RNA gives rise to helices, stem loops and pseudoknot structures.[6] More complex structures such as G-quadruplexes (G4s)[10] and i-motifs[11] fall under the category of tertiary structures. Examples of these structures are highlighted in Figure 3.

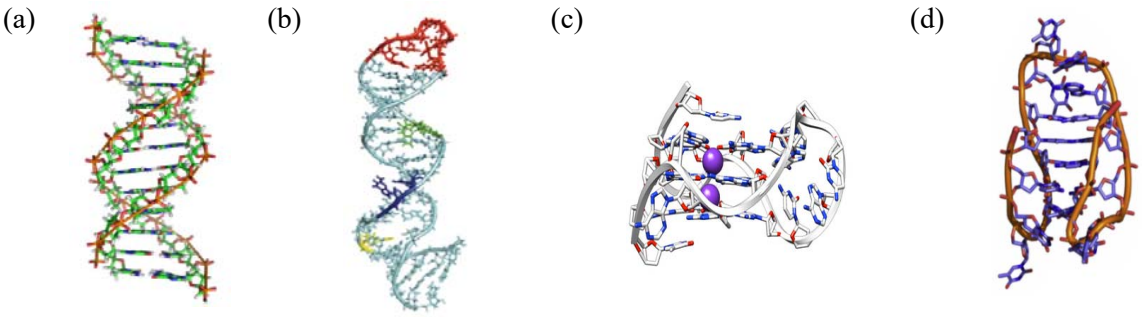

Figure 3. Representative DNA and RNA structures found in nature. (a) B-type DNA double helix,[12] (b) RNA stem loop,[13] (c) DNA G-quadruplex,[14] (d) DNA i-motif.[11]

1.2.1 G-quadruplexes – Structure and Function

G-quadruplexes (G4s) are secondary structures that have the potential to form in both G-rich DNA and RNA.[10,15] Bioinformatic studies have shown that the structures are particularity widespread in promopter regions and telomere ends of chromosomes and are thought to be involved in the regulation of gene expression. When four guanines come into contact with each other they are able to hydrogen-bond *via* Hoogsteen base-pairing to form a G-quartet that is square planar in nature. Hoogsteen base-pairing differs from conventional Watson-Crick base-pairing as N7 is also involved in the H-bonding network. Cations such as potassium and sodium coordinate with the O6 carbonyl of G to aid stability of the G-quartet (

Figure **4**a). G-quartets can stack on top of each other to form layered G4 structures (

Figure **4**b). G4s are able to form in not only DNA and RNA, but also in synthetic variants such as PNA and LNA sequences and can be bimolecular, trimolecular, tetramolecular or intramolecular, thus reflecting the inherent stability of these structures.[16,17]

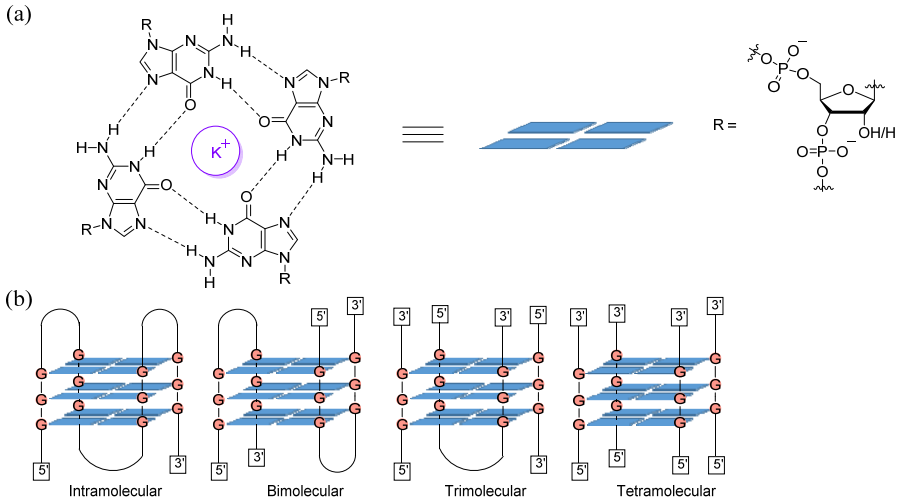

Figure 4. Graphical representation of (a) G-quartet. (b) Intra-, bi-, tri- and tetramolecular G4.

The structures of DNA and RNA G4s can be further defined by the relative direction of the strands and the orientation of their loops. Figure 5 is a schematic of the different structural types of G4s which have been identified. The assignment of G4s as parallel, *anti*-parallel or mixed is due to the directionality of the DNA or RNA strand (in the 5′ to 3′ direction) as represented by arrows in Figure 5. If all arrows are pointing the same direction then the G4 is parallel and if two are pointing up and two are pointing down then the G4 is *anti*-parallel. There are also three main types of loops that can be present depending on the G4 structure; diagonal, edgewise or propeller loops.

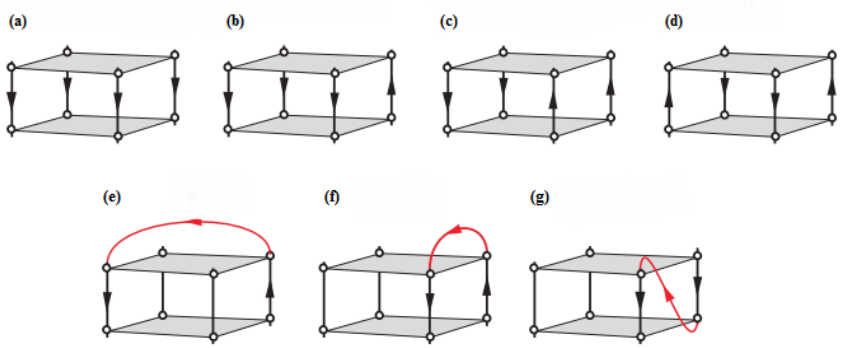

Figure 5. Four types of G-tetrad cores: (a) parallel G-tetrad core. (b) (3 + 1) G-tetrad core. (c) antiparallel G-tetrad core (up–up–down– down). (d) antiparallel G-tetrad core (up–down–up–down). Three types of loops (coloured red): (e) diagonal loop. (f) edgewise loop. (g) propeller loop. Arrows indicate the strand orientations, from 5′ → 3′.[16]

The structure of a DNA or RNA G4 can easily change depending on the length of the G-rich sequence, the cation present and the bases present in the sequence. Figure 6 gives an example of

DNA human telomeric sequences where the structure changes from *anti*-parallel to parallel to a hybrid/mixed structure as the cation is changed from Na^+ to K^+.[18]

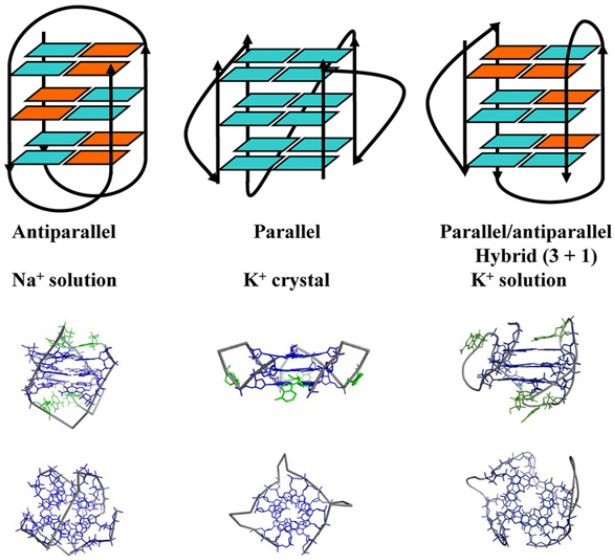

Figure 6. Structures of parallel, *anti*-parallel and mixed G-quadruplexes. Guanosine residues are coloured according to the configuration of the glycosidic bond. *Anti* guanosines are coloured aqua and *syn* guanosines are coloured orange.[18]

The change from parallel to *anti*-parallel also changes the conformation of the *N*-glycosidic bond in the guanines involved in each G-quartet (Figure 7).[15] *Anti*-parallel structures only contain the *syn* orientation (**1.19**) while parallel structures only contain the *anti* orientation (**1.12**). DNA G4s are able to form both parallel and *anti*-parallel structures under different conditions. However, RNA G4s generally only adopt the parallel structure as the *syn* conformation (**1.15**) is highly unfavourable for RNA due to steric clashes between the 3H′ of the ribose ring and the N3 position of the guanine.[15]

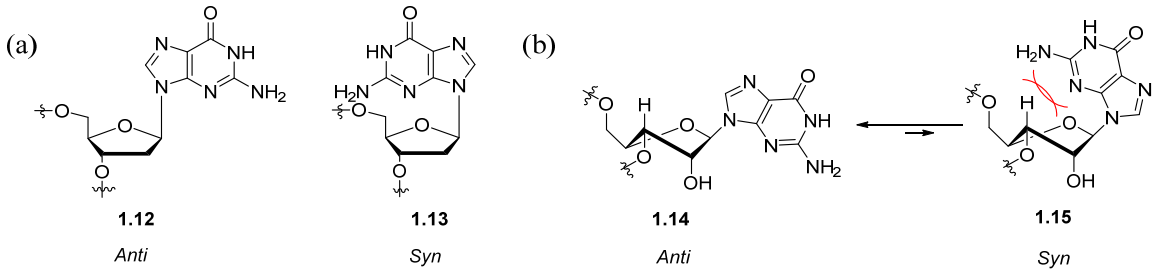

Figure 7. Purine s*yn*- and *anti*-conformations for (a) DNA, and the preferred *anti* conformation for (b) RNA.

Evidence is now emerging that G4 structures play a major regulatory role in gene expression, ranging from pre-mRNA splicing and polyadenylation through to transcription termination and telomere homeostasis.[19,20] According to bioinformatics analysis, about 376,000 G4 forming

sequences are present in the human genome[19] and many of these are found in human telomeres which contains the repeating unit d(GGGTTA)$_n$.[16] It has been hypothesised that these G4s could cause a 'block' and inhibit telomerase activity which is found to be upregulated in around 85 % of all cancers. DNA G4s are also abundant in non-teleomeric promoter regions of proto-oncogenes such as c-Myc, Bcl-2 and c-Kit. They are also overexpressed at the 5′ and 3′ ends of primary transcripts which may affect gene function. *In vitro* analysis has shown that RNA G4s are more stable[21] and it is thought that they are more likely to fold into G4s due to lack of a complementarity strand *in vivo*.[20] Although there is a large amount of published material on the possible function of DNA and RNA G4s, there is still a divide in the academic community with some believing that while G4s may fold *in vitro*, these sequences may remain unfolded *in vivo* and not play any regulatory roles within the cell.[22] However stabilisation of these structures could provide opportunities as a new drug target.

1.3 Small Molecules that Bind DNA and RNA Secondary Structures

Molecules can be designed to bind specifically to certain secondary structures of DNA or RNA. This can lead to enhanced stabilisation or destabilisation of the nucleic acid structure or to block the binding of proteins, potentially leading to favourable therapeutic effects downstream. Due to the occurrence of G4s within the cell, for example at the end of DNA telomeres, there has been an effort to design small molecules with the ability to selectively stabilise G4s to further understand the power of these structures as therapeutics.[23]

Due to the large, flat, aromatic surfaces that are present in both DNA and RNA G4s, ligand design has centred around molecules that are planar and aromatic in nature. This allows strong π-π interactions with the external guanine residues of the G4.[24] This binding mode is termed 'external stacking' or 'end stacking' and has been shown for a number of DNA G4 ligand binders.[25] Some small molecules (e.g., TmPyP4) have shown a preference for interaction with the G4 loops as well G-quartets.[26] If this is the case, the small molecules can bind in the groove created by the G4 loops. A ligand could also intercalate between the G-quartets, and this has been shown for some metallic porphyrins.[27] Ligands also tend to be cationic to allow electrostatic interactions with the negatively charged backbone of the G4.[24]

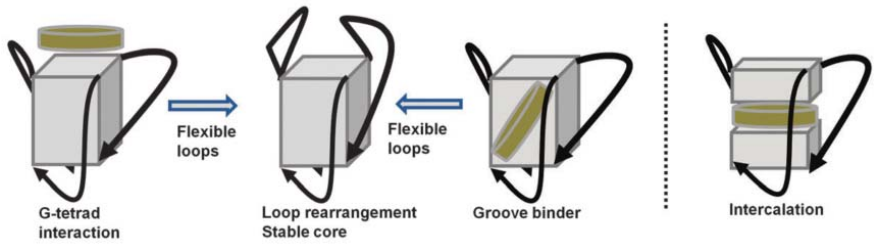

Figure 8. Schematic representation of possible G4:ligand binding.[28]

A great wealth of DNA G-quadruplex stabilisers have been reported, whereas the number of RNA G4s are much fewer even though the likelihood of RNA G4s forming is higher due to the fact that RNA is predominately single stranded within the cell.

1.3.1 DNA G4 Binding Small Molecules

A variety of molecules have been developed that allow *in situ* protonation of amino side chains or *N*-methyl pyridines, which are commonly found around an aromatic core. Protonation enhances the hydrophilicity of the molecule therefore making it more water soluble and more accessible to its biological target.[24] Pyridostatin (**1.16**) and PDC-360A (**1.17**) are two such compounds that can stabilise G4s at telomere ends and thereby disrupt telomerase function.[24]

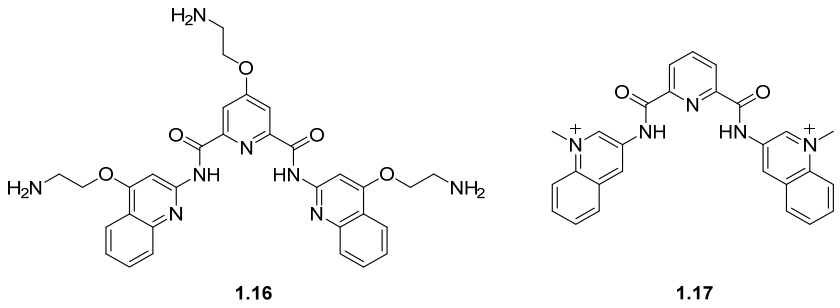

Figure 9. Structure of Pyridostatin (**1.16**) and PDC-360A (**1.17**).

Pyridostatin (**1.16**) was designed jointly by Riou and Balasubramanian[29] after realising that small molecules that contained a large aromatic surface area, to be available for π-interactions with a G4, and amino appendages, that would facilitate electrostatic interactions with the DNA backbone, provided superior G4 interaction. The design also allowed for water or cation coordination through the quindoline nitrogen lone pairs which could 'conformationally lock' the molecule into the flat ligand needed for strong binding. Initially, FRET melting assays were performed to measure the level of stabilisation pyridostatin (**1.16**) could cause for a telomeric DNA G4 over dsDNA. **1.16** exhibited a maximum stabilisation of ΔT_m 35 K at 0.18 μM of ligand

for the DNA G4, while for dsDNA a ΔT_m of 0.5 K was seen (1.0 μM ligand). Cell viability assays with a range of cancer cell lines also showed low micromolar IC_{50} values for **1.16** and analogues after 72 hours of treatment, with long term growth of HT1080 cancer cells inhibited with treatment over a 30 day timeframe.[30] It was later found that **1.16** leads to initiation of the DNA damage response within cells by causing DNA double strand breaks.[31] The *N*-methyl pyridine analogue of pyridostatin, PDC-360A (**1.17**) also demonstrates a >150-fold selectivity for G4 DNA over dsDNA.[24] Triturated PDC-360A was found to preferentially bind to chromosome ends in both healthy and tumour cells suggesting binding to putative G4s formed from telomere overhangs.[32]

Phen-DC3 (**1.18**), a phenanthroline analogue, has a near-perfect match in size to a G4. The stabilisation of the G4 forming sequence F21T (FAM-$G_3[T_2AG_3]_3$-Tamra) by Phen-DC3, was increased by over 20 °C (ΔT_m = 29.7 °C). This increased binding efficiency was reported to be from the increased aromaticity from the quinoline arms and the locked 1,10-phenanthroline backbone which allowed the planar structure of the ligand to be maintained (Figure 10).[24,33]

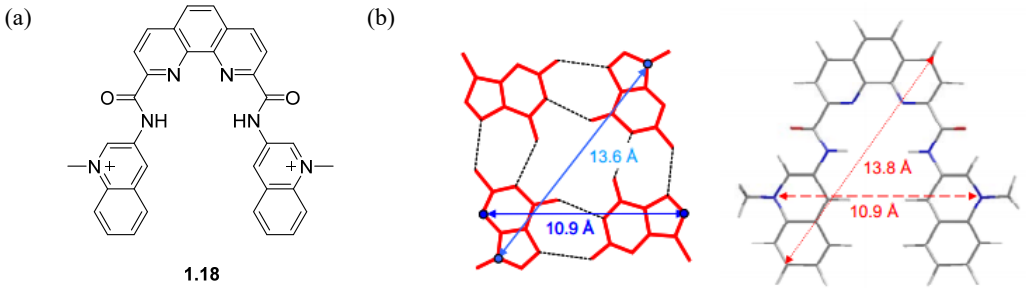

Figure 10. (a) Structure of Phen-DC3 (**1.18**). (b) Molecular lengths of standard G4 and Phen-DC3 using molecular mechanics calculations.[33]

The structure of BRACO-19 (**1.19**) came about by systematic optimisation of both the aromatic core and amino side chains by Neidle and co-workers.[34–38] Using molecular dynamics simulations, the three amino side chains of BRACO-19 have been shown to interact with the 3 grooves of a parallel DNA G4.[38] This interaction was again shown *via* crystal structure with a bimolecular DNA G4,[39] with binding *via* external stacking to the 3′ end face of the G4 (Figure 11). Utilising both FRET and SPR analysis, it was found that BRACO-19 was 31-times more selective for DNA G4s over dsDNA.[24] BRACO-19 (**1.19**) has also demonstrated high activity *in vivo*, with the ability to produce 96 % growth inhibition on mouse uterus carcinoma cell line xenografts with a 2 mg per kg per day dosing regimen.[40]

(a) (b)

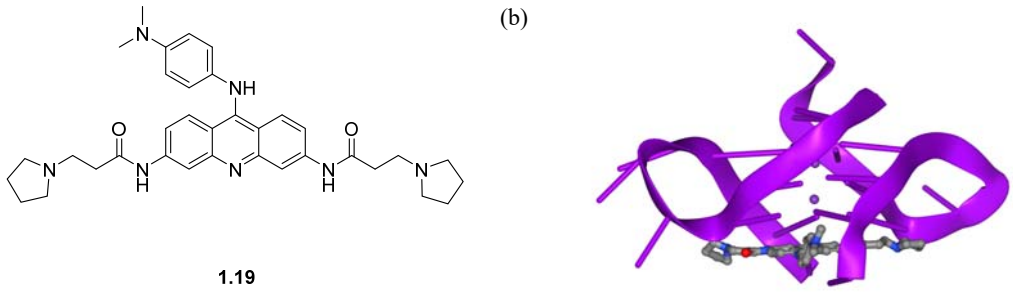

1.19

Figure 11. (a) Structure of BRACO-19 (**1.19**). (b) Crystal structure of BRACO-19 in complex with bimolecular DNA G4 (PDB id 3CE5). Bimolecular G4 coloured purple, BRACO-19 coloured grey.

Hurley *et al.*[41] tested a small library of compounds for stabilisation of the c-Myc DNA G4 found within the nuclease hypersensitive element III region of this oncogene. They found the ellipticine derivative, GQC-05 (**1.20**), to be a selective and potent stabiliser of the c-Myc G4 with a ΔT_m of 21 °C at 10 μM of compound. It also showed a 45-fold preference for the c-Myc G4 over the c-Myc dsDNA.

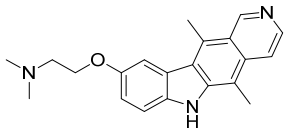

1.20

Figure 12. Structure of GQC-05 (**1.20**).

They also tested GQC-05 (**1.20**) in a range of *in vitro* assays which demonstrated that this compound was effective at inducing cytotoxicity and leading to lower levels of mRNA after transcription. They suggested that in Burkitt's lymphoma, negative superhelicity could unwind the dsDNA allowing both a G4 and i-motif to form on opposite strands. In the presence of GQC-05 (**1.20**), two equivalents could bind to the G4, leading to stabilisation and, consequently, transcriptional down regulation.

Another family of G4 binding ligands that have been researched thoroughly are porphyrins. One such example is TMPyP4 (**1.21**) which is a known DNA G4 stabilising tetracationic porphyrin.[24] Although TMPyP4 exhibits poor selectivity for G4 over dsDNA, it is able to downregulate multiple oncogenes such as c-Myc[42] and k-ras and inhibit telomerase activity (IC_{50}: 6 μM) by binding directly to G4s.[24]

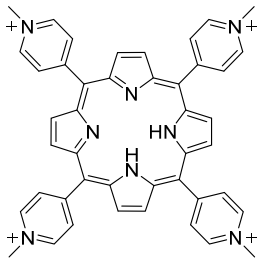

1.21

Figure 13. TMPyP4 (**1.21**).

Although TMPyP4 (**1.21**) has limited use as a selective therapeutic agent due to its structural promiscuity, there has still been a great deal of research into its interaction with DNA. It has exhibited the ability to convert *anti*-parallel G4 topologies into parallel G4 topologies[24] and has been shown to have a number of unique binding modes, including, end-stacking,[43] loop binding and intercalation between G-quartets.[26,43,44]

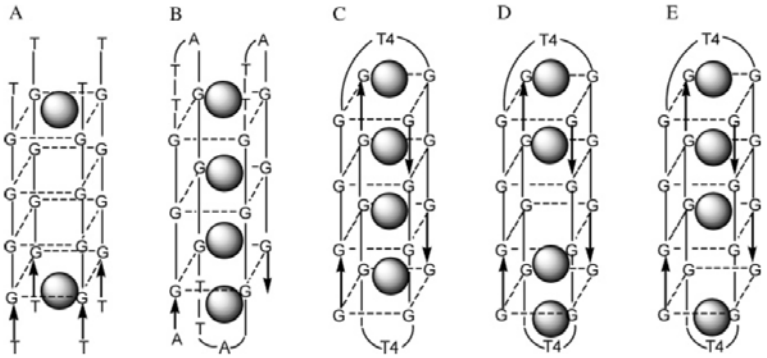

Figure 14. Proposed binding modes of TMPyP4 (**1.21**) with tetra-, bi-, and, unimolecular DNA G4s. (a) Two molecules of TMPyP4 end-stacking with the tetramolecular DNA G4 $(TG_3T)_4$. (b) TMPyP4 intercalating between two G-quartets and also end-stacking with both the lateral and diagonal loops of $AG_3(T_2AG_3)_3$. (c, d, and e) Mixture of intercalation between two G-quartets and binding to the T_4 loop of the bimolecular G4 formed from $(G_4T_4G_4)_2$.

More recently the inclusion of transition metals into ligand assemblies has been shown to dramatically increase the association of the ligand for DNA G4 structures. The positively-charged ligands exert a higher affinity for the negatively charged nucleic acid structure and the chelating ligand is furthered anchored in place due to the central metal residue which interacts with the cationic core of the G4.[45] To illustrate this the Mn(III)-complex of TMPyP4, Mn-TMPyP4 (**1.22**), exhibited a 10-fold increase in its selectivity of G4 vs dsDNA compared to its parent porphyrin (**1.21**).[24]

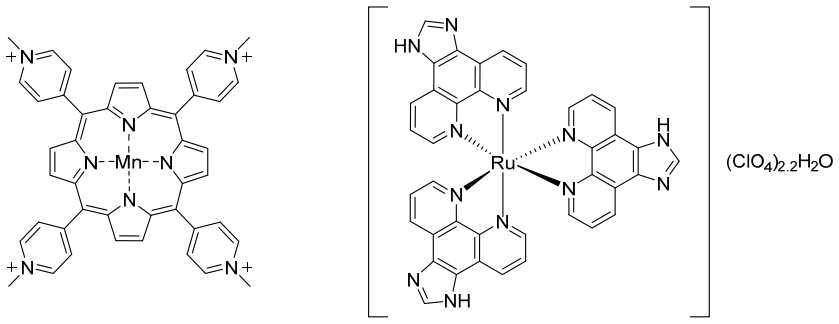

Figure 15. Structure of Mn-TMPyP4 (**1.22**) and $[Ru(ip)_3](ClO_4)_2 \cdot 2H_2O$ (**1.23**).

More recently there has been a rise in the use of ruthenium based compounds. The ruthenium (II) complex $[Ru(ip)_3](ClO_4)_2 \cdot 2H_2O$, (**1.23**), stabilises DNA G4s formed in the Bcl-2 gene and subsequently induces cell apoptosis in *in vivo* studies.[46]

1.3.2 RNA G4 Binding Small Molecules

Due to the high probability of RNA being single stranded in the cell and the extra thermodynamic stability that is afforded due to the 2′-OH, it could be imagined that RNA G4s could be a valuable therapeutic target.[28,47] However, to date there has been very little published in the literature of selective RNA G4 binding ligands. It has been hypothesised that the 2′-OH group would allow RNA selective ligands to be designed as this would present the opportunity for valuable H-bond interactions with ligands. The majority of RNA G4s also adopt parallel structures due to the 2′OH forcing the sugar pucker into the C3′-endo conformation. Again, this could lead the design of highly active ligands.[28] However, to date, there have been no examples of ligands selective for RNA G4s over DNA G4s.

Mergny *et al.* carried out a short investigation into the selectivity seen for PDC-360A towards both DNA and RNA G4s. FRET analysis was used to evaluate the ΔT_m values for 4 DNA strands and one human telomeric RNA strand when treated with 1 μM of **1.17**.

(a)

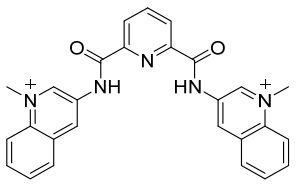

1.17

(b)

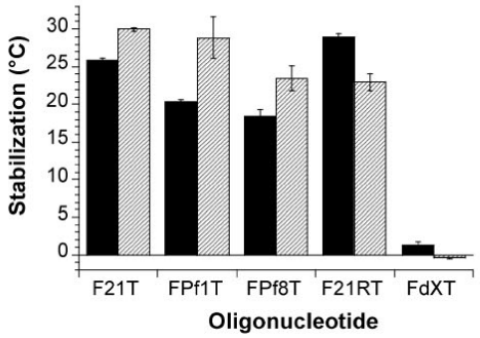

Figure 16. (a) Structure of PDC-360A (**1.17**). (b) Stabilisation observed for a number of 5′FAM and 3′TAMRA labelled oligo- and oligoribonucleotides. F21T – human telomeric sequence $(GGGTTA)_3GGG$; FPf1T – plasmodium sequence $(GGGTTTA)_3GGG$; FPf8T – plasmodium sequence $(GGGTTCA)_3GGG$; F21RT – human telomeric RNA sequence $(GGGUUA)_3GGG$; FdXT – hairpin duplex with a HEG loop $TATAGCTATAC_{18}TATAGCTATA$. Filled columns – NaCl; hatched columns – KCl+LiCl.

As seen in Figure 16, stabilisation of over 20 °C was seen for F21T, FPf1T, FRf8T and F21RT in both salt conditions. Since PDC-360A (**1.17**) has already been shown to be a highly effective DNA G4 stabiliser, it would not be expected to be selective for the human telomeric RNA sequence.

In a different study, the binding and stabilisation of PDC-360A (**1.17**), alongside two Phen-DC compounds (**1.18** and **1.24**), was explored towards a G4 formed within the 5′-UTR region of the TRF2 mRNA.[48] Using the QGRS Mapper programme, several putative G4 forming sequences within the 5′UTR region were identified. Examination using electrophoretic mobility assays of each of the DNA versions of the sequences, with increasing equivalents of **1.17**, suggested that the sequence 91TRF2G (5′-CGGGAGGGCGGGGAGGGC-3′) was the most stable and therefore, was most likely to form stable RNA G4s also. UV melting assays and CD measurements of this sequence 91TRF2G:RNA further confirmed the ability of this sequence to form a stable G4 in Na^+, K^+ and Li^+ buffers at a range of buffer and RNA concentrations. FRET melting assays were utilised to determine the ability for the three ligands **1.17**, **1.18** and **1.24** to bind 91TRF2G:RNA. Initially melting values were determined for the DNA G4 sequence F21T alone and with ligands. Then a series of competitor sequences were added with ligands to observe the binding preference by recording ΔT_m of F21T. The competitor sequences were a dsDNA sequence, 91TRF2G:RNA and a mutated version of 91TRF2G:RNA where one guanine from each G-quartet was replaced with a uridine (Mut91TRF2G:RNA – 5′-CGUGAGUGCGCUGAGGGC-3′). This would prevent the G4 from forming. As expected, each of the ligands increased the ΔT_m of F21T by > 19.2 °C in both buffer systems (Figure 17b). The addition of dsDNA did not change this selectivity. However, upon the addition of 91TRF2G:RNA, along with **1.17**, **1.18** and **1.24**, the ΔT_m of F21T dropped and no stabilisation was observed. This suggests that each of these ligands preferentially

bind to, and stabilise the RNA G4 over the DNA G4. When Mut91TRF2G:RNA was added the preferentially stabilised structure was F21T.

(a)

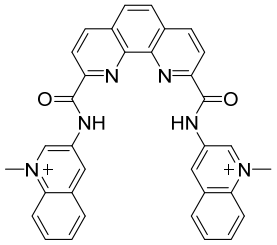

1.18

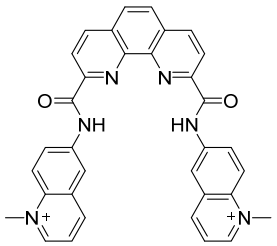

1.24

(b)

$\Delta T_{1/2}$ (°C)	No compound	1 μM Phen-DC(3)	1 μM Phen-DC(6)	1 μM 360A
100 mM NaCl				
No competitor	0.1	27.2	>29.7	25.4
Ds26	0.0	24.0	>28.1	24.0
91TRF2G:RNA	0.6	0.1	0.0	1.0
Mut91TRF2G:RNA	−0.5	24.8	>20.6	24.1
10 mM KCl + 90 mM LiCl				
No competitor	0.0	19.2	>31.6	26.5
ds26	−0.2	18.3	>31.3	26.5
91TRF2G:RNA	−0.5	0.6	−0.5	12.0
Mut91TRF2G:RNA	−1.4	17.6	>22.4	25.5

Figure 17. (a) Structure of Phen-DC3 (**1.18**) and Phen-DC6 (**1.24**). (b) FRET melting assay results of F21T with G4 ligands and 91TRF2G:RNA and Mut91TRF2G:RNA as competitors. Compounds were tested a 1 μM and are the average of n = 3 runs. Annealing and experiments carried out in 10 mM lithium cacodylate buffer at pH 7.2 with 100 mM NaCl or 10 mM KCl + 90 mM LiCl.

Using a coupled transcription-translation assay it was demonstrated that the stabilisation of the 91TRF2G:RNA G4 by the 3 ligands tested affected GFP protein translation *in vitro*. Yet, the mRNA production and stability was not affected. The authors suggested that this inhibition of GFP protein synthesis was due to targeted RNA G4 stabilisation and this could be harnessed for treatment of cancer as TRF2 has been found to be overexpressed in cancer cells.[49,50]

Another study that discovered that transcription could be inhibited by the stabilisation of RNA G4s was carried out by Balasubramanian on the 5′-UTR of the NRAS oncogene.[51] Two firefly luciferase reporter mRNA constructs were designed, one containing the RNA G4 sequence (NRAS UTR(+)Q) and the second missing this section (NRAS UTR(-)Q). Initially a derivative of PDC-360A was tested, RR92 (**1.25**), however a decrease in translation efficiency was observed for both NRAS constructs suggesting this compound was not selective for the G4 and was possibly acting *via* another mechanism (Figure 18a – b). A second derivative that exchanged the cationic alkyl amino group at the C4 position of the pyridine for a less polar fluorophenyl group provided superior selectivity for the NRAS UTR(+)Q construct over the control. A dose dependant decrease in the translation of the NRAS protein was observed from 1.25 to 10 μM for **1.26** (Figure 18c – d). A second G4 construct, NRAS UTR(+120)Q, was tested where the G4

forming sequence was relocated to 120 nt downstream of the 5′ cap. Without ligand present, translation of this construct was as efficient as that of the control construct NRAS UTR(-)Q. However, once treated with **1.26**, a dose-dependent inhibition of the translation efficiency is observed and is on par with that seen for NRAS UTR(+)Q (~ 40% at 10 μM ligand).

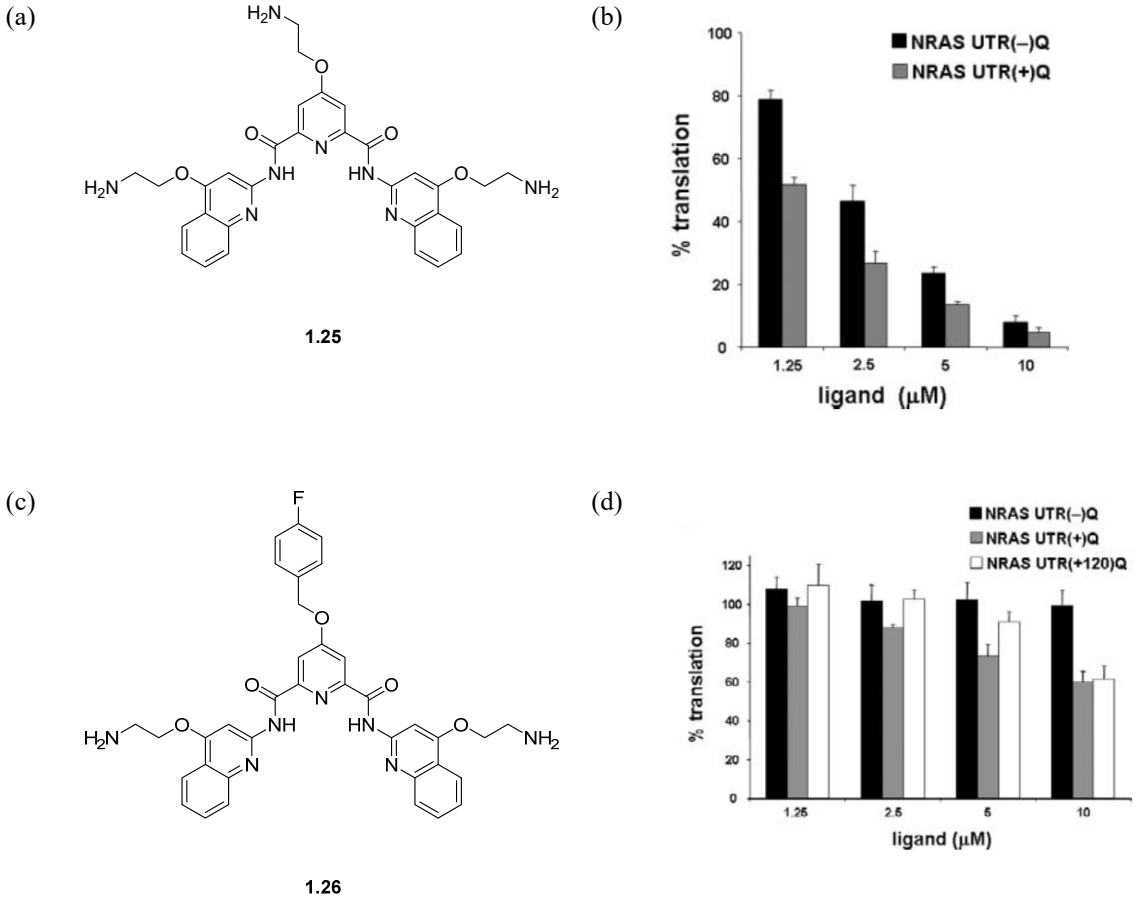

Figure 18. (a) Structure of RR82 (**1.25**). (b) Relative translation efficiencies for NRAS UTR(+)Q and NRAS UTR(-)Q treated with varying concentrations of **1.25** from luciferase assays. Reactions were normalised to control without ligand. (c) Structure of RR110 (**1.26**). (d) Relative translation efficiencies for NRAS UTR(+)Q, NRAS UTR(-)Q and NRAS UTR(+120)Q, treated with varying concentrations of **1.26** from luciferase assays. Reactions were normalised to control without ligand.[51]

^{1}H NMR spectroscopy was then conducted to look for any signal changes that would confirm binding of **1.26** to the RNA G4. A ligand titration was carried out from 0 to 5 equivalents and as the concentration increased clear line broadening and upfield shift of the imino and aromatic proton signals were observed (Figure 19a). The authors hypothesised that this was due to π – π interactions between the terminal G-quartets of the G4 and the aromatic protons of **1.26**. Hydrogen-deuterium exchange kinetics of the imino protons at 5 equivalents of **1.26** also

suggested protection of these protons from solvent by the ligand as the kinetics were slower at higher concentrations of ligand (Figure 19b).

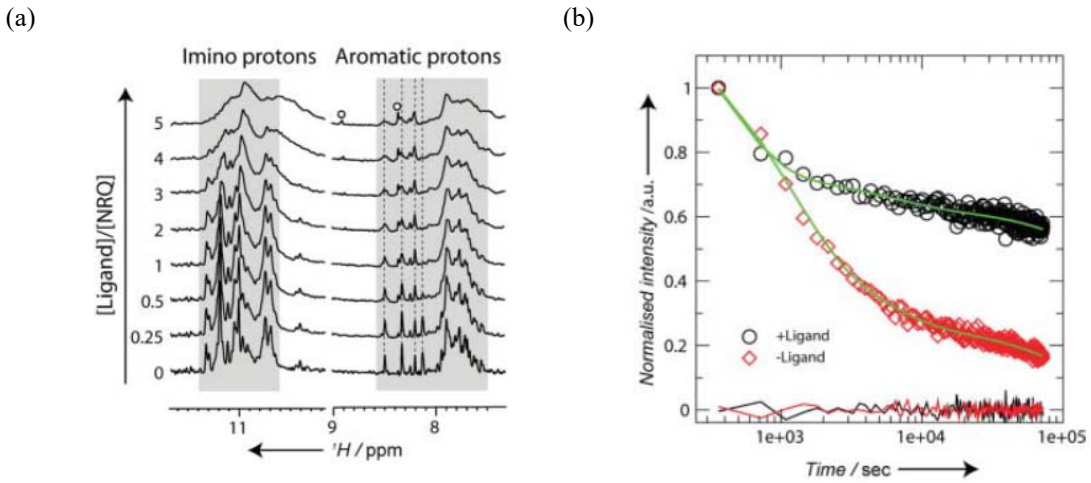

Figure 19. (a) ^{1}H NMR of imino and aromatic proton signals from ligand titration experiment. (b) Kinetics from hydrogen-deuterium exchange experiment at 5 equivalents of **1.26**.[51]

Non-coding RNA, termed TERRA, is thought to play a major role in telomere maintenance and function and has been suggested as a therapeutic target. It has been shown to form G4 structures readily due to its rUUAGGG repeating sequence. Neidle *et al.*[52] have reported a crystal structure of a TERRA•acridine complex at a resolution of 2.6 Å (Figure 20a and c). This complex was found to have two acridine (**1.27**) molecules inserted between two TERRA G4 structures. As expected the G4 adopts a parallel topology. Interestingly, few H-bond interactions are present between the ligand and the guanines of the G4, with most of the stability seemingly arising from π-π interactions. However, the UUA propeller loops were shown to be held in place by several H-bonds with the ligand (Figure 20b). Major conformational changes also take place in the loops to allow binding of **1.27**. Figure 20d shows the rotation of U6, U7 and A8, in comparison to the native form,[53] to accommodate the ligand and increase π – π stacking.

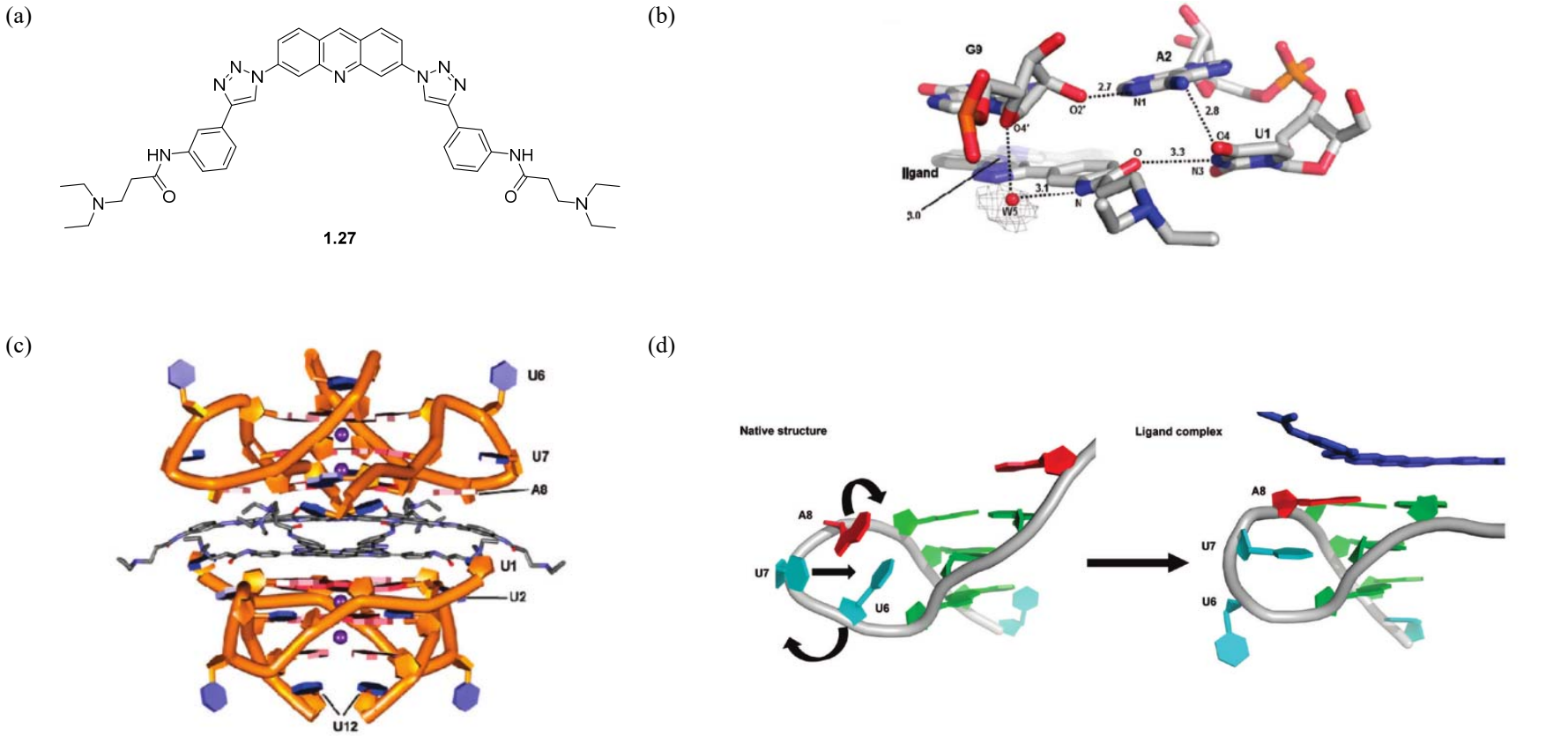

Figure 20. (a) Structure of acridine *N*,*N*'-((1,10-(acridine-3,6-diyl)bis(1*H*-1,2,3-triazole-4,1-diyl))bis(3,1-phenylene))bis- (2-(diethylamino)acetamide) (**1.27**). (b) H-bonds between the amide of **1.27**, a water molecule and the G9, A2 and U1 bases. (c) Schematic representation of the TERRA•acridine complex formed from two G4s and two ligands. Backbone of RNA = orange, ligands = grey and K^+ = purple circles (PDB id 3MIJ). (d) Schematic showing the conformational changes observed in the UUA loops region on binding of **1.27**.[52]

The overall complex was found to exhibit key differences from the corresponding DNA TERRA G4•acridine crystal structure published previously (PDB id 3QCR).[54] The DNA complex only exhibited a 1:1 binding mode and no loop involvement was observed. This is one of the few crystal structures of a RNA G4•ligand complex and should facilitate towards future ligand design.

To be able to effectively target RNA G4s, more knowledge needs to be gained on their specific role in diseases and highly selective ligands need to be designed to reduce the possibility of off-target effects within the cell.

1.4 RNA Splicing

Pre-mRNA contains sequences called exons and introns. Exons are known as the coding part of the gene and introns hold non-coding information.[55] During splicing, introns are excised from the pre-mRNA and exons are spliced together to form mature mRNA which is subsequently exported out of the nucleus to be translated into a corresponding protein.[56] The spliceosome is a large, complex macromolecular machine which regulates and catalyses the splicing process.[57] Over 150 proteins contribute to the spliceosome at different stages in the splicing process.[58,59] Five of the most important spliceosomal proteins are called small nuclear ribonuclearproteins (snRNPs). The snRNPs associate together to create a catalytic hub in which a series of transesterification reactions can take place (Figure 23).[60,61] Within each snRNP, small nuclear RNAs (snRNAs) known as U1, U2, U4, U5 and U6, are found.[62] Each snRNA has a short run of nucleotides which are complementary to the pre-mRNA to be spliced which helps to orientate and fold the pre-mRNA. The splicing cycle proceeds *via* the formation of a number of different RNA-protein complexes. A multitude of proteins bind to different sections of the pre-mRNA during the splicing cycle to control the splicing process. The four main sections of the pre-mRNA that are critical to splicing are the 5′ splice site, the adenosine branchpoint, the polypyrimidine tract and the 3′ splice site (Figure 21).[55] The 5′ and 3′ splice sites are found on the boundary of the excised intron and the retained exon. Between the splice sites, the branchpoint adenosine and the polypyrimidine tract are found, with the branchpoint adenosine found upstream of the polypyrimidine tract. The distance between the 5′ splice site and the branchpoint adenosine can be many kb in length, however, the polypyrimidine tract is only around 100 nt in length.[55]

Pre-mRNA often contains conserved sequences upstream and downstream of splice sites, which assist in splice site recognition. The most conserved nucleotides are G and T in the +1 and +2 position of the 5′ splice site, respectively.[55] In the 3′ splice site the most highly conserved

nucleotides are A and G in the -1 and -2 positions, respectively. Figure 21 highlights the consensus sequences in the 5′ and 3′ splice sites and the branch site.

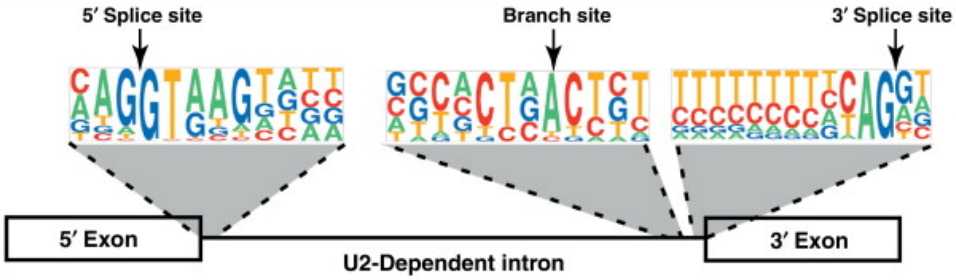

Figure 21. Consensus splice site sequence for U2-dependent intron pre-mRNAs. The larger the letter, the more conserved the nucleotide is.[63]

During the splicing process the first complex that is formed is the E complex (Figure 22). The U1 snRNP interacts with the pre-mRNA at the 5′ splice site, allowing base pairing of the short complementary sequence up to 11 nucleotides in length between U1 and the 5′ splice site.[55,57,62] The proteins U2AF35, U2AF64 and SF1 then bind to the 3′ splice site, polypyrimidine tract and the adenosine branch point, respectively. The formation of this complex defines both the 5′ and 3′ splice sites. Complex A is formed when U2 replaces SF1 at the branch point position. Again, base-pairing between the pre-mRNA and U2 stabilises this interaction, however as the base pairing is not completely complementary, the branch point adenosine creates a bulge in the sequence.[55] The next snRNPs that associate with the spliceosome are U4, U5 and U6, which form a unique tri-snRNP (termed U4/U6●U5) complex that forms complex B. Key rearrangements take place between RNA and proteins and the tri-snRNP recruits RNA helicases from U5, which cause rearrangements within the spliceosome and the expulsion of U1 and U4. This forms the active site in the B^{act} complex and is catalytically activated by the DEAH-box RNA helicase Prp2 which generates the B* complex.[64]

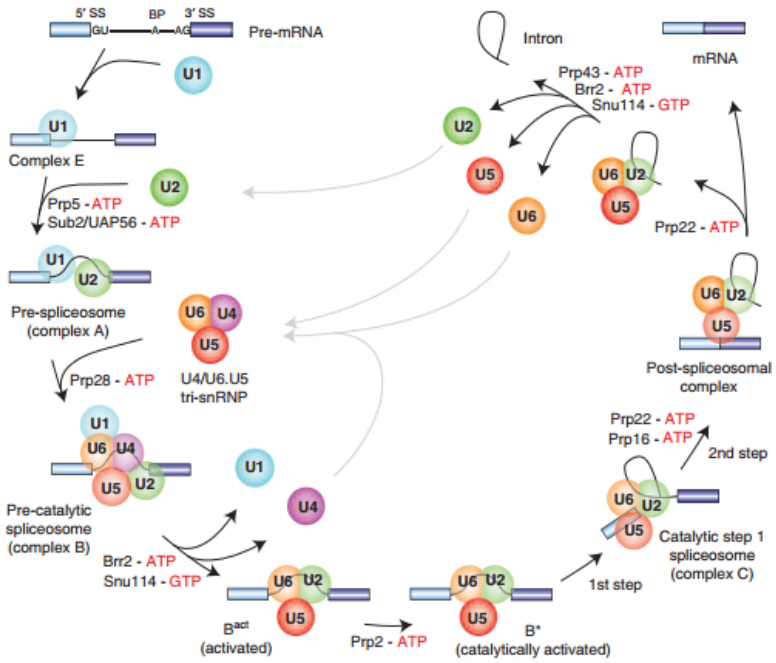

Figure 22. An overview of the process of RNA splicing catalysed by the spliceosome.[59]

U5 arranges both exon 1 and exon 2 within the active site while U6 interacts with the 5′ splice site and U2, which is still paired with the adenosine branch point. PRP8 and a preformed group of proteins called the '19 complex' complete the catalytic core and hold all the components in place ready for the first transesterification reaction (Figure 23).[55]

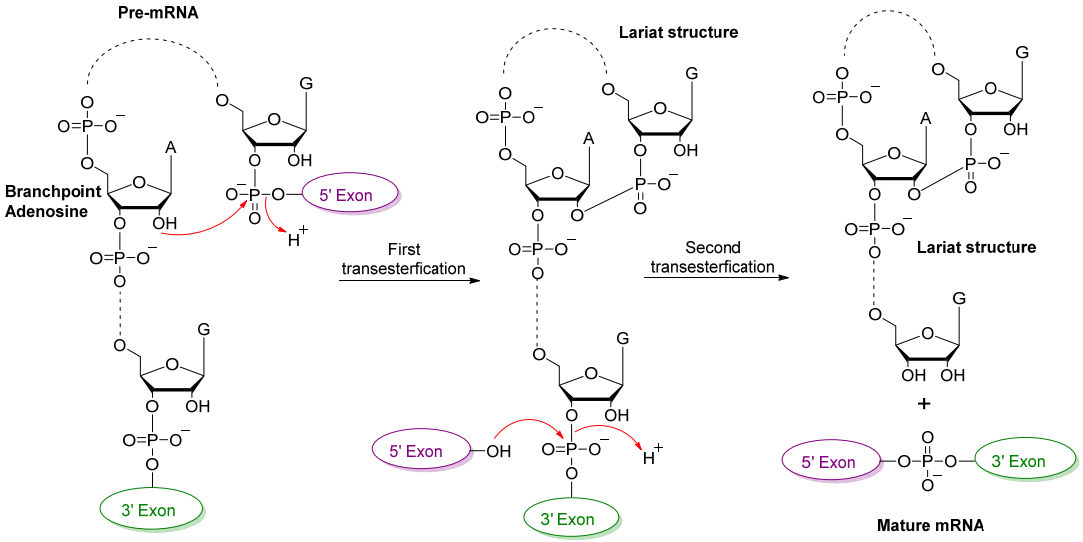

Figure 23. Mechanistic overview of the two transesterfication reactions that take place during splicing.

The branchpoint adenosine 2′-OH attacks the phosphodiester bond between the upstream exon and the intron to create a new 5′ – 2′ phosphodiester bond. This results in the displacement of the

5′ exon and subsequent formation of a looped lariat structure. The 3′-OH of the 5′ exon then attacks the phosphodiester bond between the intron and the 3′ exon to form a bond between the 5′ exon and 3′ exon and releases the lariat structure. This double transesterification process is continuous until splicing of the pre-mRNA is complete and the mature mRNA is formed (Figure 23).[55] Two magnesium ions are present during the two transesterification reactions and it is believed that they help stabilise the nucleophile and position the leaving group in both reactions. They also help to balance the negative charges that are present during splicing.[57,60,65]

1.5 Alternative Splicing

In eukaryotic cells, protein diversity is achieved by a process known as alternative splicing.[55,66] This is where a sequence of pre-mRNA encodes for multiple different RNA isoforms depending on the sequence in which the exons within the RNA are joined together. Figure 24 illustrates this process where a pre-mRNA strand produces three different RNA isoforms, which can then be translated into three different protein isoforms.[57]

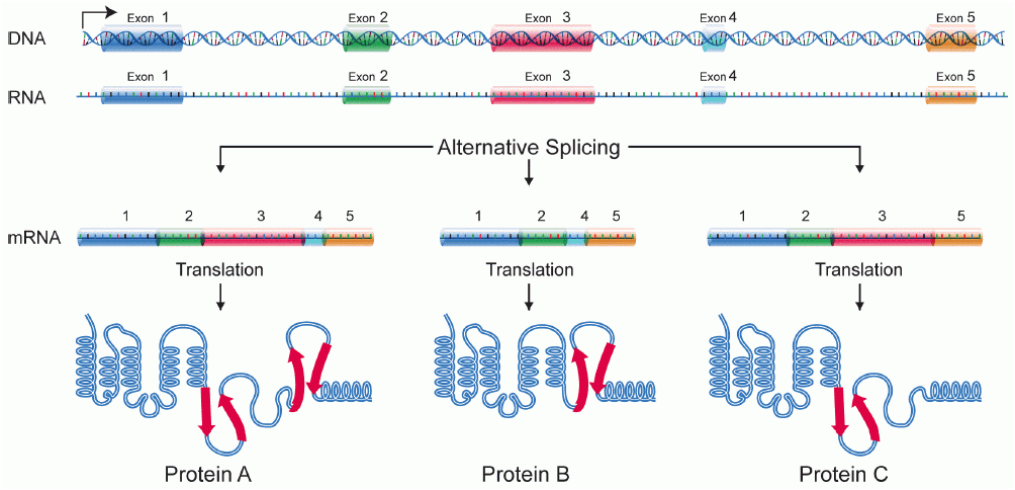

Figure 24. Schematic representation of alternative splicing in pre-mRNA.[57]

In humans, ~ 95 % of multi-exon genes undergo alternative splicing,[67,68] however, aberrant alternative splicing processes can also be the cause of disease and mutations.[69,70] Aberrant splicing can occur *via* multiple mechanisms including mutations in splicing enhancers and silencers which control the usage of splice sites by binding to splicing proteins.[71] It is therefore essential to understand the complexity of the splicing process in order to design systems to overcome unwanted splicing outcomes.

1.5.1 Mechanism of Splice Site Selection

The three main ways in which pre-mRNA can be alternatively spliced are (i) exon skipping, (ii) alternative splice sites, and (iii) the retention of introns. Exon skipping is the most common form of alternative splicing in higher eukaryotes and accounts for almost 40 % of alternative splicing events.[72] Alternative splice sites, either 5′ or 3′, account for around 8 % and 19 % of possible events, respectively. Intron retention only accounts for about 5 % of the possible alternative splicing events which can take place. However, as demonstrated in Figure 25, there are numerous other more complex ways in which splicing can occur along with the three mentioned above.

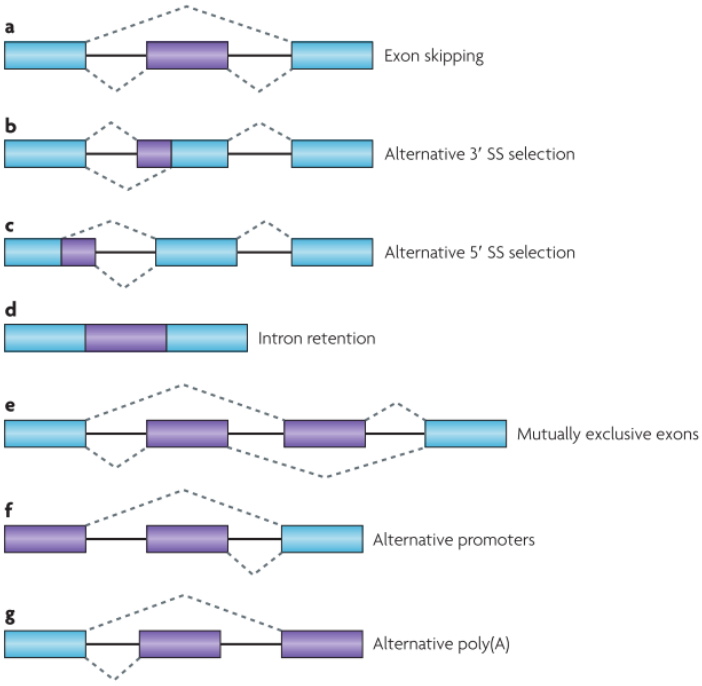

Figure 25. Overview of the main splicing pathways in eukaryotes. (a) Exon skipping (b) Use of an alternative 3′ splice site within the upstream exon. (c) Use of an alternative 5′ splice site within the upstream exon. (d) Intron retention. (e) One of two exons is spliced out of the pre-mRNA. (f) Alternative promoters initiate splicing. (g) Alternative polyadenylation sites.[72]

There are two main factors that influence splicing patterns, namely, *cis*-regulatory sequences and *trans*-acting factors.[62] *Cis*-regulatory sequences are RNA sequences that define splice site conservation and strength, length of introns and branchpoint location. *Trans*-acting factors refer to the proteins that bind to the *cis*-regulatory sequences of the pre-mRNA. 5′ and 3′ splice sites have to be highly conserved for efficient splicing to take place. The strength of these is also important and is correlated to the degree of complementarity between the splice site and the corresponding binding sequence on the appropriate snRNA.[73] This means a strong splicing signal is where there is a high degree of complementarity between the pre-mRNA binding sequence and

the protein or snRNP binding sequence. A weak splicing signal arises when multiple mutations have taken place in the binding sequences which lowers the complementarity. Mutations in the splice site can abolish splicing altogether or lead to other splice sites being used which have a higher degree of complementarity. These secondary splice sites are called cryptic splice sites and are often similar to the consensus sequence but are not active during splicing of the wild type pre-mRNA.[69] Use of a cryptic splice site can occur if the strength of the wild type splice site is not very high and a mutation occurs in the cryptic splice site to make it more complementary. The length of the introns that are being spliced out and the rate at which the pre-mRNA is transcribed by RNA polymerase II can also greatly affect splicing patterns. Transcription and splicing occur simultaneously, therefore long intronic regions give the spliceosome time to undergo splicing with the correct exons.[55] However, if introns are short then subsequent downstream exons will be transcribed before splicing is complete resulting in the production of competing exons and splice sites. If the rate of transcription is fast, then more exons will be available which could have stronger splice sites which can interfere with the removal of the current intron.

There are three main groups of splicing factors that are important in the transcription of pre-mRNA; SR (serine-arginine rich) proteins, U2AF and hnRNPs (heterogeneous ribonucleoprotein particles).[62] One important member of the SR protein family is SRSF1 (SF2/ASF) which has been found to enhance binding of U1 to the 5′ splice sites.[74] Spliceosomal activity can be blocked when SR proteins are not present, therefore SR proteins are usually referred to as ‘enhancers’ of splicing.[75] In contrast, the hnRNP family of proteins are termed ‘silencers’ of splicing.[76] In the case of hnRNP A1, it competes with U1 for the binding of the pre-mRNA in complex E which, if successful, affects the 5′ splice site selection.[73,74] SR proteins and hnRNPs bind to different sections of the RNA and this is how regulation of splice site usage occurs. The binding sites of SR proteins are known as exonic splicing enhancers (ESEs) and intronic splicing enhancers (ISEs) and are found in exons and introns respectively. hnRNPs bind to sections termed exonic splicing silencers (ESSs) and intronic splicing silencers (ISSs).[77]

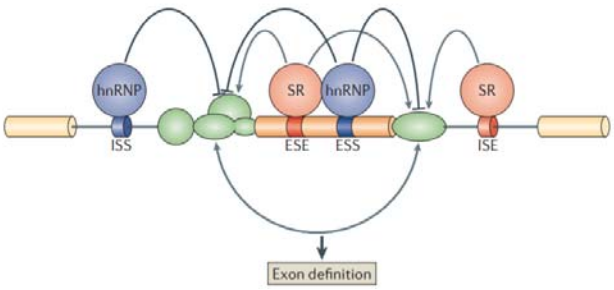

Figure 26. Sequences and factors that control the outcome of alternative splicing processes.[77]

Mutations in any of these regulatory elements can affect the recruitment of spliceosomal components which is a common way in which splicing defects arise.[71]

1.6 Aberrant RNA Splicing and Disease

Approximately 95 % of multi-exon pre-mRNAs undergo alternative splicing.[67] As a result, a large number of illnesses such as cancer and cardiovascular diseases are caused by modifications to the alternative splicing profile of wild-type pre-mRNA. Understanding the complexity underpinning aberrant splicing pathways in a disease context has the potential to open up opportunities for the development of new therapeutics.

1.6.1 Spinal Muscular Atrophy

Spinal Muscular Atrophy (SMA) is a general term for a range of diseases that are caused by the death of motor neurons in the spinal cord which lead to the slow wastage and atrophy of muscles in the body.[78] Proximal Spinal Muscular Atrophy (commonly referred to as SMA) is the most frequent genetic cause of infant death with children that exhibit the most severe form (type 0/1) rarely living longer than two years (Table 1).[79]

Table 1. Disease classifications for Spinal Muscular Atrophy [80]

Classification	Age of onset	Maximum function achieved	Prognosis	SMN 2 copy number
Type 0 very severe	Neonatal with prenatal signs	Never sits	If untreated, no survival beyond the first months after birth	¨
Type 1 severe	0-6 months	Never sits	If untreated, life expectancy < 2 years	One or two copies of SMN2 in 80% of patients
Type 2 intermediate	7–18 months	Sits but never stands	Survival into adulthood	Three copies of SMN2 in >80% of patients
Type 3 mild	>18 months	Stands and walks	Survival into adulthood	Three or four copies of SMN2 in 96% of patients
Type 4 adult	10–30 years	Stands and walks	Survival into adulthood	Four or more copies of SMN2

SMN wild type consists of two genes - SMN1 and SMN2 – which encode for the Survival of Motor Neuron (SMN) protein. When alternative splicing of SMN1 takes place, exon 7 is retained which leads to normal SMN protein levels. Both genes exhibit 99.9 % similarity however, a single C to U mutation in exon 7 in SMN2 results in exon 7 skipping 90 % of the time.[69] This translates into a non-viable SMN protein isoform and is quickly degraded. This accounts for very low SMN protein levels from the SMN2 gene.[63] SMA is characterized by low levels of the SMN protein as in 95 % of cases the SMN1 gene is absent and SMN2 can only produce a small amount of the functioning SMN protein due to the single nucleotide mutation.[78]

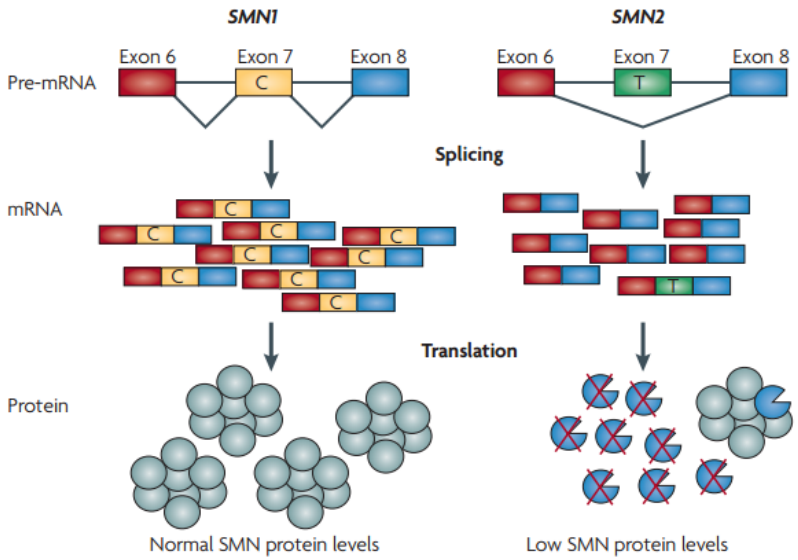

Figure 27. Schematic demonstrating the transcription and translation of wild type SMN1 and SMN2 pre-mRNA. SMN1 encodes for 100 % of SMN protein whereas SMN2 only encodes for 10 % of functioning SMN protein.[81]

Therapeutic strategies to correct the loss of functioning protein in SMA have focussed on both traditional small molecule approaches and antisense oligonucleotides (ASOs).

1.6.1.1 Splice Switching Antisense Oligonucleotides – Nusinersen (Spinraza)

A new type of treatment that has shown increasing importance within the last 30 years is ASOs.[82] ASOs are short oligonucleotides that have an affinity for ssRNA sequences and bind through traditional Watson-Crick base pairs. They generally contain 12 – 14 bases and the bases and backbone can be modified in a number of ways to (i) increase the binding to the target RNA, (ii) increase the stability of the ASO towards nuclease degradation and (iii) improve the pharmacokinetic properties.[83] In December 2016 the first ASO for treatment of SMA was approved by the FDA, Nusinersen (Spinraza™), which is a uniformly modified 18-mer ASO. The bases are a combination of methylated and non-methylated variants, held together with a 2′-*O*-(2-

methoxyethyl) backbone (5′-^{Me}U^{Me}CA^{Me}C^{Me}U^{Me}U^{Me}U^{Me}CA^{Me}UAA^{Me}UG^{Me}C^{Me}UGG-3′, Figure A1).[84] It targets an ISS within intron 7 of SMN2 and promotes the inclusion of exon 7 by displacement of hnRNP proteins which leads to fully functioning SMN protein (Figure 28).[85]

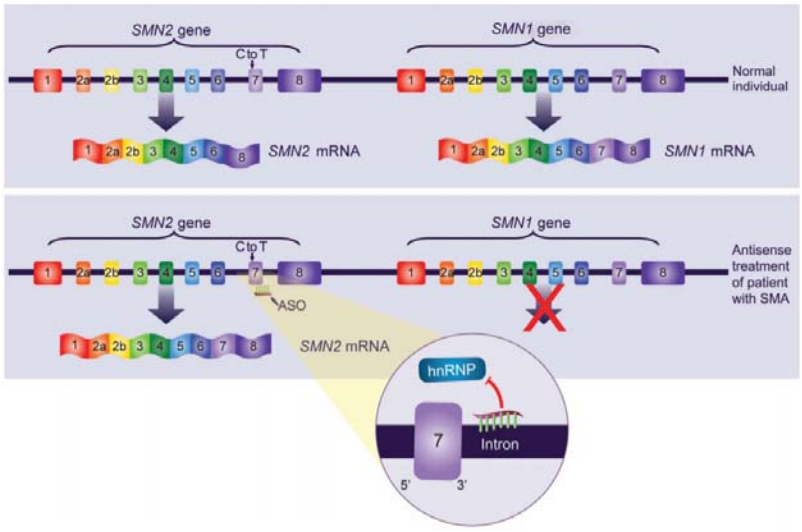

Figure 28. Mode of action of Nusinersen (Spinraza™).[85]

In Phase I clinical trials, a single dose of 1, 3, 6 or 9 mg was prescribed by injection into the cerebrospinal fluid of patients and it was found that after 9 – 14 months SMN protein levels were still elevated by more than double normal levels in the 6 and 9 mg test groups.[86]

1.6.1.2 Splice Switching Small Molecules which Enhance Production of SMN2

Small molecules, both repurposed and novel, have been extensively studied to try and treat SMA. The preferable mode of action would be by increasing the inclusion of exon 7 in SMN2, however neuroprotective drugs and scavenger mRNA-decapping enzyme (DcpS) inhibitors have also been tested.[87] To date, the two best candidates have been published by the pharmaceutical companies Roche/PTC Pharmaceuticals and Novartis. In 2014 Roche, in collaboration with PTC Pharmaceuticals, published a small molecule with a pyridopyrimidinone scaffold (**1.28**) which was capable of increasing body weight and decreasing muscular atrophy in mice with a severe form of SMA if they were treated from postnatal day 3. This lead to improved motor function and prevented neuromuscular deficits into adulthood.[88] Further lead optimization on the central core of the scaffold lead to the design of coumarin, isocoumarin and benzamide cores with (**1.30**) showing promise due to the reduction in aromaticity of the structure.[88–91]

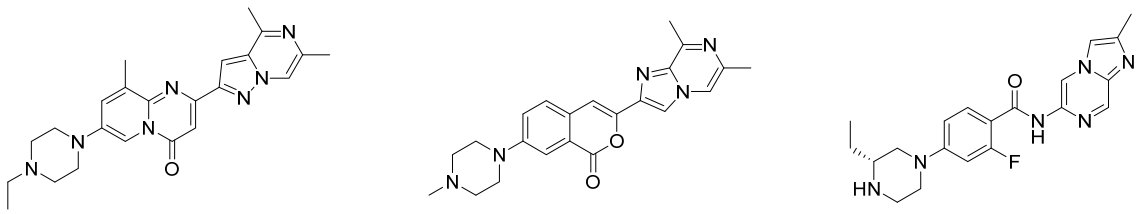

Figure 29. Structure of several small molecules published by Roche/PTC Pharmaceuticals for the treatment of SMA.[88,91]

Novartis followed Roche with the publication of a small molecule **1.31** that also greatly increased the inclusion of exon 7. The small molecule was identified by high throughput screening. qPCR and ELISA assays confirmed that an increase in SMN protein was observed in SMNΔ7 mouse myoblasts.[92] Again, this compound improved body weight and survival rate of treated mice. Investigations were carried out to try and understand the mechanism of action of **1.31** and it was found that it could stabilise a transient dsRNA complex formed between the pre-mRNA of SMN2, specifically the 5′ ss, and the U1 snRNP. The U1 snRNP is a key factor in the selection of the 5′ss during the splicing process and this stabilisation allowed the increased retention of exon 7. In surface plasmon resonance studies it was shown that the compound could not bind either the SMN2 5′ ss or U1 snRNP alone, only once in complex with each other. Once in the complex, the dissociation of the two parts was slowed fourfold. This observed interaction was further probed by 1D and 2D NMR where chemical shift changes and line broadening were seen which indicated the residues with which the compound was interacting. This allowed a computational model of the binding site of **1.31** to be obtained once superimposed on the published crystal structure of U1 snRNP (Figure 30b).

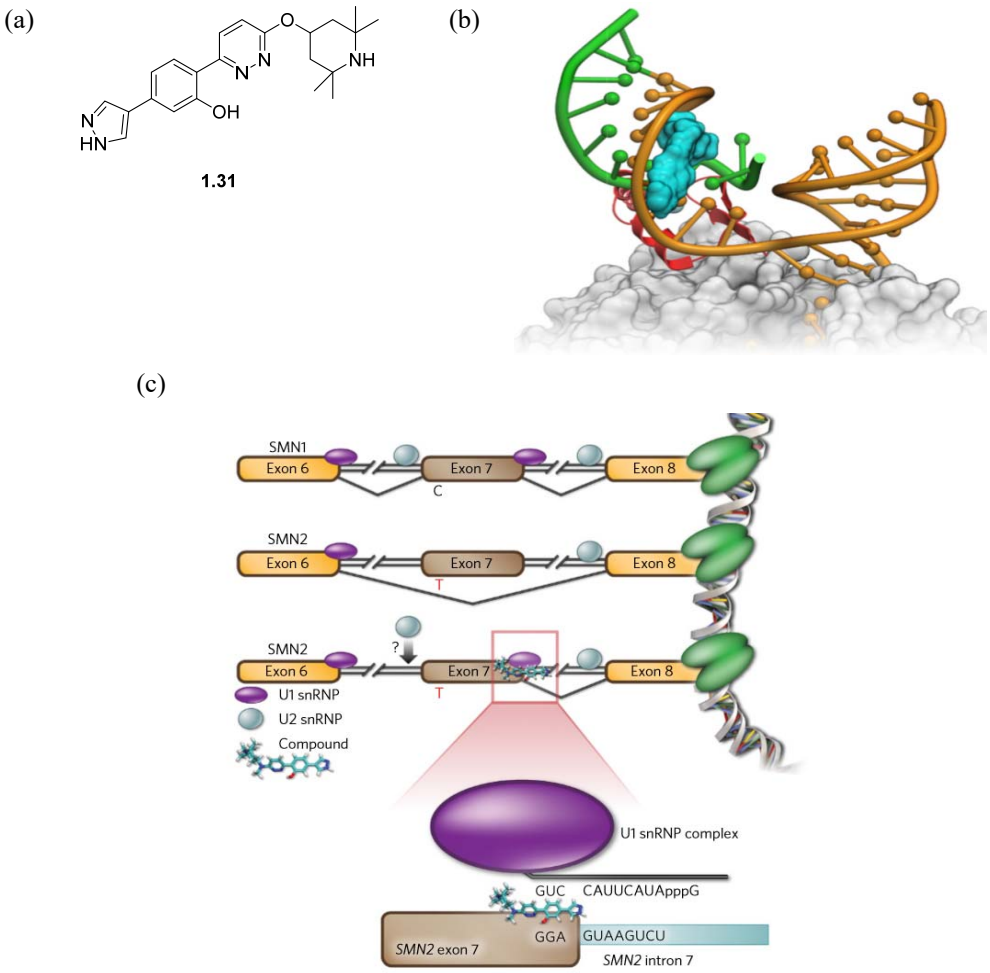

Figure 30. (a) Structure of small molecule published by Novartis for the treatment of SMA. (b) Small molecule docking site based on NMR data and known crystal structure of U1 snRNP. (c) Schematic of mechanism of action of **1.31**.[92]

Currently both Roche/PTC Pharmaceuticals (NCT02908685, NCT02913482 and NCT03032172) and Novartis (NCT02268552) have small molecules based on the structures shown in Figure 29 and Figure 30 in Phase I and Phase II clinical trials for the treatment of SMA.[93–96]

Unlike traditional protein drug targets, targeting pre-mRNA with antisense oligonucleotides or small molecules in the attempt to control disease is still a very new avenue of study. Not enough is known about disease targets and understanding how to manipulate and control pre-mRNA splicing is the key to any success using these types of therapeutics.

1.7 Bcl-2 and its Role in Apoptosis

The Bcl-2 protein family consists of 25 genes, to date, that are key regulators of programmed cell death (apoptosis) and produce antagonistic splicing variants in humans (termed anti- and pro-apoptotic isoforms).[97] Bcl-2 genes are characterised by their Bcl-2 homology (BH) domains

(BH1, 2, 3 and 4). These domains are critical for their function and determine whether they are anti- or pro-apoptotic (Figure 31a). A large number of pro-apoptotic genes only contain the BH3 domain and these can regulate apoptosis by multiple different pathways.[97]

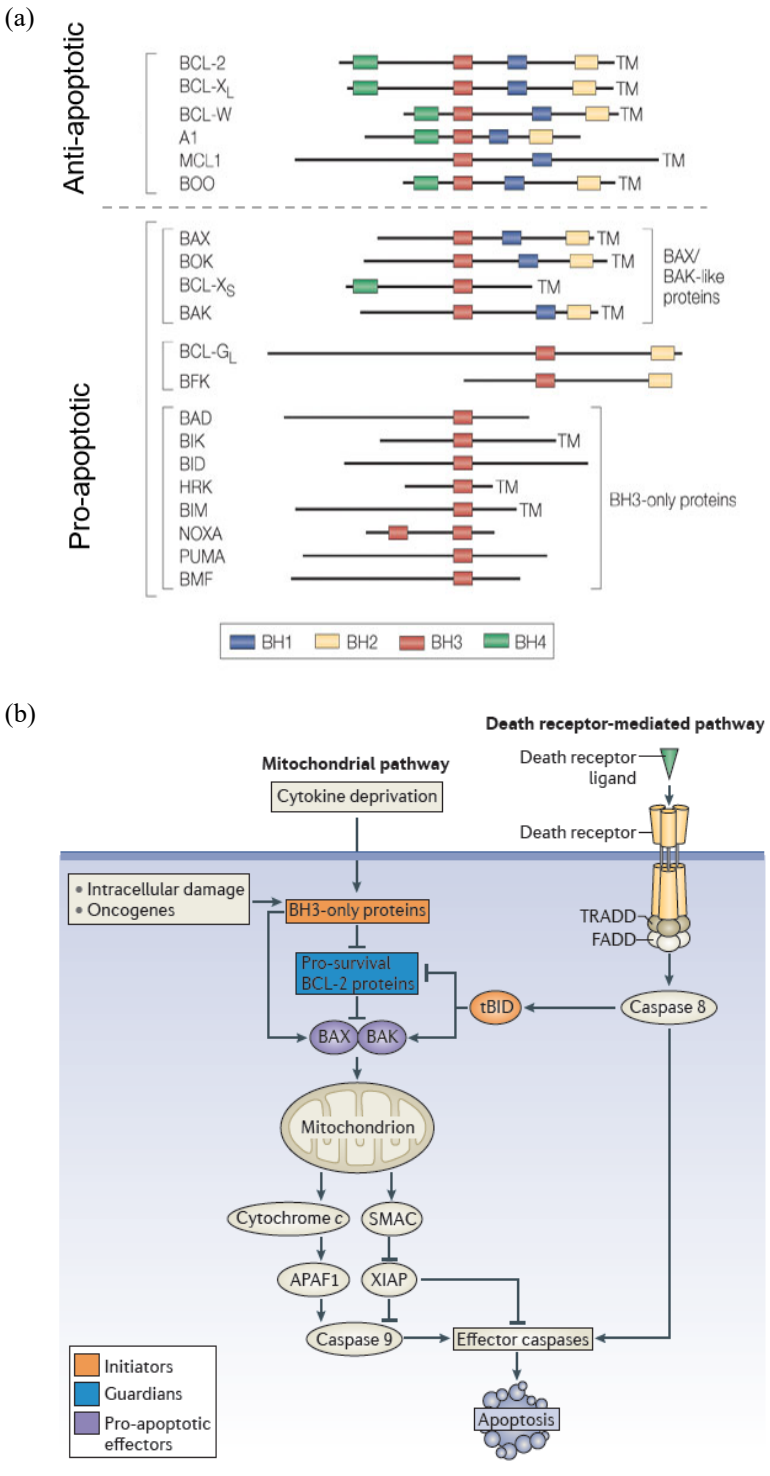

Figure 31. (a) Classification of the Bcl-2 family of proteins based on domain organization.[98] (b) Apoptotic pathway regulated by Bcl-2 proteins.[99]

There are several different proposals as to how the proteins in the Bcl-2 family express their pro- or anti-apoptotic effect on cells. Generally it is agreed that the activation of caspases (enzymes that regulate apoptotic signals within the cell)[100] must take place by Bcl-2 proteins.[99] Pro-apoptotic proteins, such as BAX or BAK, dimerize which leads to the formation of a permeability transition pore on the outer mitochondria membrane (OMM). How this dimerization process is initiated is still debated. One report states that anti-apoptotic proteins are able to block dimerization and PT pore formation by sequestering pro-apoptotic proteins.[101] While a second paper suggests BH3-only proteins such as BAD can heterodimerize with Bcl-2 and become membrane bound which allows them to exert their pro-apoptotic ability.[102] Nonetheless, the balance between pro- and anti-apoptotic proteins within the cell is critical. Once a pore opens up, cytochrome C is realised from the mitochondria into the cytosol which in turn recruits and activates APAF1 protein and caspase 9. Caspase 9 then cleaves further caspases, known as effector caspases, which execute apoptosis and organise the cell for death (Figure 31b).[101] As the dimerization of Bcl-2 proteins and the role they play in apoptosis is still not fully understood, greater understanding of this fast expanding class of proteins is needed to effectively target and manipulate programmed cell death for therapeutic purposes.[101]

1.8 Alternative Splicing of Bcl-x

The gene Bcl-x, which belongs to the Bcl-2 family of proteins, can be alternatively spliced into two mRNAs, resulting in the production of two antagonistic protein isoforms after translation.[103] Bcl-xL is the longer protein isoform (241 amino acids in length) which contains all four BH domains and inhibits apoptosis of cells, whereas the shorter isoform Bcl-xS (178 amino acids in length) induces apoptosis and only contains BH3 and 4. Bcl-xL is overexpressed in many cancer cell lines including small lung carcinoma, prostate tumours and breast cancer.[104] The alternative splicing pattern observed in Bcl-x is due to two possible 5′ splice sites available in the pre-mRNA. The upstream splice site encodes for the pro-apoptotic isoform, whilst the downstream site produces the anti-apoptotic protein isoform, as demonstrated in Figure 32. The xS/xL ratio is important in the determination of the fate of the cell. A high xS/xL ratio favours a pro-apoptotic outcome, whereas a low xS/xL ratio results in an anti-apoptotic outcome.

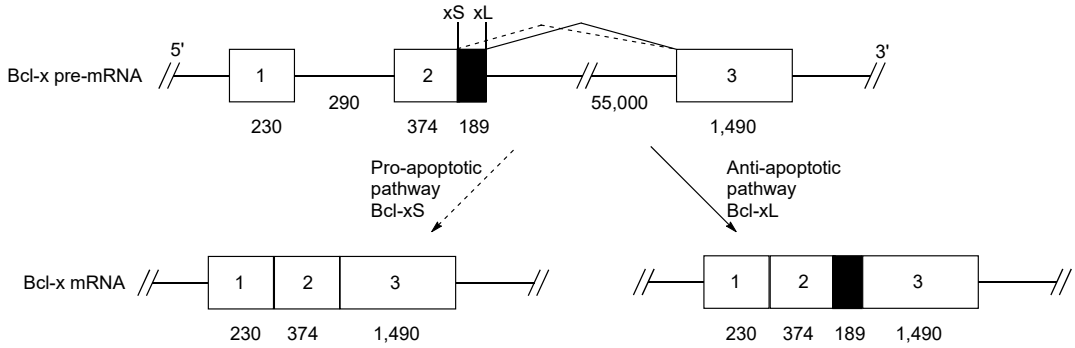

Figure 32. Schematic representation of the length of the wild type Bcl-x (top) and the two splicing isomers Bcl-xS and Bcl-xL (bottom). Length of each exon and intron is indicated by numbers below. xL and xS splice sites are labelled above the diagram with the two possible Bcl-x splicing patterns shown by the black and dotted lines above the diagram.

Exogenous control of the splicing outcomes of Bcl-x would be highly advantageous to increase apoptosis of cancer cells. This has been attempted with the use of ASOs which were designed to target and bind areas around the Bcl-xL splice site. Initially, a palette of 20-mer phosphorothioate 2′MOE modified ASOs were tested for their ability to increase Bcl-xS.[105] The best ASO was found to be ISIS 22783 (5′-CTGGATCCAAGGCTCTAGGT-3′) which binds 15 nucleotides upstream of the Bcl-xL splice site. It was demonstrated that treatment of A549 cells with 100 nM ISIS 22783 induced the formation of Bcl-xS and deceased the formation of Bcl-xL as shown in Figure 33.

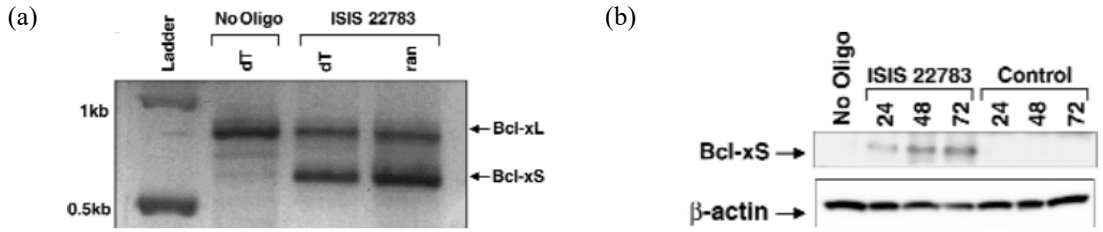

Figure 33. (a) RT-PCR analysis of A549 cells treated with 100 nM ISIS 22783. (b) Western blot assays showing levels of Bcl-xS 25, 48 and 72 hr after treatment of A549 cells with 100 nM ISIS 22783.[105]

The change in levels of the spliced RNA isoforms was also reported at the protein level. Western blot assays demonstrated that xL protein levels were decreased by 50 % 24 hours after ISIS 22783 treatment while xS protein levels were visible 10 hours after treatment and this increased continued till 72 hours after treatment. Although these results were initially promising, there has not been much investigation into other ways to control Bcl-x using other ASOs or small molecules. Very little is known about the structure of the pre-mRNA which makes targeting it difficult.

1.9 Investigating the Structure of Bcl-x Using the Model Construct Bcl-x-681

The intron between exon 2 and 3 in wild type Bcl-x pre-mRNA contains 55,000 nt which creates a system that is too long is study effectively *in vitro*. Therefore, a functional splicing construct was designed to investigate the structure of Bcl-x which would allow therapeutic targeting of this RNA. This shortened transcript preserved the sequence between the xS and xL 5′ ss but reduced the size of the intron from 55,000 nt to 241 nt and the size of exon 3 from 1,490 to 99. This transcript was termed Bcl-x-681 (Figure 34). In splicing assays this construct was found to splice as the wild type, with Bcl-xL still being the preferred isoform.[106]

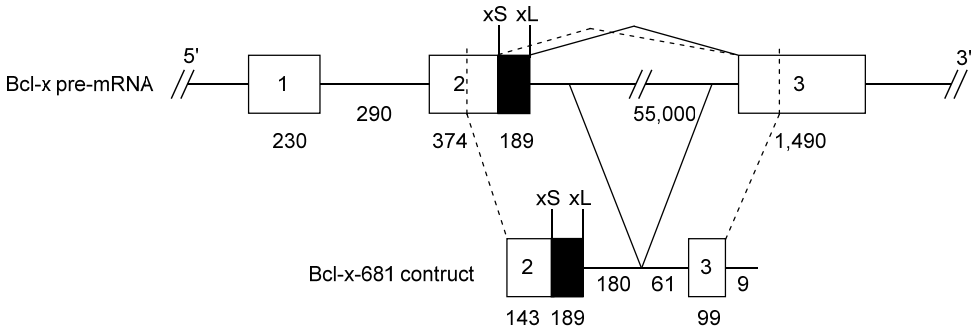

Figure 34. Schematic representation of the length of the wild type Bcl-x (top) and the functional transcript Bcl-x-681 (bottom). Length of each exon and intron is indicated by numbers below. Where the wild type RNA has been cut is represented by the black and dotted lines between the two structures.

Recently, the structure of Bcl-x-681 has been mapped by the process of RNA footprinting (Figure 35).[106] The structure is split into 4 defined areas, namely the 5′ xL splice site, the 5′ xS splice site, the intron and the 3′ splice site.

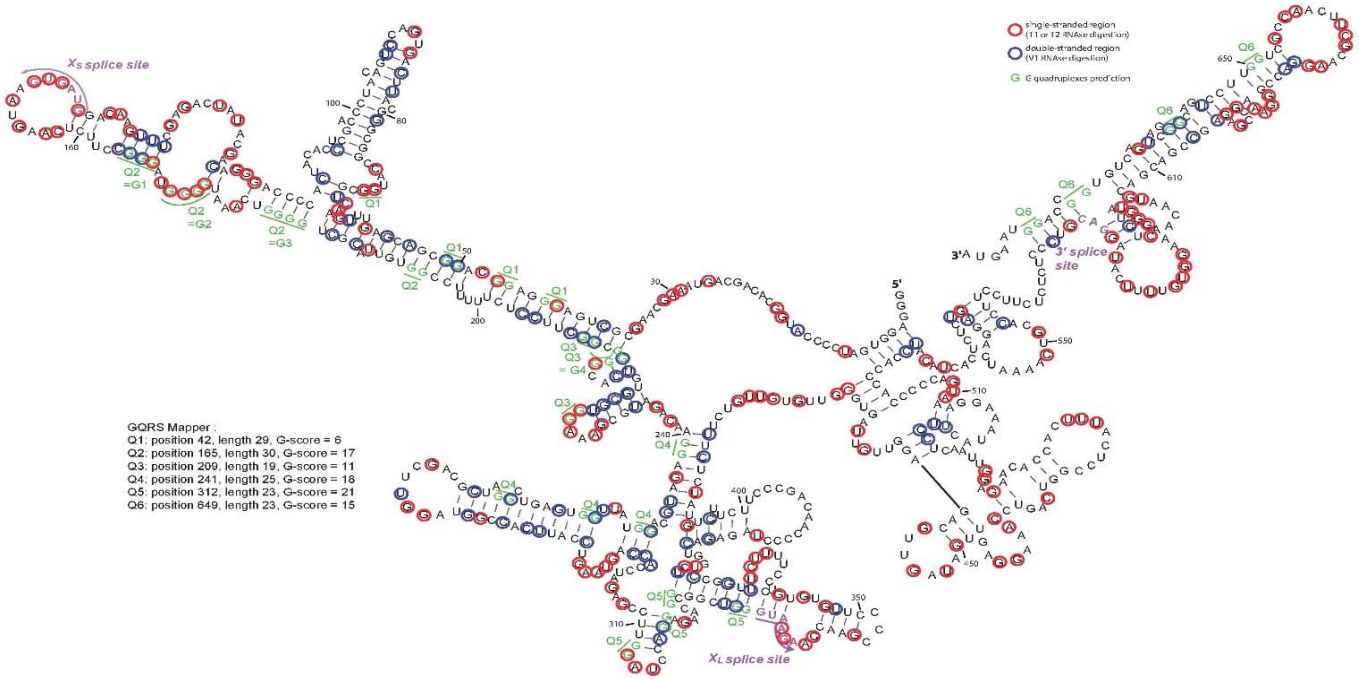

Figure 35. Structure of Bcl-x-681 as proposed by RNA footprinting.[106]

Bioinformatic analysis identified 6 possible sequences in the pre-mRNA that were predicted to form secondary RNA structures such as G-quadruplexes.[107] Each sequence was represented by a 'G-score' which denoted how likely the sequence would be able to form a G-quadruplex under physiological conditions (Table 2). The G-score is assigned according to three principles;

- The length of the loops
- Whether the loops are of similar length
- The number of potential G-quartets that could form

Table 2. Bioinformatic analysis of Bcl-x-681 showing possible G-quadruplex forming structures. The guanine groups which form the G-quartets are underlined.

Sequence Name	Nucleotide Start Position	Length	Sequence	G-score
Q1	42	29	GGGAGGCAGGCGACGAGUUUGAACUGCGG	6
Q2	165	30	GGGAUGGGGUAAACUGGGGUCGCAUUGUGG	17
Q3	209	19	GGCGGGGCACUGUGCGUGG	11
Q4	241	25	GGAGAUGCAGGUAUUGGUGAGUCGG	18
Q5	312	23	GGAUCCAGGAGAACGGCGGCUGG	21
Q6	649	23	GGUUCCUGACGGCAUGACUGUGGCCAGG	15

A G-score increases if the length of the loops are short and all loops are of similar size. More G-quartets also contributes to a higher G-score. Therefore, the higher the predicted G-score, the more likely the sequence is to form a stable G4.

Following this, mutational analysis of the sequence was conducted to see if these G4s formed and how important they were to the overall structure. The formation of G4s requires a stable H-bond network between the G-quartets in the form of Hoogsteen base pairs. If each guanine (**1.1**) is mutated for 7-deazaguanine (**1.32**), this will stop any G4 formation due to the absence of Hoogsteen base pairs.[108] However, the Watson-Crick base pairing face is not disturbed which allows the formation of stem loops.

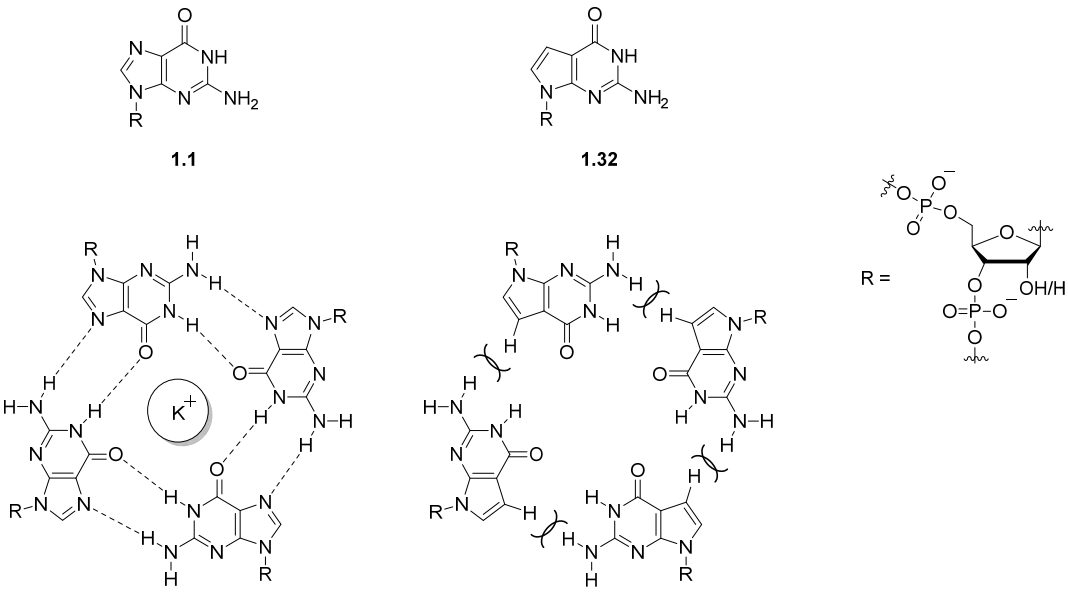

Figure 36. Representation of guanine and a G-quartet using Hoogsteen base pairing and 7-deazaguanine (**1.32**) and the lack of Hoogsteen base pairing that takes place.

7-deazaguanine (**1.32**) mapping was carried out in the Bcl-x-681 construct, which allowed information to be gathered on whether single or double stranded RNA was present throughout the structure with the use of RNAses. T1 and T2 RNAses are capable of cleaving single stranded areas of RNA, whereas V1 RNAse can only cleave double stranded sections. When these digests were compared to the footprint gathered without 7-deazaguanine mutations, it was possible to see which areas were protected from RNAses due to G4 formation. It was found that these regions were mainly located around both 5′ splice sites in the Q2 and Q5 regions discovered during bioinformatic analysis. RNAse H cleavage assays were then performed on both the native and mutated RNA, and areas within the RNA were designated either protected or accessible to the RNAse H depending on the amount of cleavage observed (< 40% cleavage = protected, > 60% cleavage = accessible). Again it was found that the sequences around both 5′ splice sites were mostly protected suggesting formation of G4 structures.[106]

1.10 Splice Switching Small Molecules of Bcl-x Targeting G4 pre-mRNA

As analysis of the structure of the Bcl-x pre-mRNA suggested the formation of putative G4 forming sequences around both the xL and xS 5′ ss, it was hypothesised that stabilisation of one, or both of these, could induce a change in the splicing ratio seen in Bcl-x. Collaborative work between Professor Ian Eperon, Dr Cyril Dominguez and Professor Glenn Burley focussed on identifying G4 stabilising ligands that could induce a splicing change in Bcl-x towards the greater formation of the pro-apoptotic isoform Bcl-xS. *In vitro* splicing assays were carried out using two

established DNA G4 stabilisers Pyridostatin[30,109] (**1.16**) and Quarfloxin[110] (**1.33**), however they did not alter the splicing pattern of Bcl-x towards the increased production of Bcl-xS.[111] Two porphyrins were then tested **1.34** and **1.21**. A slight increase in the amount of the Bcl-xS isoform was observed with TMPyP4 (**1.21**). At 5 μM and 10 μM an approximately 2-fold increase in the amount of Bcl-xS was seen, however splice switching ability was shut down once the concentration of TMPyP4 (**1.21**) reached 25 μM. Conversely, the larger porphyrin system, Zn-DIGP (**1.34**) did not switch the splicing pattern of Bcl-x towards Bcl-xS.

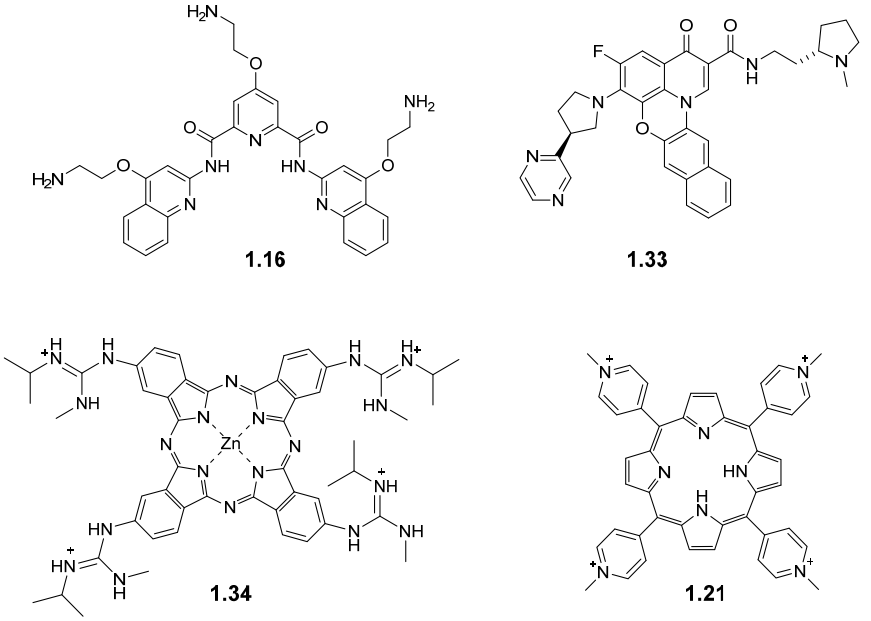

Figure 37. Structure of Pyridostatin (**1.16**), Quarfloxin (**1.33**), Zn-DIGP (**1.34**) and TmPyP4 (**1.21**).

Quindolines GSA-0902 (**1.35**) and GSA-0820 (**1.36**) have been previously shown to stabilize G4 structures.[112] In Bcl-x splicing assays both **1.35** and **1.36** decreased the xS/xL ratio by lowering the Bcl-xS product while not altering the Bcl-xL product. Changes to the splicing pattern were not dose dependent as the same results were obtained at of 10 and 40 μM for both compounds.

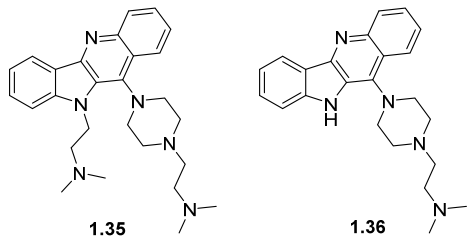

Figure 38. Structure of GSA-0902 (**1.35**) and GSA-0820 (**1.36**).

A library of ellipticines were subsequently tested in the *in vitro* splicing assays as they have been previously shown to stabilise G4s in the nuclease hypersensitive element (NHE) of both the

c-Myc proto-oncogene and the platelet-derived growth factor receptor β (PDGFR-β) signalling pathway.[41,113,114] When tested against Bcl-x it was found compounds **1.41** and **1.42** did not change the normal splicing ratios of Bcl-x, however, compounds **1.37** – **1.40** displayed a significant change towards the utilization of the Bcl- xS splice site. This lead to an increase in the xS/xL splicing ratio.

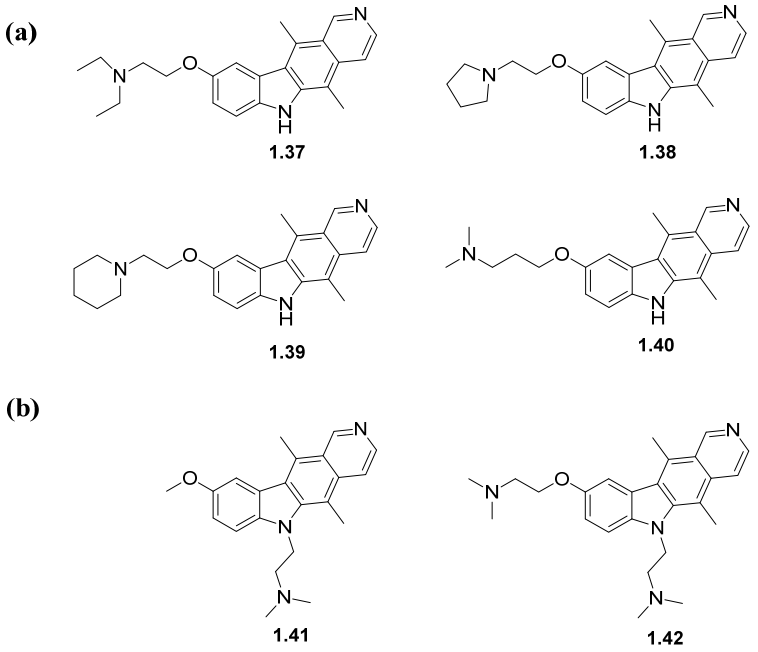

Figure 39. GQC-05 derivatives that have been tested in Bcl-x splicing assays. (a) Compounds that had a similar effect to GQC-05, increase in Bcl-xS isoform and decrease in Bcl-xL isoform **1.37** – **1.40**. (b) Compounds that had no effect on ratio of splicing isoforms **1.41** and **1.42**.

GQC-05 (**1.20**) displayed the best modulation of the splicing isoforms. The addition of 10 μM GQC-05 (**1.20**) resulted in the decrease of the amount of Bcl-xL, while Bcl-xS was increased. This result was observed in a concentration dependent manner to a maximum of 40 μM (Figure 40).

(a)

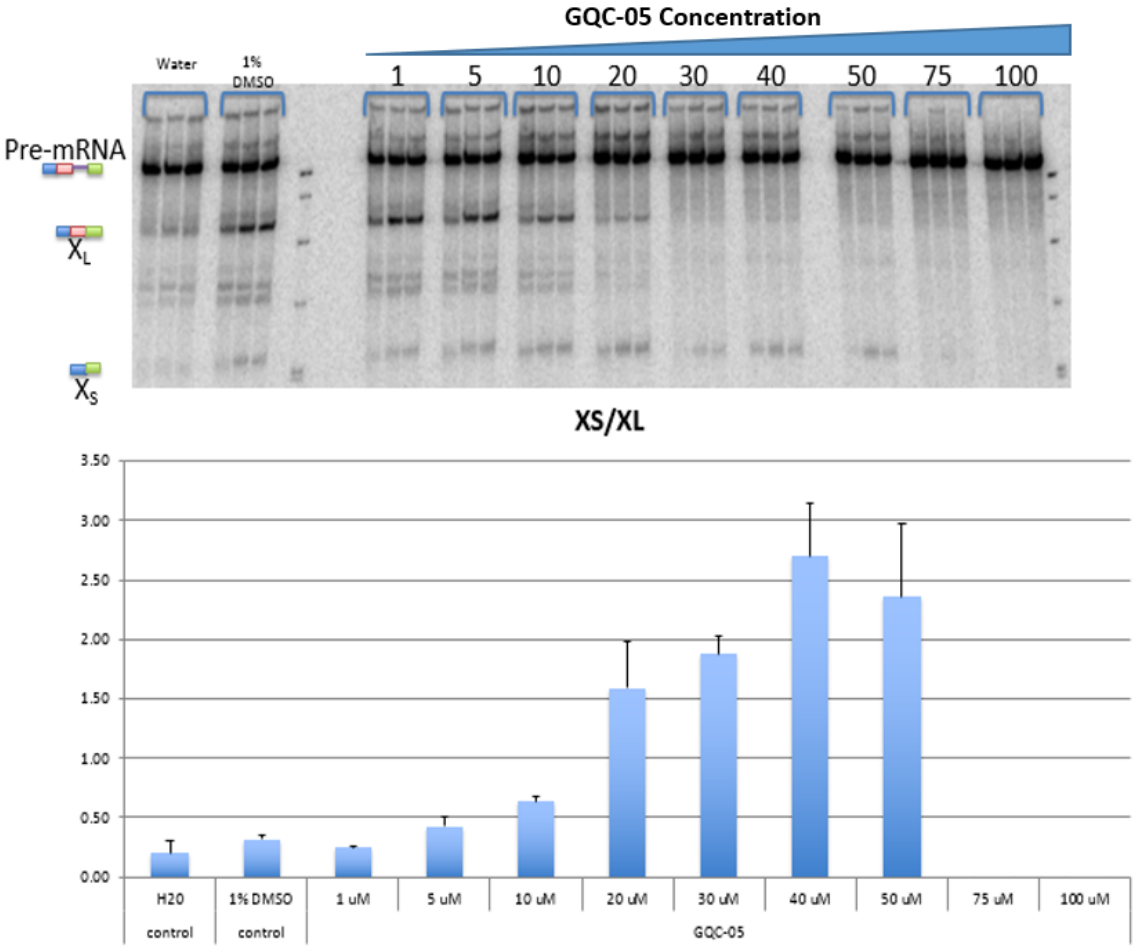

(b)

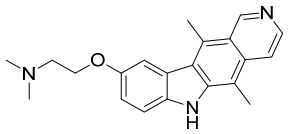

1.20

Figure 40. (a) *In vitro* splicing assay as a function of increasing [GQC-05] and results from the *in vitro* splicing assay plotted as a graph of X_S/X_L ratio *vs.* [GQC-05].[115] (b) Structure of GQC-05 (**1.20**)

HeLa cells were then treated with 10 μM GQC-05 (**1.20**) for 4 hours before the RNA was isolated and amplified by RT-PCR. Figure 41 shows a clear increase in the pro-apoptotic xS isoform and decrease in the anti-apoptotic isoform xL when treatment was carried out.

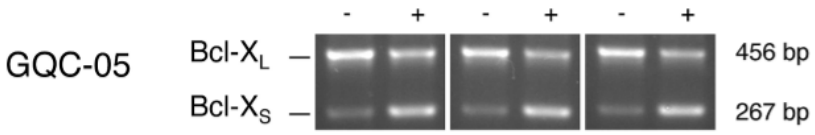

Figure 41. Agarose gel showing Bcl-xL and Bcl-xS bands associated with amplified RNA from HeLa cells treated with 10 μM GQC-05 (+) and without (-) GQC-05.[111]

As previously mentioned, the pre-mRNA of Bcl-x is very G-rich and contains multiple G-tracts that are hypothesized to form G4s under physiological conditions. It could be imagined that planar aromatic compounds such as GQC-05 (**1.20**) could be intercalating into the G-quartets or end-stacking onto the top of the G-quartets and the amino ethoxy tail of the C9 position could be interacting with the phosphate backbone to help stabilise the G4 structure.

1.11 Limitations of Current Approaches to Modulate Bcl-x Splicing.

Although Bcl-x has been known to be a member of the Bcl-2 apoptotic gene family for many years and that Bcl-xL is over expressed in multiple types of cancer, very little has been done to actively target Bcl-x to treat cancer. It is only recently that the structure of Bcl-x has been suggested and still, it is not known exactly what structures this dynamic RNA sequence could adopt and whether certain secondary structures could possibly control the xS/xL outcome. This makes selectively targeting Bcl-x with small molecules very difficult.

Initial SAR work by Eperon *et al.* has been conducted with a series of G4 stabilising molecules to determine their ability to modulate the splicing of Bcl-x towards the production of Bcl-xS.[111] G4 stabilising ligands were chosen after mutation experiments carried out on Bcl-x-681 suggested that G4s may be present close to the alternative 5′ splice sites and that the stabilisation of these may be what increases the production of Bcl-xS. However, further work is required to fully appreciate the interactions of ligands such as GQC-05 with Bcl-x, and whether this is a direct or indirect process during alternative splicing.

1.12 Hypothesis

It has been previously shown that small molecules are able to interrupt gene regulation which can lead to the apoptosis of cancerous cells.[9] Previous work has found that the ellipticine derivative GQC-05 (**1.20**) is able to alter the alternative splicing pattern of the oncogene Bcl-x, however it is not known how **1.20** induces this change. The pre-mRNA of Bcl-x is G-rich (Section 1.9, Figure 35) and could have the possibility of forming multiple G-quadruplexes *in vivo*. As **1.20** has been previously shown to stabilise DNA G-quadruplexes, it is hypothesised that the mode of action is *via* the stabilization of a select subset of G4s in Bcl-x. In doing so, **1.20** could either sequester or promote the utilization of a splice site, resulting in the observed splice switching activity (Figure 42).

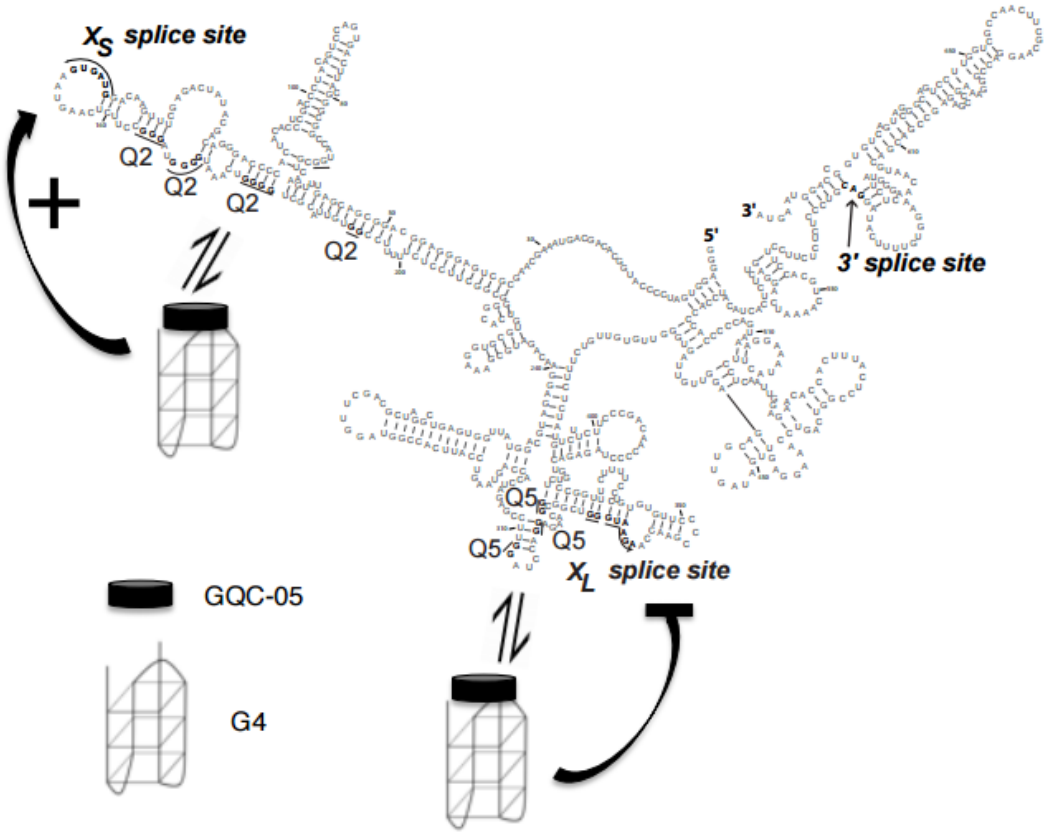

Figure 42. Possible mode of action of GQC-05 (**1.20**) on the competing xS and xL splice sites in pre-mRNA Bcl-x.[111]

2 Thesis Aims

The main objective of this PhD project is to characterise the mode of action of GQC-05 (**1.20**) on the splicing behaviour of the oncogene Bcl-x. This will be carried out by the design of a library of GQC-05 derivatives which can be used in SAR analysis. The specific aims of the project are to:

(i) Establish a modular and convergent synthetic route to access the desired ellipticine analogues.

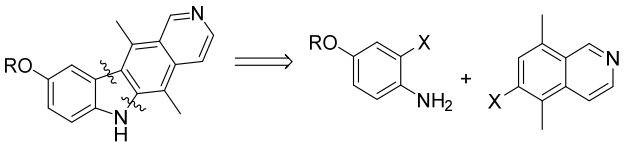

(ii) Develop an SAR profile of ellipticine analogues for use in *in vitro* Bcl-x splicing assays.

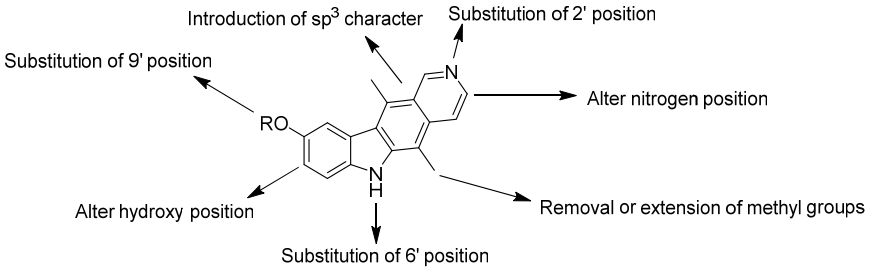

(iii) Determine the mode of binding of GQC-05 and related analogues to Bcl-x through NMR and UV melting assays.

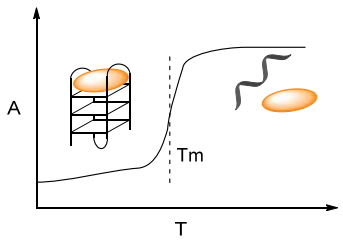

(iv) Determine the selectivity of the ellipticine analogues for other possible competing DNA structures using FRET melting assays.

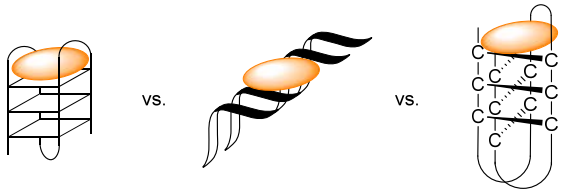

Chapter 2

Literature Routes Towards Ellipticine and Analogues

3 Ellipticine Natural Products

Ellipticine (**2.5**) was first isolated in 1959 from the *Ochrosia elliptica* tree by Goodman while the first total chemical synthesis was published by R. B. Woodward later that year.[116] Woodward's first synthesis produced **2.5** in 2 % yield over 3 steps (Scheme 1).[117] In the subsequent decades more than 30 new synthetic routes to ellipticine natural products and analogues thereof have been described, including 9-hydroxy- (**2.6**) and 9-methoxyellipticne (**2.7**), isoellipticine (**2.8**) and olivacine (**2.9**).[116] The synthetic routes are generally grouped into four major classes according to the last ring to be formed in the synthetic procedure *i.e.,* B-type, C-type, D-type or [B+C]-type. Early synthetic strategies focussed on B- or C-type routes. These required harsh conditions, often suffered from low yields and lacked the possibility to diversify the ellipticine structure. [B+C]-type routes are generally employed to produce ellipticine analogues such as 5-deazaellipticine (**2.10**).[116] More recently there have been a number of routes published which focus on the development of flexible synthetic methodologies to prepare ellipticine analogues and which can later be employed in medicinal chemistry and chemical biology applications.[118–120]

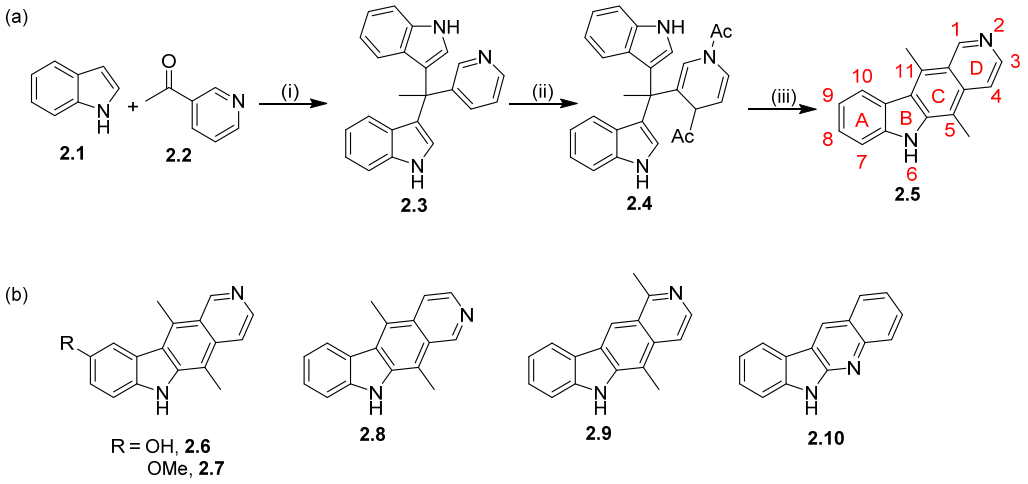

Scheme 1. (a) First total synthesis of Ellipticine (**2.5**) as proposed by Woodward.[117] Reagents and conditions: (i) CH_3COOH, $ZnCl_2$, (ii) Zn, Ac_2O, reflux, (iii) 200 °C. (b) Structure of 9-hydroxyellipticine (**2.6**), 9-methoxyellipticine (**2.7**), isoellipticine (**2.8**), olivacine (**2.9**), and 5-deazaellipticine (**2.10**).

Ellipticine and derivatives have been of interest to researchers since 1967 when Dalton *et al.* showed ellipticine (**2.5**) and 9-methoxyellipticine (**2.7**) displayed cytotoxicity in mice and human cells.[121] In the 1980s 9-methoxyellipticine (**2.7**) entered into early clinical trials for treatment of acute myeloid leukaemia,[122] however it was quickly withdrawn due to solubility issues.[123] To combat this, the pyridine nitrogen in the D-ring was methylated and the acetate salt was tested, 9-hydroxy-*N*-methylellipticinium acetate (Celiptium) (**2.11**).[116] Compound **2.11** showed positive results when tested by patients with advanced metastatic breast cancer. Remission was observed

in 25 % of patients for 18 months at a dose of 80-100 mg/m^2 per week for four weeks, however nephrotoxicity was observed and therefore the compound did not enter into further clinical trials.[124] Due to this early success, several other ellipticine derivatives entered clinical trials such as 2-(diethylamino-2-ethyl)-9-hydroxyellipticinium chloride (Datelliptium) (**2.12**). Compound **2.12** also showed a positive response against advanced metastatic breast cancer at a dose of 150 mg^{-2}/day for 5 days every 3 weeks, with the added benefit of a much reduced toxicity compared to **2.11**.[123]

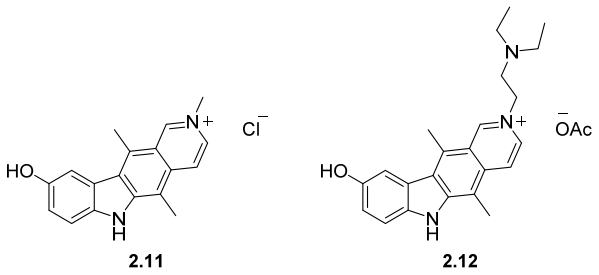

Figure 43. Structures of 9-hydroxy-*N*-methylellipticinium acetate (Celiptium) (**2.11**) and 2-(diethylamino-2-ethyl)-9-hydroxyellipticinium chloride (Datelliptium) (**2.12**).

The cytotoxicity of ellipticine (**2.5**) has been demonstrated in a large number of cancer cell lines as shown in Table 3.

Table 3. Cytotoxicity of ellipticine (**2.5**) in multiple human cancer cell lines.[125]

Cancer Cells Lines Tested	IC_{50} (µM)
Breast adenocarcinoma MCF-7	1.25±0.13
Leukemia HL-60	0.67±0.06
Leukemia CCRF-CEM	4.70±0.48
Neuroblastoma IMF-32	0.27±0.02
Neuroblastoma UKF-NB-3	0.44±0.03
Neuroblastoma UKF-NB-4	0.49±0.04
Glioblastoma U87MG	1.48±0.62

The mode of action of ellipticine and related alkaloid derivatives has been widely studied; they have been shown to disrupt multiple different processes within the cell which account for their antitumor effects.

3.1 Ellipticine Cytotoxicity: Mechanisms of Action

Ellipticine (**2.5**) and its derivatives exhibit multiple modes of action which lead to its potent antitumor properties, these include topoisomerase II inhibition, kinase inhibition and DNA intercalation.[126]

3.1.1 Ellipticine•DNA Intercalation

An intercalator is a small molecule that binds between the planar DNA base pairs.[126,127] These small molecules tend to be planar, aromatic, and hydrophobic in nature; good examples include doxorubicin (**2.13**),[127–129] ethidium bromide (**2.14**),[130,131] and thalidomide (**2.15**).[132] Unwinding of the dsDNA occurs when intercalation takes place. This can then lead to further structural changes of the dsDNA including strand lengthening and base pair twisting. Disruption of important biological processes can occur including inhibition of transcription, replication, and the DNA repair processes, as a result most DNA intercalators are mutagens.[126]

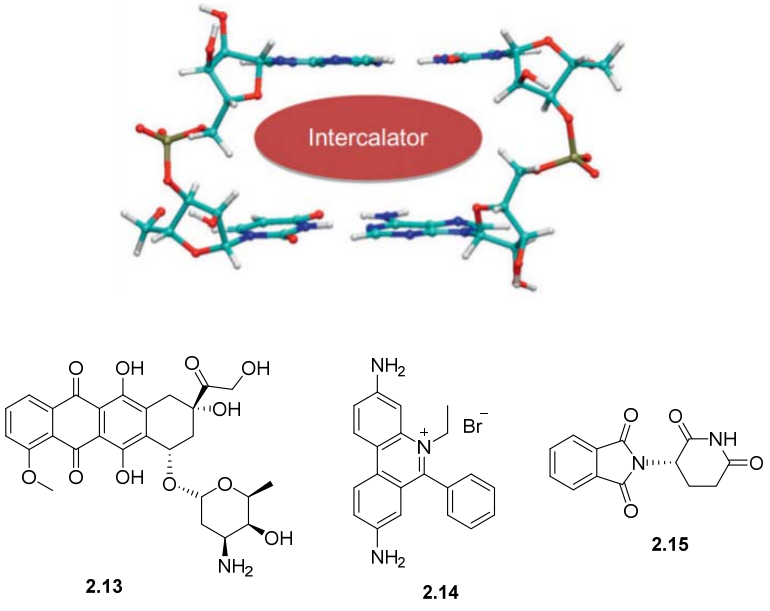

Figure 44. (a) Schematic representation of intercalation of small molecule between base pairs.[126] (b) Examples of intercalators.

Intercalators change several properties of dsDNA when bound, including the viscosity, CD spectrum, and UV absorption. Kohn *et al.*[133] studied the change in viscosity and sedimentation rate of calf thymus DNA in the presences of ellipticine (**2.5**). The results from **2.5** were compared to those from the known intercalator proflavin, and an increase in viscosity and decrease in sedimentation was observed, consistent with DNA intercalation. The degree of DNA unwinding

was determined to be 7.9 ° relative to the control compound ethidium which displayed an unwinding of 12 °. It was later found that ethidium unwinding was underestimated,[134,135] which in turn means the degree of DNA unwinding caused by **2.5** was also underestimated.

Initially, ellipticine (**2.5**) was identified as a DNA intercalator with DNA binding constants of 8.3 × 10^5 M^{-1} (pH 5) and 3.3 × 10^5 M^{-1} (pH 9), and a preference for intercalation between G-C base pairs.[116] Canals *et al.*[136] published a crystal structure of **2.5** in complex with a 6-mer oligonucleotide with the sequence d(CGATCG)$_2$. In this 6-mer duplex, two molecules of ellipticine complex within the structure at the two C-G base pairs, leaving the A-T base pair free (Figure 45).

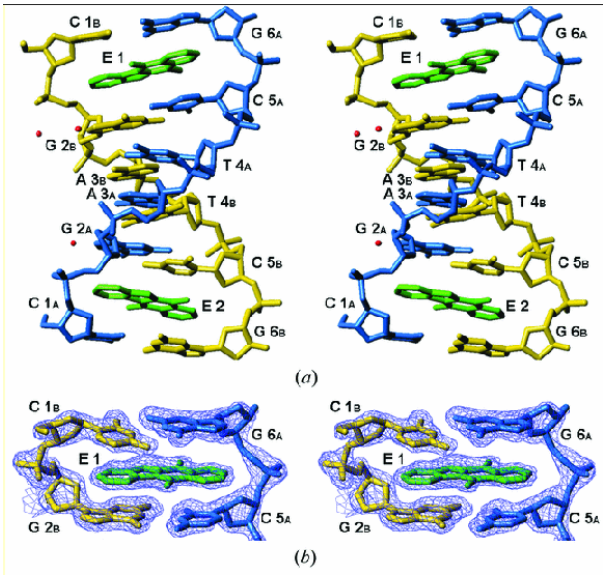

Figure 45. Crystal structure of ellipticine (**2.5**) intercalation into d(CGATCG)$_2$, 1.5 Å resolution (PDB id 1Z3F).[136]

3.1.2 Topoisomerase Inhibition

Topoisomerase I and II are enzymes that are responsible for single and double strand breaks in DNA, respectively.[126] They control the topology of DNA during nearly every DNA process within the cell to prevent positive and negative supercoiling. Once the strand break has been made, the DNA sequence are remodelled and the DNA ends are joined back together by the enzyme.[137] Small molecules such as ellipticine (**2.5**) and doxorubicin (**2.13**) can inhibit topoisomerase II.[138,139] Inhibitors such as ellipticine intercalate within the DNA strand and inhibit the ligation step leading to an increase in the amount of DNA strand breaks which ultimately leads to cell apoptosis. This form of DNA damage is considered one of the most important mechanisms which leads to ellipticine cytotoxicity.[140]

3.1.3 Biooxidation of Ellipticine

The oxidation of ellipticine (**2.5**) by human cytochrome P450 enzymes (CYPs) leads to the formation of several important ellipticine metabolites, namely 12- and 13-hydroxyellipticine (**2.22** and **2.23**). These metabolites are able to crosslink with DNA strands through the N7 of guanine to produce **2.18** and **2.25** as shown in Figure 46.[141,142]

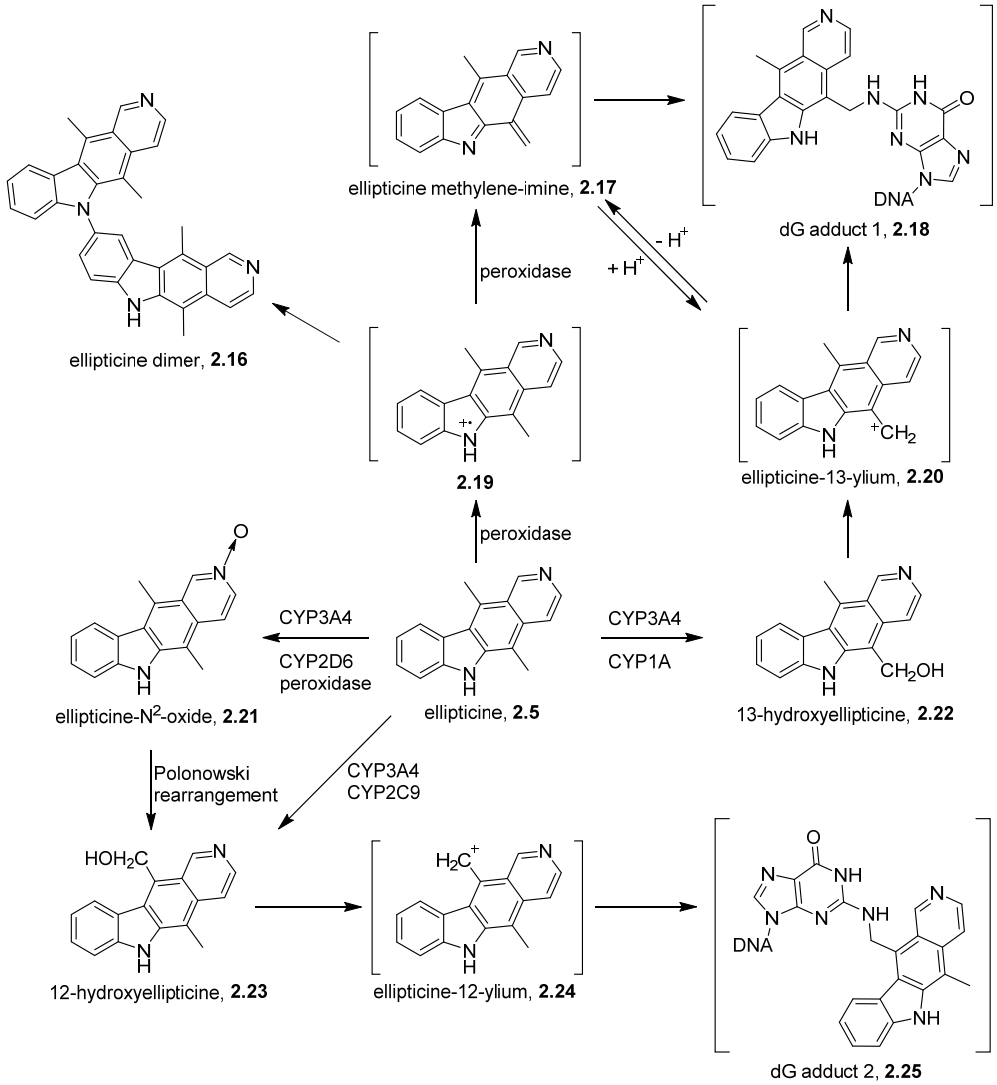

Figure 46. Mechanism of ellipticine adduct formation by peroxidases and human cytochrome P450 enzymes.[141]

Peroxidases (*e.g.*, human myeloperoxidase, bovine lactoperoxidase and horseradish peroxidase) were also able to form ellipticine adducts *via* oxidative pathways, including the ellipticine dimer **2.16**.[143] Extensive work has been carried out to see whether the formation of these ellipticine-DNA adducts is responsible for the cytotoxicity seen in cells however, to date there has not been any conclusive evidence correlating the mechanism of adduct formation with cytotoxicity.

Nevertheless, it has been suggested that this mechanism could partially explain the tumour specificity exhibited by ellipticine, as CYPs are only expressed in some tissues, e.g., breast, colon, prostate, liver, kidney and lung.[125]

3.1.4 c-Kit Kinase Inhibition

Ellipticine (**2.5**) has been shown to disrupt many different processes that affect the cell cycle. One example of this is c-Kit kinase inhibition. Cellular processes such as proliferation, differentiation, metabolism and survival are controlled by many cell surface receptors such as c-Kit kinase. Mutations in c-Kit kinase have been connected to several types of cancer in humans. In 2005[144] it was found that 9-hydroxyellipticine (**2.6**) efficiently inhibited wild-type and mutated (D816V) c-Kit kinase with an IC_{50} value of 0.4 μM while 9-methoxyellipticine (**2.7**) demonstrated an IC_{50} of 0.8 μM (WT) and 0.6 μM (D816V). This was compared to >10 μM for ellipticine (**2.5**). Docking studies demonstrated that the free hydroxyl group at C9 was important to binding and was involved in two H-bond interactions with neighbouring amino acids (lysine and glutamate). 9-methoxyellipticine (**2.7**) showed higher IC_{50} values as only one H-bond could be made (H-bond donation from lysine). The binding of ellipticine derivatives allowed the mutated enzyme to adopt a similar structural conformation as the wild-type enzyme allowing it to be active.

Ellipticine (**2.5**) and related derivatives have demonstrated their ability to be useful agents in cancer treatment due to their highly potent nature. However, the many modes of action that have been shown to date need to be fully understood before compounds can successfully advance through the clinic. High-throughput screening methods are the quickest way to find potential targets but for this to be possible, access to compounds needs to be quick and modular. Currently, most routes to ellipticine are linear, low yielding and do not easily allow structural diversification.

4 Aims of Chapter 2

A derivative of ellipticine, GQC-05 (**1.20**), had been shown to cause changes in the splicing of the known oncogene Bcl-x towards the pro-apoptotic isoform, Bcl-xS. To explore the mechanism of action of **1.20** a modular synthetic route to this ellipticine scaffold was required. The aim of this work was to survey existing synthetic routes towards this scaffold as highlighted in Figure 47.[145–149] Both C-type and D-type routes were explored to access 9-methoxyellipticine (**2.7**).

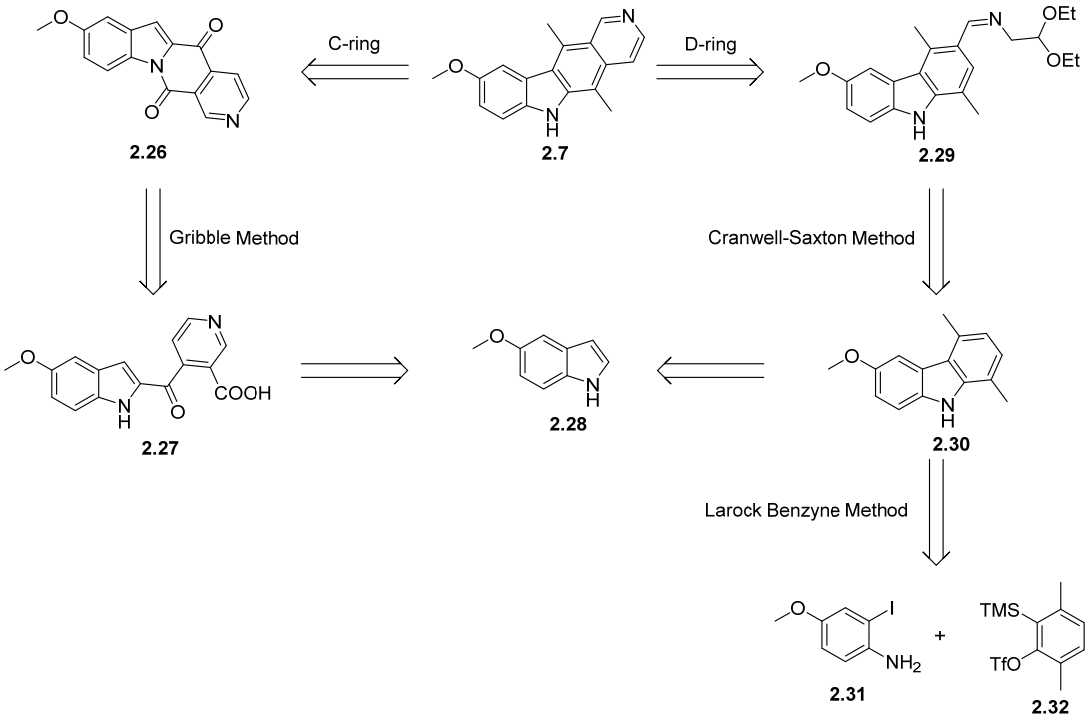

Figure 47. Routes explored towards the synthesis of 9-methoxyellipticine (**2.7**).[145–149]

5 Results and Discussion

5.1 Exploration of the Synthesis of Ellipticine using the Gribble Method

The synthetic route proposed by Gribble *et al.* was an early method which afforded 9-methoxyellipticine (**2.7**) in 47 % yield over 5 steps.[145] It involved the protection of 5-methoxy indole (**2.28**) with a sulfone before lithiation at the C-2 position and addition of 3,4-pyridinedicarboxylic anhydride to provide rings A, B and D of the ellipticine core (**2.34**). Deprotection of the indole before heating in Ac_2O afforded the ketolactam product (**2.26**). Conversion of the ketolactam into the final product **2.7** required treatment with methyllithium followed by reduction with $NaBH_4$ in EtOH.

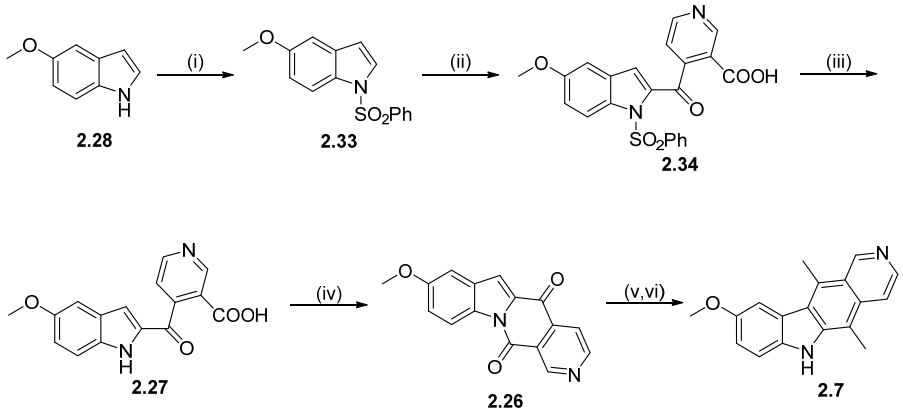

Scheme 2. Gribble's synthesis of 9-methoxyellipticine (**2.7**).[145] Reagents and conditions: (i) *n*-BuLi, $PhSO_2Cl$, -78 °C, 85 %. (ii) LDA, THF, -78 °C, 3,4-pyridinedicarboxylic anhydride, -100 °C, 76 %. (iii) K_2CO_3, $MeOH/H_2O$, reflux, quant. (iv) Ac_2O, 80-85 °C, 98 %. (v) MeLi, THF, -100 °C. (vi) $NaBH_4$, EtOH, reflux, 75 % (two steps).

This route was initially explored due to the high yield obtained for 9-methoxyellipticine (**2.7**). It was also envisaged that this route would be able to tolerate derivatisation of the A-ring without affecting the overall synthetic route. When this route was investigated 5-methoxy indole (**2.28**) was protected in a yield of 85 %. The addition of 3,4-pyridinedicarboxylic anhydride with **2.33** proceeded with 55 % yield of **2.34**. The subsequent sulfonyl deprotection was unsuccessful with the literature conditions stated, K_2CO_3 and $MeOH/H_2O$, and resulted in starting material being isolated. Harsher deprotection conditions were explored (NaOH). However, these conditions resulted in deprotection and loss of the D ring portion giving over 50 % of **2.28** after work-up.

5.2 Cranwell-Saxton Method

The Cranwell-Saxton method[146] has been extensively studied and iterative improvements have been described in recent years.[147,150,151] The initial route involved the formation of 1,4-dimethylcarbazole (**2.30**) from 5-methoxyindole (**2.28**) and 2,5-hexadione which was then formylated to give compound **2.35** (Scheme 3). This was then condensed and hydrogenated to give the amine followed by cyclisation under dry acidic conditions and dehydrogenation with Pd/C to furnish the desired ellipticine in 0.8 % over 5 steps. The formylation step was investigated by McCarthy in 2010[147] as they found that the original reaction conditions employed ($POCl_3$, DMF, TCE) produced < 30 % of the desired isomer **2.35**, with the main product usually being the *N*-formylated product. Several reaction conditions were investigated including $POCl_3$ and DMF equivalents, solvent, time and temperature. The best conditions were found to be 1.01 equivalents of both $POCl_3$ and DMF, chlorobenzene as the solvent, and a reaction temperature of 131 °C for 6.5 hours.

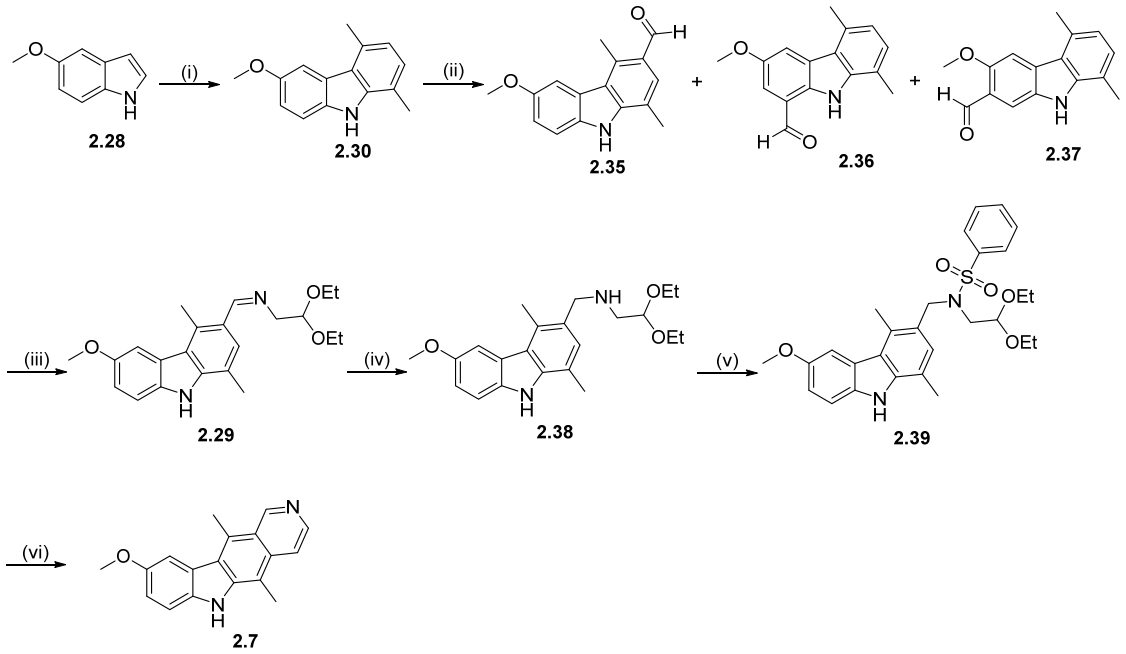

Scheme 3. Modified Cranwell-Saxton synthesis of 9-methoxyellipticine (**2.7**).[146,147] Reagents and conditions: (i) 2,5-hexadione, *p*-toluenesulfonic acid, EtOH, reflux, 2 hr, 52 %. (ii) $POCl_3$, DMF, chlorobenzene, 131 °C, 6.5 hr, 33 %. (iii) 2,2-diethoxyethan-1-amine, toluene, reflux, (iv) MeOH, $NaBH_4$, r.t., 1 hr. (v) Benzenesulfonyl chloride, pyridine, MeCN, r.t., 6 hr. (vi) 6M HCl-dioxane, reflux, 3 hr.

After the unsuccessful attempt to prepare **2.7** *via* the Gribble method (Scheme 2) the Cranwell-Saxton method was attempted. Again, it was hoped that this synthetic route would allow facile A-ring derivatisation. The condensation reaction of **2.28** with 2,5-hexadione afforded **2.30** in a 33 % yield. Extra equivalents of 2,5-hexadione and *p*-toluenesulfonic acid were required and the

reaction was stirred for a further 2 hours. McCarthy *et al.* states that the yield of the formylation of **2.30** to produce **2.35** is 22 % after separation of both side products, **2.36** and **2.37**, by column chromatography. When this reaction was carried out, only starting material and a mono-formylated carbazole product was isolated in 33 %. NMR and LCMS confirmed the structure to be the desired isomer **2.35**. The imine formation **2.29** resulted in multiple close running products being isolated after column chromatography and NMR and mass spectroscopy analysis could not decipher whether any product had been formed. Unfortunately because of the low yields and difficult purification afforded by the Cranwell-Saxton approach, different carbazole methodologies were explored.

5.3 Carbazole Formation *via* Larock's Benzyne Methodology

Larock *et al.* reported that carbazole systems could be easily accessed through coupling of iodoanilines (**2.31**) with silyaryl triflates (**2.32**) *via* a benzyne intermediate with an immediate palladium-catalysed intramolecular cyclisation.[148,149] This route was then explored to try and form the dimethyl substituted carbazole needed for 9-methoxyellipticine (**2.7**, Scheme 4).

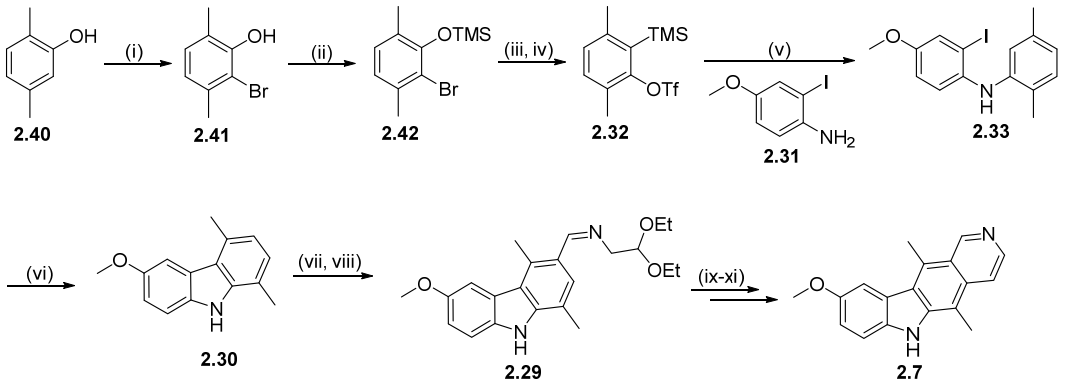

Scheme 4. Synthesis of 9-methoxyellipticine (**2.7**).[148,149] Reagents and conditions: (i) NBS, CS_2, 15 °C, 3 hr, darkness, 78 %. (ii) HMDS, 80 °C, 48 hr, darkness, 60 %. (iii) *n*-BuLi, -100 °C, 30 mins. (iv) Tf_2O, -100 °C, 30 mins, 66 % (two steps). (v) CsF, MeCN, r.t., 10 hr, (vi) 5 % $Pd(OAc)_2$, 10 % PCy_3, 100 °C, 24 hr, Ar, (vii) $POCl_3$, DMF, chlorobenzene, reflux, 6.5 hr, 22 %. (viii) aminoacetal, benzene, reflux, (ix) MeOH, $NaBH_4$, r.t., 1 hr, (x) Ns-Cl, pyridine, MeCN, r.t., 6 hr, (xi) 6M HCl-dioxane, reflux, 3 hr.

Synthesis of **2.32** was attempted using a known protocol from the commercially available dimethylphenyl compound (**2.40**).[152] Compound **2.41** was isolated after Kugelrohr distillation to give a colourless oil in a 53 % yield. Compound **2.42** was formed by TMS protection of the phenol in 60 % yield. The next stage in the protocol required **2.42** to be dissolved in THF and cooled to -100 °C before *n*-BuLi was added. The reaction was left to stir for 30 minutes in which time it

heated up slightly. Again the reaction was cooled to -100 °C before Tf_2O was added. Each time this reaction was attempted there was difficultly in maintaining the temperature at -100 °C for the length of time required. Consequently, NMR and mass spectroscopy analysis of the compound isolated revealed it to correspond to compound **2.41** not **2.32**.

2-Iodo-4-methoxyaniline (**2.31**) also had to be synthesised from the starting *p*-anisidine with a suitable iodinating reagent.[153,154] Multiple protocols were also trialled to synthesise **2.31** however, iodination of *p*-anisidine afforded starting material, iodine salts and multiple iodinated products. Due to the synthetic challenges encountered with this method, this synthetic route was also abandoned.

5.4 Synthesis of GQC-05 Derivatives

The synthesis of a small selection of GQC-05 derivatives was attempted using 9-hydroxyellipticine (**2.6**) that had been purchased commercially. These would be tested in the splicing assay of Bcl-x to see whether they had any effect on the ratio of the Bcl-x RNA isoforms. Three different GQC-05 analogues (**1.41, 1.42** and **2.43)** were proposed to investigate the importance of 9-OH and 6-NH functionalisation.[111]

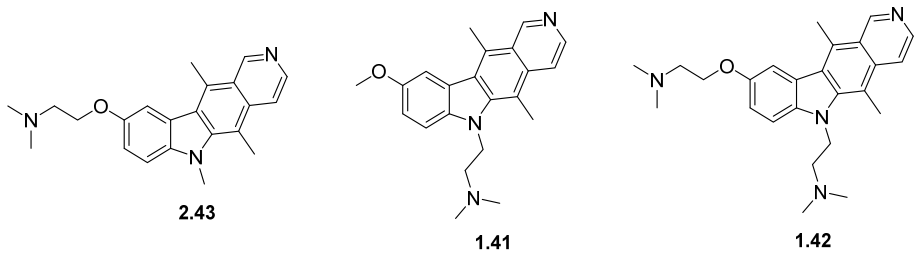

Figure 48. GQC-05 derivatives that would be synthesised for SAR analysis.

5.4.1 Preparation of *N*,*N*-dimethyl-2-((5,6,11-trimethyl-6*H*-pyrido[4,3-*b*]carbazol-9-yl)oxy) ethan-1-amine

Synthesis of the GQC-05 derivative **2.43** was explored using the procedure highlighted in Scheme 5.

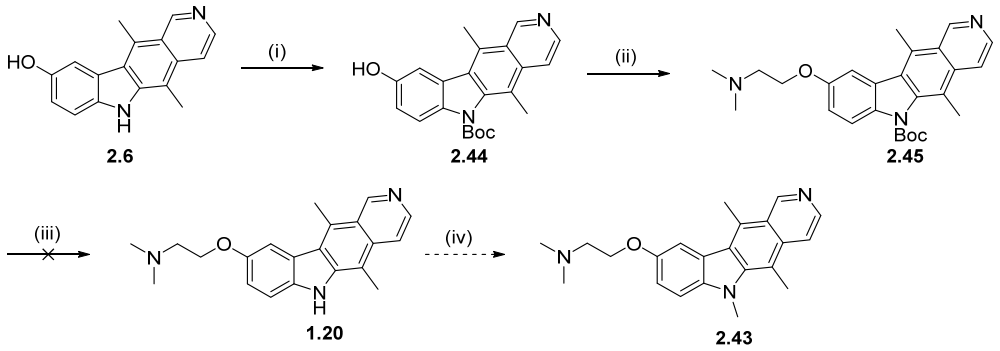

Scheme 5. Synthesis of **2.43**. Reagents and conditions: (i) Boc_2O, DMAP, MeCN, r.t., 2 hr, 59 %. (ii) 2-(Dimethylamino)ethyl methanesulfonate hydrochloride, Cs_2CO_3, DMF, 50 °C or 80 °C, 24 hr, 35 %. (iii) TFA, 2 hr. (iv) MeI, Cs_2CO_3, DMF, 50 °C, 24 hr.

Firstly, the indole nitrogen was protected using Boc_2O to afford **2.44** with an average yield of 59 % over 5 experiments. The solubility of 9-hydroxyellipticine (**2.6**) in MeCN was poor so some reactions were attempted in DMF. However, using DMF resulted in an average yield of 40 % over 3 experiments. The next step was alkylation of **2.44** with 2-(dimethylamino)ethyl methanesulfonate hydrochloride to install the dimethylaminoethyl side chain selectively on the C9 position. It was known from previous unpublished work within the group that the hydroxyl group of **2.44** was a particularly poor nucleophile and previous attempts in the laboratory reported a yield of ~50 %. Indeed, this alkylation did prove troublesome with yields of **2.45** ranging from 20−57 % with an average of 35 %. The temperature was increased to 80 °C, however no yield improvement was observed. Deprotection of the indole to produce GQC-05 (**1.20**) was then carried out. This reaction was attempted multiple times but every time several products were observed by RP-HPLC analysis and none corresponded to the product. Unfortunately, the synthesis of **2.43** could not be completed due to lack of starting material.

5.4.2 Preparation of *N*,*N*-dimethyl-2-(9-methoxy-5,11-dimethyl-6*H*-pyrido[4,3-*b*]carbazol-6-yl)ethan-1-amine

Preparation of **1.41** was carried out in a similar manner to preparative routes use to synthesise **2.43**. Protection of the indole nitrogen of **2.6** was achieved using Boc_2O with 59 % yield. MeI

was used as the methylating agent for the transformation of compound **2.44** to **2.46**, which resulted in a 60 % yield. Neat TFA was used for the Boc deprotection. This reaction produced a black TFA salt which was purified by RP-HPLC. During purification, two main peaks were observed at R_t 18-19 minutes and R_t 19-20 minutes. Both peaks were collected and analysed by LCMS which confirmed that the first peak was starting material **2.6** while the second peak had a major molecular ion of 277.2 m/z which corresponds to **2.7**. Alkylation of the indole nitrogen and purification by RP-HPLC resulting in 35 % yield of **1.41**.

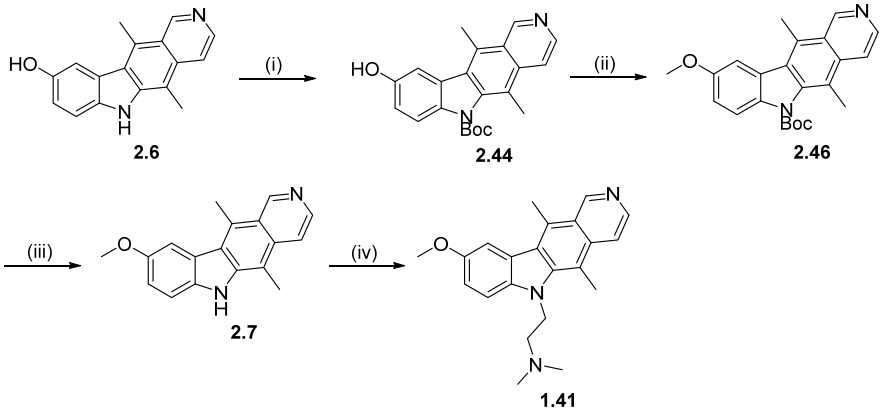

Scheme 6. Synthesis of **1.41**. Reagents and conditions: (i) Boc_2O, DMAP, MeCN, r.t., 4 hr, 59 %. (ii) MeI, Cs_2CO_3, DMF, 50 °C, 24 hr, 60 %. (iii) TFA, 4 hr, 60 %. (iv) 2-(Dimethylamino)ethyl methanesulfonate hydrochloride, Cs_2CO_3, DMF, 50 °C, 24 hr, 35 %.

5.4.3 Preparation of *N*,*N*-dimethyl-2-(9-(2-(dimethylamino)ethoxy)-5,11-dimethyl-6*H*-pyrido [4,3-*b*]carbazol-6-yl)ethan-1-amine

Using an adapted protocol[155] reported by Luniewski *et al.*, compound **1.42** was synthesised from **2.6**. The reaction was purified by RP-HPLC, resulting in a yield of 20 %.

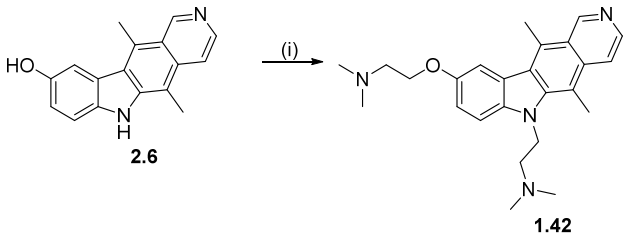

Scheme 7. Synthesis of **1.42**. Reagents and conditions: (i) 2-(Dimethylamino)ethyl methanesulfonate hydrochloride, NaOH, (50 % v/v), TBAB, DMF, 50 °C, 24 hr, 20 %.

6 Conclusions and Future Work

GQC-05 (**1.20**) has a novel effect of the alternative splicing of Bcl-x.[111] It is able to increase the amount of the pro-apoptotic mRNA isoform Bcl-xS and decrease the anti-apoptotic isoform Bcl-xL. The mechanism of action of **1.20** has not yet been proven, therefore it would be beneficial to carry out a structure activity relationship study using GQC-05 derivatives. This would allow a better understanding of what features of the small molecule are important to produce this splicing change and also allow the design of a more potent compound. To do this, a reliable route to the ellipticine core had to be investigated. There are many published synthetic procedures towards ellipticine and several of these were investigated. However, considerable difficulties were encountered when existing preparative routes were explored in order to synthesise **1.20**. Furthermore, the linearity of current synthetic strategies also posed significant limitations as a general method to prepare libraries of analogues. As a result of these limitations, work subsequently focused on establishing a modular synthetic methodology for the preparation of ellipticine small molecule libraries. The synthesis of three GQC-05 derivatives was also proposed and two of these were successfully synthesised (**1.41** and **1.42**) for use in Bcl-x splicing assays.

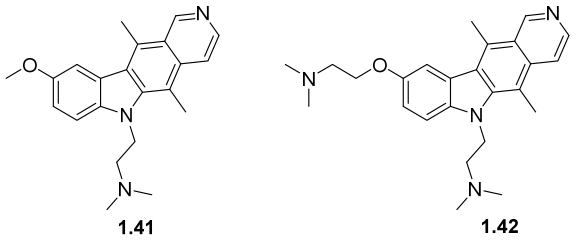

Figure 49. GCQ-05 derivatives successfully synthesised.

7 Experimental

7.1 General

Reagents and Solvents

All reagents and solvents were obtained from commercial suppliers and were used without further purification unless otherwise stated. Purification was carried out according to standard laboratory methods.[156] Dry solvents for reactions were purchased from Sigma-Aldrich and stored under nitrogen (THF, toluene). DCM, EtOAc, and petroleum ether 40 – 60° for purification purposes were used as obtained from suppliers without further purification.

Purification of Products

Thin layer chromatography was carried out using Merck silica plates coated with fluorescent indicator UV254. These were analyzed under 254 nm UV light. Normal phase flash chromatography was carried out using ZEOprep 60 HYD 40 – 63 μm silica gel. Semi-preparative reverse phase high pressure liquid chromatography (RP-HPLC) purification was carried out on a Dionex 3000 series instrument. See appendix for method and column parameters.

Spectroscopic Analysis of Products

Fourier Transformed Infra-Red (FTIR) spectra were obtained on a Shimadzu IRAffinity-1 machine. ^{1}H and ^{13}C spectra were obtained on either a Bruker AV 400 at 400 MHz, 101 MHz and 376 MHz, respectively, or Bruker DRX 500 at 500 MHz, 126 MHz and 471 MHz, respectively. Chemical shifts are reported in ppm and coupling constants are reported in Hz with MeOD referenced at 3.31 ppm (^{1}H) and 41.0 ppm (^{13}C) and DMSO-d_6 referenced at 2.50 ppm (^{1}H) and 39.52 ppm (^{13}C). High-resolution mass spectra were obtained through analysis at the EPSRC UK National Mass Spectrometry Facility at Swansea University.

LCMS was carried out on either an Agilent HPLC instrument in conjunction with an Agilent Quadrupole mass detector. Electrospray ionization (ESI) was used in all cases. GCMS was carried out on an Agilent 5975C inert MSD instrument in conjunction with a Triple-Axis mass detector. Chemical ionization (CI) was used in all cases. Analytical HPLC was carried out on a Dionex 3000 series instrument. See appendix for method and column parameters.

7.2 Compound Characterisation Data

5-Methoxy-1-(phenylsulfonyl)-1*H*-indole[145], **2.33**

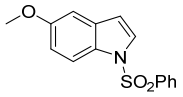

5-Methoxyindole (4 g, 27.0 mmol, 1 equiv.), powdered NaOH (2.7 g, 68.0 mmol, 2.5 equiv.) and TBAHS (90 mg, 0.27 mmol) were dissolved in DCM (116 mL) and stirred vigorously which resulted in a green solution being formed. Benzenesulfonyl chloride (7.2 g, 0.041 mmol, 1.5 equiv.) was added dropwise over a period of 1 hour. Over this time the temperature rose from 22 °C to 28 °C and the solution changed from green to a pale pink colour. After addition, the solution was left to stir for 1 hour at r.t. which resulted in a beige solution. Excess NaOH and other salts were filtered off before the filtrate was adjusted to pH 7-8 with a water wash. Afterwards, the filtrate was dried with Na_2SO_3 and decolourized with charcoal. Excess solvent was removed in *vacuo* and the product (**2.33**) was recrystallised from EtOH to give an off-white crystalline solid (6.58 g, 85 %).

^{1}H NMR (400 MHz, DMSO) δ 7.94 (dt, *J* = 8.6, 1.8 Hz, 2H), 7.83 (d, *J* = 9.0 Hz, 1H), 7.76 (d, *J* = 3.6 Hz, 1H), 7.72 – 7.66 (m, 1H), 7.62 – 7.55 (m, 2H), 7.12 (d, *J* = 2.5 Hz, 1H), 6.95 (dd, *J* = 9.0, 2.6 Hz, 1H), 6.77 (dd, *J* = 3.7, 0.7 Hz, 1H), 3.75 (s, 3H).
^{13}C NMR (101 MHz, DMSO) δ 155.9, 137.8, 133.2, 131.3, 129.1, 128.7, 126.6, 126.2, 133.9, 133.3, 108.9, 103.2, 55.1.
LRMS (GCMS BASIC_PCI_GC320) R_t = 16.603, m/z = 288.0 $[M+H]^+$

4-(5-Methoxy-1-(phenylsulfonyl)-1*H*-indole-2-carbonyl)nicotinic acid[145], **2.34**

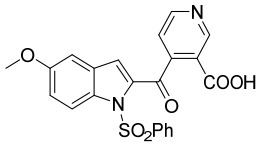

Diisopropylamine (3.6 mL, 0.26 mol, 1.1 equiv.), *n*-BuLi (2.3 mL, 0.24 mol, 1.1 equiv.) and dry THF (35 mL) were added to a round bottom flask at -78 °C, under argon, to form LDA *in situ*. Added to this was 1-(phenylsulfonyl)-5-methoxyindole (6.58 g, 0.23 mol, 1.0 equiv.) in dry THF (35 mL) *via* syringe over 5 minutes. The mixture was allowed to warm to 10 °C over 2 hours. The

light orange/yellow solution was cooled to -100 °C (liquid N_2/methanol) and treated quickly with a solution of pyridine anhydride (3.73 g, 0.025 mol, 1.1 equiv.) in dry THF (25 mL) while efficient cooling and stirring was maintained. The mixture was stirred at -100 °C for 1.5 hours before slowly being warmed to r.t. overnight. The solvent was then removed *in vacuo* and the resulting dark yellow oil was dissolved in H_2O (6 mL), acidified to pH 2-3 with 20 % HCl and then cooled to 5 °C. The resulting off-white precipitate was collected by filtration and washed with water (3 x 2 mL) to give an off-white solid. The solid was then treated with glacial HOAc (4 mL) and refluxed ntil nearly all the solid had dissolved. The solution was subsequently filtered by gravity to remove a small amount of residual solids before boiling H_2O was added until the cloudy appearance persisted for approximately 5 seconds before disappearing. The mixture was then allowed to cool to r.t. then cooled further to 10 °C. The product (**2.34**) was collected by filtration and thoroughly washed with H_2O, then freeze dried to produce an off-white crystalline solid (5.54 g, 55 %).

^{1}H NMR (400 MHz, DMSO) δ 7.95-7.90 (m, 2H), 7.82 (d, *J* = 9.0 Hz, 1H), 7.75 (d, *J* = 3.7 Hz, 1H), 7.67, (tt, *J* = 7.3, 1.2, 1H), 7.60-7.54 (m, 2H), 7.11 (d, *J* = 2.5 Hz, 1H), 6.94 (dd, *J* = 9.1, 2.6 Hz, 1H), 6.77 (dd, *J* = 3.8, 0.7 Hz, 1H), 3.74 (s, 3H).
^{13}C NMR (101 MHz, DMSO) δ 156.1, 137.0, 134.5, 131.7, 129.8, 128.7, 127.7, 126.6, 114.0, 113.7, 109.9, 104.0, 55.4.
ESI MS m/z (+ ve mode; %) 295.20 (100) $[M\text{-}SO_2Ph \text{ and } -H]^+$

4-(5-Methoxy-1*H*-indole-2-carbonyl)nicotinic acid[145], **2.35**

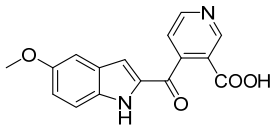

Method 1:
To a magnetically stirred solution of 4-(5-methoxy-1-(phenylsulfonyl)-1*H*-indole-2-carbonyl)nicotinic acid (112.1 mg, 0.26 mmol) in MeOH:H_2O (2.5:0.75 mL), K_2CO_3 (145.5 mg, 1.05 mmol) was added and the mixture was refluxed under N_2 for 3 hours. The mixture was cooled, and the solvent was removed *in vacuo* to give a white solid. LCMS analysis confirmed this solid to be the starting material. The solid was resubmitted to the reflux conditions for 5 hours, however again the starting material was obtained.

Method 2:

To a magnetically stirred solution of 4-(5-methoxy-1-(phenylsulfonyl)-1*H*-indole-2-carbonyl)nicotinic acid (4.83 g, 0.01 mol) in MeOH (27 mL), 2M NaOH (33mL) was added and the mixture was refluxed under N_2 overnight. The mixture was cooled, and the solvent was removed *in vacuo* to give a dark red solid. The crude product was dissolved in water (200 mL) and acidified with 20 % HCl. A white solid crashed out and this was filtered off, washed and analysed. NMR confirmed this to be 5-methoxyindole (2.10 g).

6-Methoxy-1,4-dimethyl-9H-carbazole[147], **2.30**

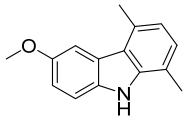

5-Methoxyindole (2.1 g, 0.014 mol, 1.0 equiv.), 2,5-hexadione (3.4 g, 0.030 mol, 2.07 equiv.) and a catalytic amount of *p*-toluenesulfonic acid were dissolved in EtOH (20 mL). The reaction mixture was heated to reflux and left to stir at reflux for 2.5 hours. TLC analysis indicated the reaction was not complete so extra 2,5-hexadione (0.5 mL) and *p*-toluenesulfonic acid was added and the reaction was left for another 2.5 hours. The reaction mixture was then cooled to room temperature and the solvent was evaporated under reduced pressure. The product was purified by silica column chromatography with the product (**2.30**) eluting with hexane-ethyl acetate (8:2) to afford an off-white solid (1.0403 g, 33 %).

^{1}H NMR (400 MHz, DMSO) δ 10.96 (s, 1H), 7.60 (d, *J* = 2.5 Hz, 1H), 7.44 (d, *J* = 8.7 Hz, 1H), 7.05 (dd, *J* = 2.4 Hz, 2H), 6.80 (d, *J* = 7.4 Hz, 1H), 3.86 (s, 3H), 2.77 (s, 3H), 2.49 (s, 3H).
^{13}C NMR (101 MHz, DMSO) δ 153.8, 139.7, 134.6, 129.6, 125.6, 123.6, 120.4, 119.4, 117.4, 113.4, 111.3, 105.3, 55.6, 20.1, 16.7.
LCMS (GCMS BASIC_PCI_GC320) R_t = 16.131, m/z = 226.1 $[M+H]^+$.

6-Methoxy-1,4-dimethyl-9*H*-carbazole-3-carbaldehyde[147], **2.35**

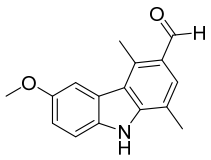

6-Methoxy-1,4-dimethylcarbazole (1.0403 g, 4.622 mmol, 1.0 equiv.) was dissolved in DMF (10 mL, 1.3 mol) and chlorobenzene (30 mL). The solution was cooled with an ice bath to 0 °C then $POCl_3$ (0.4 mL, 4.67 mmol, 1.01 equiv.) was slowly added. The reaction was then heated to 131 °C for 6.5 hours with stirring. The reaction mixture was then cooled and poured into a solution of sodium acetate (20 mL, 25 % w/w) and evaporated under pressure to afford a brown solid which was diluted with ethyl acetate and washed with water then brine and concentrated under reduced pressure to afford a crude brown oil. The product was purified by silica column chromatography with the product (**2.35**) eluting with hexane-ethyl acetate (80:20) to afford an off-white solid (390 mg, 33 %).

^{1}H NMR (400 MHz, DMSO) δ 11.55 (s, 1H), 10.36 (s, 1H), 7.72 (d, *J* = 2.3 Hz, 1H), 7.65 (s, 1H), 7.50 (d, *J* = 8.8 Hz, 1H), 7.12 (dd, *J* = 8.8, 2.4 Hz, 1H), 3.87 (s, 3H), 3.13 (s, 3H), 2.53 (s, 3H).
^{13}C NMR (101 MHz, DMSO) δ 191.0, 160.7, 159.4, 155.5, 154.0, 142.4, 134.1, 128.5, 128.4, 117.1, 113.8, 111.0, 106.7, 55.7, 15.9, 14.5.
LRMS (GCMS BASIC_PCI_GC320) R_t = 17.93, m/z = 254.1 $[M+H]^+$.

(Z)-*N*-(2,2-Diethoxyethyl)-1-(6-methoxy-1,4-dimethyl-9H-carbazol-3-yl)methanimine[147], **2.29**

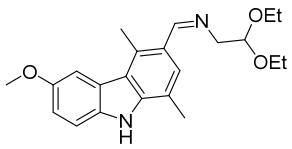

6-Methoxy-1,4-dimethyl-9*H*-carbazole-3-carbaldehyde (300.0 mg, 1.19 mmol, 1.0 equiv.) was added to a round bottom flask with 2,2-diethoxyethan-1-amine (166.0 mg, 1.25 mmol, 1.1 equiv.), dried molecular sieves and dry toluene (10 mL). The reaction was heated to reflux and left to stir overnight. The crude reaction mixture was diluted with ethyl acetate and washed with water then brine and concentrated under reduced pressure to afford a crude solid. The product was purified by silica column chromatography; however, the product could not be isolated clean.

2-Bromo-3,6-dimethylphenol[149], **2.41**

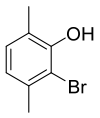

In a three-necked flask fitted with a drying tube, 2,5-dimethylphenol (5.0 g, 0.0410 mol, 1.0 equiv.) was dissolved in CS_2 (150 mL) and the mixture was degassed for 30 minutes while being protected from light. The reaction was then cooled to 15 °C and NBS (8.16 g, 0.046 mol, 1.1 equiv.) was added to the solution slowly. The mixture was stirred and warmed to room temperature over 3 hours. Afterwards the solvent was removed *in vacuo* and the residue filtered through a short silica plug and eluted with *n*-hexanes. The crude product was then purified by Kugelrohr distillation to give the desired bromophenol (**2.41**) as a colourless oil which was sensitive to light (4.35 g, 53 %).

^{1}H NMR (400 MHz, DMSO) δ 8.80 (s, 1H), 6.96 (d, *J* = 7.6 Hz, 1H), 6.72 (d, *J* = 7.6 Hz, 1H), 2.27 (s, 3H), 2.18 (s, 3H).
^{13}C NMR (101 MHz, DMSO) δ 151.7, 135.6, 128.9, 123.7, 121.4, 113.7, 22.8, 16.7.
LCMS (GCMS BASIC_PCI_GC320) R_t = 11.669, m/z = 201.0 $[M+H]^+$.

(2-Bromo-3,6-dimethylphenoxy)trimethylsilane[149], **2.42**

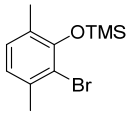

In a dry three-necked flask, under argon, 2-bromo-3,6-dimethylphenol (3.05 g, 0.0152 mol, 1.0 equiv.) and HMDS (30 mL) were added and heated to 80 °C. After 48 hours excess HMDS and NH_3 were removed *in vacuo* to give a colourless oil. The product was purified by silica column chromatography with the product (**2.42**) eluting with hexane-ethyl acetate (80:20) to afford an off-white solid (2.5 g, 60 %).
^{1}H NMR (400 MHz, DMSO) δ 7.06 (d, *J* = 7.7 Hz, 1H), 6.87 (d, *J* = 7.7 Hz, 1H), 2.31 (s, 3H), 2.18 (s, 3H), 0.29 (s, 9H).
^{13}C NMR (101 MHz, DMSO) δ 149.9, 135.1, 128.2, 126.2, 122.5, 116.7, 22.0, 16.5, 0.2.
LRMS (GCMS BASIC_PCI_GC320) R_t = 11.90, m/z = 273.0 $[M]^+$.

3,6-Dimethyl-2-(trimethylsilyl)phenyl trifluoromethanesulfonate[149], **2.32**

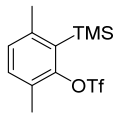

(2-Bromo-3,6-dimethylphenoxy)trimethylsilane (2.5 g, 9.15 mmol) was dissolved in dry THF (45 mL) in a round bottom flask. The solution was cooled to -100 °C (dry ice/Et_2O bath) and *n*-BuLi (0.96 mL, 1.6 M solution in hexanes, 10.07 mmol, 1.1 equiv.) was added over 5 minutes. The mixture was stirred for 30 minutes. During this time the temperature rose to -80 °C therefore the mixture was cooled again to -100 °C, then Tf_2O (1.85 mL, 10.98 mmol, 1.2 equiv.) was added over 5 minutes. The reaction mixture was stirred for 30 minutes and the temperature was allowed to rise to -80 °C. Cold saturated aq. $NaHCO_3$ (50 mL) was added, and the aqueous layer was extracted with Et_2O (3 x 50 mL). The combined organic layers were dried over Na_2SO_4, filtered and concentrated *in vacuo*. When the crude reaction mixture was analysed by NMR and LCMS it was found that the expected product had not been formed. The major product was instead 2-bromo-3,6-dimethylphenol.

2-Iodo-4-methoxyaniline[157], **2.31**

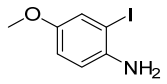

Method 1:

p-Anisidine (5.0 g, 0.04 mol, 1.0 equiv.) and sodium carbonate (4.24 g, 0.04 mol, 1.0 equiv.) were suspended in water (50 mL) and stirred for 30 minutes. The solution was cooled to 5 – 10 °C before I_2 (10.15 g, 0.04 mol, 1.0 equiv.) was added. The reaction mixture was stirred for 48 hours with regular LCMS analysis; however, only starting material was observed.

Method 2:

p-Anisidine (5.0 g, 0.04 mol, 1.0 equiv.) was dissolved in MeCN (100 mL) and NIS (10.05 g, 0.045 mol, 1.1 equiv.) and CF_3COOH (0.94 mL, 0.012 mol, 0.3 equiv.) was added at r.t. The reaction was heated to 85 °C and stirred for 5 hours. The reaction mixture was then cooled to r.t. and diluted with ethyl acetate (250 mL). The organic layer was washed with a saturated solution of sodium thiosulfate (3 x 100 mL), water (3 x 100 mL) and brine (2 x 100 mL). The organic

layer was then dried with Na_2SO_4 and reduced under vacuum to afford a dark oil. Crude ^{1}H NMR showed no product or starting material.

Method 3:

p-Anisidine (3.0 g, 0.024 mol, 1.2 equiv.) was dissolved in DCM (15 mL) under argon. ICl (3.25 g, 0.020 mol, 1.0 equiv.) was added dropwise over 5 minutes. The reaction was left to stir for 1 hour in the dark. After 1 hour TLC indicated that the starting material had been consumed. The solvent was removed under vacuum to afford a black solid (1.2077 g). The product was purified by silica column chromatography with a compound eluting with hexane-ethyl acetate (8:2). ^{1}H NMR analysis showed that the expected product had not been formed.

2-(Dimethylamino)ethyl methanesulfonate hydrochloride[158]

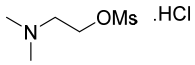

A solution of 2-dimethylaminoethanol (4.32 g, 48.5 mmol, 1 equiv.) in DCM (100 mL) was cooled to 0 °C in an ice bath. MsCl (9.39 mL, 120 mmol, 2.5 equiv.) was added dropwise. A white precipitate was formed upon complete addition of MsCl. The reaction was allowed to warm to r.t. and stirred for 3 hours, after which the product was filtered and collected. The desired product was isolated as a white/yellow solid (9.55 g, 97 %).

^{1}H-NMR: ($CDCl_3$, 400 MHz) δ 3.97 (t, *J* = 6.3 Hz, 2H), 3.53 (bt, *J* = 6.0 Hz, 2H), 3.00 (s, 6H), 2.79 (s, 3H).

^{13}C-NMR: ($CDCl_3$, 101 MHz) δ 58.0, 43.2, 38.8, 36.6.

LRMS (LCMS) R_t = 0.96, m/z 168.1 $[M+H]^+$, +ve.

tert-Butyl 9-hydroxy-5,11-dimethyl-6*H*-pyrido[4,3-*b*]carbazole-6-carboxylate, **2.44**

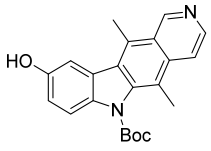

To a solution of 9-hydroxyellipticine (50 mg, 0.167 mmol, 1 equiv.) in MeCN (2 mL), Boc_2O (43.7 mg, 0.200 mmol, 1.2 equiv.) and DMAP (22.4 mg, 0.183 mmol, 1.1 equiv.) were

sequentially added. The reaction was allowed to stir at r.t. for 4 hours before being dissolved in EtOAc and adsorbed onto silica. Silica gel column chromatography was used to purify the product which eluted with 0 → 5 % MeOH/DCM. The desired product (**2.44**) was isolated as a yellow solid (40 mg, 67 %).

^{1}H NMR (400 MHz, MeOD) δ 9.60 (s, 1H), 8.34 (d, *J* = 6.3 Hz, 1H), 8.10 (d, *J* = 1.9 Hz, 1H), 7.99 (d, *J* = 6.2 Hz, 1H), 7.53 (d, *J* = 8.6 Hz, 1H), 7.30 (dd, *J* = 8.8, 2.08 Hz, 1H), 3.23 (s, 3H), 2.79 (s, 3H), 1.59 (s, 9H).
ESI MS m/z (+ ve mode; %) 363.07 (100) $[M+H]^+$.

tert-Butyl-9-(2-(dimethylamino)ethoxy)-5,11-dimethyl-6*H*-pyrido[4,3-*b*]carbazole-6-carboxylate, **2.45**

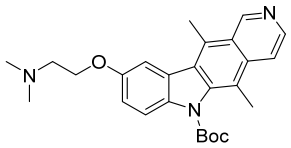

tert-Butyl 9-hydroxy-5,11-dimethyl-6*H*-pyrido[4,3-*b*]carbazole-6-carboxylate (35 mg, 0.097 mmol, 1 equiv.) and Cs_2CO_3 (79 mg, 0.242 mmol, 2.5 equiv.) were dissolved in DMF (2 mL). 2-(dimethylamino)ethyl methanesulfonate hydrochloride (20 mg, 0.967 mmol, 1 equiv.) was then added and the reaction was heated to 50 °C and left to stir for 24 hours during which time the reaction colour had changed from yellow to dark brown/purple. The reaction mixture was then cooled to room temperature and the solvent was removed *in vacuo*. The product was dissolved in MeOH then filtered to remove the Cs_2CO_3 and then finally adsorbed onto silica. Silica gel column chromatography was used to purify the product which eluted with 0 → 15 % MeOH/DCM. The desired product (**2.45**) was isolated as a yellow oil (23.9 mg, 57 %).

^{1}H NMR (400 MHz, MeOD) δ 9.62 (s, 1H), 8.29 (d, *J* = 6.9 Hz, 1H), 8.22 (d, *J* = 7.1 Hz, 1H), 7.95 (d, *J* = 2.0 Hz, 1H), 7.45 (d, *J* = 8.7 Hz, 1H), 7.34 (dd, *J* = 8.8, 2.07 Hz, 1H), 4.57 (bs, 2H), 3.06 (s, 3H), 2.97 (t, *J* = 5.8 Hz, 2H), 2.68 (s, 3H), 2.37 (s, 6H), 1.62 (s, 9H).
LRMS (ESI) m/z (+ve mode %) 434.20 (100) $[M+H]^+$.

N,*N*-Dimethyl-2-((5,11-dimethyl-6*H*-pyrido[4,3-*b*]carbazol-9-yl)oxy)ethan-1-amine[41], **1.20**

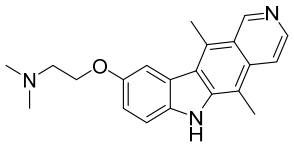

tert-Butyl-9-(2-(dimethylamino)ethoxy)-5,11-dimethyl-6*H*-pyrido[4,3-*b*]carbazole-6-carboxylate (20.5 mg, 0.047 mmol, 1 equiv.) was dissolved in TFA (3 mL) and stirred at room temperature for 1 hour. The product was dissolved in MeOH and neutralized with ammonia solution to a pH of 6-7. Excess TFA was then removed *in vacuo* to give a black crude solid. The crude material was purified by RP-HPLC to give the desired product (**1.20**) as an orange solid (3.6 mg, 23 %).

RP-HPLC: R_t = 16.3 minutes (For general conditions see Appendix, Section 6.3).
^{1}H NMR (400 MHz, DMSO) δ 11.22 (s, 1H), 9.69 (s, 1H), 8.41 (d, *J* = 6.1 Hz, 1H), 7.91 (dd, *J* = 4.1, 1.5 Hz, 2H), 7.49 (d, *J* = 8.7 Hz, 1H), 7.21 (dd, *J* = 8.8, 2.4 Hz, 1H), 4.24 (t, *J* = 5.7 Hz, 2H), 3.27 (s, 3H), 2.82 (t, *J* = 5.6 Hz, 2H), 2.78 (s, 3H), 2.36 (s, 6H).
^{13}C NMR (101 MHz, DMSO) δ 156.5, 152.1, 140.4, 137.4, 132.3, 128.3, 123.6, 115.8, 111.1, 108.9, 107.9, 57.7, 45.3, 14.3, 11.9 (not all peaks can be identified).
LRMS (ESI) m/z (+ve mode %) 348.27 (100) $[M + 14]^+$.

tert-Butyl 9-methoxy-5,11-dimethyl-6*H*-pyrido[4,3-*b*]carbazole-6-carboxylate,[159] **2.46**

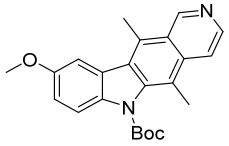

tert-Butyl 9-hydroxy-5,11-dimethyl-6*H*-pyrido[4,3-*b*]carbazole-6-carboxylate (34 mg, 0.0938 mmol, 1 equiv.) and Cs_2CO_3 (76 mg, 0.2345 mmol, 2.5 equiv.) were dissolved in DMF (2 mL). MeI (13.3 mg, 0.0938 mmol, 1 equiv.) was added and the reaction was heated to 50 °C and left to stir for 24 hours during which time the reaction colour changed from yellow to dark brown/red. The reaction mixture was then cooled and filtered to remove Cs_2CO_3 then diluted with EtOAc and washed with LiCl (x5). The combined organic layers were washed with brine, dried with Na_2SO_4 and the excess solvent was evaporated *in vacuo*. Silica gel column chromatography was used to

purify the product which eluted with 0 → 5 % MeOH/DCM to produce the desired product (**2.46**) as a yellow oil (21.2 mg, 60 %).

^{1}H NMR (400 MHz, MeOD) δ 8.76 (s, 1H), 7.99 (d, *J* = 7.0 Hz, 1H), 7.44 – 7.23 (m, 2H), 7.09 – 7.03 (m, 1H), 6.87 (d, *J* = 8.8 Hz, 1H), 3.11 (s, 3H), 2.05 (s, 3H), 1.92 (s, 3H), 1.63 (s, 9H).

LRMS (ESI) m/z (+ve mode %) 377.20 (26) $[M+H]^+$.

9-Methoxy-5,11-dimethyl-6*H*-pyrido[4,3-*b*]carbazole,[114] **2.7**

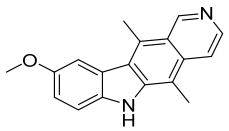

tert-Butyl 9-methoxy-5,11-dimethyl-6*H*-pyrido[4,3-*b*]carbazole-6-carboxylate (19.7 mg, 0.045 mmol, 1 equiv.) was dissolved in TFA (3 mL) and stirred at room temperature for 4 hours. Excess TFA was removed *in vacuo* then the crude material was purified by RP-HPLC to give the desired product (**2.7**) as an orange solid (13.1 mg, 90 %).

RP-HPLC: R_t 19.2 (For general conditions see Appendix, Section 6.3).

^{1}H NMR (400 MHz, MeOD) δ 9.70 (s, 1H), 8.43 (d, *J* = 7.0 Hz, 1H), 8.27 (d, *J* = 7.0 Hz, 1H), 7.71 (d, *J* = 2.4 Hz, 1H), 7.43 (d, *J* = 8.7 Hz, 1H), 7.17 (dd, *J* = 8.9, 2.39 Hz, 1H), 4.15 (s, 3H), 3.15 (s, 3H), 3.08 (s, 3H).

LRMS (ESI) m/z (+ve mode %) 277.7 (100) $[M+H]^+$.

N,*N*-Dimethyl-2-(9-methoxy-5,11-dimethyl-6*H*-pyrido[4,3-*b*]carbazol-6-yl)ethan-1-amine, **1.41**

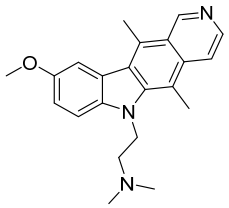

9-Methoxy-5,11-dimethyl-6*H*-pyrido[4,3-*b*]carbazole (13.1 mg, 0.05 mmol, 1 equiv.), and Cs_2CO_3 (38.6 mg, 0.12 mmol, 2.5 equiv.) were dissolved in DMF (1 mL). 2-(dimethylamino)ethyl methanesulfonate hydrochloride (9.57 mg, 0.05 mmol, 1 equiv.) was then added and the reaction

was heated to 50 °C and left to stir for 24 hours during which time the reaction colour had changed from yellow to dark brown. The reaction mixture was then cooled to room temperature and the solvent was removed *in vacuo*. The crude material was purified by RP-HPLC to give the desired product (**1.41**) as an orange solid (5.6 mg, 35 %).

RP-HPLC: R_t: 19.0 minutes (For general conditions see Appendix, Section 6.3).

^{1}H NMR (400 MHz, MeOD) δ 9.88 (s, 1H), 8.55 (s, 1H), 8.36 (d, *J* = 5.4 Hz, 1H), 8.11 (s, 1H), 7.70 (s, 1H), 7.51 (d, *J* = 9.0 Hz, 1H), 4.56 (t, *J* = 4.8 Hz, 2H), 4.31 (s, 3H), 3.72 (t, *J* = 4.8 Hz , 2H), 3.20 (s, 3H), 2.89 (s, 3H), 3.08 (s, 6H).

HRMS Exact mass calculated for $[M+H]^+$ ($C_{22}H_{26}O_1N_3$) requires m/z 348.8070, found $[M+H]^+$ m/z 348.2071.

N,*N*-Dimethyl-2-(9-(2-(dimethylamino)ethoxy)-5,11-dimethyl-6*H*-pyrido[4,3-*b*]carbazol-6-yl)ethan-1-amine,[114] **1.42**

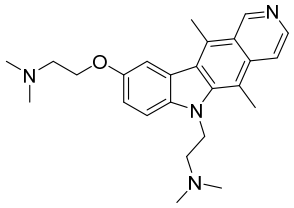

To a stirred solution of 9-hydroxyellipticine (20 mg, 0.07 mmol, 1.0 equiv.) in DMF (2 mL) was added 2-(dimethylamino)ethyl methanesulfonate hydrochloride (27.3 mg, 0.13 mmol, 2.0 equiv.), 50 % aqueous NaOH solution (0.34 mL, 0.004 mmol) and TBAB (8 mg, 0.025 mmol). The reaction was heated to 50 °C and stirred overnight. After cooling to room temperature, residual salts were removed by filtration and excess solvent was removed *in vacuo*. The crude material was purified by RP-HPLC to give the desired product (**1.42**) as an orange solid (6.9 mg, 20 %).

RP-HPLC: R_t 11.5 minutes (For general conditions see Appendix, Section 6.3).

^{1}H NMR (400 MHz, MeOD) δ 8.16 (s, 1H), 7.84 (d, *J* = 8.9 Hz, 1H), 7.53 (d, *J* = 9.1 Hz, 1H), 5.17 (t, *J* = 7.8 Hz, 2H), 4.58 (t, *J* = 4.6 Hz, 2H), 3.72 (t, *J* = 4.8 Hz, 2H), 3.59 (t, *J* = 7.8 Hz, 2H), 3.40 (s, 3H), 3.20 (s, 3H), 2.17 (s, 12H).

HRMS Exact mass calculated for $[M+H]^+$ ($C_{25}H_{33}O_1N_4$) requires m/z 405.2649, found $[M+H]^+$ m/z 405.2645.

Chapter 3

Development of a Convergent, Step-efficient Synthesis of an Ellipticine Analogue Library

8 Palladium Cross Coupling Chemistry

Reactions which can form C-C bonds are the most important and well-studied reactions in the field of chemistry. This is demonstrated by the fact that no fewer than 5 Nobel Prizes have been awarded in this area alone. Palladium metal can be used to efficiently catalyse C-C bond forming reactions, as well as C-Heteroatom bonds.[160–165] Within the last 60 years palladium cross coupling chemistry has been established in both industrial and academic settings and applied in the synthesis of countless natural products, fine chemicals and pharmaceutically relevant compounds.[166] In general, palladium catalysed cross coupling involves the reaction of an organic electrophile (typically an aryl halide) with a corresponding nucleophile. Nucleophiles can range from metals and metalloids such as zinc, magnesium, tin, boron, and silicon, to heteroatoms such as nitrogen, oxygen, and sulfur. Terminal alkynes and alkenes have also been used as successfully coupling partners to produce extended hybridized systems (Figure 50).

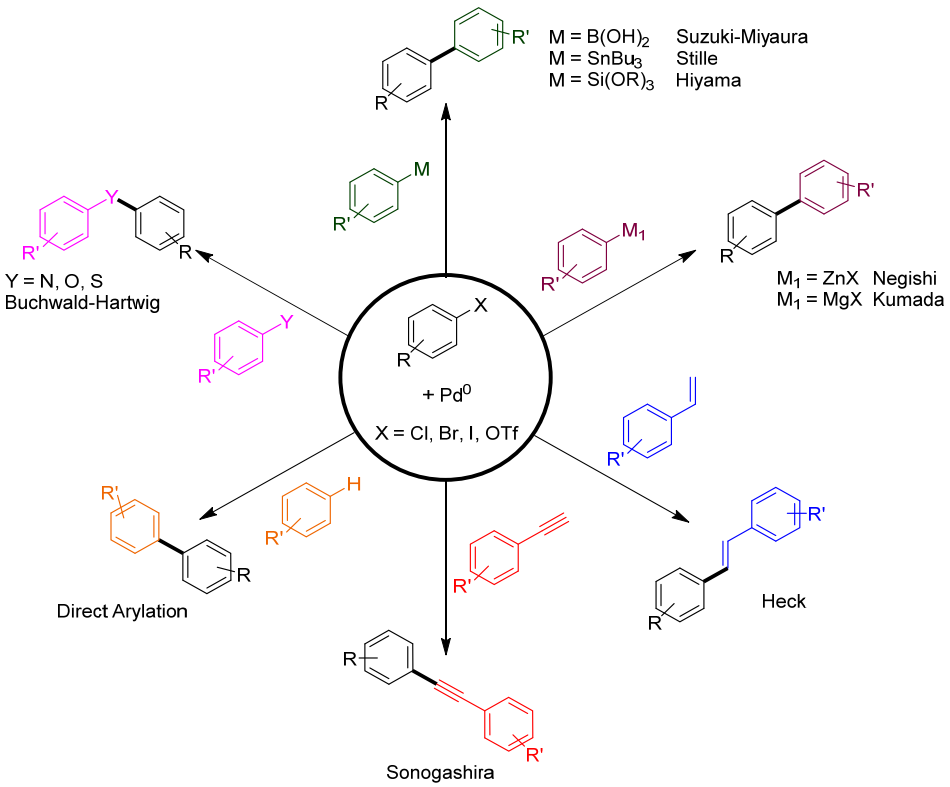

Figure 50. Overview of palladium cross coupling reactions.

8.1 Buchwald-Hartwig Amination

First discovered in 1995 by both Stephen L. Buchwald[165] and John F. Hartwig,[167] the Buchwald-Hartwig amination reaction allows the coupling of a range of amines — including primary anilines, nitrogen containing heterocycles, and amides — with aryl halides under catalytic conditions. Coupling with ammonia under mild conditions to produce primary arylamines has also been shown, even in the presence of base sensitive functional groups.[168,169] Initially, the formation of arylamines was demonstrated by Migita with the coupling of aryl bromide **3.1** and tin amide **3.2** to form aniline **3.3**.[170,171] However, the reaction scope was limited and the use of toxic tin compounds was undesirable.

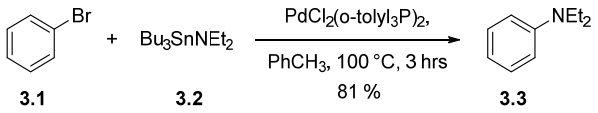

Scheme 8. Coupling of benzyl bromide and tin amides.[170]

The first examples of tin free aryl-amine coupling was demonstrated by both Buchwald[165] and Hartwig[167] independently using the bulky inorganic bases NaO*t*Bu and LiHMDS, respectively and employing aryl bromides of type **3.4** along with secondary amines (eg., **3.5**) to produce **3.6** (Scheme 9).

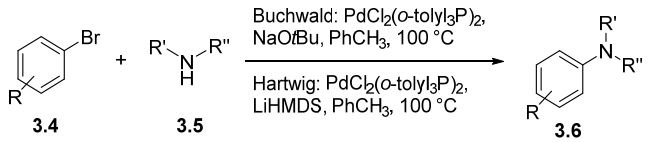

Scheme 9. Tin free coupling of aryl bromides and amines.[165,167]

The catalytic cycle (Scheme 10) for the Buchwald-Hartwig amination begins with the oxidative addition of a Pd^0 species into an aryl halide bond. This Pd^0 species **3.9** can be formed from stable Pd^{II} salts **3.8** such as $Pd(OAc)_2$ or $PdCl_2$. Reduction and activation of the Pd source must take place before the reaction can proceed and this can typically be achieved with the use of a Et_3N or by excess phosphine ligand (Figure 51).

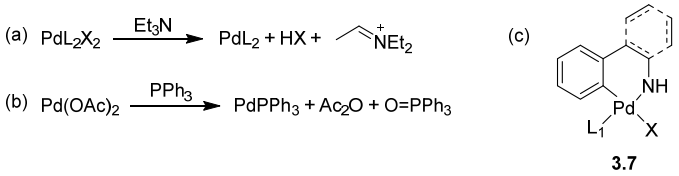

Figure 51. (a) and (b) Methods to generate Pd^0. (c) Buchwald pre-catalyst general structure.

This pre-activation step can be omitted if a Pd^0 active catalyst such as $Pd(PPh_3)_4$ or $Pd_2(dba)_3$ is used or alternatively, a stable pre-catalyst (**3.7**) is employed in the reaction (Figure 51c). Pre-catalysts are Pd^0 complexes consisting of stable, bulky diaryl phosphine ligands based on the Buchwald ligand set. Many of these pre-catalysts are now commercially available and can be an attractive alternative to the traditional Pd^{II} salt and ligand combination. Once the catalytically active Pd^0 species is formed, oxidative addition of Pd^0 into the aryl halide bond can occur to give complex **3.11**. This is the rate determining step in the catalytic cycle[167] with electron-withdrawing groups (EWGs) increasing the rate of this step, while election-donating groups (EDGs) decrease the rate. Next amine binding can occur resulting in complex **3.13**, which is then followed by deprotonation of the amine by a suitable base which leads to **3.16**. Both strong and weak bases are tolerated with the choice of base dependent on the substrate being coupled and presence of sensitive functional groups. The final step in the catalytic cycle is reductive elimination of the coupled product **3.17** and regeneration of Pd^0 **3.9**. If a bidentate ligand is used this holds the aryl and amine components in a 4-coordinate species with *cis* geometry which aids in reductive elimination from the catalyst.[172,173]

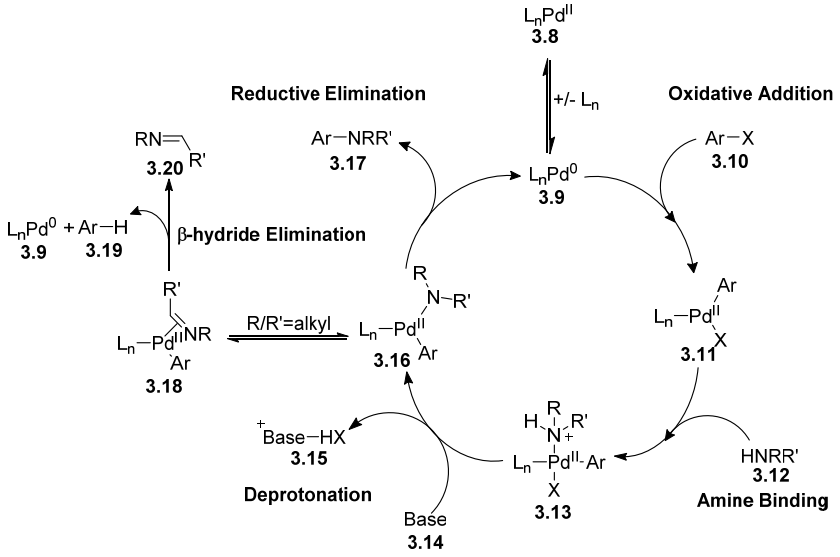

Scheme 10. Catalytic cycle of the Buchwald-Hartwig amination reaction.

The imine side product **3.20** that can be formed from Buchwald-Hartwig aminations occurs if either of the R groups present on the amine have a β-hydride that can undergo elimination.[174] A 3-coordinate species formed from a monodentate ligand enhances the β-hydride elimination pathway.[172] The use of bidentate ligands were initially shown to decrease the rate of this side reaction, however bulky biaryl phosphines have demonstrated the same ability.[175,176] This side process still forms one of the major limitations associated with the Buchwald-Hartwig amination

reaction due to the ease of the formation of the β-hydride eliminated product with alkyl amines. Although a wide range of nitrogen nucleophiles can be used, including amines, amides and nitrogen heterocycles, intensive screening should be carried out to find the best combination of ligand, base and solvent as preferred reaction conditions can vary widely.

A major ongoing development to the Buchwald-Hartwig amination reaction is the ligands employed. The first generation ligands used were simple phosphine ligands such as **L1** – **L4** (Figure 53).[165] It was initially hypothesised that increasing the steric bulk of these ligands would minimise the unwanted β-hydride elimination pathway.[177] However, once bidentate ligands (**L5** – **L8**) were discovered to be successful, it was realised that the bite angle that the ligand accommodated around the Pd centre and the ligand electronics were more important than the overall bulk (Figure 52).[172]

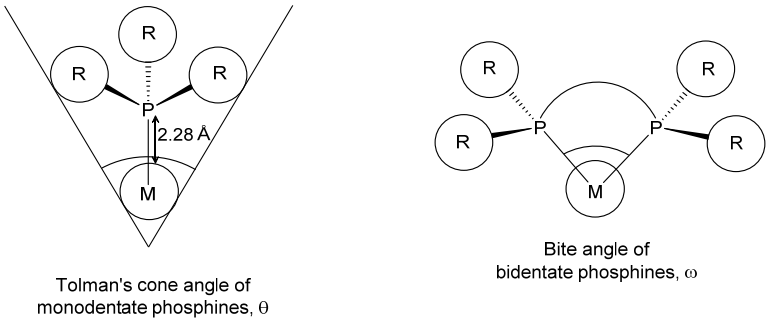

Figure 52. Illustration of Tolman's cone angle of monodentate phosphines and the bite angle of bidentate phosphines.[178]

The next significant advance in the ligand set used was the development of diaryl phosphine ligands (**L10** – **L15**) by Buchwald for the use in Buchwald-Hartwig aminations and Suzuki-Miyaura couplings.[175,176,179] The design of these ligands allows the steric and the electronic effects to be carefully controlled by altering the R groups on both the phosphine and the aryl rings (Figure 53).[180,181] While phosphines and diaryl phosphines are clearly the most abundantly utilised ligands in Buchwald-Hartwig aminations, *N*-heterocylic carbenes (NHCs) have also shown promise.[182–185] The advantages of NHCs over simple phosphines (e.g., **L1**) are well documented.[186,187] NHCs appear to have similar electronic properties to phosphines, as both are capable of strong σ-donation (due to the singlet carbene electrons) and limited π-back-donation. However it has been found that the NHCs exhibited a much greater σ-donating ability than even the most Lewis basic phosphine, PCy_3.[188]

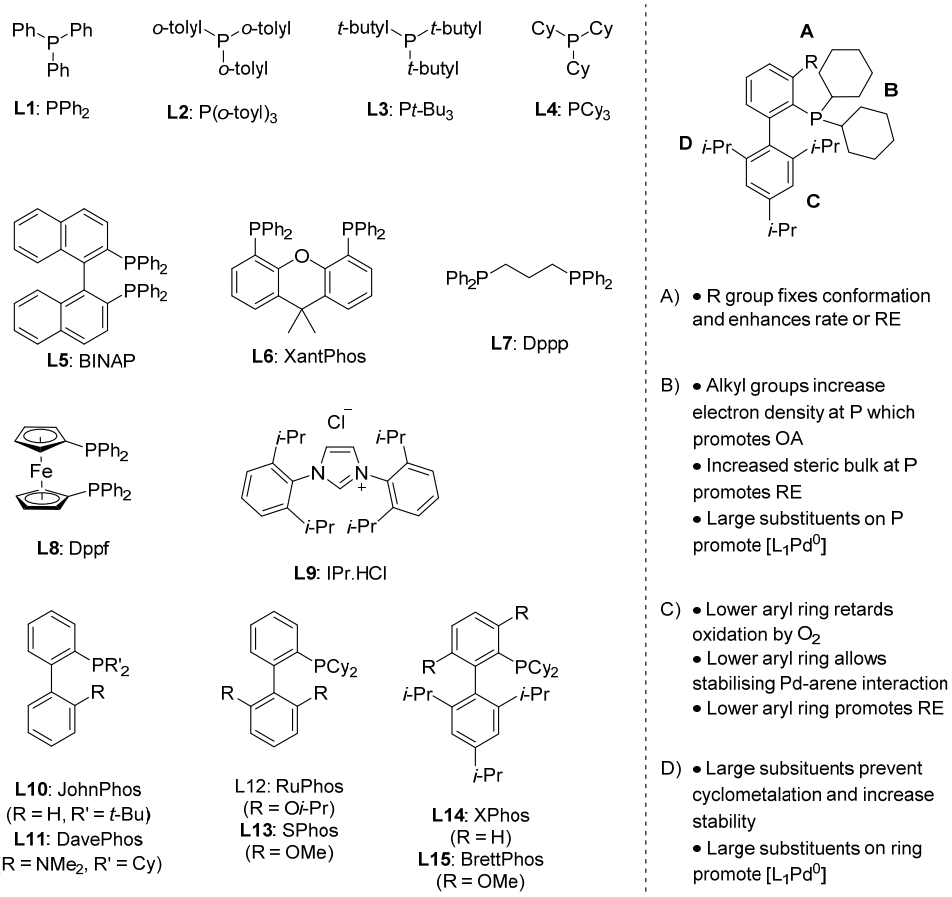

Figure 53. Ligands successfully applied in the Buchwald-Hartwig amination reaction and important structural features of diarylphoshine type ligands.[180,181] OA = oxidation addition. RE = reductive elimination.

8.2 Direct Arylation

Reactions such as the Suzuki-Miyaura and Negishi cross couplings have widespread application throughout synthetic organic chemistry.[189–193] This is due to the fact that the conditions employed are usually mild and a large number of functional groups can be tolerated which results in high yielding, selective reactions.[194] However, both coupling partners need to be preactivated, one with a halogen (typically X = Br, I) and the other with a metal (Scheme 11, Entry (i)). The synthesis of these preactivated starting materials can require several steps and can be wasteful, costly and time consuming. The removal of stoichiometric amounts of metal and halogen by-products is also a concern, especially on industrial scales. It could be envisaged that if the metal coupling partner could be replaced with something more benign, such as a halogen (X = Cl) or even a hydrogen, then these reactions would be cleaner and more efficient. The ideal case would be the coupling of two C-H bonds (Scheme 11, Entry (iii)). However, this is unrealistic due to the energy that would need to be put into the reaction to overcome the strength of the C-H bonds. This approach would

also lead to selectivity issues if there was more than two C-H bonds available for coupling. Currently the best approach would be the substitution of one of the preactivated species (preferably the metal) with an arene (Scheme 11, Entry (ii)). This area of research is defined as direct arylation *via* C-H activation.

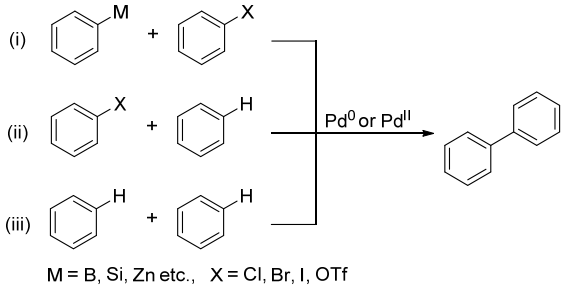

Scheme 11. Possible C-C bond forming routes. **(i)** The use of two preactivated substrates. **(ii)** The use of one preactivated substrate. **(iii)** The direct coupling of two arenes.

Several different types of direct arylation strategies exist which help to control the regioselectivity of reactions. These include using (i) directing groups, (ii) tethers, or (iii) electronic effects.[195] The use of oxidative coupling conditions have also been employed to drastically improve the yield of some reactions (Scheme 12, Entry (iv)).

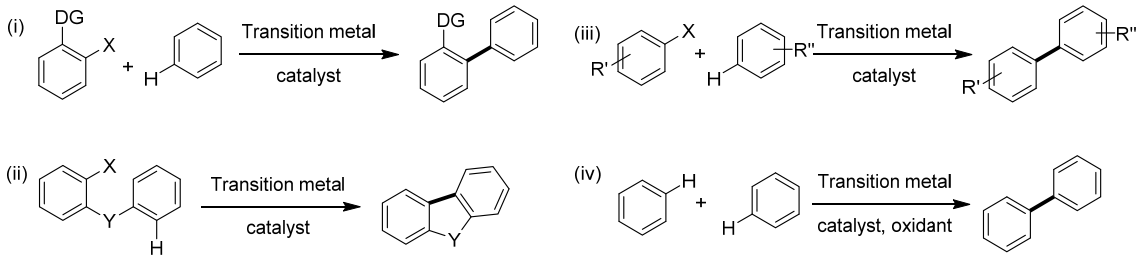

Scheme 12. Strategies used to control direct arylation.[195]

To date multiple different transitions metals, including Pd, Rh, and Ru, have been shown to be applicable to direct arylation reactions.[196] The mechanism by which direct arylation reactions proceed is heavily influenced by the choice of transition metal employed, the base, ligand, solvent, and coupling partners chosen.[197] It is generally accepted that the metal catalyst will oxidatively add into the aryl-halide bond to give an intermediate such as **3.22** (Scheme 13). Several different mechanisms have then been proposed by different academics however, as previously mentioned, they are very reaction specific.[198–205]

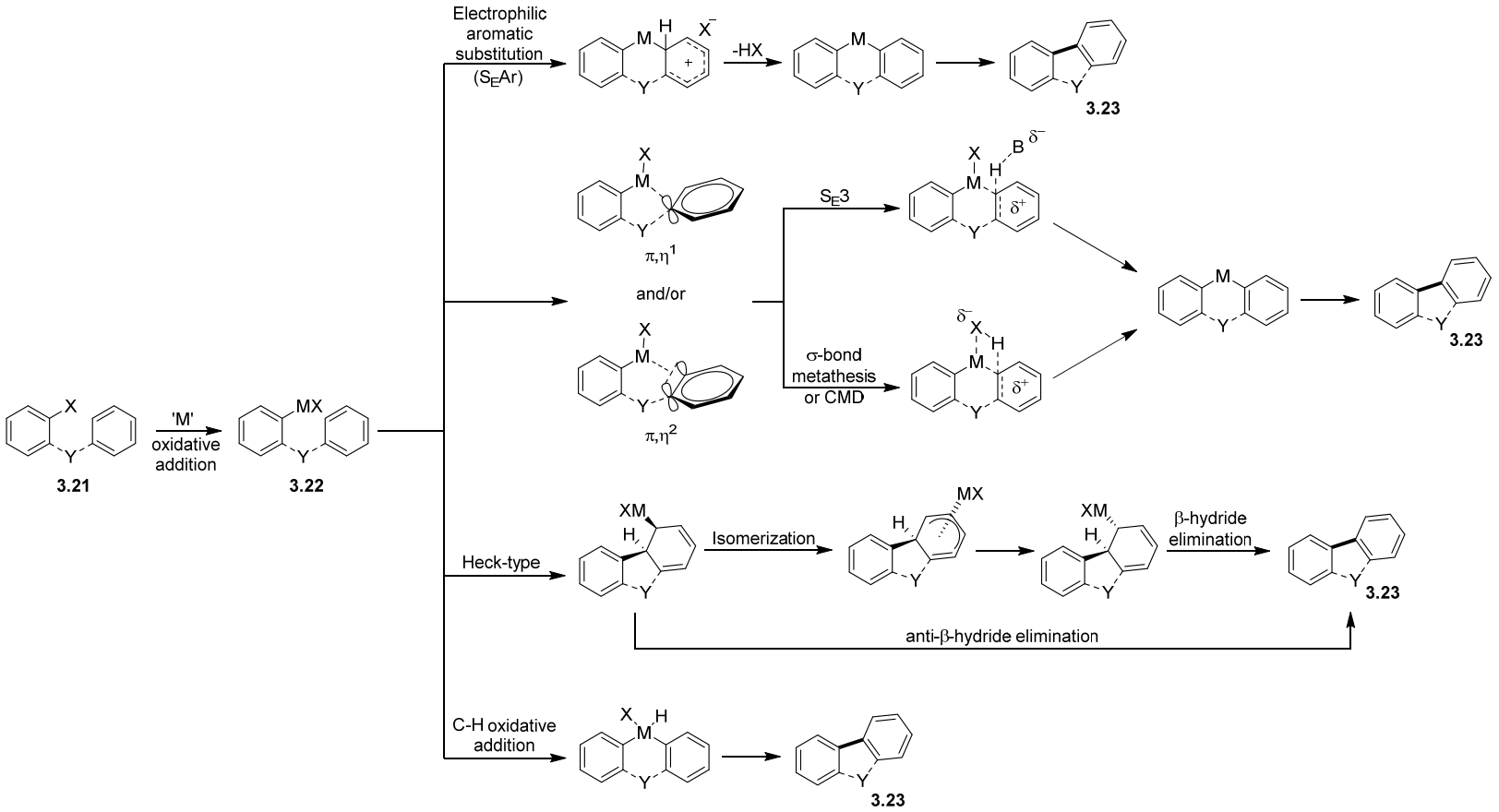

Scheme 13. Possible mechanisms for direct arylation *via* C-H activation.[198–205]

8.2.1 Mechanism of Palladium Catalysed Direct Arylations

To elucidate the mechanisms of reactions, kinetic isotope effects (KIEs) are often studied as these can convey important information on the rate determining step (RDS) in a reaction. Rate constants are measured for a reaction where the starting material is isotopically labelled then the ratio of k_L/k_H is calculated. Traditionally deuterium is installed in place of hydrogen as this gives the best kinetic isotope results due to the 100 % increase in mass.[206] Primary KIEs suggest that the RDS occurs when the bond to the isotopically labelled atom is being either formed or broken. Secondary KIEs arise if this bond formation or breaking is not the RDS.[207] In relation to palladium catalysed direct arylation reactions, if a primary KIE is observed then this is strong evidence that C-H bond cleavage and Pd-C bond formation is happening simultaneously. This points to either a substitution electrophilic trimolecular (S_E3) mechanism or σ-bond metathesis mechanism (sometimes referred to as concerted metalation deprotonation (CMD)). A S_E3 mechanism arises when the acidic proton is abstracted by an external base as the Pd-C bond is being formed. On the other hand, if an anionic ligand is present on the palladium centre, then this can remove the proton while the Pd-C bond is formed *via* σ-bond metathesis (Scheme 13).[208]

Work initially by Echavarren,[209,210] and followed on by Fagnou,[211–215] has shown intramolecular direct arylations favour electrophilic palladation pathways with proton extraction carried out either by ligands coordinated to the palladium centre or by external bases, such as carbonate or pivalate. These routes were initially proposed by Echavarren and Maseras while examining the selectivity of **3.24** under palladium catalysed direct arylation conditions (Table 4).

Table 4. Direct arylation selectivity studies.[209]

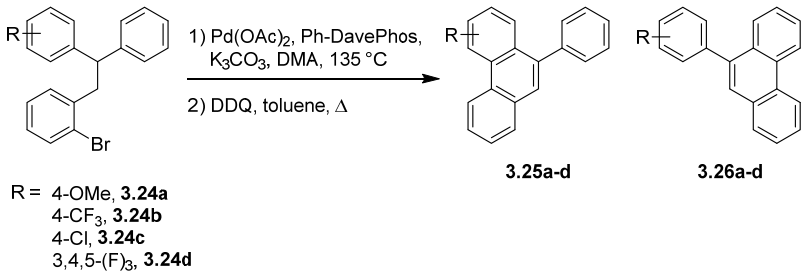

R = 4-OMe, **3.24a**
4-CF_3, **3.24b**
4-Cl, **3.24c**
3,4,5-$(F)_3$, **3.24d**

Entry	Substrate	Yield (%)	Ratio (3.25/3.26)
1	**3.24a**	90	1.1:1
2	**3.24b**	71	1.3:1
3	**3.24c**	66	1.5:1
4	**3.24d**	82	25:1

They found consistent selectivity for the substituted ring, even when bearing electron donating (OMe) and highly electron withdrawing (3,4,5-$(F)_3$) groups. A large KIE of 5.0 was observed which, along with the selectivity, was not consistent of a reaction proceeding *via* a S_EAr mechanism. Their conclusion was that the reaction proceeded *via* proton abstraction either by an external base or a ligand attached to the metal centre. This was then further examined using DFT modelling which concluded that both assisted processes were much more favourable than an unassisted one (by under 20 kcal/mol).[210]

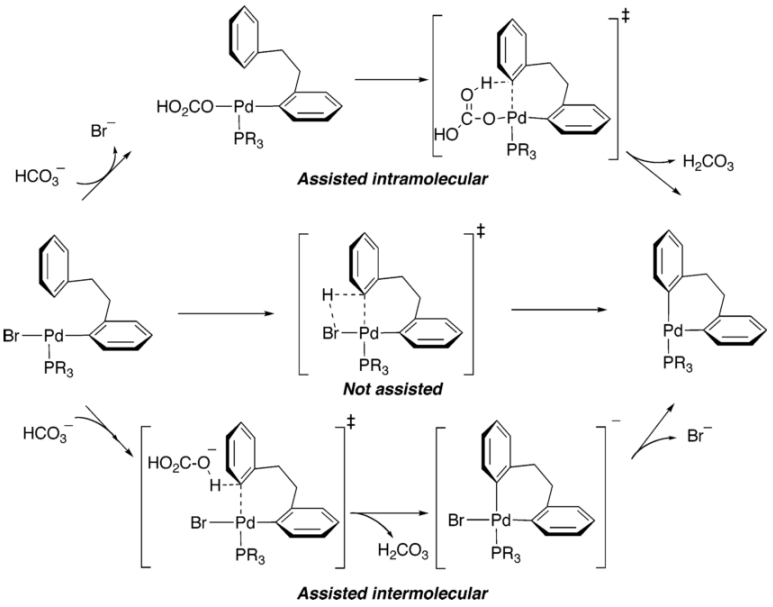

Figure 54. Possible catalytic cycles for palladium catalysed direct arylation.[210]

Work in the Fagnou laboratory discovered that electron withdrawing ligands were particularly effective in direct arylation processes, especially for more challenging substrates such as the synthesis of the 7-membered ring compound **3.28**. This was demonstrated with the intramolecular direct arylation of **3.27** where a low yield of 35 % was achieved with Ph-DavePhos (**L16**), while the CF_3 containing biaryl **L17** produced a 92 % yield after 6 hours heating. Again the KIE was measured at 3.5 which again suggested a CMD mechanism.[211]

Table 5. Effects of ligand on formation of 7-membered ring **3.28**.[211]

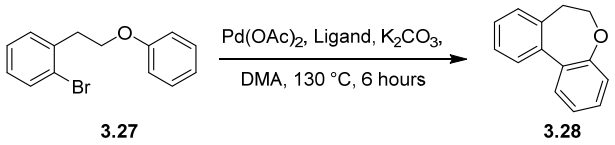

3.27 **3.28**

Entry	Ligand	Yield (%)[a]
1	**L16**	35
2	**L17**	92

[a] Yield determined by GCMS, n = 3.

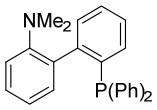

L16

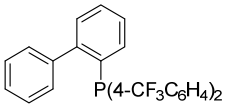

L17

Fagnou also discovered that the use of pivalic acid as an additive gave superior results in direct arylation reactions. A selection of carboxylic acid additives were examined in the reaction of **3.29**, with an increase in bulk of the additive having positive effects on yield (Table 6). It was hypothesised that this reaction again was proceeding through either a CMD or S_E3 mechanism or both (KIE = 5.4).[216]

Table 6. Effects of carboxylic acid additive on formation of **3.30**.[216]

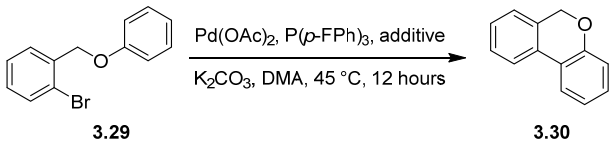

3.29 **3.30**

Entry	Additive	Yield (%)[a]
1		31
2		32
3		63
4		100

[a] Yield determined by GCMS

Increasing evidence suggests that CMD or σ-bond metathesis mechanisms are favoured for intramolecular direct arylation reactions catalysed by palladium. There have been several reports of C-H activation mechanisms, however computational studies have suggested that this process is energetically more costly and requires the oxidation of the palladium centre to a Pd(IV) species.[203] Also, as previously mentioned, KIEs from example reactions do not suggest S_EAr are

at play. Unfortunately, general reaction conditions seem difficult to predict which makes optimisation of reaction conditions necessary every time.

8.3 Carbazole formation *via* Sequential Buchwald-Hartwig Amination and Direct Arylation

Carbazoles are synthetically useful structures and are the core to many natural products and biologically active compounds.[217] There are many synthetic procedures in the literature to form the carbazole core including classic reactions such as the Borsche–Drechsel cyclization,[218,219] or transition metal mediated cyclisation of 2-aminobiaryls,[214,220,221] Larock's benzyne synthesis[148,149] and routes from functionalised and unfunctionalized indoles.[146,222–224] Carbazoles have also been successfully constructed *via* consecutive Pd-catalysed Buchwald-Hartwig amination and direct arylation separately by Ackermann,[225,226] Bedford,[227–229] Buchwald,[230] and Fagnou.[212,213]

The first example of this one pot process was shown by Bedford *et al.,* to synthesise the *N*-methyl and *N*-benzyl protected carbazoles of type **3.33**.[227] Electron donating and neutral aryl bromides (**3.32)** along with electron withdrawing and neutral 2-chloroanilines (**3.31**) were tolerated, with yields ranging from 27 – 61 % (Scheme 14). However, the use of *N*-H anilines impeded the reaction after the Buchwald-Hartwig amination.

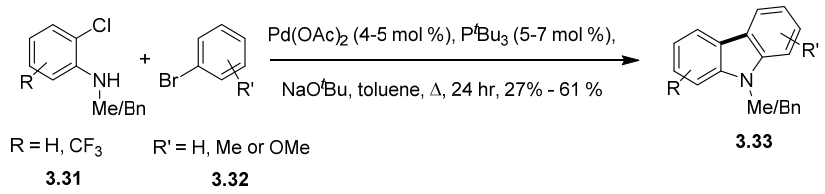

Scheme 14. General synthesis of a range of *N*-substituted carbazoles *via* consecutive Pd-catalysed Buchwald-Hartwig amination and direct arylation.[227]

Four years later Bedford published a second paper where *N*-H carbazoles were efficiently synthesised with the aid of microwave heating which allowed high temperatures to be reached.[228] The synthesis of the natural product Clausine P (**3.37**) was achieved, along with several other carbazoles containing EDGs on both the aryl bromide and the 2-chloroaniline. Interestingly, it was found that if the reaction was performed in a one-pot manner under microwave conditions then the best solvent was toluene. However, if the reactions were carried out separately by thermal means then toluene was more efficient for the Buchwald-Hartwig amination and 1,4-dioxane was more efficient for the direct arylation reaction.

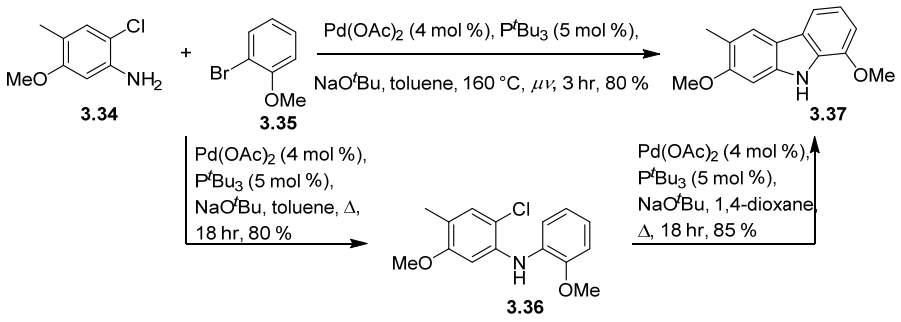

Scheme 15. Synthesis of Clausine P (**3.37**).[228]

Ackermann and Althammer[225] showed that inexpensive dichloroarenes (eg., **3.39**) could be successfully coupled with *N*-H and *N*-Ph anilines using $Pd(OAc)_2$, PCy_3, K_3PO_4, and NMP heated at 130 °C thermally for 18 hours to form a range of carbazoles. This is exemplified by the synthesis of the natural carbazole product Murrayafoline A (**3.40**) with comparable yields from coupling of **3.38** with both 1,2-dichlorobenzene (**3.39a**) and 1-bromo-2-chlorobenzene (**3.39b**).

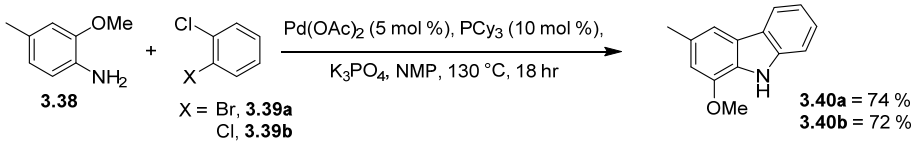

Scheme 16. The synthesis of Murrayafoline A (**3.40**).[225]

A solvent study found that polar aprotic solvents such as NMP and DMA performed better in the synthesis of *N*-H carbazoles (**3.43**), while non-polar solvents such as toluene caused the reaction to stall after the Buchwald-Hartwig amination (Table 7, Entry 1). They also found that a more concentrated reaction solution resulted in a lower yield (Table 7, Entry 10 *vs.* 11).

Table 7. Optimisation study for the synthesis of *N*-H carbazole **3.43**.

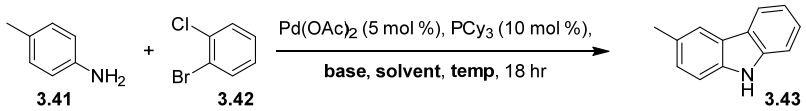

3.41 3.42 3.43

Entry	Solvent	Base	Temp (°C)	Yield (%)[a]
1	Toluene (0.1 M)	NaO^{t}Bu	105	N/A[b]
2	DMA (0.1 M)	K_2CO_3	130	60
3	DMA (0.1 M)	Cs_2CO_3	130	51
4	DMA (0.1 M)	K_3PO_4	130	79
5	DMF (0.1 M)	K_3PO_4	130	6[c]
6	DMPU (0.1 M)	K_3PO_4	130	<2[c]
7	NMP (0.1 M)	K_3PO_4	130	81
8	NMP (0.1 M)	K_2CO_3	130	76
9	NMP (0.1 M)	K_3PO_4	100	53
10	NMP (0.5 M)	K_3PO_4	130	69
11	NMP (1.0 M)	K_3PO_4	130	25[c]

[a] Yields of isolated products.
[b] Reaction stalled after Buchwald-Hartwig amination. Yield of diarylamine intermediate was 94 %.
[c] GC conversion.

9 Aims of Chapter 3

Although there is a considerable number of published routes towards the natural product ellipticine, many of them do not allow the ability to functionalise the structure with ease. The routes tend to be linear in nature and low yields are prevalent. The aim of this work was to develop a highly modular alternative to existing approaches *via* a consecutive Pd-catalysed Buchwald-Hartwig amination and direction arylation (Scheme 17).[228,231] This would provide access to the ellipticine core (**3.45**) from 2-chloroaniline (**3.46)**, which is cheap and has many analogues readily available, and 6-bromoisoquinoline-5,8-dione (**3.47**), which would require initial synthesis. Then methylation and reduction could be used to install the dimethyl groups of ellipticine (**3.44**).

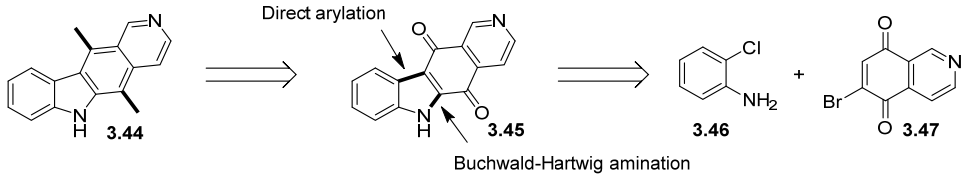

Scheme 17. Proposed retrosynthesis of ellipticine.

Once optimised, the limitations of this route will be explored and will be used to build a compound library of ellipticine analogues which could be tested in Bcl-x splicing assays to establish SAR information.

10 Results and Discussion

10.1 Pd-Catalysed Carbazole Formation by a Sequential Buchwald-Hartwig Amination/Direct Arylation Process

The conditions published by both Bedford and Ackermann for carbazole formation were initially investigated to see whether they would be a suitable starting point for the synthesis of the ellipticine core. The work by Bedford *et al.* looked appealing as carbazoles of type **3.49** could be formed in 3 hours under microwave irradiation in 79 % yield (Scheme 18).

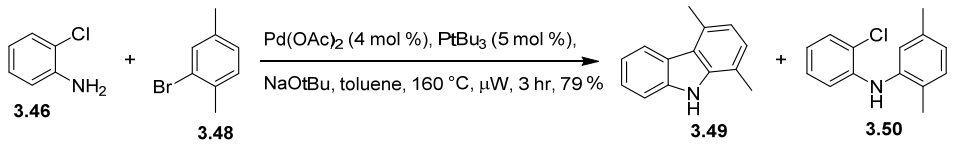

Scheme 18. Synthesis of 1,4-dimethyl-9*H*-carbazole (**3.49**).[228]

Using the literature conditions and reagents, only 26 % of **3.49** was isolated. The diarylamine intermediate **3.50** was also isolated during purification. Next, conditions developed by Ackermann were explored.[226] A small selection of reactions were run to optimise the reaction conditions to prepare carbazole **3.43** (Table 8). In Entry 1, 1,2-dichlorobenzene was reacted with 4-methylaniline (**3.41**) at a temperature of 145 °C. Unfortunately the major product was the Buchwald intermediate **3.52** (41 %), with no **3.43** being isolated. The temperature was increased to 170 °C (Entries 2 and 3), and also the ligand was changed to the tetrafluoroborate salt of PCy_3, $HPCy_3BF_4$. When 1,2-dichlorobenzene was employed, LCMS analysis after 18 hours of heating showed the major product to be the Buchwald intermediate **3.52** by LCMS analysis. Conversely, when 1-bromo-2-chlorobenzene was utilised the reaction proceeded well with 41 % of 3-methyl-*9H*-carbazole **3.43** being isolated. Synthesis of **3.43** was then conducted on a 1 g scale using these conditions, which resulted in a yield of 64 %.

Table 8. Synthesis of 3-methyl-9*H*-carbazole (**3.43**).[226]

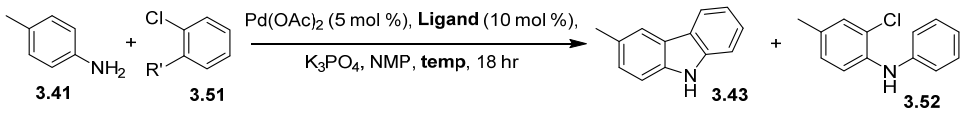

3.41 3.51 3.43 3.52

Entry	R_1	Temperature (°C)	Ligand	Major Product	Yield (%)
1	Cl	145	PCy_3	**3.52**	41
2	Cl	170	$HPCy_3BF_4$	3:1 **3.52** : **3.43**	Not isolated
3	Br	170	$HPCy_3BF_4$	**3.42**	64

Using the conditions above, the synthesis of 1,4-dimethyl-9*H*-carbazole (**3.49**) was reattempted. This time 49 % of **3.49** was isolated at a 1.6 mmol scale and 52 % at a 5.4 mmol scale. As anticipated, the major side product was the diarylamine intermediate (Scheme 19).

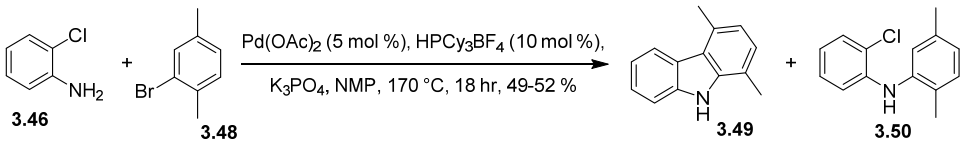

3.46 3.48 3.49 3.50

Scheme 19. Synthesis of 1,4-dimethyl-9*H*-carbazole (**3.49**).

Conditions where the Buchwald-Hartwig amination and C-H activation step were attempted separately were also investigated. For the first step in the reaction the conditions were altered to use the highly active catalyst BrettPhos **L15** which has shown superior results in the coupling of aryl mesylates and the monoarylation of primary amines.[230,232] A high yield of 72 % was achieved for compound **3.53** (Scheme 20).

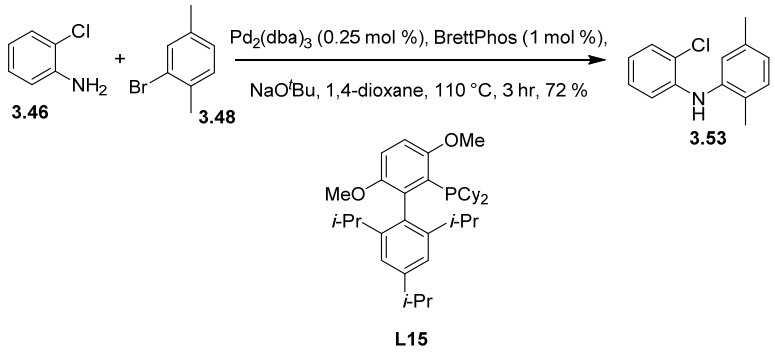

3.46 3.48 3.53 L15

Scheme 20. Synthesis of *N*-(2-chlorophenyl)-2,5-dimethylaniline (**3.53**).

The subsequent preparation of the carbazole **3.49** from **3.53** *via* direct arylation was attempted using two different conditions (Scheme 21, Conditions A and B, respectively). Conditions A were the coupling conditions previously reported in Scheme 19 and these afforded **3.49** in a reasonable

65 % yield. However the two-step process had a slightly lower overall yield than the one-step process in Scheme 19 (47 % vs 52 %).

It has been proposed that direct arylation reactions that proceed through a concerted deprotonation pathway can be promoted by the addition of PivOH by facilitating the deprotonation of **3.53**.[216,231,233] Conditions were adapted from Buchwald[233] for the direct arylation of **3.53**, unfortunately these conditions resulted in a considerable drop in the yield of **3.49** (11 %).

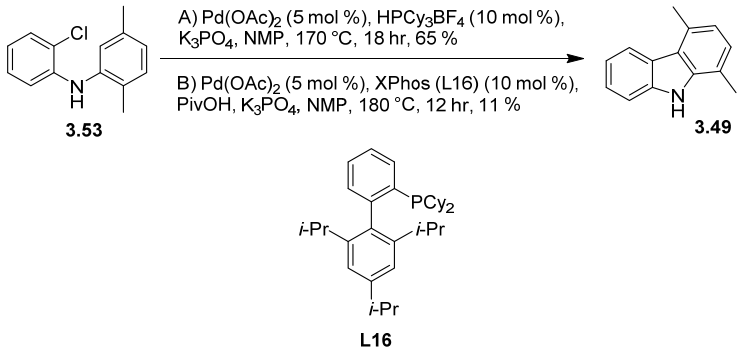

Scheme 21. Synthesis of 1,4-dimethyl-9*H*-carbazole (**3.49**)..

As a proof of concept, the coupling of 2-chloroaniline (**3.46**) and 6-bromoisoquinoline (**3.54**) was attempted to prepare **3.55** which would furnish the tetracyclic core of ellipticine in one step (Scheme 22).

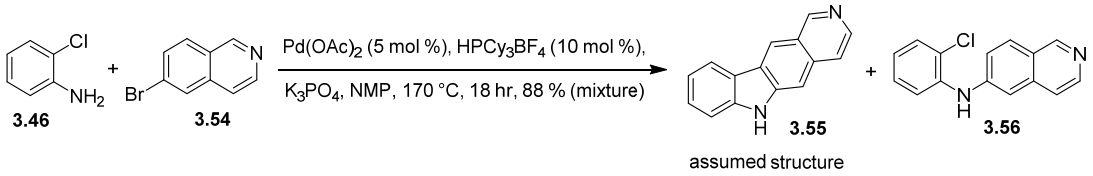

Scheme 22. Synthesis of 6*H*-pyrido[4,3-*b*]carbazole (**3.55**).

Unfortunately this reaction provided a mixture of both the desired product **3.55** and the diarylamine intermediate (**3.56**) even after column chromatography, with the intermediate being the major product (3:2 ratio by LCMS). It was concluded that further optimisation of the reaction conditions were required for the preparation of the ellipticine core.

10.2 Optimisation of Conditions for the Tetracyclic Ellipticine core by a Sequential Buchwald-Hartwig Amination/Direct Arylation Process

The variables of temperature, solvent, ligand and base were investigated to probe the reaction conditions required for the sequential Buchwald-Hartwig amination and direct arylation using 2-chloroaniline (**3.46**) and 6-bromoisoquinoline (**3.54**) to yield the ellipticine analogue **3.55**. Microwave irradiation was utilized to reduce reaction times.[228] Initially a selection of polar non-protic and non-polar solvents that had high boiling points were tested. The Pd source, ligand and base were kept the same as the conditions for *N*-H carbazole synthesis (Scheme 22). Initial test reactions were carried out at 160 °C and the time was shortened to 3 hours (Scheme 23).

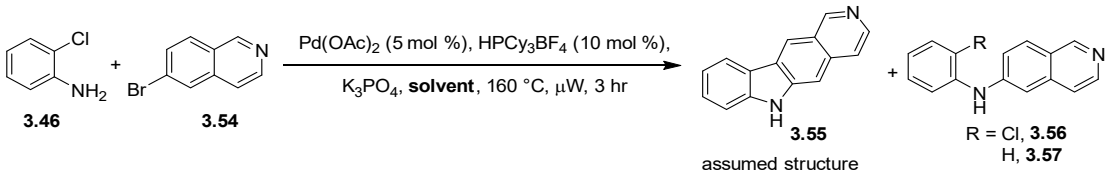

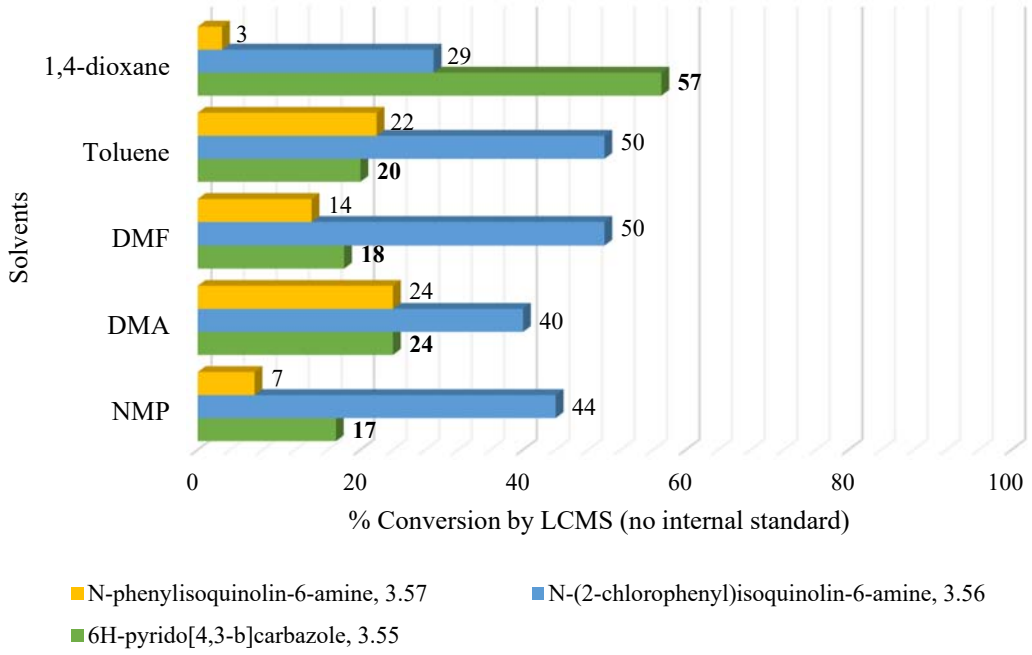

Scheme 23. Screen of solvents for the synthesis of 6*H*-pyrido[4,3-*b*]carbazole (**3.55**). Percentage conversion to product shown in bold on graph. No internal standard used, Percentage conversion measured by LCMS.

After 3 hours, it was clear that 1,4-dioxane provided superior results over the other solvents tested including toluene which is commonly used in these types of transformations.[197] It was also noted that the reaction profile by LCMS analysis looked much cleaner when 1,4-dioxane was employed

which was expected to make purification of these reactions easier. Reactions run with toluene, DMF, DMA and NMP gave low conversions to the desired product **3.55**. Interestingly, over 20 % conversion to the dehalogenated side product **3.57** was observed with toluene and DMA.

A screen of several ligands and bases was examined using an Anton Paar microwave, which can process up to 40 samples at a time. However, all the reactions performed much worse than expected, with low yields of both the product **3.55** and intermediate **3.56** (Table A1). It was believed that the high temperatures needed for the reaction were not being reached, thus not allowing the reactions to proceed. A second screen was then attempted, which employed 4 different ligands and 3 commonly used bases, using a single sample microwave. The reactions were heated using microwave irradiation held at 160 °C for 6 hours before being analysed by RP-HPLC. The best results were obtained using K_3PO_4 in combination with the electron rich dialkylbiaryl phosphine Buchwald ligand DavePhos in 1,4-dioxane (Scheme 24). Pleasingly, none of the reactions produced traceable amounts of the dehalogenated side product **3.57**.

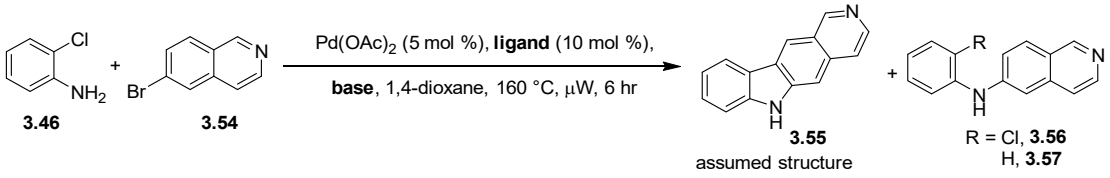

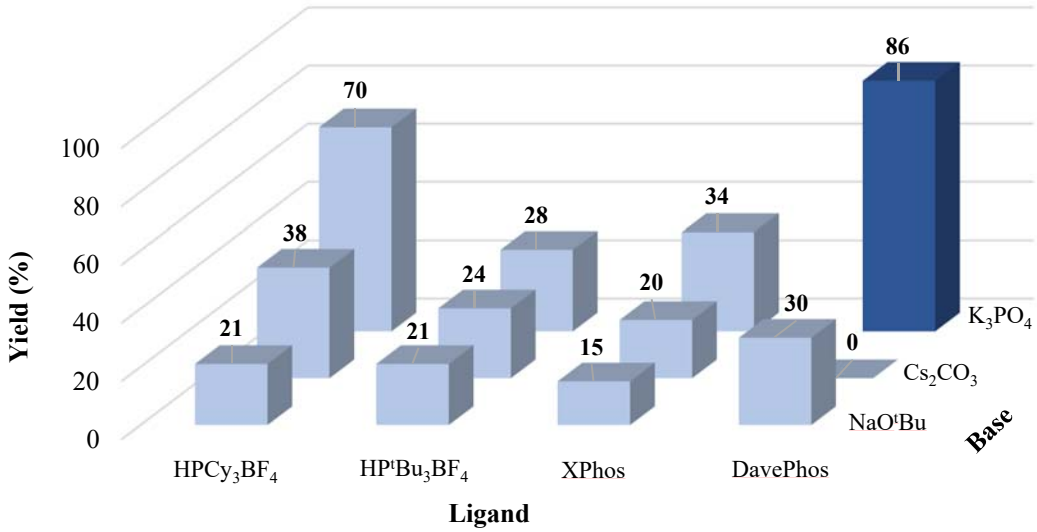

Scheme 24. Screen of ligands and bases for the synthesis of 6*H*-pyrido[4,3-*b*]carbazole (**3.55**). % yield determined by RP-HPLC analysis. Yields shown in bold on graph.

When this screen was initially run it was anticipated that the regioisomer that had formed was **3.55**. However, after further analysis by 2D NMR, it was found that the product isolated was

actually regioisomer **3.55b**. Positions 5 and 8 of 6-bromoisoquinoline are the most electrophilic[234] and therefore more susceptible to the direct arylation reaction. After the Buchwald-Hartwig amination has taken place, the isoquinoline is tethered in place at the 6 position therefore the direct arylation will take place at the nearest electrophilic site (position 5 over position 7). This reactivity has previously been documented by Fagnou using naphthalene systems.[213]

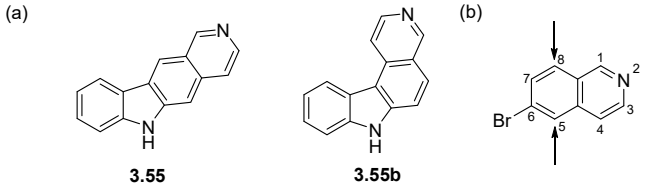

Figure 55. (a) Possible regioisomers that could form from the sequential Buchwald-Hartwig amination and direct arylation reaction. (b) Most electrophilic sites of 6-bromoisoquinoline highlighted by arrows.

Although this reactivity was disappointing as it did not provide the correct regioisomer for the ellipticine core, the product isolated would still be useful to test as a G4 stabilising ligand.

10.3 Synthesis of Library of Buchwald-Hartwig Amination Compounds

With optimized conditions for a sequential Buchwald-Hartwig direct arylation established, the scope of this methodology to synthesise a palette of fused heterocyclic compounds was explored. It was noted that using different microwave systems, gave varied reaction profiles and the appearance of the double amination product **3.58** was occasionally observed (Figure 56). To allow full control over each step of the reaction, the methodology was altered to heat the reaction at 120 °C for 30 minutes to allow the Buchwald-Hartwig reaction to go to completion before subsequently heating the reaction to 160 °C for 8 hours. This was to ensure that no 6-bromoisoquinoline was left after 30 minutes, preventing an undesirable second amination reaction from taking place.

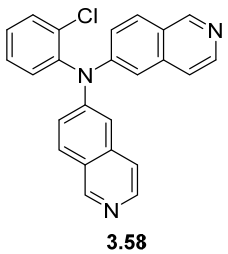

Figure 56. Unwanted side product obtained with different microwave instruments.

Using this method, a palette of 19 diarylamine compounds (**3.61a – 3.61s**) were prepared with isolated yields that ranged from 8 – 99 % (Scheme 25). The conditions tolerated a range of

electron donating (**3.61a**, **b**, **e**, **i**, **l – o** and **q – r**) and electron withdrawing (**3.61c**, **d**, **f** and **g**) 2-chloroanilines with a selection of bromo-heteroaryls. sp^3 character was introduced by coupling with chromane and 2,5-dihydrofuran derivatives (**3.61o – q**). Pleasingly, the quinone derivative **3.61r** was isolated in a 98 % yield, however coupling of the unprotected phenol only produced **3.61s** in an 8 % yield. Compound **3.61d** was isolated in 83 % yield, however harsher heating conditions had to be employed. Unfortunately naphthalene, benzimidazole, indole and indazole compounds (**3.61u – y**) did not couple at all, with only starting material remaining after heating.

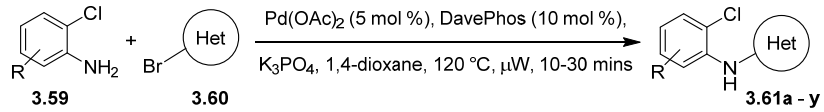

3.59 **3.60** **3.61a - y**

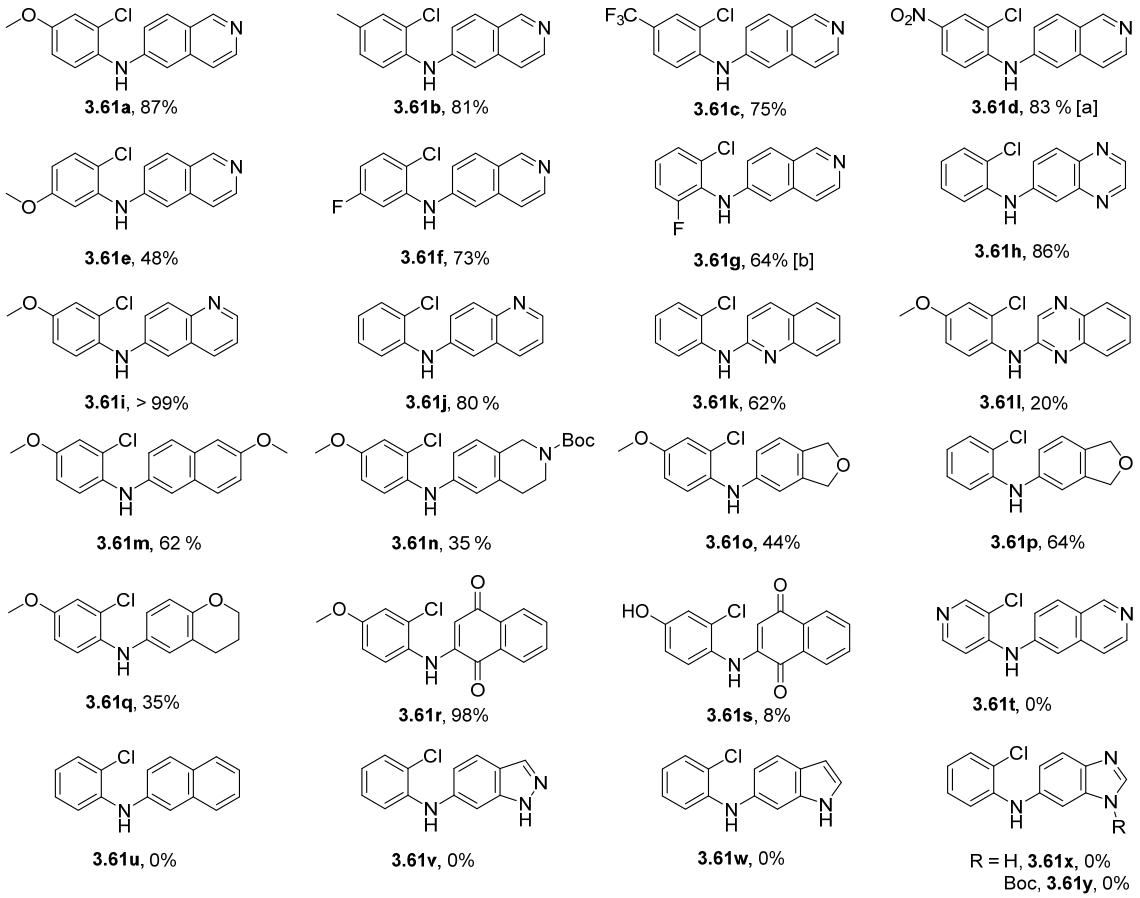

[a] At 160 °C for 6 hr. [b] At 120 °C for 10 mins. Yield determined by RP-HPLC analysis.

Scheme 25. Substrate scope for microwave-assisted Buchwald-Hartwig amination

Notably, the reaction of 4-methoxy-2-chloroaniline and 6-bromoquinoline produced diarylamine **3.61i** in quantitative yield. In the reaction of 2-chloro-4-methoxyaniline and 2-bromoquinoxaline,

the double amination **3.61z** and full cyclisation **3.62f** side products (Figure 57) were also isolated in 23 % and 16 % yield, respectively.

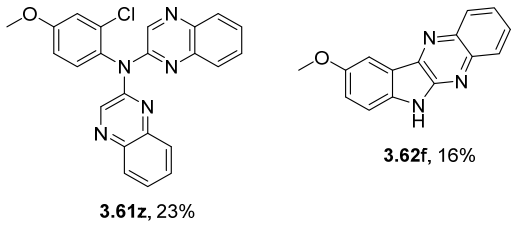

3.61z, 23% **3.62f**, 16%

Figure 57. Side products obtained from reaction of 2-chloro-4-methoxyaniline and 2-bromoquinoxaline.

10.4 Optimisation of 'One-pot' Reactions Conditions to Prepare the Ellipticine Core

The domino reaction was then explored in a one-pot, two-step methodology. A selection of electron donating and withdrawing 2-chloroanilines and nitrogen rich heterocycles were tolerated, producing compounds **3.62a – g** in 11 – 88 % yield (Scheme 26). It was envisaged that if coupling with 2-bromonaphthalene-1,4-dione was successful, this would provide a route to install the dimethyl substituents of ellipticine, *via* methylation and reduction in an efficient manner, avoiding difficulties generally found in previous methods.[145,235] Fortunately, this analogue performed well in the two-step reaction with isolated yields of 34 – 90 % obtained for a variety of A-ring coupling partners (**3.62h – k**).

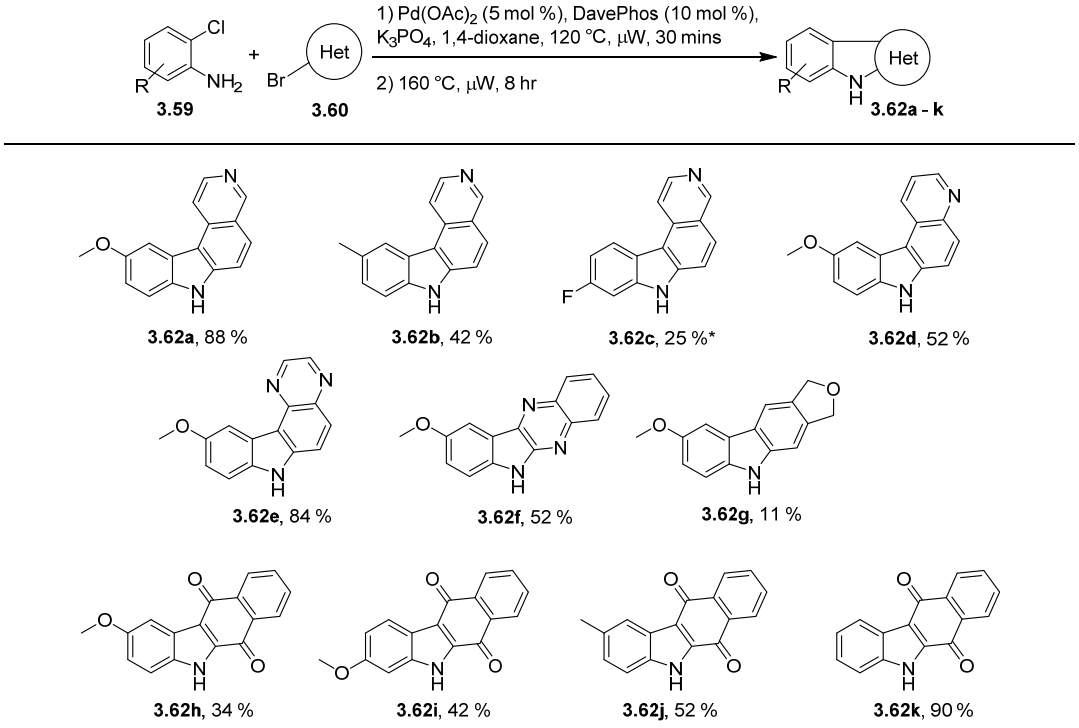

Scheme 26. Substrate scope for microwave-assisted C-H activation/direct arylation. * Product isolated as a mixture with diarylamine intermediate.

10.5 Methylation and reduction to produce ellipticine

Previous preparative methods of the ellipticine core have used a dione functionality to install the dimethyl groups of ellipticine (**2.5**).[236,237] It was proposed that treatment with MeLi and reduction with $NaBH_4$, or similar, would allow installation of the dimethyl groups in the coupled dione core of **3.62h**. Conditions were adapted from Gribble *et al.*,[145] using substrate **3.62h**, however it was found that only the monomethylated product **3.63** was obtained (70 %, Scheme 27).

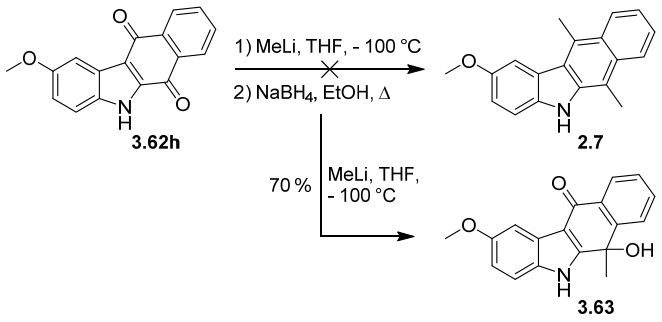

Scheme 27. Attempted synthesis of 2-methoxy-6,11-dimethyl-5*H*-benzo[*b*]carbazole (**2.7**).

It was envisaged that the lone pair from the nitrogen was in resonance with the carbonyl at the 11-position, reducing the electronegativity of this position. Protecting the nitrogen with a benzyl group reduces this resonance problem and should allow the installation of both methyl groups.[238]

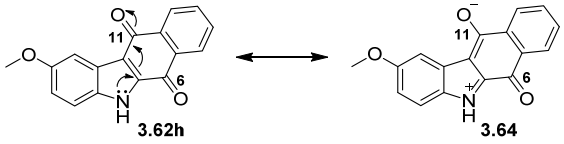

Figure 58. Hypothesised formation of methylation side product 6-hydroxy-2-methoxy-6-methyl-5,6-dihydro-11*H*-benzo[*b*]carbazol-11-one (**3.63**).

However, the monomethylated product **3.63** was isolated in a 70 % yield and provided access to unsaturated C-ring derivatives of the ellipticine core. This could allow facile installation of a number of nucleophilic species in the C6 position in future, including labelled alkyl groups which could provide important information about the metabolism and interaction of these compounds in the body.

10.6 Synthesis of ellipticine C/D ring fragment

In order to complete the synthesis of ellipticine (**2.5**) a suitable C/D ring fragment had to be synthesised**.** A route to quindoline derivative **3.67** had been proposed by Miller and Moock[239] which involved Friedel-Crafts acylation of 2-bromo-1,4-dimethylbenzene (**3.48**), followed by oxidation to **3.65**, and then reduction to produce **3.66**. Ozonolysis with ammonium hydroxide reduction furnishes **3.67** in 69 % overall yield. Synthesis was attempted with 1,4-dimethylbenzene (**3.68**), however dehydration of the cyclic alcohol **3.70** towards the indene **3.71** could not be performed. Analysis of the product formed by NMR and LCMS did not show any peaks that would be associated with the desired product.

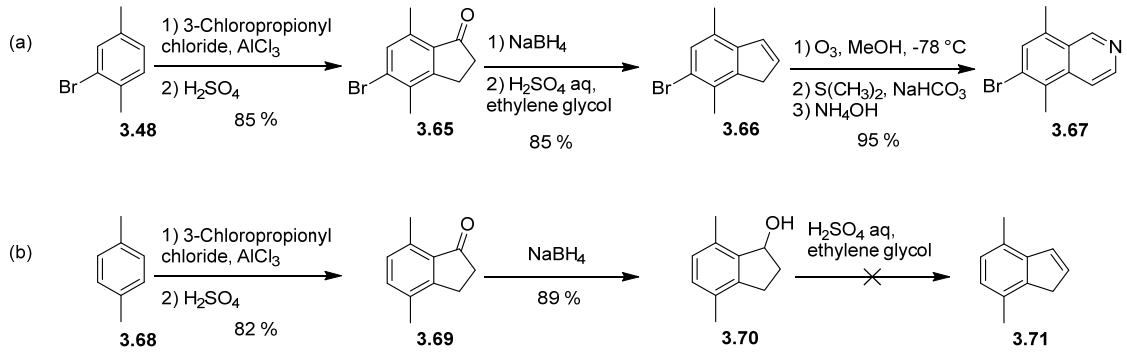

Scheme 28. Synthesis of (a) 6-bromo-5,8-dimethylisoquinoline[239] (**3.67**) and (b) 4,7-dimethyl-1*H*-indene (**3.71**).

A second route to **3.67** was performed using an extended Pomeranz-Fritsch[240] synthesis of isoquinolines, which was similar to the process applied in the Cranwell-Saxton[146] ellipticine synthesis. Mono-formylation of **3.72** and subsequent imine formation was achieved in high yields for both steps, 85 % and 78 % respectively. Reduction of the imine and sulfonyl protection produces **3.74** in a 53 % yield. The final step in the synthesis of **3.67** proved problematic. NMR and LCMS analysis releveled multiple products formed from the cyclisation step, including suspected cyclisation intermediates. However, even after subsequently resubmitting the reaction mixture back to the reaction conditions to force the reaction to completion, the required product **3.67** could not be isolated.

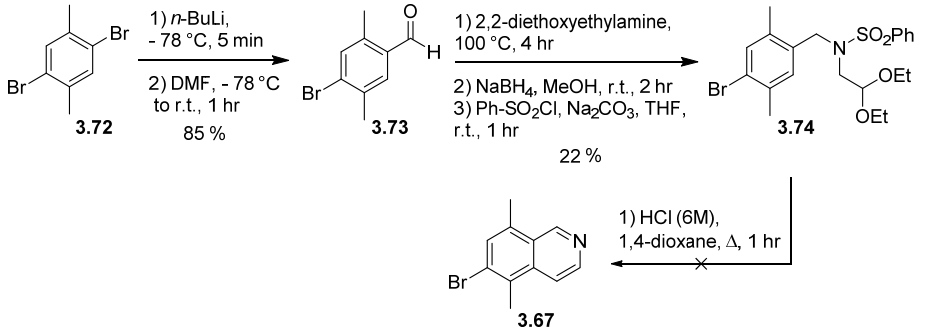

Scheme 29. Synthesis of 6-bromo-5,8-dimethylisoquinoline (**3.67**).

A procedure for the synthesis of **3.47** was discovered starting from either isoquinolin-5-amine (**3.75a**)[241] or isoquinolin-5-ol (**3.75b**).[242] Double bromination and oxidation could deliver the isoquinoline dione **3.47** in two steps which, based on coupling reactions with the naphthalene equivalent, should be successful in the one pot coupling procedure described above for the synthesis of ellipticine (Scheme 26).

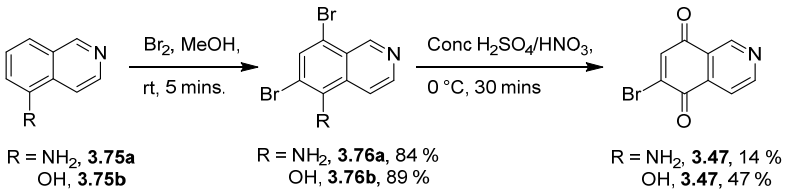

Scheme 30. Synthesis of 6-bromoisoquinoline-5,8-dione (**3.47**).

When this synthetic route was tested, **3.76a** and **b** were successfully isolated in 84 % and 89 % yield from **3.75a** and **b**, respectively. Reactions with NBS and HBr were also attempted, however these proved unsuccessful. The oxidation reaction proved particularly challenging with fresh HNO_3 and H_2SO_4 proving most effective. Consistent work up and purification of the reaction mixture across batches proved difficult. Compound **3.47** was isolated however, in 14 % and 47 %

yield from **3.76a** and **b**, respectively. CrO_3 with acetic acid was also utilised for the oxidation, but this again was unsuccessful and gave only starting material.

With **3.47** in hand, this substrate was used in the consecutive Buchwald-Hartwig direct arylation reaction represented in Scheme 31. Initially a small scale test reaction was run and analysed by LCMS only, with 2-chloroaniline (**3.46**) and **3.47**. The optimised heating conditions were not applied in this reaction, as at this point in the project they had not been developed, therefore the reaction vessel was heated to 160 °C for only 6 hours. LCMS analysis of the crude reaction mixture confirmed the major product to be the Buchwald-Hartwig amination intermediate **3.79a**, with a second, minor peak corresponding to the expected mass of the product **3.45**. This reaction was then repeated using the optimised heating conditions with 4-methoxy-2-chloroaniline (**3.77**). Compound **3.78** was isolated (15 %), however it was not pure by NMR analysis although the major peak by LCMS corresponded to **3.78**. Over 50 % of the starting aniline was recovered but none of **3.47**. The other major side product was the uncyclised Buchwald-Hartwig intermediate **3.79b** (10 %). After heating for 8.5 hours, a considerable amount of black substance was found coating the reaction vessel. This was thought to be palladium black which is believed to have contributed to the low yield observed due to catalyst inactivation.[243,244]

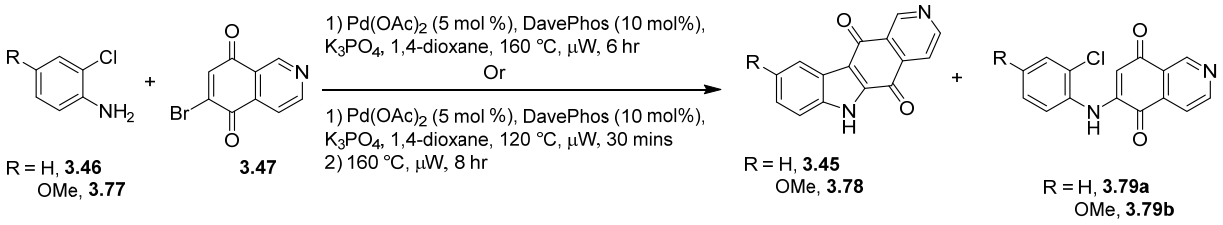

Scheme 31. Synthesis of 5*H*-pyrido[4,3-*b*]carbazole-5,11(6*H*)-dione (**3.45**) and 9-methoxy-5*H*-pyrido[4,3-*b*]carbazole-5,11(6*H*)-dione (**3.78**).

Unfortunately **3.78** could not be isolated in a higher yield in the time frame of the project however, initial investigations (Scheme 26) suggest that this reaction should proceed without any difficulties.

11 Conclusions and Future Work

In summary, a consecutive Buchwald-Hartwig amination/direct arylation reaction under microwave irradiation was developed. This strategy was demonstrated to be a step efficient approach to prepare the backbone of the natural product ellipticine. This general procedure to compounds of this class is highly modular and allows the efficient synthesis of a library of tetracyclic compounds as well as uncyclized diarylamines. Work has successfully been carried out to synthesize the appropriate C/D ring fragment for ellipticine and this has been trialled in the cross coupling reaction to produce 9-methoxy-5*H*-pyrido[4,3-*b*]carbazole-5,11(6*H*)-dione (**3.78**). Unfortunately the yield of this was low, however it is expected that this was due to practical experimental difficulties rather than a failure in the synthetic route. Further work is needed to increase the yield of this step to be comparable with yields from the similar naphthalene dione compounds.

Initially, installation of the dimethyl groups was carried out on 2-methoxy-5*H*-benzo[*b*]carbazole-6,11-dione (**3.62h**), however it was found that the lone pair from N5 was in resonance with the dione which afforded a different reactivity than was initially expected. This stalled the reaction after the first methylation, nevertheless this will allow access to asymmetric compounds of this type which have not been seen in the literature before. To allow both methyl groups to be installed successfully, it is envisaged that protection of the indole nitrogen will need to be investigated.[238]

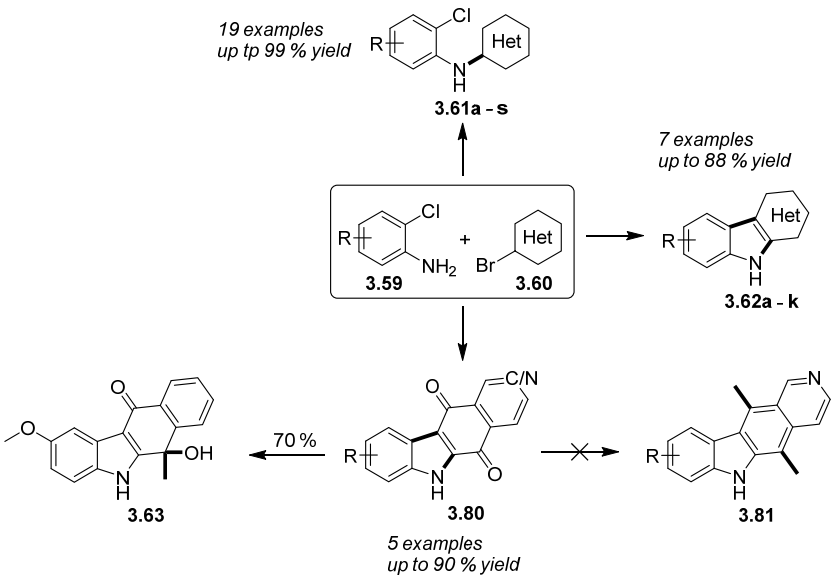

Scheme 32. Summary of synthetic route developed towards the ellipticine backbone and related compounds.

12 Experimental

12.1 General

Reagents and Solvents

All reagents and solvents were obtained from commercial suppliers and were used without further purification unless otherwise stated. Purification was carried out according to standard laboratory methods.[156] Dry solvents for reactions were purchased from Sigma-Aldrich and stored under nitrogen (1,4-dioxane, toluene, NMP, DMF and DMA). DCM, EtOAc, and petroleum ether 40 – 60° for purification purposes were used as obtained from suppliers without further purification.

Experimental Details

Microwave reactions were carried out in capped 2 – 5 mL microwave vials purchased from Biotage. Reactions were carried out at elevated temperatures and pressures using a Biotage Initiator Robot Eight and Sixty microwave.

Purification of Products

Thin layer chromatography was carried out using Merck silica plates coated with fluorescent indicator UV254. These were analyzed under 254 nm UV light. Normal phase flash chromatography was carried out using ZEOprep 60 HYD 40 – 63 µm silica gel. Semi-preparative reverse phase high pressure liquid chromatography (RP-HPLC) purification was carried out on a Dionex 3000 series instrument using an Ace 5 C18-300 250mm x 21.2 mm i.d column. See Appendix for further details.

Spectroscopic Analysis of Products

Fourier Transformed Infra-Red (FTIR) spectra were obtained on a Shimadzu IRAffinity-1 machine. ^{1}H, ^{13}C and ^{19}F NMR spectra were obtained on either a Bruker AV 400 at 400 MHz, 101 MHz and 376 MHz, respectively, or Bruker DRX 500 at 500 MHz, 126 MHz and 471 MHz, respectively. Some ^{13}C and 2D NMR was carried out on a Bruker AVANCEII+ 600 NMR at 600.13 MHz. Chemical shifts are reported in ppm and coupling constants are reported in Hz with MeOD referenced at 3.31 ppm (^{1}H) and 41.0 ppm (^{13}C) and DMSO-d_6 referenced at 2.50 ppm (^{1}H) and 39.52 ppm (^{13}C). High-resolution mass spectra were obtained through analysis at the EPSRC UK National Mass Spectrometry Facility at Swansea University.

LCMS was carried out on either an Agilent HPLC instrument in conjunction with an Agilent Quadrupole mass detector, or an Agilent 1100 HPLC instrument in conjunction with a Waters Micromass ZQ 2000/4000 mass detector. Electrospray ionization (ESI) was used in all cases. GCMS was carried out on an Agilent 5975C inert MSD instrument in conjunction with a Triple-Axis mass detector. Chemical ionization (CI) was used in all cases. Analytical RP-HPLC was carried out on an Agilent 1100 series instrument. See appendix for all method and column parameters.

12.2 General Experimental Procedures

General Procedure for Microwave Assisted Buchwald-Hartwig Amination/Direct Arylation Screen

For example, using $HPCy_3BF_3$ and K_3PO_4 to synthesise 6*H*-pyrido[4,3-*b*]carbazole, **3.55**[245]

6-Bromoisoquinoline (40.0 mg, 0.19 mmol, 1.0 equiv.), 2-chloroaniline (29.4 mg, 0.23 mmol, 1.2 equiv.), $Pd(OAc)_2$ (2.16 mg, 5.0 mol%), DavePhos (7.57 mg, 10 mol%) and K_3PO_4 (122 mg, 0.58 mmol, 3.0 equiv.) were added to a dry microwave vial (2 – 5 mL). 1,4-dioxane (2 mL, 0.1 mol/L) was added and the lid was secured to the vial. The vial was evacuated and purged with argon 3 times and heated at 160 °C for 6 hours under microwave irradiation . An aliquot of the crude reaction mixture was taken (10 uL into 470 uL DMSO), filtered through Mini-Uniprep™ Syringless Filters (GE Healthcare Life Sciences), and analysed by RP-HPLC to calculate RP-HPLC yield. All reactions were sampled in duplicate.

^{1}H NMR (500 MHz, DMSO) δ 12.72 (s, 1H), 9.75 (s, 1H), 9.05 (d, *J* = 6.1 Hz, 1H), 8.81 – 8.67 (m, 2H), 8.39 (d, *J* = 8.9 Hz, 1H), 8.18 (d, *J* = 8.9 Hz, 1H), 7.80 (d, *J* = 8.1 Hz, 1H), 7.60 (td, *J* = 7.8, 1.08 Hz, 1H), 7.48 (td, *J* = 7.7, 1.00 Hz, 1H).
^{13}C NMR (101 MHz, DMSO) δ 146.5, 142.2, 139.1, 134.5, 127.8, 126.0, 122.2, 121.2, 121.9, 118.9, 117.7, 113.0, 112.7.
LRMS (LCMS_High pH, 2 minutes method) R_t = 1.00, m/z = 218.9 $[M + H]^+$.

Table 9. Optimisation of the Reaction Conditions for the One-pot Synthesis of the Ellipticine Core[a]

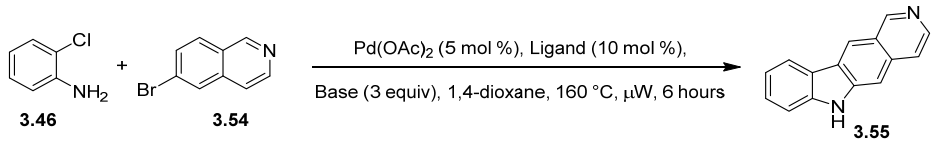

3.46 3.54 3.55

Entry [a]	Ligand	Base	Yield (%) [b]
1	$HPCy_3BF_4$	K_3PO_4	70
2	$HPCy_3BF_4$	Cs_2CO_3	38
3	$HPCy_3BF_4$	NaO^tBu	21
4	$HP^tBu_3BF_4$	K_3PO_4	28
5	$HP^tBu_3BF_4$	Cs_2CO_3	24
6	$HP^tBu_3BF_4$	NaO^tBu	21
7	XPhos	K_3PO_4	34
8	XPhos	Cs_2CO_3	20
9	XPhos	NaO^tBu	15
10	**DavePhos**	**K_3PO_4**	**86**
11	DavePhos	Cs_2CO_3	0
12	DavePhos	NaO^tBu	30

[a] **Reaction conditions: 3.46** (1.2 equiv.), **3.54** (1 equiv.), $Pd(OAc)_2$ (5 mol%), ligand (10 mol%), base (3 equiv.), 1,4-dioxane (2 mL), 160 °C, *μv*, 6 hr. [b] Determined by RP-HPLC analysis.

General Procedure for Microwave Assisted Buchwald-Hartwig Amination

For example, for *N*-(2-chloro-4-methoxyphenyl)isoquinolin-6-amine, **3.62a**

6-Bromoisoquinoline (100 mg, 0.48 mmol, 1 equiv.), 4-methoxy-2-chloroaniline (90.9 mg, 0.58 mmol, 1.2 equiv.), $Pd(OAc)_2$ (5.4 mg, 5 mol%), DavePhos (18.9 mg, 10 mol%) and K_3PO_4 (306 mg, 1.44 mmol, 3 equiv.) were added to a dry microwave vial (2 – 5 mL). 1,4-dioxane (5 mL, 0.1 mol/L) was added and the lid was secured to the vial. The vial was evacuated and purged with argon 3 times and heated at 120 °C for 30 minutes under microwave irradiation . The reaction was cooled, diluted with water (25 mL) and filtered through celite. The organic phase was then extracted with DCM (3 x 50 mL), dried with $MgSO_4$, filtered and the solvent was removed *in vacuo*. The crude compound was purified by silica column chromatography, petroleum ether (40 – 60 °C):ethyl acetate (100:0 → 30:70) to afford the pure compound (**3.62a**) as a brown solid (119 mg, 87 %).

General Procedure for Consecutive Buchwald-Hartwig Amination/Direct Arylation

For example, for 9-methoxy-6*H*-pyrido[4,3-*b*]carbazole, **3.62a**

6-bromoisoquinoline (100 mg, 0.48 mmol, 1 equiv.), 4-methoxy-2-chloroaniline (90.9 mg, 0.58 mmol, 1.2 equiv.), $Pd(OAc)_2$ (5.4 mg, 5 mol%), DavePhos (18.9 mg, 10 mol%) and K_3PO_4 (306 mg, 1.44 mmol, 3 equiv.) were added to a dry microwave vial (2 – 5 mL). 1,4-dioxane (5 mL, 0.1 mol/L) was added and the lid was secured to the vial. The vial was evacuated and purged with argon 3 times and heated at 120 °C for 30 minutes then heated at 160 °C under microwave irradiation . The reaction was cooled, diluted with water (25 mL) and filtered through celite. The organic phase was then extracted with DCM (3 x 50 mL), dried with $MgSO_4$, filtered and the solvent was removed *in vacuo*. The crude compound was purified by RP-HPLC (C18) to afford the pure compound (**3.62a**) as an orange solid (105 mg, 88 %).

12.3 Compound Characterisation Data

1,4-Dimethyl-9*H*-carbazole,[147] **3.49**

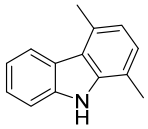

Method 1:

K_3PO_4 (998 mg, 4.7 mmol, 3.0 equiv.), $Pd(OAc)_2$ (18 mg, 5 mol%) and $HPCy_3BF_4$ (74 mg, 10 mol%) were dissolved in dry NMP (16 mL) in a flame-dried Schlenk flask and back-filled with argon three times. 2-chloroaniline (242 mg, 1.9 mmol, 1.2 equiv.) and 2-bromo-1,4-dimethylbenzene (300 mg, 1.6 mmol, 1.0 equiv.) were added and the reaction mixture was back-filled with argon again before being heated to 170 °C and left overnight to stir under argon. The reaction mixture was cooled, filtered through a celite column and the solvent was removed under vacuum in an oil bath at 170 °C. The crude reaction mixture was columned in hexane:ethyl acetate (95:5) to give the desired product (**3.49**) as an off-white crystalline compound (153.1 mg, 49 %).

Method 2:

To an oven dried Schlenk flask was added *N*-(2-chlorophenyl)-2,5-dimethylaniline (166 mg, 0.716 mmol, 1.0 equiv.), $Pd(OAc)_2$ (8 mg, 5 mol%), XPhos (33 mg, 10 mol%), K_3PO_4 (304 mg,

1.43 mmol, 2.0 equiv.) and pivalic acid (73 mg, 0.716 mmol, 1.0 equiv.). The reaction flask was evacuated and backfilled with argon. NMP (4 mL) was added and the reaction was heated to 180 °C for 12 hours. After 12 hours the reaction mixture was cooled to room temperature, washed with water and the combined aqueous layers were extracted with EtOAc. The organic layers were combined, dried with Na2SO4, and concentrated in vacuo. The crude product was purified by silica gel column chromatography using hexane:ethyl acetate (0 to 20 %) to give the desired product (**3.49**) as an off-white crystalline compound (14.2 mg, 11 %).

Method 3:

To an oven dried Schlenk flask was added *N*-(2-chlorophenyl)-2,5-dimethylaniline (100 mg, 0.43 mmol, 1.0 equiv.), $Pd(OAc)_2$ (5 mg, 5 mol%), $HPCy_3BF_4$ (16 mg, 10 mol%), K_3PO_4 (276 mg, 1.30 mmol, 3 equiv.). The reaction flask was evacuated and backfilled with argon. NMP (4 mL) was added and the reaction was heated to 180 °C overnight. The reaction mixture was cooled, filtered through a celite column and the solvent was removed under vacuum in an oil bath at 170 °C. The crude product was purified by silica gel column chromatography using hexane:ethyl acetate (0 to 20 %) to give the desired product (**3.49**) as an off-white crystalline compound (54.2 mg, 65 %).

^{1}H NMR (400 MHz, DMSO) δ 11.15 (s, 1H), 8.11 (d, *J* = 7.9 Hz, 1H), 7.53 (dd, *J* = 7.4, 0.7 Hz, 1H), 7.38 (ddd, *J* = 8.1, 7.1, 1.1 Hz, 1H), 7.17 (ddd, *J* = 8.1, 7.2, 1.0 Hz, 1H), 7.09 (d, *J* = 7.7 Hz, 1H), 6.86 (d, *J* = 7.7 Hz, 1H), 2.77 (s, 3H), 2.52 (s, 3H).
^{13}C NMR (101 MHz, DMSO) δ 139.7, 138.9, 129.5, 125.7, 124.6, 123.3, 122.0, 120.4, 119.9, 118.5, 117.3, 110.8, 20.2, 16.7.
LRMS (GCMS OP_GC320_DELAY9) R_t = 15.051, m/z = 196.1 $[M + H]^+$.

3-Methyl-9*H*-carbazole,[147] **3.43**

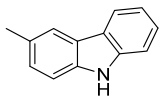

K_3PO_4 (3.3 g, 15.6 mmol, 3.0 equiv.), $Pd(OAc)_2$ (58 mg, 5 mol%) and $HPCy_3BF_4$ (191 mg, 10 mol%) were dissolved in dry NMP (40 mL) in a flame-dried Schlenk flask and back-filled with argon three times. 4-methylaniline (669 mg, 6.2 mmol, 1.2 equiv.) and 1-bromo-2-chlorobenzene (1.0 g, 5.2 mmol, 1.0 equiv.) were added and the reaction mixture was back-filled with argon again before being heated to 170 °C and left overnight to stir under argon. The reaction mixture was cooled, filtered through a celite column and the solvent was removed under vacuum in an oil

bath at 170 °C. The crude reaction mixture was columned in hexane:ethyl acetate (95:5) to give the desired product (**3.43**) as an off-white crystalline compound (604 mg, 64 %).

^{1}H NMR (500 MHz, DMSO) δ 11.07 (s, 1H), 8.05 (d, *J* = 7.7 Hz, 1H), 7.89 (d, *J* = 0.5 Hz, 1H), 7.44 (d, *J* = 8.1 Hz, 1H), 7.38 – 7.31 (m, 2H), 7.20 (dd, *J* = 8.2, 1.1 Hz, 1H), 7.11 (td, *J* = 7.5, 0.9 Hz, 1H), 2.46 (s, 3H).
LRMS (GCMS BASIC_PCI_GC320) R_t = 14.719, m/z = 182.1 $[M + H]^+$.

N-(2-chlorophenyl)-2,5-dimethylaniline, **3.50**

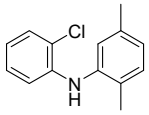

$Pd_2(dba)_3$ (7 mg, 0.25 mol%), BrettPhos (14 mg, 1 mol%) and NaO^{t}Bu (288 mg, 3.0 mmol, 3.0 equiv.) were dissolved in dry dioxane (2 mL) in a dry Schlenk flask, purged with argon and left to stir for 10 minutes. 2-chloroaniline (153 mg, 1.2 mmol, 1.2 equiv.) and 2-bromo-*p*-xylene (185 mg, 1.0 mmol, 1.0 equiv.) were added to the reaction mixture and the reaction again was purged with argon, heated to 100 °C and left for 2 hours. The reaction mixture was cooled to room temperature and the solvent was removed under reduced pressure. The crude reaction mixture was purified by silica gel column chromatography, hexane:ethyl acetate (95:5) to give the desired product (**3.50**) as an off white crystalline solid (166 mg, 72 %).

^{1}H NMR (400 MHz, DMSO) δ 7.36 (dd, *J* = 8.0, 1.27 Hz, 1H), 7.17 – 7.07 (m, 2H), 6.95 (s, 1H), 6.87 (m, 2H), 6.76 (td, *J* = 7.6, 1.4 Hz, 1H), 6.57 (dd, *J* = 8.1, 1.1 Hz, 1H), 2.23 (s, 3H), 2.09 (s, 3H).
^{13}C NMR (126 MHz, DMSO) δ 142.1, 139.9, 135.8, 130.6, 129.5, 128.78, 127.7, 124.7, 124.2, 120.5, 119.5, 116.0, 20.6, 17.2.
MP 72-75 °C.
IR (solid) υ_{max} 3427, 2922, 2855, 1591, 1321, 1037, 811, 752 cm^{-1}.
HRMS Exact mass calculated for $[M+H]^+$ ($C_{14}H_{15}NCl$) requires m/z 232.0847, found $[M+H]^+$ m/z 232.0839

6*H*-pyrido[4,3-*b*]carbazole, [246] **3.55**

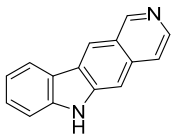

K_3PO_4 (764 mg, 3.6 mmol), $Pd(OAc)_2$ (13 mg, 5 mol%) and $HPCy_3BF4$ (44 mg, 10 mol%) were dissolved in dry NMP (10 mL). 2-chloroaniline (184 mg, 1.4 mmol, 1.2 equiv.) and 2-bromoisoquinoline (250 mg, 1.2 mmol, 1.0 equiv.) were added and the reaction mixture was heated to 180 °C in an oven dried Schlenk flask overnight. The reaction mixture was cooled and diluted with water and washed with diethyl ether. The organic layers were combined, washed with brine, dried with Na_2CO_3, filtered and concentrated in *vacuo*. The crude compound was purified by silica column chromatography, DCM:MeOH (85:15), which resulted in the formation of two products as an inseparable mixture (229.5 mg, 88 %).

LRMS (LCMS) R_t = 6.585, m/z = 219.1 $[M + H]^+$, +ve, 217.1 $[M – H]^+$, –ve.
R_t = 6.713, m/z = 257.0 $[M + 3H]^+$, +ve.

N-(2-chloro-4-methoxyphenyl)isoquinolin-6-amine, **3.61a**

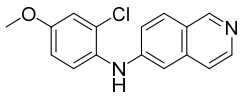

6-Bromoisoquinoline (100 mg, 0.48 mmol, 1 equiv.), 4-methoxy-2-chloroaniline (90.9 mg, 0.58 mmol, 1.2 equiv.), $Pd(OAc)_2$ (5.4 mg, 5 mol%), DavePhos (18.9 mg, 10 mol%) and K_3PO_4 (306 mg, 1.44 mmol, 3 equiv.) were added to a dry microwave vial (2 – 5 mL). 1,4-dioxane (5 mL, 0.1 mol/L) was added and the lid was secured to the vial. The vial was evacuated and purged with argon 3 times and heated at 120 °C for 30 minutes under microwave irradiation. The reaction was cooled, diluted with water (25 mL) and filtered through celite. The organic phase was then extracted with DCM (3 x 50 mL), dried with $MgSO_4$, filtered and the solvent was removed *in vacuo*. The crude compound was purified by silica column chromatography, petroleum ether (40 – 60 °C):ethyl acetate (100:0 → 30:70) to afford the pure compound (**3.61a**) as a brown solid (119 mg, 87 %).

^{1}H NMR (500 MHz, MeOD) δ 8.87 (s, 1H), 8.13 (d, *J* = 5.7 Hz, 1H), 7.86 (d, *J* = 8.9 Hz, 1H), 7.41 (d, *J* = 6.0 Hz, 1H), 7.38 (d, *J* = 8.8 Hz, 1H), 7.25 (dd, *J* = 8.8, 2.2 Hz, 1H), 7.12 (d, *J* = 2.9 Hz, 1H), 6.96 (dd, *J* = 8.8, 2.9 Hz, 1H), 6.79 (d, *J* = 2.1 Hz, 1H), 3.84 (s, 3H).

^{13}C NMR (126 MHz, MeOD) δ 157.8, 150.1, 149.0, 141.1, 138.4, 130.7, 130.6, 129.0, 127.4, 119.5, 119.3, 119.3, 115.2, 113.5, 103.4, 54.9.

IR υ_{max} (solid) 2920, 2849, 2112, 1737, 1614, 1493, 1473, 1209, 1037, 846 cm^{-1}.

HRMS Exact mass calculated for $[M + H]^+$ ($C_{16}H_{14}O_1N_2Cl$) requires *m*/*z* 285.0789, found $[M + H]^+$ *m*/*z* 285.0790.

N-(2-chloro-4-methylphenyl)isoquinolin-6-amine, **3.61b**

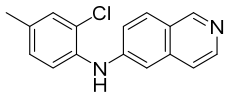

6-Bromoisoquinoline (100 mg, 0.48 mmol, 1 equiv.), 4-methyl-2-chloroaniline (81.7 mg, 0.58 mmol, 1.2 equiv.), $Pd(OAc)_2$ (5.4 mg, 5 mol%), DavePhos (18.9 mg, 10 mol%) and K_3PO_4 (306 mg, 1.44 mmol, 3 equiv.) were added to a dry microwave vial (2 – 5 mL). 1,4-dioxane (5 mL, 0.1 mol/L) was added and the lid was secured to the vial. The vial was evacuated and purged with argon 3 times and heated at 120 °C for 30 minutes under microwave irradiation. The reaction was cooled, diluted with water (25 mL) and filtered through celite. The organic phase was then extracted with DCM (3 x 50 mL), dried with $MgSO_4$, filtered and the solvent was removed *in vacuo*. The crude compound was purified by silica column chromatography, petroleum ether (40 – 60 °C):ethyl acetate (100:0 → 30:70) to afford the pure compound (**3.61b**) as a brown solid (105 mg, 81 %).

^{1}H NMR (400 MHz, MeOD) δ 8.92 (s, 1H), 8.18 (d, *J* = 5.7 Hz, 1H), 7.91 (d, *J* = 8.9 Hz, 1H), 7.47 (d, *J* = 6.0 Hz, 1H), 7.40 (d, *J* = 8.2 Hz, 1H), 7.36 (s, 1H), 7.35 (dd, *J* = 8.8, 2.2 Hz, 1H), 7.18 (ddd, *J* = 8.1, 2.1, 0.5 Hz, 1H), 7.02 (d, *J* = 2.1 Hz, 1H), 2.37 (s, 3H).

^{13}C NMR (101 MHz, MeOD) δ 151.7, 149.2, 142.7, 139.7, 136.9, 136.8, 131.7, 130.4, 129.5, 129.3, 125.6, 125.1, 121.4, 120.8, 106.1, 20.7.

IR υ_{max} (solid) 3217, 2920, 2851, 1607, 1473, 1495, 1300, 817 cm^{-1}.

HRMS Exact mass calculated for $[M + H]^+$ ($C_{16}H_{14}N_2Cl$) requires *m*/*z* 269.0840, found $[M + H]^+$ *m*/*z* 269.0842.

N-(2-chloro-4-(trifluoromethyl)phenyl)isoquinolin-6-amine, **3.61c**

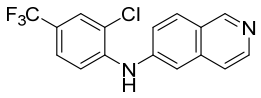

6-Bromoisoquinoline (100 mg, 0.48 mmol, 1 equiv.), 4-trifluoromethyl-2-chloroaniline (113 mg, 0.58 mmol, 1.2 equiv.), $Pd(OAc)_2$ (5.4 mg, 5 mol%), DavePhos (18.9 mg, 10 mol%) and K_3PO_4 (306 mg, 1.44 mmol, 3 equiv.) were added to a dry microwave vial (2 – 5 mL). 1,4-dioxane (5 mL, 0.1 mol/L) was added and the lid was secured to the vial. The vial was evacuated and purged with argon 3 times and heated at 160 °C for 6 hours under microwave irradiation. The reaction was cooled, diluted with water (25 mL) and filtered through celite. The organic phase was then extracted with DCM (3 x 50 mL), dried with $MgSO_4$, filtered and the solvent was removed *in vacuo*. The crude compound was purified by silica column chromatography, petroleum ether (40 – 60 °C):ethyl acetate (100:0 → 30:70) to afford the pure compound (**3.61c**) as a yellow crystalline solid (116 mg, 75 %).

^{1}H NMR (500 MHz, DMSO) δ 9.12 (s, 1H), 8.71 (s, 1H), 8.35 (d, *J* = 5.8 Hz, 1H), 8.03 (d, *J* = 8.7 Hz, 1H), 7.88 (s, 1H), 7.64 – 7.61 (m, 3H), 7.55 (dd, *J* = 8.9, 2.2 Hz, 1H), 7.49 (d, *J* = 2.0 Hz, 1H).

^{13}C NMR (126 MHz, DMSO) δ 151.4, 143.3 (t, *J* = 44.4 Hz), 136.6, 129.0, 127.3 (q, *J* = 3.8 Hz), 125.2 (q, *J* = 3.6 Hz), 124.8, 124.8, 123.6, 122.7, 122.5, 122.3, 122.0, 121.8, 119.4 (d, *J* = 8.2 Hz), 110.3.

^{19}F NMR (471 MHz, DMSO) δ -60.20.

IR υ_{max} (solid) 2921, 2853, 1608, 1324, 1104, 1080, 885, 822 cm^{-1}.

HRMS Exact mass calculated for $[M + H]^+$ ($C_{16}H_{11}N_2ClF_3$) requires *m/z* 323.0557, found $[M + H]^+$ *m/z* 323.0558.

N-(2-chloro-4-nitrophenyl)isoquinolin-6-amine, **3.61d**

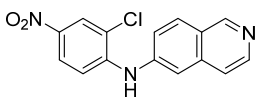

6-Bromoisoquinoline (100 mg, 0.48 mmol, 1 equiv.), 4-nitro-2-chloroaniline (99 mg, 0.58 mmol, 1.2 equiv.), $Pd(OAc)_2$ (5.4 mg, 5 mol%), DavePhos (18.9 mg, 10 mol%) and K_3PO_4 (306 mg, 1.44 mmol, 3 equiv.) were added to a dry microwave vial (2 – 5 mL). 1,4-dioxane (5 mL, 0.1

mol/L) was added and the lid was secured to the vial. The vial was evacuated and purged with argon 3 times and heated at 160 °C for 8 hours under microwave irradiation. The reaction was cooled, diluted with water (25 mL) and filtered through celite. The organic phase was then extracted with DCM (3 x 50 mL), dried with $MgSO_4$, filtered and the solvent was removed *in vacuo*. The crude compound was purified by silica column chromatography, petroleum ether (40 – 60 °C):ethyl acetate (100:0 → 30:70) to afford the pure compound (**3.61d**) as a yellow crystalline solid (89 mg, 62 %).

^{1}H NMR (400 MHz, DMSO) δ 9.21 (s, 1H), 9.08 (s, 1H), 8.43 (d, *J* = 5.6 Hz, 1H), 8.35 (d, *J* = 2.7 Hz, 1H), 8.12 (d, *J* = 8.9 Hz, 1H), 8.11 (dd, *J* = 9.1, 2.7 Hz, 1H), 7.74 (d, *J* = 1.7 Hz, 1H), 7.71 (d, *J* = 5.7 Hz, 1H), 7.65 (dd, *J* = 9.0, 2.01 Hz, 1H), 7.53 – 7.46 (m, 1H).
^{13}C NMR (126 MHz, DMSO) δ 151.7, 146.2, 143.4, 142.0, 139.7, 136.3, 129.2, 125.9, 125.2, 124.3, 123.1, 121.0, 119.7, 115.8, 114.4.
IR υ_{max} (solid) 3218, 3066, 2924, 1582, 1506, 1333 cm^{-1}.
HRMS Exact mass calculated for $[M + H]^+$ ($C_{15}H_{11}O_2N_3Cl$) requires *m*/*z* 300.0534, found $[M + H]^+$ *m*/*z* 300.0537.

N-(2-chloro-5-methoxyphenyl)isoquinolin-6-amine, **3.61e**

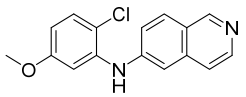

6-Bromoisoquinoline (100 mg, 0.48 mmol, 1 equiv.), 5-methoxy-2-chloroaniline (90.9 mg, 0.58 mmol, 1.2 equiv.), $Pd(OAc)_2$ (5.4 mg, 5 mol%), DavePhos (18.9 mg, 10 mol%) and K_3PO_4 (306 mg, 1.44 mmol, 3 equiv.) were added to a dry microwave vial (2 – 5 mL). 1,4-dioxane (5 mL, 0.1 mol/L) was added and the lid was secured to the vial. The vial was evacuated and purged with argon 3 times and heated at 120 °C for 30 minutes under microwave irradiation. The reaction was cooled, diluted with water (25 mL) and filtered through celite. The organic phase was then extracted with DCM (3 x 50 mL), dried with $MgSO_4$, filtered and the solvent was removed *in vacuo*. The crude compound was purified by silica column chromatography, petroleum ether (40 – 60 °C):ethyl acetate (100:0 → 30:70) to afford the pure compound (**3.61e**) as a yellow solid (65.7 mg, 48 %).

^{1}H NMR (400 MHz, DMSO) δ 9.02 (s, 1H), 8.40 (s, 1H), 8.27 (d, *J* = 5.8 Hz, 1H), 7.94 (d, *J* = 8.9 Hz, 1H), 7.53 (d, *J* = 6.0 Hz, 1H), 7.47 – 7.39 (m, 2H), 7.14 (d, *J* = 2.0 Hz, 1H), 7.01 (d, *J* = 2.8 Hz, 1H), 6.74 (dd, *J* = 8.9, 2.9 Hz, 1H), 3.75 (s, 3H).

^{13}C NMR (101 MHz, DMSO) δ 158.8, 151.1, 145.8, 143.0, 139.0, 137.0, 130.7, 128.9, 123.5, 120.4, 119.0, 117.8, 110.5, 108.5, 106.1, 55.4.

IR υ_{max} (solid) 3219, 2830, 2923, 2851, 1582, 1471, 848 cm^{-1}.

HRMS Exact mass calculated for $[M + H]^+$ ($C_{16}H_{14}ON_2Cl$) requires *m*/*z* 285.0789, found $[M + H]^+$ *m*/*z* 285.0790.

N-(2-chloro-5-fluorophenyl)isoquinolin-6-amine, **3.61f**

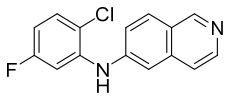

6-Bromoisoquinoline (100 mg, 0.48 mmol, 1 equiv.), 5-fluoro-2-chloroaniline (84 mg, 0.58 mmol, 1.2 equiv.), $Pd(OAc)_2$ (5.4 mg, 5 mol%), DavePhos (18.9 mg, 10 mol%) and K_3PO_4 (306 mg, 1.44 mmol, 3 equiv.) were added to a dry microwave vial (2 – 5 mL). 1,4-dioxane (5 mL, 0.1 mol/L) was added and the lid was secured to the vial. The vial was evacuated and purged with argon 3 times and heated at 120 °C for 30 minutes under microwave irradiation. The reaction was cooled, diluted with water (25 mL) and filtered through celite. The organic phase was then extracted with DCM (3 x 50 mL), dried with $MgSO_4$, filtered and the solvent was removed *in vacuo*. The crude compound was purified by silica column chromatography, petroleum ether (40 – 60 °C):ethyl acetate (100:0 → 30:70) to afford the pure compound (**3.61f**) as a yellow solid (86.2 mg, 73 %).

^{1}H NMR (400 MHz, DMSO) δ 9.06 (s, 1H), 8.52 (s, 1H), 8.31 (d, *J* = 5.8 Hz, 1H), 7.98 (d, *J* = 8.9 Hz, 1H), 7.60 – 7.53 (m, 2H), 7.48 (dd, *J* = 8.9, 2.2 Hz, 1H), 7.30 (td, *J* = 6.6, 2.9 Hz, 1H), 7.29 (s, 1H), 6.94 (ddd, *J* = 9.1, 8.4, 3.0, 1H).

^{13}C NMR (101 MHz, DMSO) δ 161.2 (d, *J* = 243.6 Hz), 151.3, 144.7, 143.2, 140.2 (d, *J* = 10.8 Hz), 136.9, 131.4 (d, *J* = 9.8 Hz), 129.0, 124.0, 120.8, 120.5 (d, *J* = 3.2 Hz), 119.2, 110.6 (d, *J* = 23.2 Hz), 108.4 (d, *J* = 25.6 Hz), 107.7.

^{19}F NMR (470 MHz, DMSO) δ -113.03.

IR υ_{max} (solid) 3213, 2920, 2849, 1843, 1731, 1588, 1471, 1426, 1292, 1110, 851 cm^{-1}.

HRMS Exact mass calculated for $[M + H]^+$ ($C_{15}H_{11}N_2ClF$) requires *m*/*z* 273.0589, found $[M + H]^+$ *m*/*z* 273.0592.

N-(2-chloro-6-fluorophenyl)isoquinolin-6-amine, **3.61g**

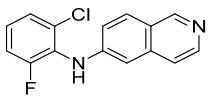

6-Bromoisoquinoline (100 mg, 0.48 mmol, 1 equiv.), 6-fluoro-2-chloroaniline (84 mg, 0.58 mmol, 1.2 equiv.), $Pd(OAc)_2$ (5.4 mg, 5 mol%), DavePhos (18.9 mg, 10 mol%) and K_3PO_4 (306 mg, 1.44 mmol, 3 equiv.) were added to a dry microwave vial (2 – 5 mL). 1,4-dioxane (5 mL, 0.1 mol/L) was added and the lid was secured to the vial. The vial was evacuated and purged with argon 3 times and heated at 120 °C for 10 minutes under microwave irradiation. The reaction was cooled, diluted with water (25 mL) and filtered through celite. The organic phase was then extracted with DCM (3 x 50 mL), dried with $MgSO_4$, filtered and the solvent was removed *in vacuo*. The crude compound was purified by silica column chromatography, petroleum ether (40 – 60 °C):ethyl acetate (100:0 → 30:70) to afford the pure compound (**3.61g**) as an off white solid (95.7 mg, 73 %).

^{1}H NMR (500 MHz, DMSO) δ 9.0 (s, 1H), 8.53 (s, 1H), 8.23 (d, *J* = 5.9 Hz, 1H), 7.91 (d, *J* = 8.8 Hz, 1H), 7.48 (d, *J* = 7.7 Hz, 1H), 7.46 (d, *J* = 5.9 Hz, 1H), 7.42 – 7.33 (m, 2H), 7.24 (dd, *J* = 8.8, 1.97 Hz, 1H), 6.61 (s, 1H).

^{13}C NMR (101 MHz, DMSO) δ 158.5 (d, *J* = 248.5 Hz), 151.2, 146.7, 143.1, 137.0, 132.1 (d, *J* = 3.2 Hz), 128.8, 127.4 (d, *J* = 9.0 Hz), 126.3, 126.1, 126.1 (d, *J* = 3.3 Hz), 123.2, 118.8 (d, *J* = 11.9 Hz), 115.6 (d, *J* = 20.8 Hz), 103.6.

^{19}F NMR (470 MHz, DMSO) δ -115.90.

IR υ_{max} (solid) 3636, 2918, 2849, 1733, 1627, 1473, 1448, 898 cm^{-1}.

HRMS Exact mass calculated for $[M + H]^+$ ($C_{15}H_{11}N_2ClF$) requires *m/z* 273.0589, found $[M + H]^+$ *m/z* 273.0590.

N-(2-chlorophenyl)quinoxalin-6-amine, **3.61h**

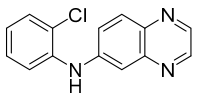

6-Bromoquinoxaline (101 mg, 0.48 mmol, 1 equiv.), 2-chloroaniline (73.6 mg, 0.58 mmol, 1.2 equiv.), $Pd(OAc)_2$ (5.4 mg, 5 mol%), DavePhos (18.9 mg, 10 mol%) and K_3PO_4 (306 mg, 1.44 mmol, 3 equiv.) were added to a dry microwave vial (2 – 5 mL). 1,4-dioxane (5 mL, 0.1 mol/L) was added and the lid was secured to the vial. The vial was evacuated and purged with argon 3 times and heated at 120 °C for 30 minutes under microwave irradiation. The reaction was cooled,

diluted with water (25 mL) and filtered through celite. The organic phase was then extracted with DCM (3 x 50 mL), dried with $MgSO_4$, filtered and the solvent was removed *in vacuo*. The crude compound was purified by RP-HPLC (C18) to afford the pure compound (**3.61h**) as a green solid (105 mg, 86 %)

^{1}H NMR (500 MHz, MeOD) δ 8.72 (d, *J* = 1.7 Hz, 1H), 8.62 (d, *J* = 1.8 Hz, 1H), 8.56 (s, 1H), 7.92 (d, *J* = 9.1 Hz, 1H), 7.16 (dd, *J* = 9.0, 2.5 Hz, 1H), 7.57 (d, *J* = 8.0 Hz, 1H), 7.53 (d, *J* = 7.8 Hz, 1H), 7.38 (t, *J* = 8.0 1H), 7.20 – 7.14 (m, 2H).
^{13}C NMR (126 MHz, MeOD) δ 145.9, 145.5, 144.1, 141.7, 138.2, 137.9, 130.4, 129.9, 128.1, 126.8, 125.0, 123.7, 123.0, 107.8.
IR υ_{max} (solid) 3414, 3247, 3053, 2116, 1588, 1456, 1197, 1181, 1132, 745 cm^{-1}.
HRMS Exact mass calculated for $[M + H]^+$ ($C_{14}H_{11}N_3Cl$) requires *m*/*z* 256.0636, found $[M + H]^+$ *m*/*z* 256.0638.

N-(2-chloro-4-methoxyphenyl)quinolin-6-amine, **3.61i**

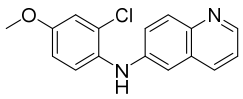

6-Bromoquinoline (100 mg, 0.48 mmol, 1 equiv.), 4-methoxy-2-chloroaniline (90.9 mg, 0.58 mmol, 1.2 equiv.), $Pd(OAc)_2$ (5.4 mg, 5 mol%), DavePhos (18.9 mg, 10 mol%) and K_3PO_4 (306 mg, 1.44 mmol, 3 equiv.) were added to a dry microwave vial (2 – 5 mL). 1,4-dioxane (5 mL, 0.1 mol/L) was added and the lid was secured to the vial. The vial was evacuated and purged with argon 3 times and heated at 120 °C for 30 minutes under microwave irradiation. The reaction was cooled, diluted with water (25 mL) and filtered through celite. The organic phase was then extracted with DCM (3 x 50 mL), dried with $MgSO_4$, filtered and the solvent was removed *in vacuo*. The crude compound was purified by RP-HPLC to afford the pure compound (**3.61i**) as an orange solid (137 mg, > 99 %).

^{1}H NMR (500 MHz, MeOD) δ 8.69 (dd, *J* = 5.3, 1.4 Hz, 1H), 8.60 (d, *J* = 8.4 Hz, 1H), 7.98 (d, *J* = 9.2 Hz, 1H), 7.74 (dd, *J* = 8.3, 5.2 Hz, 1H), 7.69 (dd, *J* = 9.4, 2.4 Hz, 1H), 7.40 (d, *J* = 8.7 Hz, 1H), 7.15 (d, *J* = 3.0 Hz, 1H), 7.04 (d, *J* = 2.6 Hz, 1H), 6.99 (d, *J* = 8.7, 2.8 Hz, 1H), 3.85 (s, 3H).
^{13}C NMR (101 MHz, DMSO) δ 157.3, 146.3, 141.7, 140.2, 135.6, 130.4, 130.4, 130.2, 127.8, 124.9, 124.4, 121.8, 115.3, 114.4, 104.6, 55.6.
IR υ_{max} (solid) 3280, 3089, 2084, 1668, 1205, 1119, 829, 796 cm^{-1}.

HRMS Exact mass calculated for $[M + H]^+$ ($C_{16}H_{14}ON_2Cl$) requires *m*/*z* 285.0789, found $[M + H]^+$ *m*/*z* 285.0790.

N-(2-chlorophenyl)quinolin-6-amine, **3.61j**

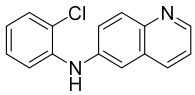

6-Bromoquinoline (100 mg, 0.48 mmol, 1 equiv.), 2-chloroaniline (73.6 mg, 0.58 mmol, 1.2 equiv.), $Pd(OAc)_2$ (5.4 mg, 5 mol%), DavePhos (18.9 mg, 10 mol%) and K_3PO_4 (306 mg, 1.44 mmol, 3 equiv.) were added to a dry microwave vial (2 – 5 mL). 1,4-dioxane (5 mL, 0.1 mol/L) was added and the lid was secured to the vial. The vial was evacuated and purged with argon 3 times and heated at 120 °C for 30 minutes under microwave irradiation. The reaction was cooled, diluted with water (25 mL) and filtered through celite. The organic phase was then extracted with DCM (3 x 50 mL), dried with $MgSO_4$, filtered and the solvent was removed *in vacuo*. The crude compound was purified by silica column chromatography, petroleum ether (40 – 60 °C):ethyl acetate (100:0 → 30:70) to afford the pure compound (**3.61j**) as a dark yellow solid (98.2 mg, 80 %)

^{1}H NMR (500 MHz, MeOD) δ 8.60 (dd, *J* = 4.3, 1.6 Hz, 1H), 8.11 (d, *J* = 8.4 Hz, 1H), 7.90 (d, *J* = 9.1 Hz, 1H), 7.58 (dd, *J* = 9.1, 2.5 Hz, 1H), 7.45 (dd, *J* = 8.2, 4.2 Hz, 1H), 7.45 (dd, *J* = 8.2, 1.2 Hz, 1H), 7.40 (dd, *J* = 8.3, 4.4 Hz, 1H), 7.34 (d, *J* = 2.5 Hz, 1H), 7.28 – 7.24 (m, 1H), 7.03 – 6.98 (m, 1H).

^{13}C NMR (101 MHz, DMSO) δ 147.3, 143.7, 141.8, 139.4, 134.2, 130.2, 129.8, 129.1, 128.0, 124.9, 123.3, 123.2, 121.6, 121.2, 109.4.

IR υ_{max} (solid) 3319, 2920, 2851, 1586, 1515, 1303, 837, 744 cm^{-1}.

HRMS Exact mass calculated for $[M + H]^+$ ($C_{15}H_{12}N_2Cl$) requires *m*/*z* 255.0684, found $[M + H]^+$ *m*/*z* 255.0684.

N-(2-chlorophenyl)quinolin-2-amine, **3.61k**

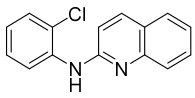

2-Bromoisoquinoline (100 mg, 0.48 mmol, 1 equiv.), 2-chloroaniline (73.6 mg, 0.58 mmol, 1.2 equiv.), $Pd(OAc)_2$ (5.4 mg, 5 mol%), DavePhos (18.9 mg, 10 mol%) and K_3PO_4 (306 mg, 1.44 mmol, 3 equiv.) were added to a dry microwave vial (2 – 5 mL). 1,4-dioxane (5 mL, 0.1 mol/L) was added and the lid was secured to the vial. The vial was evacuated and purged with argon 3 times and heated at 120 °C for 30 minutes under microwave irradiation. The reaction was cooled, diluted with water (25 mL) and filtered through celite. The organic phase was then extracted with DCM (3 x 50 mL), dried with $MgSO_4$, filtered and the solvent was removed *in vacuo*. The crude compound was purified by silica column chromatography, petroleum ether (40 – 60 °C):ethyl acetate (100:0 → 30:70) then by RP-HPLC (C18) afford the pure compound (**3.61k**) as a white crystalline solid (62.4 mg, 62 %).

^{1}H NMR (500 MHz, DMSO) δ 10.12 (s, 1H), 8.34 (d, *J* = 8.9 Hz, 1H), 8.05 (d, *J* = 6.6 Hz, 1H), 7.89 (d, *J* = 8.1 Hz, 1H), 7.78 – 7.66 (m, 2H), 7.63, (dd, *J* = 8.0, 1.2 Hz, 1H), 7.51- 7.41 (m, 2H), 7.33 (t, *J* = 7.7 Hz, 1H), 7.26 (d, *J* = 9.1 Hz, 1H).

^{13}C NMR (101 MHz, DMSO) δ 159.1, 158.8, 153.1, 141.6, 140.0, 134.2, 131.7, 130.3, 128.4, 127.8, 127.0, 124.7, 122.6, 121.0, 113.4.

IR υ_{max} (solid) 2729, 1941, 1681, 1184, 1129, 757, 723 cm^{-1}.

HRMS Exact mass calculated for $[M + H]^+$ ($C_{15}H_{12}N_2Cl$) requires *m*/*z* 255.0684, found $[M + H]^+$ *m*/*z* 255.0684.

N-(2-chloro-4-methoxyphenyl)quinoxalin-2-amine, **3.61l**

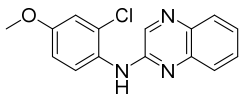

2-Bromoquinoxaline (101 mg, 0.48 mmol, 1 equiv.), 4-methoxy-2-chloroaniline (90.9 mg, 0.58 mmol, 1.2 equiv.), $Pd(OAc)_2$ (5.4 mg, 5 mol%), DavePhos (18.9 mg, 10 mol%) and K_3PO_4 (306 mg, 1.44 mmol, 3 equiv.) were added to a dry microwave vial (2 – 5 mL). 1,4-dioxane (5 mL, 0.1 mol/L) was added and the lid was secured to the vial. The vial was evacuated and purged with argon 3 times and heated at 120 °C for 30 minutes under microwave irradiation. The reaction was cooled, diluted with water (25 mL) and filtered through celite. The organic phase was then extracted with DCM (3 x 50 mL), dried with $MgSO_4$, filtered and the solvent was removed *in*

vacuo. The crude compound was purified by silica column chromatography, petroleum ether (40 – 60 °C):ethyl acetate (100:0 → 30:70) to afford the pure compound (**3.61l**) as a yellow crystalline solid (27.2 mg, 20 %).

^{1}H NMR (500 MHz, DMSO) δ 9.0 (s, 1H), 8.64 (s, 1H), 7.92 (d, *J* = 9.0 Hz, 1H), 7.84 (dd, *J* = 8.1, 1.0 Hz, 1H), 7.61 – 7.53 (m, 2H), 7.43 (ddd, *J* = 8.4, 7.4, 1.7 Hz, 1H), 7.15 (d, *J* = 3.0 Hz, 1H), 7.00 (d, *J* = 9.0, 2.9 Hz, 1H), 3.81 (s, 3H).
^{13}C NMR (101 MHz, DMSO) δ 156.6, 150.5, 140.8, 139.8, 137.1, 129.9, 128.9, 128.4, 128.0, 126.9, 126.2, 124.7, 114.6, 113.6, 55.7.
IR υ_{max} (solid) 3332, 2929, 1536, 1499, 1212, 758 cm^{-1}.
HRMS Exact mass calculated for $[M+H]^+$ ($C_{15}H_{13}ON_3Cl$) requires m/z 286.0742, found $[M+H]^+$ m/z 286.0743.

N-(2-chloro-4-methoxyphenyl)-*N*-(quinoxalin-2-yl)quinoxalin-2-amine, **3.61z**

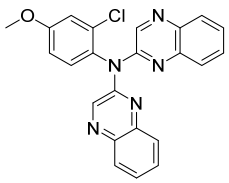

2-Bromoquinoxaline (101 mg, 0.48 mmol, 1 equiv.), 4-methoxy-2-chloroaniline (90.9 mg, 0.58 mmol, 1.2 equiv.), $Pd(OAc)_2$ (5.4 mg, 5 mol%), DavePhos (18.9 mg, 10 mol%) and K_3PO_4 (306 mg, 1.44 mmol, 3 equiv.) were added to a dry microwave vial (2 – 5 mL). 1,4-dioxane (5 mL, 0.1 mol/L) was added and the lid was secured to the vial. The vial was evacuated and purged with argon 3 times and heated at 120 °C for 30 minutes under microwave irradiation. The reaction was cooled, diluted with water (25 mL) and filtered through celite. The organic phase was then extracted with DCM (3 x 50 mL), dried with $MgSO_4$, filtered and the solvent was removed *in vacuo*. The crude compound was purified by silica column chromatography, petroleum ether (40 – 60 °C):ethyl acetate (100:0 → 30:70) to afford the pure compound (**3.61z**) as a yellow crystalline solid (45.4 mg, 23 %).

^{1}H NMR (500 MHz, DMSO) δ 8.83 (s, 2H), 8.04 (d, *J* = 8.0 Hz, 2H), 7.76 – 7.73 (m, 4H), 7.73 – 7.69 (m, 2H), 7.58 (d, *J* = 8.8 Hz, 1H), 7.32 (d, *J* = 2.9 Hz, 1H), 7.12 (dd, *J* = 8.7, 2.9 Hz, 1H), 2.89 (s, 3H).
^{13}C NMR (126 MHz, DMSO) δ 160.1, 150.9, 142.0, 140.5, 139.3, 133.6, 132.8, 131.4, 131.1, 129.1, 128.5, 127.9, 116.4, 115.6, 56.4.

IR υ_{max} (solid) 2920, 2843, 1493, 1223, 758 cm^{-1}.

HRMS Exact mass calculated for $[M+H]^+$ ($C_{23}H_{17}ON_5Cl$) requires m/z 414.1116, found $[M+H]^+$ m/z 414.1114.

N-(2-chloro-4-methoxyphenyl)-6-methoxynaphthalen-2-amine, **3.61m**

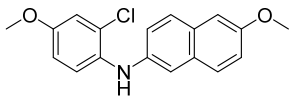

2-Bromo-6-methoxynaphthalene (100 mg, 0.42 mmol, 1 equiv.), 4-methoxy-2-chloroaniline (80 mg, 0.51 mmol, 1.2 equiv.), $Pd(OAc)_2$ (4.74 mg, 5 mol%), DavePhos (16.5 mg, 10 mol%) and K_3PO_4 (269 mg, 1.27 mmol, 3 equiv.) were added to a dry microwave vial (2 – 5 mL). 1,4-dioxane (4.4 mL, 0.1 mol/L) was added and the lid was secured to the vial. The vial was evacuated and purged with argon 3 times and heated at 120 °C for 30 minutes under microwave irradiation. The reaction was cooled, diluted with water (25 mL) and filtered through celite. The organic phase was then extracted with DCM (3 x 50 mL), dried with $MgSO_4$, filtered and the solvent was removed *in vacuo*. The crude compound was purified by RP-HPLC (C18) twice to afford the pure compound (**3.61m**) as a red oil (82 mg, 62 %).

^{1}H NMR (400 MHz, DMSO) δ 7.65 (d, *J* = 8.8 Hz, 1H), 7.55 (s, 1H), 7.52 (d, *J* = 9.0 Hz, 1H), 7.30 (d, *J* = 8.8 Hz, 1H), 7.20 – 7.15 (m, 2H), 7.11 (d, *J* = 2.9 Hz, 1H), 7.02 (dd, *J* = 9.0, 2.6 Hz, 1H), 6.99 (d, *J* = 2.1 Hz, 1H), 6.92 (dd, *J* = 8.8, 2.9 Hz, 1H), 3.81 (s, 3H), 3.77 (s, 3H).

^{13}C NMR (101 MHz, DMSO) δ 155.3, 155.0, 141.3, 133.0, 129.6, 128.7, 127.5, 127.5, 127.3, 124.2, 119.6, 118.5, 115.1, 114.0, 108.8, 106.1, 55.6, 55.0.

IR υ_{max} (solid) 3401, 2931, 2830, 1504, 1223, 803 cm^{-1}

HRMS Exact mass calculated for $[M + H]^+$ ($C_{18}H_{18}O_2NCl$) requires *m*/*z* 314.0942, found $[M + H]^+$ *m*/*z* 314.0945.

tert-Butyl 6-((2-chloro-4-methoxyphenyl)amino)-3,4-dihydroisoquinoline-2(1*H*)-carboxylate, **3.61n**

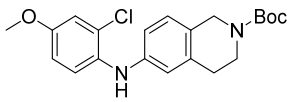

tert-Butyl-6-bromo-3,4-dihydroisoquinoline-2(1*H*)-carboxylate (100 mg, 0.32 mmol, 1 equiv.), 4-methoxy-2-chloroaniline (60.5 mg, 0.38 mmol, 1.2 equiv.), $Pd(OAc)_2$ (3.59 mg, 5 mol%), DavePhos (12.6 mg, 10 mol%) and K_3PO_4 (204 mg, 0.96 mmol, 3 equiv.) were added to a dry microwave vial (2 – 5 mL). 1,4-dioxane (3.33 mL, 0.1 mol/L) was added and the lid was secured to the vial. The vial was evacuated and purged with argon 3 times and heated at 120 °C for 30 minutes under microwave irradiation. The reaction was cooled, diluted with water (25 mL) and filtered through celite. The organic phase was then extracted with DCM (3 x 50 mL), dried with $MgSO_4$, filtered and the solvent was removed *in vacuo*. The crude compound was purified RP-HPLC (C18) twice to afford the pure compound (**3.61n**) as a brown oil (66 mg, 35 %).

^{1}H NMR (500 MHz, MeOD) δ 7.17 (d, *J* = 8.9 Hz, 1H), 6.98 (d, *J* = 2.8 Hz, 1H), 6.91 (d, *J* = 8.2 Hz, 1H), 6.78 (dd, *J* = 8.9, 2.8 Hz, 1H), 6.72 (dd, *J* = 8.3, 2.4 Hz, 1H), 6.65 (d, *J* = 2.1 Hz, 1H), 4.43 (s, 2H), 2.75 (s, 3H), 3.56 (t, *J* = 5.7 Hz, 2H), 2.70 (t, *J* = 5.9 Hz, 2H), 1.47 (s, 9H).
^{13}C NMR (101 MHz, MeOH) δ 156.7, 156.6, 144.7, 136.6, 134.8, 127.9, 127.7, 123.7, 118.4, 117.2, 116.3, 115.5, 115.2, 114.5, 81.2, 56.3, 56.2, 30.0, 28.8.
IR υ_{max} (solid) 2972, 2836, 1668, 1614, 1502, 1162, 1130 cm^{-1}.
HRMS Exact mass calculated for $[M + H]^+$ ($C_{21}H_{26}O_3N_1Cl_1$) requires *m*/*z* 389.1626, found $[M + H]^+$ *m*/*z* 389.1627.

N-(2-chloro-4-methoxyphenyl)-1,3-dihydroisobenzofuran-5-amine, **3.61o**

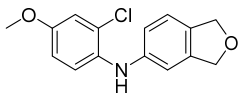

5-Bromo-1,3-dihydroisobenzofuran (95.7 mg, 0.48 mmol, 1 equiv.), 4-methoxy-2-chloroaniline (90.9 mg, 0.58 mmol, 1.2 equiv.), $Pd(OAc)_2$ (5.4 mg, 5 mol%), DavePhos (18.9 mg, 10 mol%) and K_3PO_4 (306 mg, 1.44 mmol, 3 equiv.) were added to a dry microwave vial (2 – 5 mL). 1,4-dioxane (5 mL, 0.1 mol/L) was added and the lid was secured to the vial. The vial was evacuated and purged with argon 3 times and heated at 120 °C for 30 minutes under microwave irradiation. The reaction was cooled, diluted with water (25 mL) and filtered through celite. The organic phase was then extracted with DCM (3 x 50 mL), dried with $MgSO_4$, filtered and the solvent was

removed *in vacuo*. The crude compound was purified by RP-HPLC (C18) to afford the pure compound (**3.61o**) as a brown oil (59 mg, 44 %).

^{1}H NMR (500 MHz, MeOD) δ 7.21 (d, *J* = 8.7 Hz, 1H), 7.07 (d, *J* = 8.0 Hz, 1H), 7.01 (d, *J* = 2.9 Hz, 1H), 6.84 – 6.79 (m, 2H), 6.76 (s, 1H), 4.98 (d, *J* = 4.0 Hz, 4H), 3.77 (s, 3H).
^{13}C NMR (101 MHz, DMSO) δ 155.4, 144.9, 140.0, 132.8, 128.9, 127.6, 124.7, 121.4, 115.0, 114.8, 114.0, 107.3, 72.5, 72.2, 55.6.
IR υ_{max} (solid) 3377, 2834, 1495, 1279, 1209, 1041, 807 cm^{-1}.
HRMS Exact mass calculated for $[M + H]^+$ ($C_{15}H_{15}O_2NCl$) requires *m*/*z* 276.0786, found $[M + H]^+$ *m*/*z* 276.0788.

N-(2-chlorophenyl)-1,3-dihydroisobenzofuran-5-amine, **3.61p**

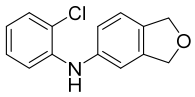

5-Bromo-1,3-dihydroisobenzofuran (95.7 mg, 0.48 mmol, 1 equiv.), 2-chloroaniline (73.6 mg, 0.58 mmol, 1.2 equiv.), $Pd(OAc)_2$ (5.4 mg, 5 mol%), DavePhos (18.9 mg, 10 mol%) and K_3PO_4 (306 mg, 1.44 mmol, 3 equiv.) were added to a dry microwave vial (2 – 5 mL). 1,4-dioxane (5 mL, 0.1 mol/L) was added and the lid was secured to the vial. The vial was evacuated and purged with argon 3 times and heated at 120 °C for 30 minutes under microwave irradiation. The reaction was cooled, diluted with water (25 mL) and filtered through celite. The organic phase was then extracted with DCM (3 x 50 mL), dried with $MgSO_4$, filtered and the solvent was removed *in vacuo*. The crude compound was purified by RP-HPLC (C18) to afford the pure compound (**3.61p**) as a grey crystalline solid (75.1 mg, 64 %).

^{1}H NMR (500 MHz, MeOD) δ 7.34 (dd, *J* = 8.1, 1.4 Hz, 1H), 7.19 (dd, *J* = 8.2, 1.5 Hz, 1H), 7.16 (d, *J* = 8.0 Hz, 1H), 7.14 – 7.09 (m, 1H), 7.04 – 7.00 (m, 2H), 6.81 (td, *J* = 7.6, 1.5 Hz, 1H), 5.02 (s, 4H).
^{13}C NMR (101 MHz, MeOD) δ 143.6, 142.3, 141.5, 133.5, 130.9, 128.5, 123.7, 122.6, 121.9, 120.5, 118.3, 113.2, 74.3, 74.2.
IR υ_{max} (solid) 3316, 2851, 1594, 1489, 1447, 1313, 1028, 753 cm^{-1}.
HRMS Exact mass calculated for $[M + H]^+$ ($C_{14}H_{13}ONCl$) requires *m*/*z* 246.0680, found $[M + H]^+$ *m*/*z* 246.0683.

N-(2-chloro-4-methoxyphenyl)chroman-6-amine, **3.61q**

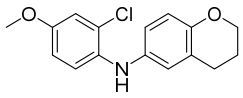

6-Bromochromane (100 mg, 0.5 mmol, 1 equiv.), 4-methoxy-2-chloroaniline (88.8 mg, 0.56 mmol, 1.2 equiv.), $Pd(OAc)_2$ (5.26 mg, 5 mol%), DavePhos (18.5 mg, 10 mol%) and K_3PO_4 (299 mg, 1.41 mmol, 3 equiv.) were added to a dry microwave vial (2 – 5 mL). 1,4-dioxane (4.89 mL, 0.1 mol/L) was added and the lid was secured to the vial. The vial was evacuated and purged with argon 3 times and heated at 120 °C for 30 minutes under microwave irradiation. The reaction was cooled, diluted with water (25 mL) and filtered through celite. The organic phase was then extracted with DCM (3 x 50 mL), dried with $MgSO_4$, filtered and the solvent was removed *in vacuo*. The crude compound was purified RP-HPLC (C18) to afford the pure compound (**3.61q**) as a brown oil (50.7 mg, 35 %).

^{1}H NMR (500 MHz, MeOD) δ 6.97 (d, *J* = 9.0 Hz, 1H), 6.94 (d, *J* = 2.8 Hz, 1H), 7.76 – 6.72 (m, 2H), 6.71 – 6.69 (m, 1H), 6.63 (d, *J* = 8.6 Hz, 1H), 4.11 (t, *J* = 5.1 Hz, 2H), 3.74 (s, 3H), 2.73 (t, *J* = 6.5 Hz, 2H), 2.00 – 1.92 (m, 2H).

^{13}C NMR (101 MHz, DMSO) δ 153.7, 148.8, 136.8, 134.8, 124.2, 122.5, 120.5, 119.1, 117.6, 116.6, 115.0, 113.9, 65.6, 55.6, 24.4, 22.0.

IR υ_{max} (solid) 3390, 2860, 2931, 2832, 1614, 1495, 1205, 1039 cm^{-1}.

HRMS Exact mass calculated for $[M + H]^+$ ($C_{16}H_{17}O_2NCl$) requires *m*/*z* 290.0942, found $[M + H]^+$ *m*/*z* 290.0944.

2-((2-Chloro-4-methoxyphenyl)amino)naphthalene-1,4-dione, **3.61r**

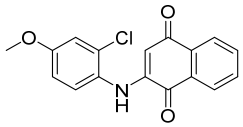

2-Bromonaphthalene-1,4-dione (114 mg, 0.48 mmol, 1 equiv.), 4-methoxy-2-chloroaniline (90.6 mg, 0.58 mmol, 1.2 equiv.), $Pd(OAc)_2$ (5.4 mg, 5 mol%), DavePhos (18.9 mg, 10 mol%) and K_3PO_4 (306 mg, 1.44 mmol, 3 equiv.) were added to a dry microwave vial (2 – 5 mL). 1,4-dioxane (5 mL, 0.1 mol/L) was added and the lid was secured to the vial. The vial was evacuated and purged with argon 3 times and heated at 120 °C for 30 minutes under microwave irradiation. The

reaction was cooled, diluted with water (25 mL) and filtered through celite. The organic phase was then extracted with DCM (3 x 50 mL), dried with $MgSO_4$, filtered and the solvent was removed *in vacuo*. The crude compound was purified by silica column chromatography, petroleum ether (40 – 60 °C):ethyl acetate (100:0 → 30:70) and 5 % NEt_3 to afford the pure compound (**3.61r**) as a dark red crystalline solid (147 mg, 98 %).

^{1}H NMR (500 MHz, DMSO) δ 9.02 (s, 1H), 8.06 (dd, *J* = 7.6, 0.9 Hz, 1H), 7.94 (dd, *J* = 7.5, 0.9 Hz, 1H), 7.86 (td, *J* = 7.5, 1.2 Hz, 1H), 7.79 (td, *J* = 7.4, 1.3 Hz, 1H), 7.36 (d, *J* = 8.8 Hz, 1H), 7.22 (d, *J* = 2.9 Hz, 1H), 7.04 (dd, *J* = 8.8, 2.9 Hz, 1H), 6.83 – 6.66 (m, 1H), 3.82 (s, 3H).
^{13}C NMR (101 MHz, DMSO) δ 182.1, 181.3, 158.9, 147.9, 135.0, 132.7, 132.6, 131.2, 130.3, 129.5, 127.3, 126.0, 125.4, 115.1, 114.3, 102.3, 55.8.
IR υ_{max} (solid) 3323, 3018, 2938, 1610, 1575, 1486, 1030 cm^{-1}.
HRMS Exact mass calculated for $[M+H]^+$ ($C_{17}H_{13}O_3NCl$) requires m/z 314.0578, found $[M+H]^+$ m/z 314.0582.

2-((2-Chloro-4-hydroxyphenyl)amino)naphthalene-1,4-dione, **3.61s**

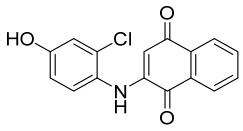

2-Bromonaphthalene-1,4-dione (114 mg, 0.48 mmol, 1 equiv.), 4-amino-3-chlorophenol hydrochloride (103 mg, 0.58 mmol, 1.2 equiv.), $Pd(OAc)_2$ (5.4 mg, 5 mol%), DavePhos (18.9 mg, 10 mol%) and K_3PO_4 (306 mg, 1.44 mmol, 3 equiv.) were added to a dry microwave vial (2 – 5 mL). 1,4-dioxane (5 mL, 0.1 mol/L) was added and the lid was secured to the vial. The vial was evacuated and purged with argon 3 times and heated at 120 °C for 30 minutes under microwave irradiation. The reaction was cooled, diluted with water (25 mL) and filtered through celite. The organic phase was then extracted with DCM (3 x 50 mL), dried with $MgSO_4$, filtered and the solvent was removed *in vacuo*. The crude compound was purified by RP- HPLC (C18) to afford the pure compound (**3.61s**) as a purple solid (12.2 mg, 8.0 %).
^{1}H NMR (500 MHz, DMSO) δ 10.10 (s, 1H), 8.94 (s, 1H), 8.06 (d, *J* = 7.7 Hz, 1H), 7.93 (d, *J* = 7.5 Hz, 1H), 7.86 (td, *J* = 7.5, 1.07 Hz, 1H), 7.78 (td, *J* = 7.5, 1.2 Hz, 1H), 7.24 (d, *J* = 8.7 Hz, 1H), 6.98 (d, *J* = 2.6 Hz, 1H), 6.85 (dd, *J* = 8.7, 2.7 Hz, 1H), 5.30 (s, 1H).
^{13}C NMR (101 MHz, DMSO) δ 182.0, 181.2, 157.2, 147.7, 134.9, 132.6, 130.9, 130.3, 129.6, 129.6, 126.0, 125.6, 125.3, 116.3, 115.3, 102.0.

IR υ_{max} (solid) 3346, 3319, 1603, 1527, 1287, 1207, 775 cm^{-1}.

HRMS Exact mass calculated for $[M+H]^+$ ($C_{16}H_{11}O_3NCl$) requires m/z 300.0422, found $[M+H]^+$ m/z 300.0425.

10-Methoxy-7*H*-pyrido[3,4-*c*]carbazole, **3.62a**

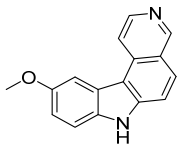

6-Bromoisoquinoline (100 mg, 0.48 mmol, 1 equiv.), 2-chloro-4-methoxyaniline (90.9 mg, 0.58 mmol, 1.2 equiv.), $Pd(OAc)_2$ (5.4 mg, 5 mol%), DavePhos (18.9 mg, 10 mol%) and K_3PO_4 (306 mg, 1.44 mmol, 3 equiv.) were added to a dry microwave vial (2 – 5 mL). 1,4-dioxane (5 mL, 0.1 mol/L) was added and the lid was secured to the vial. The vial was evacuated and purged with argon 3 times and heated at 120 °C for 30 minutes then 160 °C for 8 hours under microwave irradiation. The reaction was cooled, diluted with water (25 mL) and filtered through celite. The organic phase was then extracted with DCM (3 x 50 mL), dried with $MgSO_4$, filtered and the solvent was removed *in vacuo*. The crude compound was purified by RP-HPLC (C18) twice to afford the pure compound (**3.62a**) as a brown solid (105 mg, 88 %).

^{1}H NMR (500 MHz, DMSO) δ 12.72 (s, 1H), 9.76 (s, 1H), 9.12 (d, *J* = 6.8 Hz, 1H), 8.72 (d, *J* = 6.8 Hz, 1H), 8.38 (d, *J* = 9.0 Hz, 1H), 8.17 (d, *J* = 8.9 Hz, 1H), 8.13 (d, *J* = 2.3 Hz, 1H), 7.74 (d, *J* = 8.9 Hz, 1H), 7.25 (dd, *J* = 8.8, 2.5 Hz, 1H), 3.99 (s, 3H).

^{13}C NMR (101 MHz, DMSO) δ 155.0, 145.8, 142.5, 134.8, 134.1, 133.9, 127.4, 122.7, 122.4, 118.9, 117.9, 115.5, 113.5, 112.7, 104.3, 56.0.

IR υ_{max} (solid) 3150, 3044, 2099, 1651, 1621, 1190, 1132, 835, 723 cm^{-1}.

HRMS Exact mass calculated for $[M + H]^+$ ($C_{16}H_{13}ON_2$) requires *m*/*z* 249.1022, found $[M + H]^+$ *m*/*z* 249.1024.

10-Methyl-7*H*-pyrido[3,4-*c*]carbazole, **3.62b**

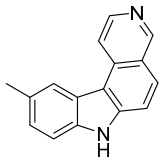

6-Bromoisoquinoline (100 mg, 0.48 mmol, 1 equiv.), 2-chloro-4-methylaniline (81.7 mg, 0.578 mmol, 1.2 equiv.), $Pd(OAc)_2$ (5.4 mg, 5 mol%), DavePhos (18.9 mg, 10 mol%) and K_3PO_4 (306 mg, 1.44 mmol, 3 equiv.) were added to a dry microwave vial (2 – 5 mL). 1,4-dioxane (5 mL, 0.1 mol/L) was added and the lid was secured to the vial. The vial was evacuated and purged with argon 3 times and heated at 120 °C for 30 minutes then 160 °C for 8 hours under microwave irradiation. The reaction was cooled, diluted with water (25 mL) and filtered through celite. The organic phase was then extracted with DCM (3 x 50 mL), dried with $MgSO_4$, filtered and the solvent was removed *in vacuo*. The crude compound was purified by silica column chromatography, petroleum ether (40 – 60 °C):ethyl acetate (100:0 → 30:70) then by RP-HPLC (C18) afford the pure compound (**3.62b**) as a yellow solid (46.4 mg, 42 %).

^{1}H NMR (400 MHz, DMSO) δ 12.65 (s, 1H), 9.73 (s, 1H), 9.05 (d, *J* = 6.7 Hz, 1H), 8.72 (d, *J* = 6.5 Hz, 1H), 8.53 (s, 1H), 8.36 (d, *J* = 8.9 Hz, 1H), 8.15 (d, *J* = 8.9 Hz, 1H), 7.69 (d, *J* = 8.8 Hz, 1H), 7.42 (dd, *J* = 8.3, 1.0 Hz, 1H), 2.60 (s, 3H).
^{13}C NMR (101 MHz, DMSO) δ 146.0, 142.4, 137.4, 134.7, 133.9, 130.6, 127.6, 127.5, 122.4, 122.4, 121.6, 119.0, 117.9, 112.7, 112.4, 21.3.
IR υ_{max} (solid) 3193, 3163, 3048, 2088, 1660, 1584, 1179, 1127, 798 cm^{-1}.
HRMS Exact mass calculated for $[M + H]^+$ ($C_{16}H_{13}N_2$) requires *m*/*z* 233.10736, found $[M + H]^+$ *m*/*z* 233.1073.

9-Fluoro-7*H*-pyrido[3,4-*c*]carbazole, **3.62c**

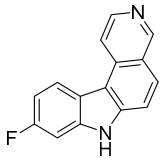

6-Bromoisoquinoline (100 mg, 0.48 mmol, 1 equiv.), 2-chloro-5-fluoroaniline (84 mg, 0.58 mmol, 1.2 equiv.), $Pd(OAc)_2$ (5.4 mg, 5 mol%), DavePhos (18.9 mg, 10 mol%) and K_3PO_4 (306 mg, 1.44 mmol, 3 equiv.) were added to a dry microwave vial (2 – 5 mL). 1,4-dioxane (5 mL, 0.1 mol/L) was added and the lid was secured to the vial. The vial was evacuated and purged with

argon 3 times and heated at 120 °C for 30 minutes then 160 °C for 8 hours under microwave irradiation. The reaction was cooled, diluted with water (25 mL) and filtered through celite. The organic phase was then extracted with DCM (3 x 50 mL), dried with $MgSO_4$, filtered and the solvent was removed *in vacuo*. The crude compound was purified by silica column chromatography, petroleum ether (40 – 60 °C):ethyl acetate (100:0 → 30:70) then by RP-HPLC (C18) afford the compound (**3.62c**) as a brown solid (28.6 mg, 25 %). A second impurity was observed in the NMR's.

^{1}H NMR (500 MHz, DMSO) δ 12.79 (s, 1H), 9.74 (s, 1H), 9.03 (d, *J* = 6.6 Hz, 1H), 8.78 – 8.72 (m, 2H), 8.38 (d, *J* = 8.9 Hz, 1H), 8.18 (d, *J* = 8.9 Hz, 1H), 7.60 (dd, *J* = 9.6, 2.3 Hz, 1H), 7.33 (td, *J* = 9.1, 2.4 Hz, 1H).

^{13}C NMR (101 MHz, DMSO) δ 160.9 (d, *J* = 241.0 Hz), 146.7, 142.9, 139.9 (d, *J* = 12.6 Hz), 134.6, 134.0, 128.7, 127.7, 123.4 (d, *J* = 10.3 Hz), 122.6, 119.0, 118.5, 117.6, 117.5, 112.8, 109.6 (d, *J* = 24.5 Hz), 99.1 (d, *J* = 26.1 Hz).

^{19}F NMR (470 MHz, DMSO) δ -114.62, -107.54 (impurity).

IR υ_{max} (solid) 3132, 3070, 2088, 1660, 1363, 1127, 825 cm^{-1}.

HRMS Exact mass calculated for $[M + H]^+$ ($C_{15}H_{10}N_2F$) requires *m*/*z* 237.0823, found $[M + H]^+$ *m*/*z* 237.0823.

10-Methoxy-7*H*-pyrido[2,3-*c*]carbazole, **3.62d**

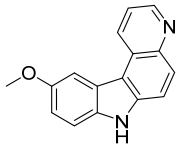

6-Bromoquinoline (100 mg, 0.48 mmol, 1 equiv.), 2-chloro-4-methoxyaniline (90.9 mg, 0.58 mmol, 1.2 equiv.), $Pd(OAc)_2$ (5.4 mg, 5 mol%), DavePhos (18.9 mg, 10 mol%) and K_3PO_4 (306 mg, 1.44 mmol, 3 equiv.) were added to a dry microwave vial (2 – 5 mL). 1,4-dioxane (5 mL, 0.1 mol/L) was added and the lid was secured to the vial. The vial was evacuated and purged with argon 3 times and heated at 120 °C for 30 minutes then 160 °C for 8 hours under microwave irradiation. The reaction was cooled, diluted with water (25 mL) and filtered through celite. The organic phase was then extracted with DCM (3 x 50 mL), dried with $MgSO_4$, filtered and the solvent was removed *in vacuo*. The crude compound was purified by RP-HPLC (C18) twice to afford the pure compound (**3.62d**) as a brown solid (62.1 mg, 52 %).

^{1}H NMR (500 MHz, DMSO) δ 12.17 (s, 1H), 9.66 (d, *J* = 8.8 Hz, 1H), 9.04 (dd, *J* = 5.1, 1.1 Hz, 1H), 8.22 (d, *J* = 9.1 Hz, 1H), 8.11 (d, *J* = 7.1 Hz, 1H), 8.10 (s, 1H), 8.00 (dd, *J* = 8.5, 5.0 Hz, 1H), 7.67 (d, *J* = 8.9 Hz, 1H), 7.20 (dd, *J* = 8.9, 2.4 Hz, 1H), 3.98 (s, 3H).

^{13}C NMR (101 MHz, DMSO) δ 158.2, 157.4, 154.4, 141.9, 137.7, 136.9, 134.2, 124.9, 122., 121.8, 120.4, 115., 113.2, 113.2, 103.8, 55.9.

IR υ_{max} (solid) 3174, 3070, 3007, 2088, 1668, 1190, 1121. 807 cm^{-1}.

HRMS Exact mass calculated for $[M + H]^+$ ($C_{16}H_{13}ON_2$) requires *m*/*z* 249.1022, found $[M + H]^+$ *m*/*z* 249.1024.

10-Methoxy-7*H*-pyrazino[2,3-*c*]carbazole, **3.62e**

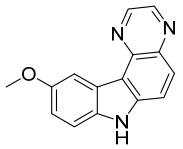

6-Bromoquinoxaline (100 mg, 0.48 mmol, 1 equiv.), 2-chloro-4-methoxyaniline (90.5 mg, 0.57 mmol, 1.2 equiv.), $Pd(OAc)_2$ (5.38 mg, 5 mol%), DavePhos (18.9 mg, 10 mol%) and K_3PO_4 (304 mg, 1.43 mmol, 3 equiv.) were added to a dry microwave vial (2 – 5 mL). 1,4-dioxane (4.97 mL, 0.1 mol/L) was added and the lid was secured to the vial. The vial was evacuated and purged with argon 3 times and heated at 120 °C for 30 minutes then 160 °C for 8 hours under microwave irradiation. The reaction was cooled, diluted with water (25 mL) and filtered through celite. The organic phase was then extracted with DCM (3 x 50 mL), dried with $MgSO_4$, filtered and the solvent was removed *in vacuo*. The crude compound was purified by RP-HPLC (C18) twice to afford the pure compound (**3.62e**) as a dark red crystalline solid (99.7 mg, 84 %).

^{1}H NMR (500 MHz, DMSO) δ 11.97 (s, 1H), 9.04 (d, *J* = 2.0 Hz, 1H), 8.86 (d, *J* = 2.0 Hz, 1H), 8.29 (d, *J* = 2.5 Hz, 1H), 8.05 (d, *J* = 8.9 Hz, 1H), 7.98 (d, *J* = 8.9 Hz, 1H), 7.61 (d, *J* = 8.8 Hz, 1H), 7.13 (dd, *J* = 8.7, 2.6 Hz, 1H), 3.91 (s, 3H).

^{13}C NMR (126 MHz, DMSO) δ 154.1, 144.2, 141.2, 140.3, 139.5, 138.7, 133.8, 126.5, 123.3, 118.1, 115.0, 114.5, 112.7, 104.4, 55.5.

IR υ_{max} (solid) 3191, 1673, 1540, 1476, 1142 cm^{-1}.

HRMS Exact mass calculated for $[M + H]^+$ ($C_{15}H_{12}ON_3$) requires *m*/*z* 250.0975, found $[M + H]^+$ *m*/*z* 250.0975.

9-Methoxy-6*H*-indolo[2,3-*b*]quinoxaline,[247] **3.62f**

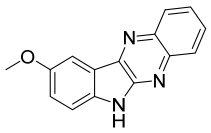

2-Bromoquinoxaline (100 mg, 0.48 mmol, 1 equiv.), 2-chloro-4-methoxyaniline (90.5 mg, 0.57 mmol, 1.2 equiv.), $Pd(OAc)_2$ (5.38 mg, 5 mol%), DavePhos (18.9 mg, 10 mol%) and K_3PO_4 (304 mg, 1.43 mmol, 3 equiv.) were added to a dry microwave vial (2 – 5 mL). 1,4-dioxane (4.97 mL, 0.1 mol/L) was added and the lid was secured to the vial. The vial was evacuated and purged with argon 3 times and heated at 120 °C for 30 minutes then 160 °C for 8 hours under microwave irradiation. The reaction was cooled, diluted with water (25 mL) and filtered through celite. The organic phase was then extracted with DCM (3 x 50 mL), dried with $MgSO_4$, filtered and the solvent was removed *in vacuo*. The crude compound was purified by RP-HPLC (C18) to afford the pure compound (**3.62f**) as an orange solid (61.7 mg, 52 %).

^{1}H NMR (500 MHz, DMSO) δ 9.22 (s, 1H), 8.80 (d, *J* = 8.2 Hz, 1H), 8.14 (dd, *J* = 8.1, 1.2 Hz, 1H), 8.09 (d, *J* = 2.2 Hz, 1H), 8.00 (d, *J* = 8.9 Hz, 1H), 7.87 (ddd, *J* = 8.7, 7.9, 1.3 Hz, 1H), 7.69 (t, *J* = 7.6 Hz, 1H), 7.33 (dd, *J* = 9.0, 2.3 Hz, 1H), 4.04 (s, 3H).
^{13}C NMR (151 MHz, DMSO) δ 157.6, 146.0, 140.5, 138.4, 135.2, 130.2, 130.0, 130.0, 129.1, 125.7, 122.0, 116.3, 115.9, 97.4, 56.2.
IR υ_{max} (solid) 2920, 2849, 1755, 1586, 1463, 1142 cm^{-1}.
HRMS Exact mass calculated for $[M + H]^+$ ($C_{15}H_{12}ON_3$) requires *m*/*z* 250.0975, found $[M + H]^+$ *m*/*z* 250.0974.

8-Methoxy-3,5-dihydro-1*H*-furo[3,4-*b*]carbazole, **3.62g**

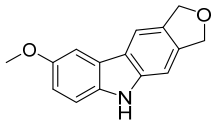

5-Bromo-1,3-dihydrobenzofuran (95.7 mg, 0.48 mmol, 1 equiv.), 2-chloro-4-methoxyaniline (90.9 mg, 0.58 mmol, 1.2 equiv.), $Pd(OAc)_2$ (5.4 mg, 5 mol%), DavePhos (18.9 mg, 10 mol%) and K_3PO_4 (306 mg, 1.44 mmol, 3 equiv.) were added to a dry microwave vial (2 – 5 mL). 1,4-dioxane (5 mL, 0.1 mol/L) was added and the lid was secured to the vial. The vial was evacuated and purged with argon 3 times and heated at 120 °C for 30 minutes then 160 °C for 8 hours under

microwave irradiation. The reaction was cooled, diluted with water (25 mL) and filtered through celite. The organic phase was then extracted with DCM (3 x 50 mL), dried with $MgSO_4$, filtered and the solvent was removed *in vacuo*. The crude compound was purified by silica column chromatography, petroleum ether (40 – 60 °C):ethyl acetate (100:0 → 30:70) to afford the pure compound (**3.62g**) as a brown crystalline solid (12.5 mg, 11 %).

^{1}H NMR (500 MHz, DMSO) δ 10.98 (s, 1H), 7.96 (s, 1H), 7.64 (d, *J* = 2.3 Hz, 1H), 7.35 (d, *J* = 8.7 Hz, 1H), 7.32 (s, 1H), 6.99 (dd, *J* = 8.8, 2.5 Hz, 1H), 5.11 (s, 4H), 3.83 (s, 3H).
^{13}C NMR (101 MHz, DMSO) δ 152.9, 140.4, 137.2, 135.0, 129.2, 122.5, 122.3, 114.5, 112.2, 111.6, 103.2, 102.9, 72.5, 72.2, 55.6.
IR υ_{max} (solid) 3396, 2918, 2845, 1461, 1437, 1209, 1023, 846 cm^{-1}.
HRMS Exact mass calculated for $[M - H]^+$ ($C_{15}H_{12}O_2N$) requires *m*/*z* 238.0868, found $[M - H]^+$ *m*/*z* 238.0871.

2-Methoxy-5*H*-benzo[*b*]carbazole-6,11-dione,[248] **3.62h**

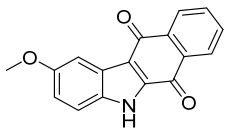

2-Bromonaphthalene-1,4-dione (114 mg, 0.48 mmol, 1 equiv.), 2-chloro-4-methoxyaniline (90.9 mg, 0.57 mmol, 1.2 equiv.), $Pd(OAc)_2$ (5.4 mg, 5 mol%), DavePhos (18.9 mg, 10 mol%) and K_3PO_4 (306 mg, 1.44 mmol, 3 equiv.) were added to a dry microwave vial (2 – 5 mL). 1,4-dioxane (5 mL, 0.1 mol/L) was added and the lid was secured to the vial. The vial was evacuated and purged with argon 3 times and heated at 120 °C for 30 minutes then 160 °C for 8 hours under microwave irradiation. The reaction was cooled, diluted with water (25 mL) and filtered through celite. The organic phase was then extracted with DCM (3 x 50 mL), dried with $MgSO_4$, filtered and the solvent was removed *in vacuo*. The crude compound was purified by silica column chromatography, petroleum ether (40 – 60 °C):ethyl acetate (100:0 → 30:70) and 5 % NEt_3 to afford the pure compound (**3.62h**) as a brown solid (44.7 mg, 34 %).

^{1}H NMR (400 MHz, DMSO) δ 13.02 (s, 1H), 8.11 (td, *J* = 7.9, 1.5 Hz, 2H), 7.86 (td, *J* = 7.5, 1.5 Hz, 1H), 7.81 (td, *J* = 7.4, 1.7 Hz, 1H), 7.63 (d, *J* = 2.5 Hz, 1H), 7.51 (d, *J* = 9.1 Hz, 1H), 7.10 (dd, *J* = 9.0, 2.6 Hz, 1H), 3.86 (s, 3H).
^{13}C NMR (101 MHz, DMSO) δ 182.3, 177.2, 157.0, 137.0, 134.2, 133.4, 133.1, 132.8, 126.0, 124.9, 118.4, 117.0, 115.0, 102.1, 55.4.

IR υ_{max} (solid) 3178, 1668, 1640, 1588, 1220, 1104 cm^{-1}.

HRMS Exact mass calculated for $[M + H]^+$ ($C_{17}H_{12}O_3N$) requires *m*/*z* 278.0812, found $[M + H]^+$ *m*/*z* 278.0814.

3-Methoxy-5*H*-benzo[*b*]carbazole-6,11-dione,[248] **3.62i**

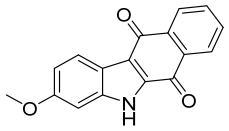

2-Bromonaphthalene-1,4-dione (114 mg, 0.48 mmol, 1 equiv.), 2-chloro-5-methoxyaniline (103 mg, 0.578 mmol, 1.2 equiv.), $Pd(OAc)_2$ (5.4 mg, 5 mol%), DavePhos (18.9 mg, 10 mol%) and K_3PO_4 (306 mg, 1.44 mmol, 3 equiv.) were added to a dry microwave vial (2 – 5 mL). 1,4-dioxane (5 mL, 0.1 mol/L) was added and the lid was secured to the vial. The vial was evacuated and purged with argon 3 times and heated at 120 °C for 30 minutes then 160 °C for 8 hours under microwave irradiation. The reaction was cooled, diluted with water (25 mL) and filtered through celite. The organic phase was then extracted with DCM (3 x 50 mL), dried with $MgSO_4$, filtered and the solvent was removed *in vacuo*. The crude compound was purified by silica column chromatography, petroleum ether (40 – 60 °C):ethyl acetate (100:0 → 30:70) and 5 % NEt_3 to afford the pure compound (**3.62i**) as an orange solid (55.6 mg, 42 %).

^{1}H NMR (400 MHz, DMSO) δ 12.89 (s, 1H), 8.11 – 8.03 (m, 3H), 7.86 – 7.77 (m, 2H), 7.02 (dd, *J* = 8.8, 2.3 Hz, 1H), 6.98 (d, *J* = 2.0 Hz, 1H), 3.85 (s, 3H).

^{13}C NMR (101 MHz, DMSO) δ 180.6, 176.8, 159.4, 139.8, 136.4, 134.0, 133.9, 133.2, 132.7, 126.0, 125.9, 123.2, 118.0, 117.9, 115.5, 95.1, 55.4.

IR υ_{max} (solid) 2918, 2849, 1662, 1197, 1104 cm^{-1}.

HRMS Exact mass calculated for $[M + H]^+$ ($C_{17}H_{12}O_3N$) requires *m*/*z* 278.0812, found $[M + H]^+$ *m*/*z* 278.0815.

2-Methyl-5*H*-benzo[*b*]carbazole-6,11-dione,[249] **3.62j**

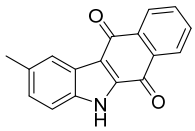

2-Bromonaphthalene-1,4-dione (114 mg, 0.48 mmol, 1 equiv.), 2-chloro-4-methylaniline (81.7 mg, 0.58 mmol, 1.2 equiv.), $Pd(OAc)_2$ (5.4 mg, 5 mol%), DavePhos (18.9 mg, 10 mol%) and K_3PO_4 (306 mg, 1.44 mmol, 3 equiv.) were added to a dry microwave vial (2 – 5 mL). 1,4-dioxane (5 mL, 0.1 mol/L) was added and the lid was secured to the vial. The vial was evacuated and purged with argon 3 times and heated at 120 °C for 30 minutes then 160 °C for 8 hours under microwave irradiation. The reaction was cooled, diluted with water (25 mL) and filtered through celite. The organic phase was then extracted with DCM (3 x 50 mL), dried with $MgSO_4$, filtered and the solvent was removed *in vacuo*. The crude compound was purified by silica column chromatography, petroleum ether (40 – 60 °C):ethyl acetate (100:0 → 30:70) and 5 % NEt_3 to afford the pure compound (**3.62j**) as an orange solid (78.4 mg, 52 %).

^{1}H NMR (500 MHz, DMSO) δ 13.00 (s, 1H), 8.11 (dd, *J* = 7.5, 1.1 Hz, 1H), 8.10 (dd, *J* = 7.5, 1.2 Hz, 1H), 8.01 (s, 1H), 7.85 (td, *J* = 7.4, 1.4 Hz, 1H), 7.81 (td, *J* = 7.5, 1.4 Hz, 1H), 7.49 (d, *J* = 8.4 Hz, 1H), 7.28 (dd, *J* = 8.5, 1.3 Hz, 1H), 2.46 (s, 3H).

^{13}C NMR (101 MHz, DMSO) δ 180.3, 177.5, 137.1, 136.9, 134.2, 134.1, 133.4, 133.2, 132.7, 128.9, 126.1, 126.0, 124.3, 121.6, 116.9, 113.6, 21.3.
IR υ_{max} (solid) 3178, 2916, 2854, 1638, 1385, 1216 cm^{-1}.
HRMS Exact mass calculated for $[M + H]^+$ ($C_{17}H_{12}O_2N$) requires *m*/*z* 262.0863, found $[M + H]^+$ *m*/*z* 262.0865.

5*H*-benzo[*b*]carbazole-6,11-dione,[250] **3.62k**

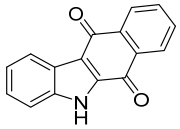

2-Bromonaphthalene-1,4-dione (114 mg, 0.48 mmol, 1.0 equiv.), 2-chloroaniline (73.6 mg, 0.58 mmol, 1.2 equiv.), $Pd(OAc)_2$ (5.4 mg, 5 mol%), DavePhos (18.9 mg, 10 mol%) and K_3PO_4 (306.3 mg, 1.44 mmol, 3.0 equiv.) were added to a dry microwave vial (2 – 5 mL). 1,4-dioxane (5 mL, 0.1 mol/L) was added and the lid was secured to the vial. The vial was evacuated and purged with argon 3 times and heated at 120 °C for 30 minutes then 160 °C for 8 hours under microwave

irradiation. The reaction was cooled, diluted with water (25 mL) and filtered through celite. The organic phase was then extracted with DCM (3 x 50 mL), dried with $MgSO_4$, filtered and the solvent was removed *in vacuo*. The crude compound was purified by silica column chromatography, petroleum ether (40 – 60 °C):ethyl acetate (100:0 → 30:70) and 5 % NEt_3 to afford the pure compound (**3.62k**) as an orange solid (107 mg, 90 %).

^{1}H NMR (500 MHz, DMSO) δ 13.12 (s, 1H), 8.21 (d, *J* = 8.0 Hz, 1H), 8.11 (ddd, *J* = 9.5, 7.3, 1.2 Hz, 2H), 7.86 (td, *J* = 7.6, 1.4 Hz, 1H), 7.82 (td, *J* = 7.5, 1.5 Hz, 1H), 7.60 (d, *J* = 8.3 Hz, 1H), 7.45 (ddd, *J* = 8.5, 6.8, 1.0 Hz, 1H), 7.37 (ddd, *J* = 8.3, 6.9, 0.7 Hz, 1H).
^{13}C NMR (101 MHz, DMSO) δ 180.3, 177.6, 138.3, 137.2, 134.2, 134.1, 133.2, 132.6, 126.9, 126.1, 126.0, 123.9, 123.9, 122.3, 117.3, 113.9.
IR υ_{max} (solid) 3256, 2923, 2851, 1646, 1398, 1214, 1147, 1015 cm^{-1}.
HRMS Exact mass calculated for $[M+H]^+$ ($C_{16}H_{10}O_2N$) requires m/z 248.0706, found $[M+H]^+$ m/z 248.0708.

2-Methoxy-6,11-dimethyl-5*H*-benzo[*b*]carbazole[251], **2.7**

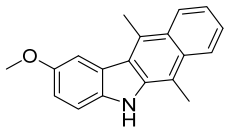

A magnetically stirred suspension of 2-methoxy-5*H*-benzo[*b*]carbazole-6,11-dione (20 mg, 0.07 mmol, 1.0 equiv.) in dry THF (5 mL) was heated under Ar at 40-50 °C for 20-30 minutes to effect dissolution, and the resulting orange solution was then rapidly cooled to -78 °C and treated over 30 s *via* syringe with MeLi (1.60 M in Et_2O, 113 µL, 0.18 mmol, 2.5 equiv.). The resulting brown solution was stirred at -85 °C for 1.5 hours and then allowed to warm to -10 °C over 3 hours. A crude LCMS sample was ran but only one methylation had taken place. The reaction mixture was cooled to -78 °C again and 1.5 equiv. MeLi (67.6 µL, 0.108 mmol, 1.5 equiv.) was added to the yellow-orange solution and left to warm to room temperature over 3 hours . A second crude LCMS sample was taken which still only showed one methylation has taken place. This suggested that this synthetic route was not suitable to obtain **2.7**.

6-Hydroxy-2-methoxy-6-methyl-5,6-dihydro-11*H*-benzo[*b*]carbazol-11-one, **3.63**

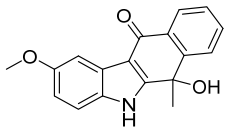

A magnetically stirred suspension of 2-methoxy-5*H*-benzo[*b*]carbazole-6,11-dione (20 mg, 0.07 mmol, 1.0 equiv.) in dry THF (5 mL) was heated under Ar at 40-50 °C for 20-30 minutes to effect dissolution, and the resulting orange solution was then rapidly cooled to -78 °C and treated over 30 s *via* syringe with MeLi (1.60 M in Et_2O, 113 µL, 0.18 mmol, 2.5 equiv.). The resulting brown solution was stirred at -85 °C for 1.5 hours and then allowed to warm to -10 °C over 3 hours. A crude LCMS sample was ran but only one methylation had taken place. The reaction mixture was cooled to -78 °C again and 1.5 equiv. MeLi (67.6 µL, 0.108 mmol, 1.5 equiv.) was added to the yellow-orange solution and left to warm to room temperature over 3 hours . A second crude LCMS sample was taken which still only showed one methylation has taken place. Distilled H_2O (2 mL) was added, the mixture was stirred for 5 minutes then the organic layer was extracted with $CHCl_3$, dried with $MgSO_4$, filtered and the solvent was removed *in vacuo*. The crude compound was purified by silica column chromatography, petroleum ether (40 – 60 °C):ethyl acetate (100:0 → 30:70) to afford the pure compound (**3.63**) as an orange solid (15.0 mg, 70 %).

^{1}H NMR (500 MHz, DMSO) δ 12.25 (s, 1H), 8.12 (dd, *J* = 7.9, 1.3 Hz, 1H), 7.88 (dd, *J* = 8.0, 0.8 Hz, 1H), 7.71 – 7.64 (m, 2H), 7.51 (td, *J* = 7.5, 1.1 Hz, 1H), 7.39 (d, *J* = 8.8 Hz, 1H), 6.90 (dd, *J* = 8.7, 2.5 Hz, 1H), 6.33 (s, 1H), 3.82 (s, 3H), 1.75 (s, 3H).

^{13}C NMR (101 MHz, DMSO) δ 179.2, 155.7, 155.2, 148.1, 132.2, 131.8, 131.7, 127.8, 126.7, 125.4, 125.4, 113.2, 113.1, 109.3, 103.2, 66.9, 55.6, 33.0.

IR υ_{max} (solid) 3394, 2256, 1655, 1024, 997, 762 cm^{-1}.

HRMS Exact mass calculated for $[M+H]^+$ ($C_{18}H_{16}O_3N$) requires m/z 294.1125, found $[M+H]^+$ m/z 294.1127.

3-Chloro-1-(2,5-dimethylphenyl)propan-1-one[252]

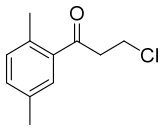

To an ice cold solution of $AlCl_3$ (1.5 g, 1.13 mol, 1.2 equiv.) in dry DCM (5 mL) 3-chloropropionyl chloride (1.2 g, 0.94 mol, 1.0 equiv.) in dry DCM (5 mL) was added slowly over 15 minutes. A solution of *p*-xylene (1.0g, 0.94 mol, 1.0 equiv.) in dry DCM (5 mL) was added dropwise over 5 minutes. The ice bath was removed and the solution was heated to room temperature and left to stir for 4 hours. Ice cold water was added and the DCM was removed *in vauco*. The aqueous layer was extracted with Et_2O and the combined organic layers were washed with 50 mL 8 % $NaCO_3$ solution then with water and dried with $NaSO_4$, and evaporated to dryness. The crude compound was recrystallised in petroleum ether to produce a yellow solid (1.8 g, 79 % yield).

^{1}H NMR (400 MHz, DMSO) δ 7.60 (s, 1H), 7.26 (dd, *J* = 7.6 Hz, 1.2 Hz, 1H), 7.19 (d, *J* = 7.6 Hz, 1H), 3.90 (t, *J* = 6.2 Hz, 2H), 3.45 (t, *J* = 6.2 Hz, 2H), 2.37 (s, 3H), 2.34 (s, 3H).
^{13}C NMR (101 MHz, DMSO) δ 200.8, 137.1, 135.1, 134.0, 132.1, 131.5, 129.2, 43.4, 39.8, 20.4, 20.2.
LRMS (GCMS BASIC_PCI_GC320) R_t = 12.35, m/z = 197.0 $[M+H]^+$.

4,7-Dimethyl-2,3-dihydro-1*H*-inden-1-one[253], **3.69**

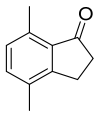

3-Chloro-1-(2,5-dimethylphenyl)propan-1-one (1.46 g, 0.704 mol, 1.0 equiv.) was dissolved in H_2SO_4 conc (1 mL) in a round bottom and heated to 95 °C for 2 hours. The reaction mixture was diluted with Et_2O and washed with water, brine, dried and concentrated *in vacuo* to give the pure product (**3.69**) as a solid (0.99 g, 84 % yield).

^{1}H NMR (400 MHz, MeOD) δ 7.30 (d, *J* = 7.5 Hz, 1H), 7.04 (d, *J* = 7.5 Hz, 1H), 3.02 – 2.95 (m, 2H), 2.67 – 2.62 (m, 2H), 2.55 (s, 3H), 2.32 (s, 3H).
^{13}C NMR (101 MHz, DMSO) δ 208.4, 154.0, 134.1, 133.2, 132.2, 131.6, 127.6, 34.8, 22.4, 15.4, 14.6.
LRMS (GCMS BASIC_PCI_GC320) R_t = 11.86, m/z = 161.1 $[M+H]^+$.

4,7-Dimethyl-2,3-dihydro-1*H*-inden-1-ol[253], **3.70**

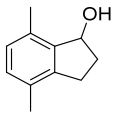

A solution of 5-bromo-4,7-dimethyl-2,3-dihydro-1*H*-inden-1-one (0.99 g, 6.2 mmol, 1.0 equiv.) in EtOH (20 mL) was cooled in an ice bath to 0 °C and $NaBH_4$ (0.16 g, 4.17 mmol, 0.67 equiv.) was added slowly over 5 minutes. The reaction was heated to r.t. and left to stir for 2 hours. The solvent was removed under vacuum and water was added. The aqueous mixture was extracted with diethyl ether and the combined organic layers were washed with brine, dried and concentrated *in vacuo* to give the pure product (**3.70**) as a yellow solid (0.89 g, 89 %).

^{1}H NMR (500 MHz, DMSO) δ 6.93 (d, *J* = 7.6 Hz, 1H), 6.86 (d, *J* = 7.6 Hz, 1H), 5.11 (td, *J* = 6.8, 3.0 Hz, 1H), 4.82 (d, *J* = 6.8 Hz, 1H), 2.89 (quin., *J* = 8.0 Hz, 1H), 2.65-2.59 (m, 1H), 2.25-2.18 (m, 1H), 1.90-1.84 (3, 1H), 2.30 (s, 3H), 2.17 (s, 3H).
^{13}C NMR (101 MHz, DMSO) δ 143.4, 142.0, 131.6, 130.3, 128.4, 127.5, 73.6, 34.5, 28.4, 18.3, 17.8.
LRMS (GCMS BASIC_PCI_GC320) R_t = 11.79, m/z = 161.1 $[M+H]^+$.

4,7-Dimethyl-1*H*-indene[254], **3.71**

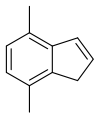

4,7-Dimethyl-2,3-dihydro-1*H*-inden-1-ol (0.89 g, 5.6 mmol, 1.0 equiv.) and *p*-TsOH (11.0 mg, 0.06 mmol) were dissolved in benzene (140 mL) and heated to reflux for 3 hours. The reaction mixture was cooled and the solvent was evaporated under pressure to produce an orange solid. The crude material was purified by silica column chromatography hexane:ethyl acetate (95:5). The NMR did not appear clean and the peaks were not well defined therefore **3.71** was not isolated.

4-Bromo-2,5-dimethylbenzaldehyde[120], **3.73**

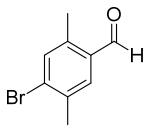

A solution of 2,5-dibromo-*p*-xylene (2.64 g, 10 mmol, 1.0 equiv.) and THF (5 mL) was made and cooled to – 78 °C. *n*-BuLi (4.4 mL, 10.5 mmol, 1.05 equiv.) was added dropwise slowly over 10 minutes. The reaction mixture was left to stir at -78 °C for 10 minutes. DMF (1.6 mL, 20 mmol, 2.0 equiv.) was added and the solution was warmed to r.t. and stirred overnight. NH_4Cl (aq) (40 mL) was added and the aqueous layer was extracted with diethyl ether (2 x 70 mL). The organic layer was washed with brine (100 mL), dried and concentrated *in vacuo* to give an orange oil. The crude compound was purified by silica column chromatography, hexane:ethyl acetate (80:20), to give the product (**3.73**) as an off white solid (1.8 mg, 85 %).

^{1}H NMR (500 MHz, DMSO) δ 10.13 (s, 1H), 7.70 (s, 1H), 7.55 (s, 1H), 2.53 (s, 3H), 2.34 (s, 3H)
^{13}C NMR (101 MHz, DMSO) δ 192.4, 139.3, 135.4, 134.9, 133.7, 133.1, 133.0, 21.7, 17.8.
LRMS (GCMS Basic_PCI_GC320) R_t = 11.808, m/z = 213.0 $[M + H]^+$.

1-(4-Bromo-2,5-dimethylphenyl)-*N*-(3,3-diethoxypropyl)methanimine[255]

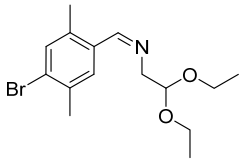

A solution of 4-bromo-2,5-dimethylbenzaldehyde (2.16g, 10.1 mmol, 1.0 equiv.) in toluene (dry), 40 mL, containing 2,2-diethoxyethanamine (1.5 mL, 10.6 mmol, 1.05 equiv.) was heated to reflux with Deak-Stark apparatus for around 4 hours. . Removal of the solvent afford the imine as an oil. The crude compound was purified by silica column chromatography, hexane:ethyl acetate (80:20), to give an orange solid (2.6 g, 78 %).

^{1}H NMR (500 MHz, DMSO) δ 8.51 (s, 1H), 7.71 (s, 1H), 7.49 (s, 1H), 4.74 (t, *J* = 5.4 Hz, 1H), 3.69 (dd, *J* = 5.2, 1.2 Hz, 2H), 3.67-3.60 (m, 2H), 3.54-3.47 (m, 2H), 2.43 (s, 3H), 2.33 (s, 3H), 1.11 (t, *J* = 6.8 Hz, 6H).
^{13}C NMR (101 MHz, DMSO) δ 160.8, 137.1, 134.7, 134.0, 133.3, 129.2, 126.1, 103.9, 101.4, 633.9, 61.5, 21.8, 17.9, 15.4, 15.3.
LRMS (GCMS Basic_PCI_GC320) R_t = 14.92, m/z = 328.0 $[M + H]^+$.

N-(4-bromo-2,5-dimethylbenzyl)-3,3-diethoxypropan-1-amine[255], **3.74**

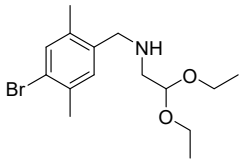

Sodium borohydride (1.5 g, 40.0 mmol, 5 equiv.) was added in portions to a stirred mixture of 1-(4-bromo-2,5-dimethylphenyl)-*N*-(3,3-diethoxypropyl)methanimine (2.62 g, 8.0 mmol, 1 equiv.) in methanol at 22 °C. The mixture was stirred for 1 hour and concentrated to dryness *in vacuo*, the residue was dissolved in ethyl ether (60 mL), and the ether solution was washed with water. The ether solution was cooled to 0 °C and acidified with a saturated solution of NH_4Cl. The separated solid was collected by filtration, combined with the acidic aqueous layer, and diluted with water. This mixture was cooled to 0 °C and basified with 10 M NaOH to pH 10 and extracted with chloroform. The organic layer was washed with water then brine, dried and evaporated to dryness to produce the desired product (**3.74**) as an orange solid (1.41 g, 53 %).

^{1}H NMR (400 MHz, DMSO) δ 7.35 (s, 1H), 7.26 (s, 1H), 4.53 (t, *J* = 5.5 Hz, 1H), 3.63 (s, 2H), 3.62 – 3.55 (m, 2H), 3.50 – 3.42 (m, 2H), 2.60 (d, *J* = 5.7 Hz, 2H), 2.29 (s, 3H), 2.24 (s, 3H), 1.18 – 1.05 (m, 6H).

^{13}C NMR (101 MHz, DMSO) δ 136.3, 135.3, 134.3, 132.8, 130.4, 122.1, 101.3, 61.8, 50.4, 49.3, 20.5, 16.4, 13.8.

LRMS (LCMS) R_t = 8.12, m/z = 286.0 $[M–OEt]^+$, +ve.

N-(4-bromo-2,5-dimethylbenzyl)-*N*-(3,3-diethoxypropyl)benzenesulfonamide[255],

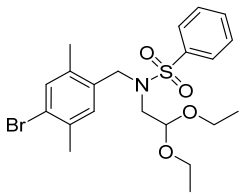

To a stirred solution of *N*-(4-bromo-2,5-dimethylbenzyl)-3,3-diethoxypropan-1-amine (1.41g, 4.28 mmol, 1.0 equiv.) in THF (40 mL) a 2.5 % solution of Na_2CO_3 (23 mL) and benzenesulfonyl chloride (0.76g, 4.28 mmol, 1.0 equiv.) was added. The reaction mixture was stirred for 1 hour at room temperature after which water was added and the reaction mixture was extracted with chloroform. The combined organic layers were washed with saturated sodium hydrogencarbonate solution and water and then evaporated under reduced pressure. The crude material was purified by silica column chromatography hexane:ethyl acetate (0 – 30 %). An off-white solid (1.03 g, 53 %) was collected.

^{1}H NMR (400 MHz, DMSO) δ 7.88 (d, *J* = 8.4 Hz, 2H), 7.72 (tt, *J* = 7.5, 1.3 Hz, 1H), 7.64 (t, *J* = 7.9 Hz, 2H), 7.38 (s, 1H), 7.06 (s, 1H), 4.35 (s, 2H), 4.30 (t, *J* = 5.3 Hz, 1H), 3.48 – 3.42 (m, 2H), 3.25 – 3.19 (m, 2H), 3.12 (d, *J* = 5.4 Hz, 2H), 2.21 (d, *J* = 5.4 Hz, 6H), 0.98 (t, *J* = 7.0 Hz, 6H).
^{13}C NMR (101 MHz, DMSO) δ 139.1, 136.1, 134.0, 134.0, 133.1, 133.0, 130.9, 19.4, 127.0, 122.6, 100.7, 62.1, 50.2, 50.0, 21.9, 17.7, 15.0.
LRMS (LCMS) R_t = 9.77, m/z = 330.0 [M – SO_2Ph], +ve, m/z = 353.9 [M–$CH_2CHO(Et)_2$]$^+$, -ve.

6-Bromo-5,8-dimethylisoquinoline[120], **3.67**

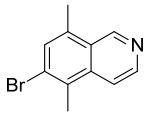

To a stirring solution of *N*-(4-bromo-2,5-dimethylbenzyl)-*N*-(3,3-diethoxypropyl)benzenesulfonamide (1.03 g, 2.158 mmol, 1.0 equiv.) in dioxane (53 mL) was added HCl (6.0 M, 10 mL) and the reaction was heated to reflux for 6 hours. The reaction mixture was cooled to room temperature and analysed by NMR and GC/MS did not confirm this as none of the major peaks gave the mass of the starting material or expected product. The solid was resubmitted to the original reaction conditions, however 10 mL HCl was added and the reaction was left to reflux for 6 hours. By TLC a new less polar spot had been formed. The crude mixture was columned to collect this new spot, however once analysed by NMR and GC/MS it did not completely resemble

the expected product. The two major peaks of the GC/MS trace have a mass of 252 (RT: 13.3 minutes) and 170 (RT: 17.8 minutes). The expected mass of the product is 236.11. The major peak at 13.3 minutes corresponds to M + 16 $[M+O]^+$ and contains the expected M + 2 peak of a compound containing bromine.

6,8-Bibromoisoquinolin-5-amine[241], **3.76a**

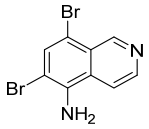

A solution of bromine (1.1 mL, 0.02 mol, 3.1 equiv.) in methanol (11 mL) was added slowly at RT to a methanolic solution (11 mL) containing 5-aminoisoquinoline (1.0 g, 6.94 mmol, 1.0 equiv) under stirring for 45 minutes. After complete addition, the excess bromine was removed by treatment with excess sodium thiosulphate, diluted with DCM and washed with water. The organic layer was then dried using anhydrous sodium sulphate, and concentrated in vacuo to afford a crude yellow solid. The crude material was purified by silica column chromatography petroleum ether (40 – 60 °C):ethyl acetate (0 – 70 %) to give the desired product (**3.76a**) as a yellow solid (1.75 g, 84 %).

^{1}H NMR (500 MHz, DMSO) δ 9.30 (s, 1H), 8.58 (d, *J* = 5.8 Hz, 1H), 8.17 (d, *J* = 6.0 Hz, 1H), 7.93 (s, 1H), 6.41 (s, 2H).
^{13}C NMR (101 MHz, DMSO) δ 150.8, 143.1, 141.5, 134.3, 126.8, 125.4, 115.7, 105.4, 104.0.
LRMS (LCMS) R_t = 7.34, m/z = 302.9 [M + H], +ve, m/z = 300.9 $[M – H]^+$, - ve.

6,8-Bibromoisoquinolin-5-ol, **3.76b**

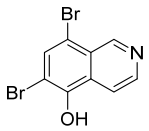

A solution of bromine (2.0 mL, 0.01 mol, 1.0 equiv.) in methanol (20 mL) was added slowly at RT to a methanolic solution (20 mL) containing 5-hydroxyisoquinoline (2.0 g, 0.01 mol, 1.0 equiv.) and NaHCO3 (2.0 g, 0.03 mol, 3.0 equiv.) under stirring for 3 hours. After complete addition, the excess bromine was removed by treatment with excess sodium bisulphate, diluted with DCM and washed with water. The organic layer was then dried using anhydrous sodium sulphate, and concentrated in vacuo to afford a crude yellow solid. The crude material was

purified by silica column chromatography petroleum ether (40 – 60 °C):ethyl acetate (0 – 70 %) to give the desired product (**3.76b**) as a yellow solid (3.6 g, 89 %).

^{1}H NMR (500 MHz, DMSO) δ 10.78 (s, 1H), 9.37 (s, 1H), 8.67 (d, *J* = 5.9 Hz, 1H), 8.12 – 8.07 (m, 2H).
^{13}C NMR (101 MHz, DMSO) δ 149.8, 149.5, 141.5, 135.0, 130.4 116.2, 111.2, 110.6.
LRMS (LCMS) R_t = 6.86, m/z = 303.9 [M + H], +ve.
IR υ_{max} (solid) 2916, 2116, 1372, 1045, 829 cm^{-1}.
HRMS Exact mass calculated for $[M+H]^+$ ($C_9H_6ONBr_2$) requires m/z 301.8811, found $[M+H]^+$ m/z 301.8815.

6-Bromoisoquinoline-5,8-dione[241], **3.74**

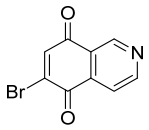

Method 1:
6,8-Dibromoisoquinolin-5-amine (1.0 g, 3.31 mol, 1 equiv.) was dissolved *in situ* in 3.86 mL of conc. sulphuric acid at 0 °C. To the above mixture, a solution of nitric acid (90 % fuming, 3.9 mL) and water (0.7 mL), was added dropwise for 30 minutes at 0 °C. The reaction mixture was then extracted by dichloromethane, and the organic layer was dried over anhydrous sodium sulphate. Finally, the dried solution was concentrated *in vacuo* to give a crude reddish brown solid. The crude material was purified by silica column chromatography petroleum ether (40 – 60 °C):ethyl acetate (0 – 70 %) to give the desired product (**3.74**) as a brown solid (110 mg, 14 %).
Method 2:
6,8-Dibromoisoquinolin-5-ol (1.0 g, 3.30 mol, 1 equiv.) was dissolved in situ in 3.87 mL of conc. sulphuric acid. To the above mixture, a solution of nitric acid (90 % fuming, 0.5 mL) and water (1.0 mL), was added dropwise for 30 minutes at 0°C. The reaction mixture was then extracted by dichloromethane, and the organic layer was dried over anhydrous sodium sulphate. Finally, the dried solution was concentrated *in vacuo* to give a crude reddish brown solid. The crude material was purified by silica column chromatography petroleum ether (40 – 60 °C):ethyl acetate (0 – 70 %) to give the desired product (**3.74**) as an orange solid (370 mg, 47 %).

^{1}H NMR (400 MHz, DMSO) δ 9.17 (s, 1H), 9.10 (d, *J* = 5.0 Hz, 1H), 7.92 (d, *J* = 5.0 Hz, 1H), 7.77 (s, 1H).

^{13}C NMR (101 MHz, DMSO) δ 182.3, 177.6, 155.5, 148.5, 147.7, 139.1, 136.5, 124.7, 119.1.
HRMS Exact mass calculated for $[M+H]^+$ ($C_9H_5O_2NBr$) requires m/z 237.9504, found $[M+H]^+$ m/z 237.9503.

9-Methoxy-5*H*-pyrido[4,3-*b*]carbazole-5,11(6*H*)-dione[256], **3.79b**

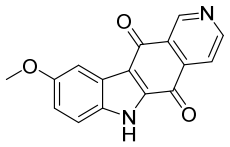

6-Bromoisoquinoline-5,8-dione (57.4 mg, 0.24 mmol, 1.0 equiv.), 2-chloro-4-methoxyaniline (45.5 mg, 0.29 mmol, 1.2 equiv.), $Pd(OAc)_2$ (2.7 mg, 5 mol%), DavePhos (9.4 mg, 10 mol%) and K_3PO_4 (154 mg, 0.72 mmol, 3.0 equiv.) were added to a dry microwave vial (2 – 5 mL). 1,4-dioxane (2.5 mL, 0.1 mol/L) was added and the lid was secured to the vial. The vial was evacuated and purged with argon 3 times and heated at 120 °C for 30 minutes then 160 °C for 8 hours under microwave irradiation . The reaction was cooled, diluted with water (25 mL) and filtered through celite. The organic phase was then extracted with DCM (3 x 50 mL), dried with $MgSO_4$, filtered and the solvent was removed *in vacuo*. The crude compound was purified by silica column chromatography, petroleum ether (40 – 60 °C):ethyl acetate (100:0 → 30:70) and 5 % NEt_3 to afford the impure compound (**3.79b**) as an orange oil (10.2 mg, 15 %).

LRMS (LCMS) R_t = 6.79, m/z = 279.0 [M + H], +ve, m/z = 277.0 $[M – H]^+$, - ve.

Chapter 4

Exploration of the Binding Profile and Splicing Efficiency of Putative G-quadruplex Stabilisers

UV Analysis: This work was carried out by the author

FRET Analysis: This work was kindly carried out by Dr Elise P. Wright at the University of East Anglia

NMR Analysis: This work was carried out by the author with guidance from Dr John Parkinson

Splicing Assays: This work was kindly carried out by Hatice Esenkaya at the University of Leicester

13 Techniques to Characterize Biomolecule•Ligand Interactions

There are several commonly used analytical techniques employed to investigate important biomolecule•ligand interactions, whether the biomolecule is DNA, RNA or protein-based. These include UV and Förster resonance energy transfer (FRET) melting assays, circular dichroism (CD) and nuclear magnetic resonance (NMR). UV, FRET and CD analysis can provide general information about the overall structure of the biomolecule and how this changes on addition of the ligand. The stability of the structure can also be investigated used UV and FRET melting analysis. On the other hand, NMR can be employed either as a HTS method to screen positive biomolecule•ligand interactions or as an aid to probe the intimate bonding interactions between the biomolecule and ligand. An introduction to the theory behind several of these techniques will be explained before results will be presented from the use of these techniques to study the interaction of ellipticine ligands previously synthesised with Bcl-x RNA and also probe the selectivity of the ligands with other DNA sequences.

13.1 UV spectrometry

Molecules that contain π-systems or non-bonding electrons can be promoted to an excited state by the absorption of energy from UV (10 – 400 nm) or visible light (390 – 700 nm). The wavelength of light absorbed determines the electronic transition that takes place, however in the UV-visible region only transitions from n → π* and π → π* are possible. The purine and pyrimidine bases that make up nucleic acids absorb light within the UV region of the electromagnetic spectrum, with an absorbance maximum at 260 nm. Duplex structures such as dsDNA are held together through π-interactions, H-bonds and hydrophobic effects. The H-bonds within dsDNA reduce the resonance of the aromatic system within the bases which, in turn, reduces the ability of dsDNA to absorb light.[257] On denaturing or 'melting' of a dsDNA, the H-bonds between the DNA strands are broken and the absorbance of the DNA increases in a phenomenon termed hyperchromicity (h_r). On denaturation, the absorbance can increase by up to 25 %[258] and this change leads to a very distinct sigmoidal curve when absorbance is plotted over temperature (Figure 59). The phenomenon is also observed in RNA species whereby the transition from structured assemblies, such as G4s, to the individual strands can be followed.[259]

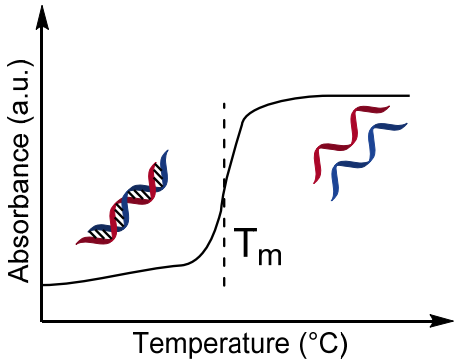

Figure 59. Schematic representation of the melting profile of dsDNA. Melting temperature is represented by T_m.

The temperature at which half of the complex has melted is defined as the T_m and this can be deduced from the melting profile of the complex. Generally higher T_m values are measured for oligonucleotides that have a high G-C content due to the increased number of H-bonds.[260,261] This technique is often used to examine the stabilisation a small molecule has on an oligonucleotide sequence. Theoretically, if a ligand binds to a nucleic acid, e.g., in the major groove of a double helix or to the end of G4, then a higher temperature is required to first dissociate the ligand from the oligonucleotide then melt the strand. This produces a characteristic shift of the curve to the right.[262]

For unimolecular G4s, the melting temperature is largely independent of oligonucleotide concentration and temperature ramp rate.[263] This is because the folding and unfolding of unimolecular G4s is rapid in comparison to the timescale of the melting experiment. On the other hand, the melting temperatures of bi-, tri- and tetramolecular G4s are highly dependent on oligonucleotide concentration.[264,265]

Although UV melting has been heavily used in the literature to understand the stability of oligonucleotide structures, there are several downsides to the technique. One of the major disadvantages is that the change in absorbance for a double stranded oligonucleotide at 260 nm is only ~ 25 % which produces fairly low resolution data. Large volumes of oligonucleotide solutions can also be required depending on the instrument used and the technique is low throughput as instruments can only record 6 – 8 samples at a time.[258]

13.2 Förster resonance energy transfer (FRET)

Förster resonance energy transfer (FRET) is a technique that was first theorised by Theodor Förster[266,267] to describe the transfer of energy from the excited state of one fluorophore (donor) to a second fluorophore (acceptor) *via* a nonradiative process.[268] The efficiency of this energy

transfer is proportional to the inverse sixth-distance between the fluorophores as shown in Equation 1.

$$E = \frac{1}{1 + \left(\frac{r}{R_o}\right)^6}$$

Equation 1. FRET efficiency (E) is dependent on the distance between the donor and acceptor (r) and the Förster distance (R_o) where energy transfer efficiency for the system is 50 %.[269]

FRET is a very sensitive technique and has been adapted to successfully measure distances of 10 – 100 Å.[270] The three most important factors to consider to successfully apply FRET in an experimental setting are: (i) selecting two FRET pairs where the emission of the donor fluorophore overlaps with the absorption of the acceptor, (ii) ensuring the distance between these two groups is under 100 Å, and (iii) ensuring information about the orientation of the transition dipoles of the fluorophores is known for maximum energy transfer. If the dipoles are oriented parallel to one another, then maximum energy transfer is measured across the system. If they are perpendicular, energy transfer is limited. For most experimental systems this orientation is approximated due to the flexibility in fluorophore orientation. However, if the fluorophores are locked in one orientation, say by two covalent linkages, then this factor needs to be taken into account.[268,271] This concept is represented in Figure 60 with the common FRET pair fluorescein and rhodamine.

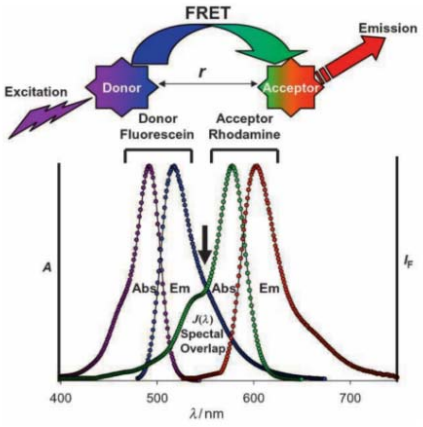

Figure 60. Schematic showing the FRET process and excitation and emission spectra of the commonly used FRET pair fluorescein and rhodamine.[270]

FRET has been applied to determine the structure and dynamics of many biomolecules, including DNA and RNA. If the target biomolecule is labelled with a FRET pair, information can be gathered on the distance and orientation of the fluorophores which can allow the overall folding of the biomolecule to be understood.

Traditionally, the folding and dynamics of nucleic acids can be monitored by FRET when the donor and acceptor fluorophores are both installed on the oligonucleotide. Tor *et al.*[272] used a different approach to follow the binding of aminoglycoside ligands to a loop contained within A-site tRNA. They replaced a uridine residue close to the binding site with a modified residue that contained the FRET donor fluorophore. They then labelled the aminoglycoside ligand with the FRET acceptor fluorophore. This meant that if no ligand was bound, fluorescence from only the donor would be measured. However, on ligand binding, fluorescence from the donor would decrease and acceptor fluorescence would increase. This methodology also allowed them to treat the ligand-bound complex with competitive ligands that were unlabelled, which again would display a change in fluorescence output (Figure 61a).

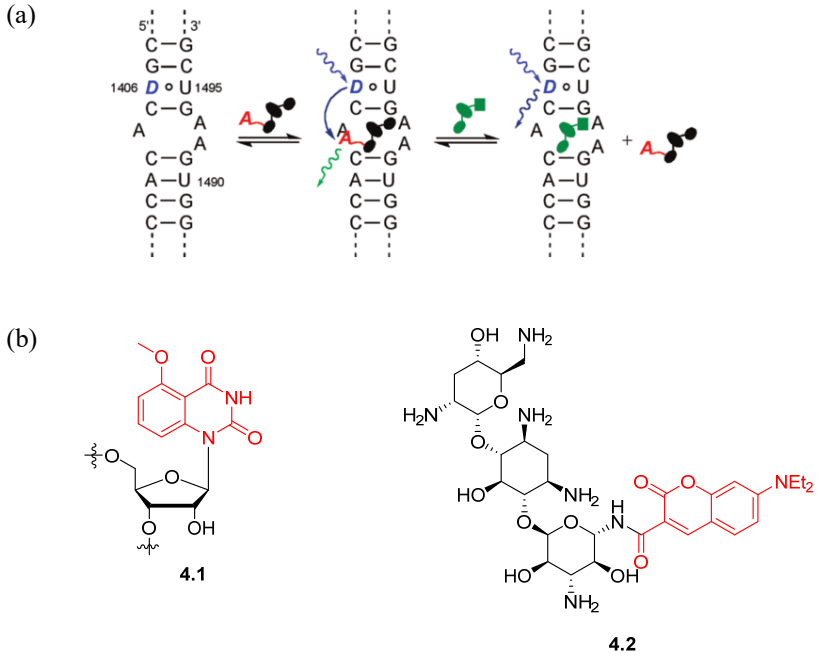

Figure 61. (a) Schematic of theory behind FRET binding assay, using fluorophore labelled RNA and ligand. D = modified residue with donor fluorophore. A = ligand with acceptor fluorophore. Green shape = competitive unlabelled ligand. (b) Structure of 5-methoxy-quinazoline-2,4-(1*H*,3*H*)-dione modified nucleotide (**4.1**) and 7-diethylamino-coumarin-3-carboxylic acid modified aminoglycoside (**4.2**) used in study.[272]

The FRET pair chosen was important as they could not be large enough that they would disrupt the overall tRNA structure but an acceptable spectral overlap also had to be achieved. This lead to the design and synthesis of the uracil analogue 5-methoxy-quinazoline-2,4-(1*H*,3*H*)-dione (**4.1**) as the donor and 7-diethylaminocoumarin-3-carboxylic acid (**4.2**) as the acceptor (Figure 61b, fluorophore highlighted in red).

On titration of the fluorophore labelled aminoglycoside, a decrease in the donor emission at 395 nm was observed along with a distinct increase in the acceptor emission observed at 473 nm

(Figure 62a). This suggested that the aminoglycoside ligand was coming into close proximity to the tRNA and binding. Competition studies were subsequently carried out with a range of unlabelled competitor aminoglycosides. As expected, if the competitor ligand had a stronger binding affinity for the tRNA, then an increase in the donor emission and decrease in the acceptor emission was witnessed (Figure 62b).[272]

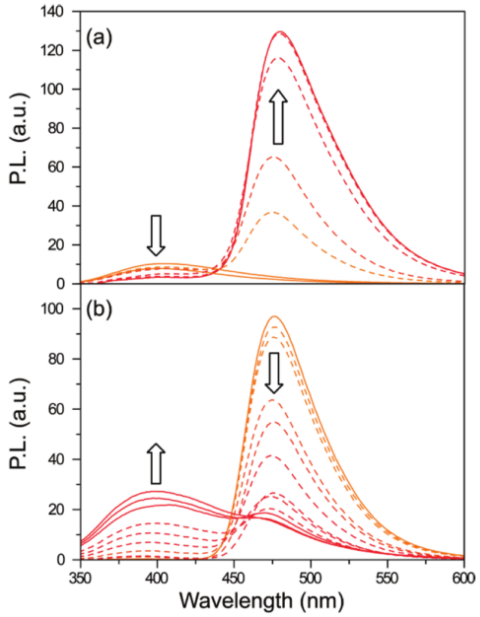

Figure 62. (a) Example FRET spectra from binding studies of labelled aminoglycosides. (b) Example FRET spectra from competition reactions with unlabelled competitor ligands.[272]

13.3 FRET-based Melting Assays

FRET has been used extensively to assess the stabilisation of small molecule ligands on DNA and RNA structures.[29,46,257,273,274] Like UV-melting analysis, if a ligand stabilises the oligonucleotide structure, then the temperature at which the oligonucleotide denatures will be higher in comparison to the control. When the oligonucleotide is structured, fluorescence is quenched due to the close proximity of the donor and acceptor ligands. Upon melting, the distance between the donor and acceptor increases, which increases the level of fluorescence from the donor. If a small molecule ligand is bound to the oligonucleotide structure and provides stabilisation, then the increase in the donor fluorescence will be observed at a higher temperature upon oligonucleotide melting (Figure 63).[275] As FRET is directly related to the distance between the donor and acceptor, it is far more sensitive than UV-melting.[257] It has been reported that increases in fluorescence upon complex melting can be as much as 10-fold. [258]

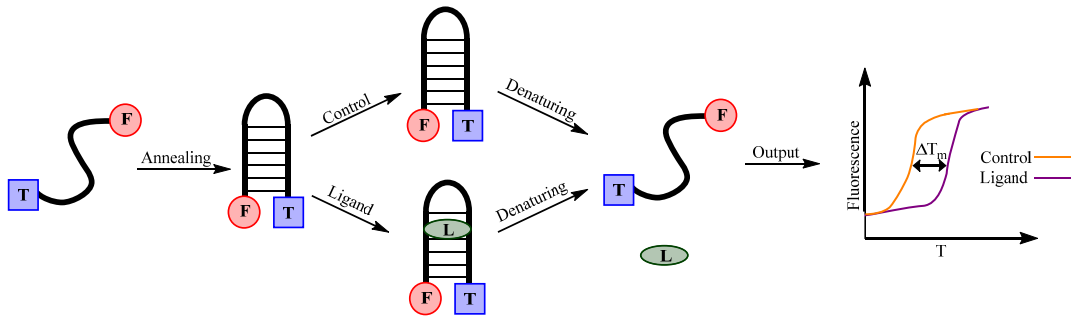

Figure 63. Schematic representation of FRET-based melting assays. F = FAM, T = TAMRA and L = ligand.

Recently Mergny tested the selectivity of a range of well-known G4 stabilising ligands on a palette of G4s.[276] The G4s used in the study adopted a range of different topologies which were characterised by CD to ensure the addition of the donor and acceptor groups did not disrupt G4 formation. A suite of 6 G4 stabilising ligands were chosen to investigate the selectivity of these for parallel *vs* antiparallel structures (Figure 64). A control DNA duplex was also tested.[276]

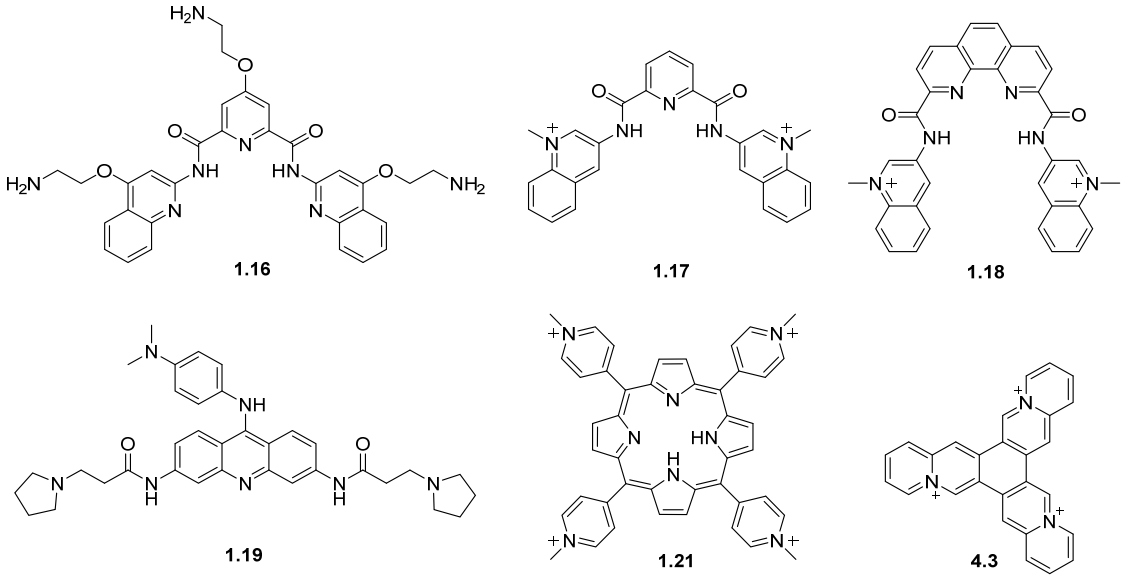

Figure 64. G4 stabilising ligands tested.[276]

All 6 ligands induced the stabilization of G4 structures when analysed by FRET melting assay. All ligands showed selectivity for the DNA G4 over the dsDNA control apart from TmPy4 (**1.21**) which revealed a 5.7 °C ΔT_m for the dsDNA control. Ligands **1.16**, **1.17** and **1.21** did not show any selectivity for either of the parallel or *anti*-parallel G4 structures. Ligands **1.17** and **4.3** both demonstrated a preference for binding the mixed G4 21g, with a ΔT_m of 19.8 and 24.4 °C, respectively. However, this is still not a high enough discrimination of one G4 structure over another to consider either of these ligands as a sequence selective G4 stabiliser.

Table 10. ΔT_m (°C) values for a range of DNA G4s and duplex control when stabilised with 6 G4 ligands. FRET melting assay measured in 10 mM lithium cacodylate (pH 7.2), 10 mM K^+. NS = no stabilisation was observed. P = parallel, a-p = *anti*-parallel, and mix = mixture of parallel, *anti*-parallel and 3 + 1 G4. Notable results in bold.

	Oligonucleotide and ΔTm (°C) Values on Ligand Addition						
Ligand	**25Ceb p**	**c-Myc p**	**Bom17 a-p**	**TBA a-p**	**21CTA a-p**	**21g mix**	**dsDNA control**
Pyridostatin (1.16)	4 ± 1	6 ± 2	5 ± 2	6 ± 2	8 ± 3	8 ± 3	NS
360A (1.17)	6.1 ± 0.4	12 ± 1	9.8 ± 0.5	10.6 ± 0.4	12.3 ± 0.9	**19.8 ± 0.7**	NS
PhenDC3 (1.18)	6.7 ± 0.7	11.2 ± 0.7	5.7 ± 0.9	8 ± 1	11.5 ± 0.5	17.3 ± 0.7	NS
Braco19 (1.19)	4 ± 1	6 ± 2	6 ± 1	6 ± 1	8 ± 2	11 ± 3	NS
TmPyP4 (1.21)	16 ± 2	19 ± 1	19 ± 1	20 ± 2	19 ± 1	25 ± 1	**5.7 ± 0.7**
TrisQ (4.3)	13.8 ± 0.2	17.9 ± 0.2	4 ± 1	7 ± 1	16.1 ± 0.1	**24.4 ± 0.1**	NS

The ligand induced stabilisation of other DNA structures can also be accurately measured with FRET. Waller *et al.* tested the stabilisation of a range of DNA i-motifs by the drug mitoxantrone (**4.4**) and derivatives of **4.4** (Figure 65).[274] i-motif structures are formed from cytosine rich sequences at acidic pH values and stabilised by the formation of hemi-protonated cytosine-cytosine base pairs. Small molecules have been shown to further bind and stabilise i-motifs, however they are understudied in comparison to their G-rich partner the G4.[11] Generally the most efficient binding is found at slightly acidic pH values, however this is not representative of physiological conditions. Therefore it is worthwhile to test for any ligand stabilisation at neutral pH. i-motifs also have a transitional pH where 50 % of the solution is folded. For the human telomeric i-motif (hTeloC) this is found at pH 6.0, whereas the c-Myc i-motif (c-MycC) is pH 6.6.[274]

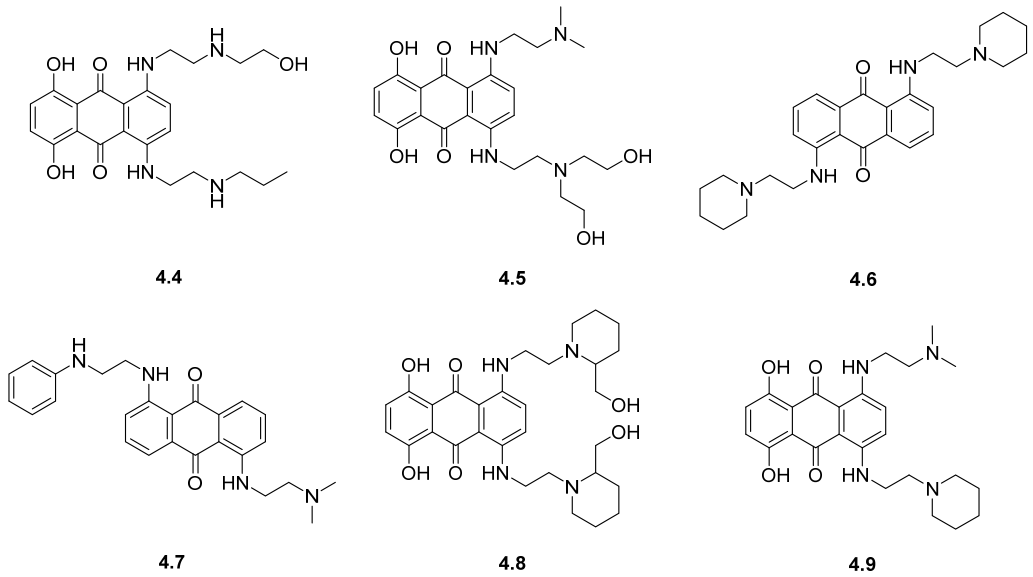

Figure 65. Structure of mitoxantrone (**4.4**) and analogues tested in FRET melting assays.[274]

The results of the FRET melting assay (Table 11) demonstrated that **4.4** could afford a high stabilisation to both the hTeloC and c-MycC i-motifs. At a pH of 5.5, high ΔT_m values – indicative of stabilization - were observed for both structures (45 and 41 °C, respectively). As the pH was increased to the transitional pH for the i-motif and then to neutral pH, this ligand was still able to provide stabilisation. This suggests that at neutral pH, **4.4** is able to induce the folding of the i-motif, which was unknown in the literature at the time. A large preference is also observed for the i-motif structures over the dsDNA control, however, this was not the case with the hTeloG sequence where a fairly high stabilisation of 23 °C was reported. The 5 mitoxantrone derivatives (**4.5** – **4.9**) did not show the same level of stabilisation towards the i-motif structures as the parent compound. In fact, ligands **4.6** and **4.9** were very poor stabilisers of all sequences tested with ΔT_m values ≤ 14.0 °C.

Table 11. ΔT_m (°C) values for a range of DNA i-motifs, G4 and duplex control when stabilised with 6 anthraquinone ligands at 10 μM. FRET melting assay measured in 10 mM sodium cacodylate (pH 7.2), 100 mM NaCl. NS = no stabilisation was observed. Notable results in bold.[274]

	Oligonucleotide and ΔTm (°C) Values on Ligand Addition							
Ligand	**hTeloC pH 5.5**	**hTeloC pH 6.0**	**hTeloC pH 7.4**	**c-MycC pH 5.5**	**c-MycC pH 6.6**	**c-MycC pH 7.4**	**hTeloG pH 7.4**	**dsDNA pH 7.4**
4.4	**45 ± 6.9**	35 ± 2.9	27 ± 1.1	**41 ± 4.5**	38 ± 2.9	29 ± 0.8	**23 ± 3.4**	9.4 ± 1.5
4.5	12 ± 3.4	19 ± 3.5	11 ± 0.2	18 ± 6.0	19 ± 2.8	15 ± 1.6	13 ± 1.6	2.6 ± 0.7
4.6	4.6 ± 2.1	5.9 ± 2.5	11 ± 0.7	3.6 ± 1.4	7.5 ± 3.0	11 ± 0.8	7.2 ± 2.2	0 ± 1.6
4.7	3.9 ± 0.1	17 ± 1.8	NS	6.6 ± 2.4	6.8 ± 2.1	NS	0.4 ± 0.7	-1.9 ± 2.4
4.8	12 ± 0.6	21 ± 1.1	11 ± 0.4	12± 0.5	30 ± 3.1	15 ± 1.3	10 ± 3.2	2.3 ± 0.7
4.9	0.2 ± 1.5	0.2 ± 0.7	13 ± 3.2	1.5 ± 0.3	10 ± 2.8	14 ± 0.8	7.6 ± 0.8	0.5 ± 0.8

As demonstrated above, FRET melting assays are able to provide accurate information on the ability of a small molecule to induce stabilisation of DNA or RNA structures. This remains a valuable technique which is used routinely and has the advantage of having readily available tools for automation, allowing analysis of a large number of samples using a multi-well plate reader.[257]

13.4 NMR structural characterisation of RNA

NMR is a valuable experimental technique that can help visualise dynamic biological processes including the equilibrium observed between RNA and a ligand.[277] In the case of understanding ligand binding to an RNA structure, both ^{1}H NMR and NOESY experiments can be conducted on the free RNA to assign the unbound state. ^{13}C, ^{31}P, COSY and TOCSY NMR can aid in the confirmation of the structure. The ligand can then be titrated into the NMR sample and any

possible structural changes can be followed by analysing the shift, disappearance or appearance of key residues.[277] This technique can be used to understand the binding of small molecules to G4 structures.[278] The equilibrium dissociation constant (K_D) is a measure of the overall strength of binding between the RNA sequence and the ligand and can also give information about the kinetics involved in the binding event.[279]

$$\text{RNA} + \text{Ligand} \underset{k_{off}}{\overset{k_{on}}{\rightleftharpoons}} \text{RNA•Ligand complex}$$

$$where \quad K_D = \frac{[RNA][Ligand]}{[RNA \bullet ligand]} = \frac{k_{off}}{k_{on}}$$

Equation 2. Equilibrium that exists between oligonucleotide and ligand[277] and the equilibrium dissociation constant for the binding event.[279]

Due to the distinct NMR differences between G4s and other oligonucleotide structures, e.g., duplexes or stem-loops, conformational changes on ligand binding can also be observed.

13.4.1 Analysis of G-Quadruplex NMR

RNA structures are generally challenging to assign because of the following factors:[280]

(i) As RNA is mainly found in A-form this means that the nucleotides experience very similar chemical environments which leads to similar chemical shifts.

(ii) Similar coupling patterns for C and U makes unequivocal assignment difficult.

(iii) The inter-residue H1′ – H2′ coupling is small and can be difficult to observe (≤ 1 Hz). This is due to the C3-endo sugar pucker confirmation adopted by RNA. [281]

(iv) Overlapping of sugar resonances H2′, H3′ and H4′ protons makes assignment difficult.

(v) Finally, the change from B-type to A-type conformation in most RNA structures increases the distance between the H1′ and neighbouring aromatic protons. This causes a loss in the intensity of cross-peaks seen between these protons. However, this overall conformational change in the RNA increases the cross-peak intensity between the aromatic and H2′ protons instead.

However, one advantage of assigning RNA G4s is the presence of diagnostic G imino resonances in ^{1}H NMR.[282] The imino residues present from H1 protons involved in Hoogsteen base pairs can

be found between 10.5 – 12 ppm. This is an upfield shift compared to imino protons forming a Watson-Crick G-C base-pairstructures (11 – 14 ppm) and can therefore be analysed easily.

The determination of the overall structure and topology of a RNA G4 can be assigned by carrying out an nOe 'walk' between the aromatic H8 protons and the adjacent imino H1 protons of each guanine (distance ~4.7 Å).[283]

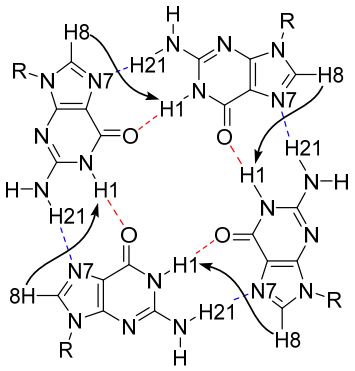

Figure 66. Schematic of aromatic-imino H8-H1 NMR walk that can be carried out across G-quartets. Distance between H8-H1 protons is roughly 5 Å. Black solid line = walk. Blue dashed line = amino interactions. Red dashed line = imino interactions.

Like conventional NMR backbone walking used extensively in the assignment of dsDNA structures, the aromatic-anomeric region can be traced in a G4. This allows important information to be obtained on the conformation of each guanine, i.e., whether they are *syn* or *anti*, as each pattern gives a different aromatic-anomeric signal intensity (Figure 67).[278] In an *anti-anti* conformation, it is possible to follow the interactions between the H8 and H1′ protons of each base. If the next base is orientated in a *syn* fashion then the H1′-H8 inter residue signal is lost. This is also true for a *syn-syn* geometry. However, with a *syn-syn* and *syn-anti* orientation, a signal appears from H8-H1′ inter residue interactions.[278]

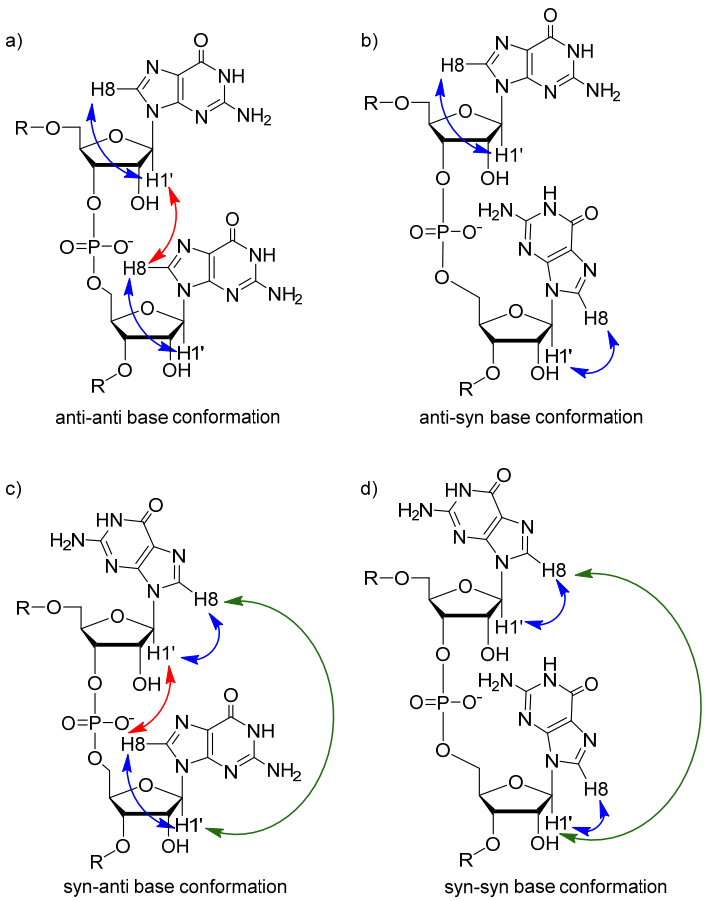

Figure 67. Schematic of possible aromatic-anomeric H8-H1′ NMR walk that can be carried out along the backbone of the RNA G4. Blue lines = H8-H1′ intra residue interactions. Red lines = H1′-H8 inter residue interactions. Green lines = H8-H1′ inter residue interactions.

Due to the large percentage of peak overlap, researchers often employ methods to simplify the NMR spectra to ensure full and accurate assignment is carried out. One of the best ways to carry this out is by the introduction of isotopic labels into the RNA.

13.4.2 RNA Labelling Techniques

Isotopic labelling of the bases is often utilised to overcome the difficulty in assigning RNA structures due to the flexibility of the structure and the peak degeneracy and overlap observed. The most common types of isotopic labelling are ^{13}C, ^{15}N and ^{2}H.[284–286] The power of this technique is demonstrated in Figure 68 where the use of deuterated bases has greatly simplified the NOESY spectra from an RNA tetraloop structure.[287] This now allows an internucleotide ‘walk’ to be carried out which allows full structural assignment to be conducted.

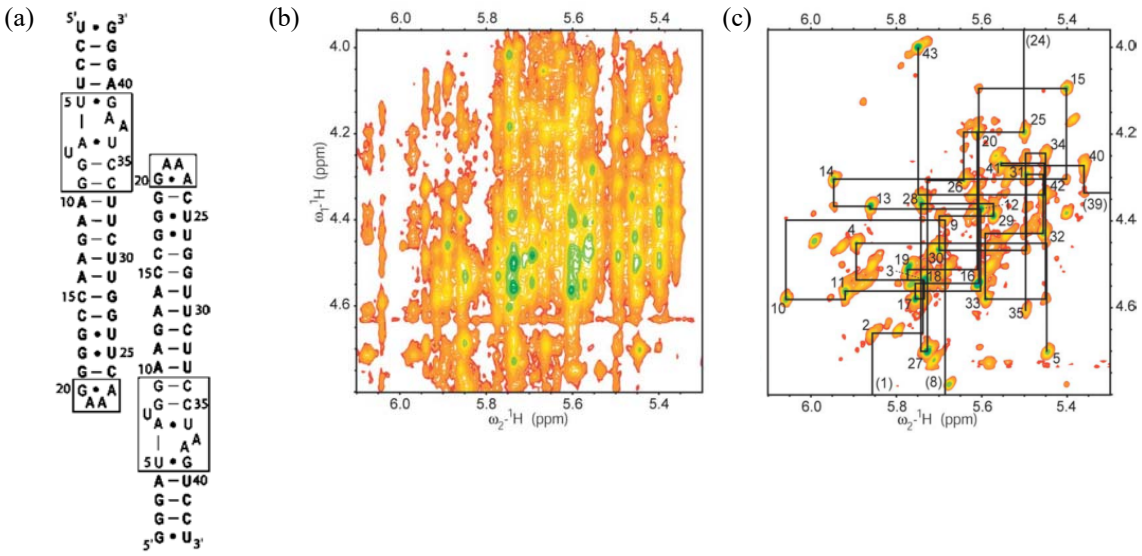

Figure 68. (a) Secondary structure of the RNA tetraloop. (b) 900 MHz NOESY of a RNA tetraloop structure. (c) 900 MHz NOESY of the same RNA tetraloop structure with selective installation of ^{2}H isotope residues.[287]

Recently, ^{19}F labels have been used to probe the structure of putative G4 forming sequences by fluorine NMR, including in living cells.[288] The use of fluorine NMR is highly advantageous due to the simplified spectra that is obtained which makes following changes to the RNA structure facile. ^{19}F NMR is also highly sensitive.[289] For example, separate signals are obtained for single stranded RNA, G4 RNA and higher order G4 structures as demonstrated in Figure 69. This change in chemical shift can also be seen for the interaction of a ligand with a G4 structure.[290]

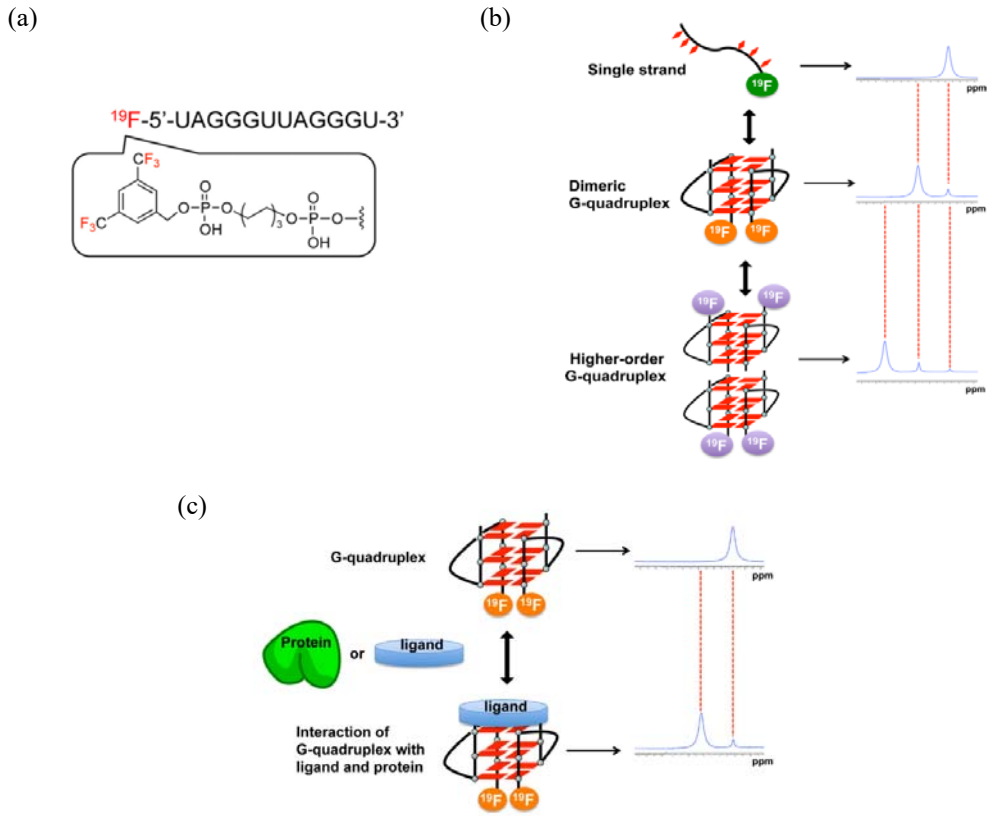

Figure 69. (a) ^{19}F labelling strategy using 3,5 bis(trifluoromethyl)phenyl moiety. Representation of the signals observed for different ^{19}F labelled RNA strands depending on the (a) structure[288] or (b) free and bound state.[290]

This form of NMR analysis cannot provide intimate details of the bonding pattern between the guanine residues of the G4, however it can provide a high throughput screening method to identify RNA G4 stabilising ligands. Depending on the method used to incorporate the isotopically labelled nucleotide into the RNA strand, the amount of isotopic label present in the final strand can vary greatly from one or two bases, to over half of the strand (Figure 70). The most common techniques are solid phase chemical synthesis, splint ligation and position selective labelling of RNA (PLOR).[286]

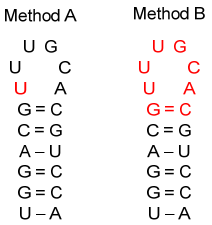

Figure 70. Incorporation of isotopically labelled bases can vary on the method used. In this example Method A (e.g., splint ligation) is only able to incorporate one isotopically labelled uracil whereas Method B (e.g., PLOR) can incorporate multiple isotopically labelled nucleotides in the loop region. Letters in red = isotopically labelled nucleotides.

Solid phase chemical synthesis of isotopically labelled RNA strands can incorporate both labelled and non-labelled nucleotides using traditional resin phosphoramidite chemistry.[291] This process allows for the greatest flexibility in the overall strand design with the ability to incorporate labels at any position within strand. The process can also be fully automated using an appropriate DNA/RNA synthesizer. One main downside to this method however, is that oligoribonucleotides of longer than 50 nt can be difficult to produce in high yield and purity.[273] The process can also be limited by the commercial availability of appropriately labelled phosphoramidites or the synthetic capability of making them. This process was employed by Hansen and Kreutz[292] while investigating the dynamics of an A-site RNA system by NMR. They incorporated isotopic labels synthetically on all four bases then engineered these site specifically into the RNA strand where they expected to see changes in the chemical environment.

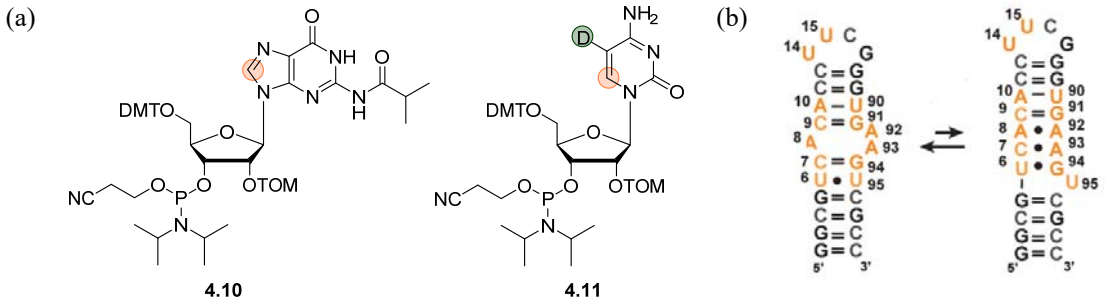

Figure 71. (a) Example of two isotopically labelled phosphoramidites that can be installed using solid phase chemical synthesis. ^{13}C labels coloured orange and ^{2}H labels coloured green.[293] (b) Isotopically labelled A-site RNA. Isotopic labels are represented by orange letters.[292]

The assembly of larger RNA strands can be accomplished by the use of splint ligation techniques which allows shorter RNA strands to be joined together with the help of T4 DNA or RNA ligase (Figure 72).[286] The shorter RNA strands, which can be constructed using solid phase chemical synthesis or *in vitro* transcription, are ligated to a template DNA strand which brings the 3′ end of one strand in close enough proximity to the 5′ end of the second strand that T4 DNA ligase can join them together.[294] T4 RNA ligase can also be used, however this requires single stranded RNA to be present at the ends being joined together.[295] The main two drawbacks to this method is that it cannot be automated and the ligation efficiency can vary greatly which limits the quantity of labels being introduced.

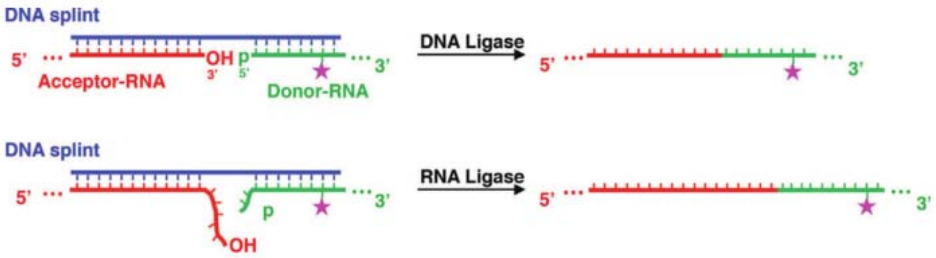

Figure 72. Chemical split ligation using both T4 DNA and RNA ligase.[286]

A technique that combines both the generation of chemically diverse oligoribonucleotides and the ability to efficiently synthesise long oligoribonucleotides at milligram scale would be highly advantageous. PLOR addresses both of these issues, while also benefiting from being an automated process.[296] This process utilises a 'pause-restart' method for the addition of ribonucleoside triphosphates (rNTPs) to a DNA templated RNA sequence using T7 RNA polymerase (Figure 73).[286 296]

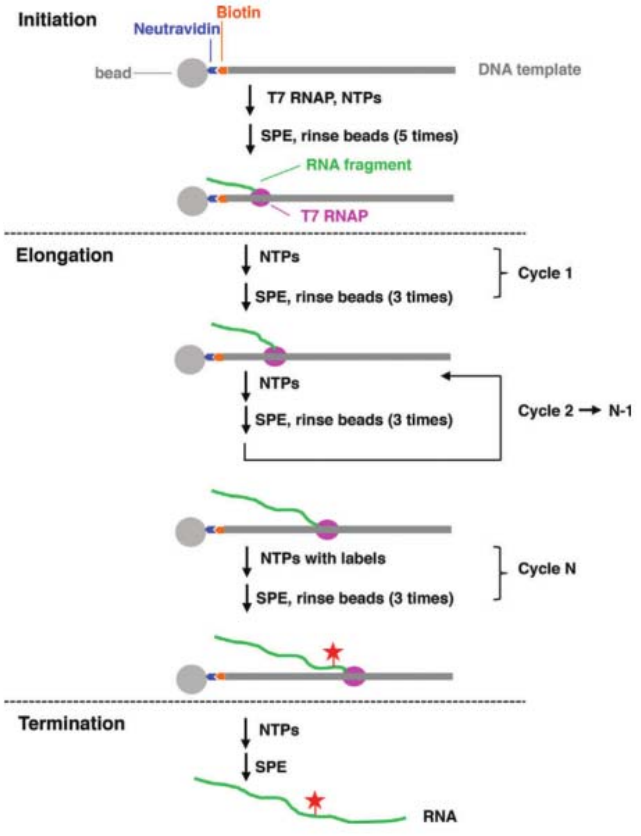

Figure 73. Schematic of PLOR. DNA template with biotin label is represented in grey. T7 RNA polymerase (T7 RNAP) is represented in purple. The extending RNA sequence is represented in green with the site specific isotopic label represented by a red star. Each elongation process is controlled by the addition of rNTPs.[286]

Each of these above methods can be used to efficiently produce isotopically labelled RNA which should allow for the simplification of RNA structural assignment by NMR and hopefully increase the amount of published work in this area, as further research is needed to fully understand the structure and function of RNA and how it can targeted for therapeutic goals using small molecules.

13.5 NMR of RNA G-Quadruplex•Ligand Complexes

To date there has only been 3 NMR RNA G4 structures[297–299] published in the PDB database and no NMR RNA•ligand complex structures published.[300] Several papers have been published however, that utilise NMR as a method to analyse the binding of RNA and G4 binding ligands. Changes in signals in ^{19}F NMR spectroscopy can be representative of a binding event taking place. As mentioned previously (Figure 69), a change in chemical shift is observed in ^{19}F NMR between bound and unbound G4's. Xu *et al.* used this approach to monitor the binding of pyridostatin and the telomeric protein TRF2 to telomere RNA. They were able to follow the change in RNA structure from free, unbound G4 to ligand bound G4 upon pyridostatin titration. The formation of a higher order structure when the ligand was present in excess was also observed. Plotting the ligand bound G4 peak areas from the ^{19}F signals versus the ligand concentration allowed a dissociation constant to be determined.

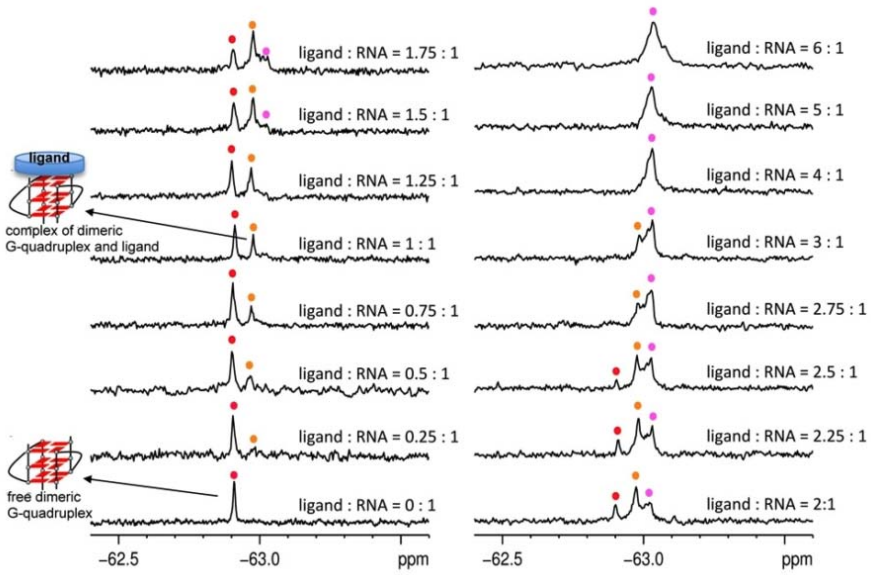

Figure 74. ^{19}F NMR of free G4, bound G4 and further binding of pyridostatin.[290]

Although ^{19}F NMR has been shown to be useful in following the binding of a G4 ligand, it does not give intimate details about the interactions between the ligand and RNA. A large set of aptamers have been discovered that bind GTP as a ligand.[301,302] Using NMR, the aptamer V-GTP has been shown to form a G4 on GTP binding. In fact, using both unlabelled and $^{15}N/^{13}C$ labelled RNA and GTP, Wöhnert *et al.,*[303] demonstrated that GTP inserts itself into one of the G-quartets in the G4 structure. In the absence of ligand, the RNA exists as an A-form helix with two internal bulges. Initial 1D and 2D NMR of the unlabelled RNA demonstrated that full assignment of the bound and unbound RNA would be difficult owing to considerable signal overlap and line broadening due to a dynamic system. However, some important information could still be gathered by the use of isotopically labelled RNA and ligand. On the addition of GTP the formation of a G4 structure can be observed by the appearance of characteristic peaks within the imino region of the ^{1}H NMR spectrum. This was further confirmed by carrying out ^{1}H, ^{15}N-HSQC NMR experiments on ^{15}N labelled GTP where one signal corresponding to GTP imino proton can be observed in the G4 imino region (Figure 75d and e).

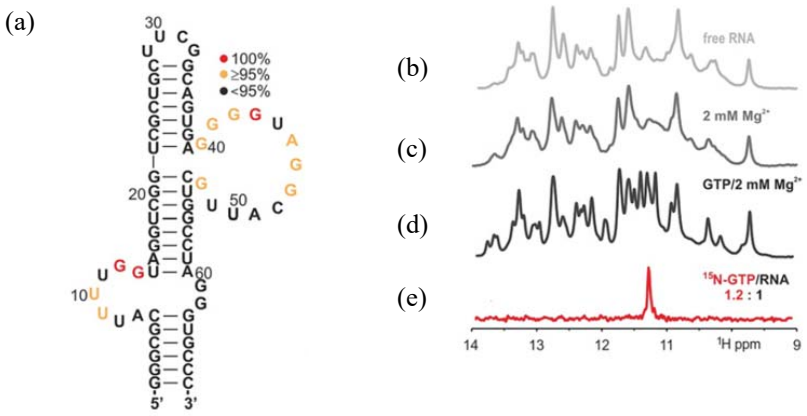

Figure 75. (a) Proposed secondary structure of the V-GTP aptamer in the absence of GTP. ^{1}H imino proton spectra of (b) free RNA in potassium phosphate buffer, (b) free RNA with the addition of 2mM Mg^{2+}, (c) RNA with the addition of 1 equivalent of GTP and (d) interaction between RNA and ^{15}N labelled GTP in ^{1}H, ^{15}N-HSQC NMR experiments.[303]

Correlations were also observed between the H8 and imino protons of the GTP and the neighbouring guanines (Figure 76b). This suggested that the GTP ligand was integrated into one of the G-quartet layers and acting like a regular guanine. To further test this theory, K^+ cations were replaced with NH_4^+ to interrogate the correlations between GTP and the NH_4^+ protons. NH_4^+ has previously been shown to replace K^+ in the cation binding pocket within the centre of a G-quartet. The NH_4^+ cation protons are then protected from exchange with the bulk solvent and no signals are seen when NMR experiments are conducted.

(a) (b)

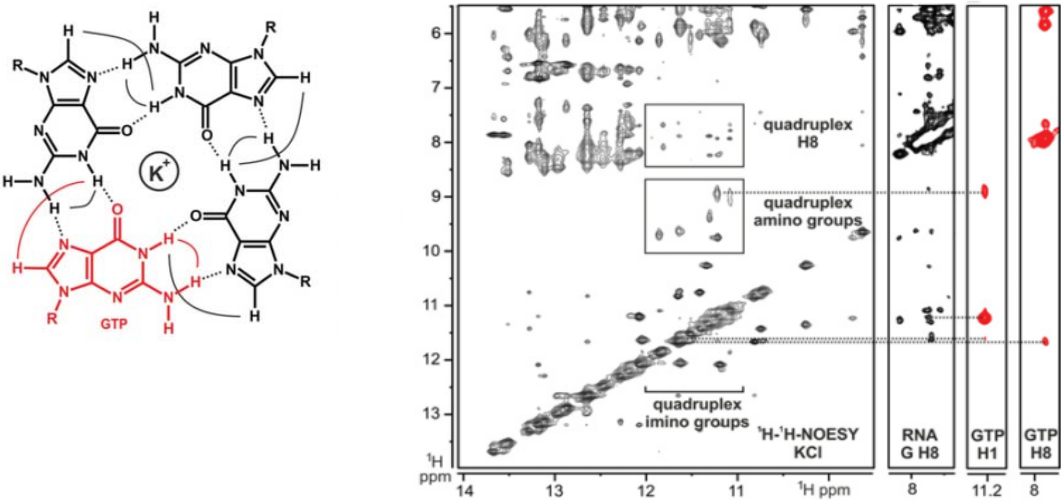

Figure 76. (a) Structure of G-quartet with GTP showing possible nOe correlations that could be observed by NMR. (b) Main spectrum = NOESY spectrum of unlabelled RNA and GTP. Smaller boxes from left to right = 2D-^{1}H,^{1}H-plane from a ^{13}C-edited NOESY-HSQC spectrum recorded with a ^{15}N,^{13}C-guanine-labeled RNA and unlabelled GTP. ^{15}N- and ^{13}C-edited NOESY-HSQC experiments recorded for samples containing ^{15}N,^{13}C-labeled ligand GTP and unlabelled RNA.[303]

13.6 *In vitro* Splicing Assays

Alternative splicing is a vital cellular process for the production of proteins from the DNA that encodes for them. It is understood that around 95 % of eukaryotic genes can be alternatively spliced,[67] therefore an inherent understanding of this process for each gene is highly important. This is especially true when it is now becoming apparent that many diseases and disorders are caused by aberrant alternative splicing events.[69,70]

One way in which to analyse the splicing process of a gene, in an isolated setting, is by using *in vitro* splicing assays. This technique, first described by Mayeda and Krainer,[304] involves the splicing of a ^{32}P labelled pre-mRNA transcript in HeLa nuclear extract. After the splicing reaction has been carried out the products produced can be separated on a denaturing polyacrylamide gel using polyacrylamide gel electrophoresis (PAGE). The product bands from the different splicing isoforms can then be visualised using a phosphorimager which allows easy quantification of the levels of different splicing isoforms (Figure 77). This process allows investigation and optimisation of each step of the splicing process due to the isolated nature of the experiment. Importantly, the efficiency of both transesterification reactions can be followed and any stalling throughout the whole splicing process can be visualised.[115,305]

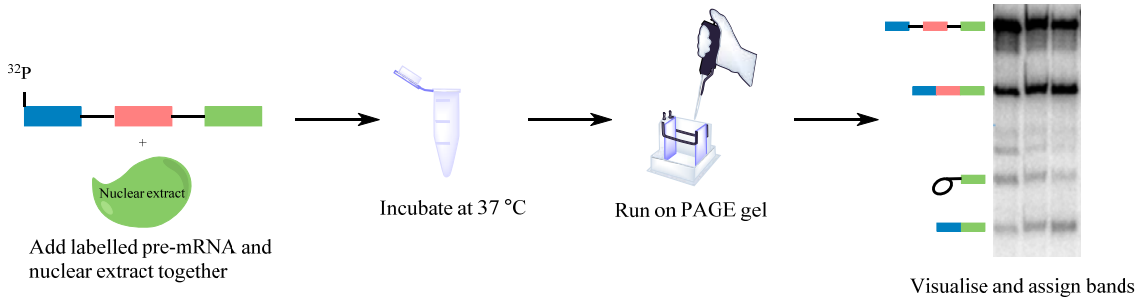

Figure 77. Simplified schematic showing steps to carry out *in vitro* splicing assay.

For the investigation into the effect that small molecules[306–308] or ASO splicing modulators[309] have on an alternative splicing process, *in vitro* splicing assays are fundamental as they provide a quick and accurate way to investigate changes to the splicing ratios of alternatively spliced isoforms that may have occurred.

13.7 *In vitro* Splicing of Bcl-x

The oncogene Bcl-x can be alternatively spliced to give two mRNA isoforms, Bcl-xL and xS. The ratio between these can be observed on a denatured polyacrylamide (PAGE) gel with an *in vitro* splicing assay. Weldon *et al.,*[106] previously created a shortened pre-mRNA transcript of Bcl-x, termed Bcl-x-681, which was found to splice at ~ 50 % efficiency after two hours and display a xS/xL ratio of 0.2.[115] Figure 78 shows the shortened Bcl-x transcript Bcl-x-681 used in all Bcl-x splicing assays and also the splicing gel obtained after up to two hours of reaction. It can be seen that any unspliced pre-mRNA is retained at the top of the PAGE gel, while the products from the splicing process are separated within the gel according to their molecular weight.

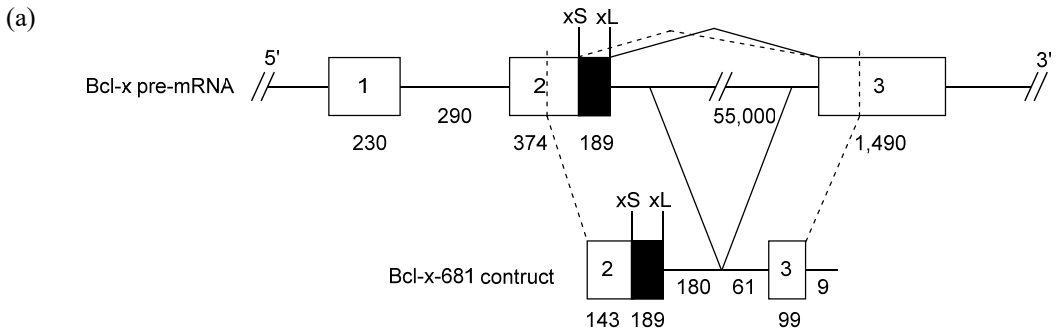

(b)

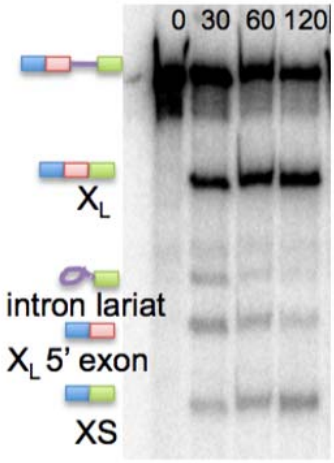

Figure 78. (a) Schematic representation of the length of the wild type Bcl-x (top) and the functional transcript Bcl-x-681 (bottom). Length of each exon and intron is indicated by numbers below. Where the wild type RNA has been cut is represented by the black and dotted lines between the two structures. (b) PAGE gel of Bcl-x splicing reaction after 0, 30, 60, and 120 minutes. Each band is assigned on the left hand side of the gel.[115]

Using *in vitro* splicing assays Weldon *et al.,* first demonstrated the apparent splicing modulation effect GQC-05 (**1.20**) had on Bcl-x (40-fold increase in xS/xL ratio, Figure 79).

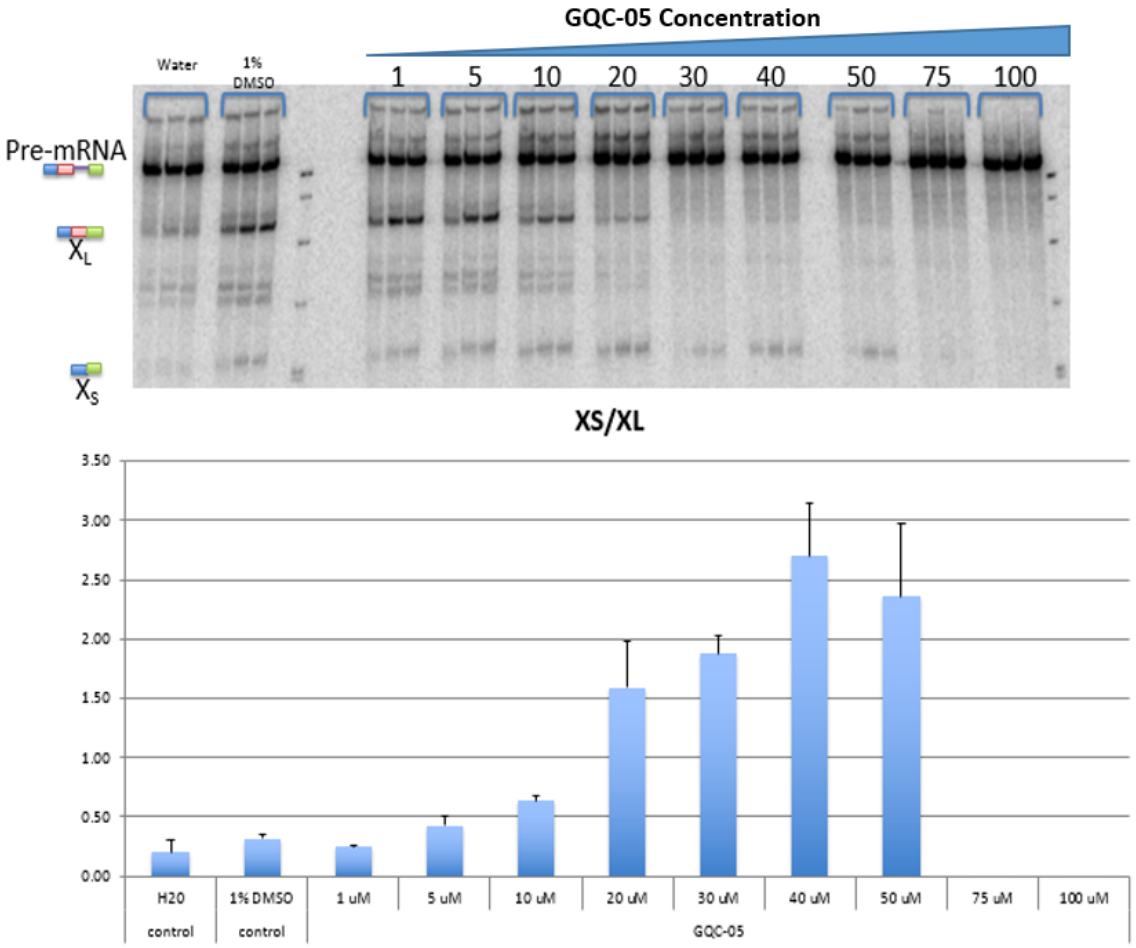

Figure 79. *In vitro* splicing assay as a function of increasing [GQC-05] and results from the *in vitro* splicing assay plotted as a graph of X_S/X_L ratio vs. [GQC-05].[115]

As previously explained in Chapter 1 Section 1.10, a range of **1.20** derivatives were also examined to see whether they were able to alter the splicing ratio in favour of the pro-apoptotic isoform Bcl-xS. The results of the SAR screen suggested several compounds had the same effect as GQC-05 however, some compounds did not change the splicing ratio (Figure 80).

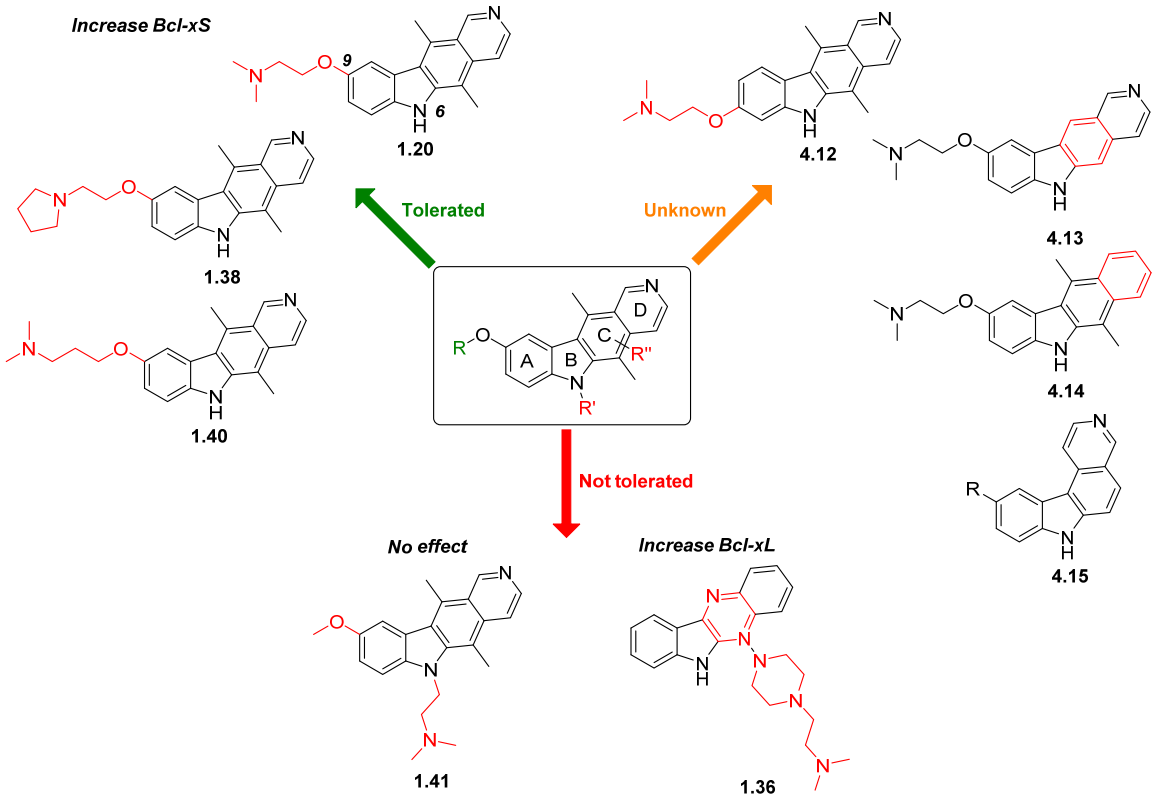

Figure 80. Overview of SAR results from previous Bcl-x studies with a range of ellipticine small molecules and possible other derivatives that would be tested.

Generally functionalisation on the 9′ position was tolerated, as long as the carbazole amine was free. If this amine was substituted with a dimethylamino tail (**1.41**) then no change in the wild type splicing ratio was observed. Interestingly, quindoline derivatives such as **1.36** were found to act in a conflicting manner to GQC-05 and actually increased the anti-apoptotic isoform xL. What was unknown however, was whether (i) movement of the dimethylamino chain, (ii) loss of the two C-ring methyl groups, (iii) loss of the pyridine nitrogen, or (iv) a different regioisomer would have a favourable or detrimental effect on the splicing efficiency. Evaluation of compounds of type **4.12 – 4.15** would further the SAR work that had already been carried out and could lead to the discovery of a more potent splicing inducer and could possibly elucidate an initial mode of action of these ellipticine compounds.

14 Aims of Chapter 4

Bcl-x splicing assays have demonstrated that GQC-05 is able to alter the splicing of Bcl-x in favour of the pro-apoptotic isoform Bcl-xS.[111] The working hypothesis of the mechanism of action of GQC-05 is that it stabilises G4 structures present within wild type Bcl-x. Previously GQC-05 has been shown by Hurley *et al.,* to be capable of selectively stabilising a DNA G4 in the c-Myc gene preferentially over other types of nucleic acid structures.[41] Results from our collaborators in Leicester University have shown the possibility of G4 structures forming in multiple regions of Bcl-x (681nt) wild type RNA, specifically in the Q2 and Q5 regions.[106] The overall objective of this chapter is to explore the binding characteristics of a range of putative G4 stabilisers synthesised in Chapters 2 and 3 with the Q2 region of Bcl-x.

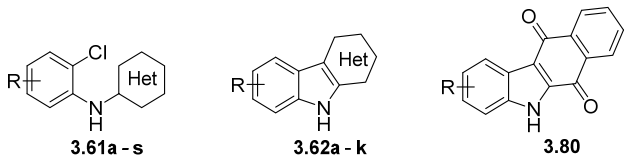

Figure 81. General scaffolds of the compounds that will be used in this chapter to analyse the binding characteristics of Bcl-x Q2.

The specific aims of this chapter are to:

(i) Investigate the stabilisation properties of ellipticine derivatives **3.62** and **3.80** (Figure 81) on Bcl-x Q2 using UV-melting.

(ii) Investigate the affinity and selectivity that ellipticine derivatives **3.61, 3.62** and **3.80** (Figure 81) have towards a range of DNA structures by FRET melting.

(iii) Examine the binding interactions between Bcl-x Q2 and GQC-05 using NMR spectroscopy.

(iv) Investigate whether ellipticine derivatives **3.61, 3.62** and **3.80** (Figure 81) have the ability to modulate the splicing ratio of Bcl-x-683 by *in vitro* splicing assays.

15 Results and Discussion

15.1 UV-Vis Melting Analysis of Q2 Bcl-x RNA

Initially the UV melt of the free Q2 Bcl-x RNA (5′-CCGGGAUGGGGUAAAC UGGGGUCGCAUUGUGGCC-3′) was tested at a number of different RNA concentrations. The buffer and KCl conditions were kept consistent with those used in the CD experiments (20 mM potassium phosphate pH 7.0 and 100 mM KCl).[106] The samples were initially heated to 90 °C quickly then cooled slowly to break up any higher order RNA structures. Each UV melt experiment was carried out in triplicate and was recorded at λ = 260 nm from 20 to 90 °C, with a heating rate of 0.5 °C/min. RNA concentrations were examined at 0.5, 1, 2, 3, 4, 5, 10, and 20 μM however only the experiments with 2, 3, 4, and 5 μM RNA gave suitable sigmoid curves (Figure 82). The experiments carried out using low or high RNA concentrations gave sigmoid curves with poor signal to noise ratio. A Boltzmann sigmoid was fitted to the data to allow a T_m value to be determined.

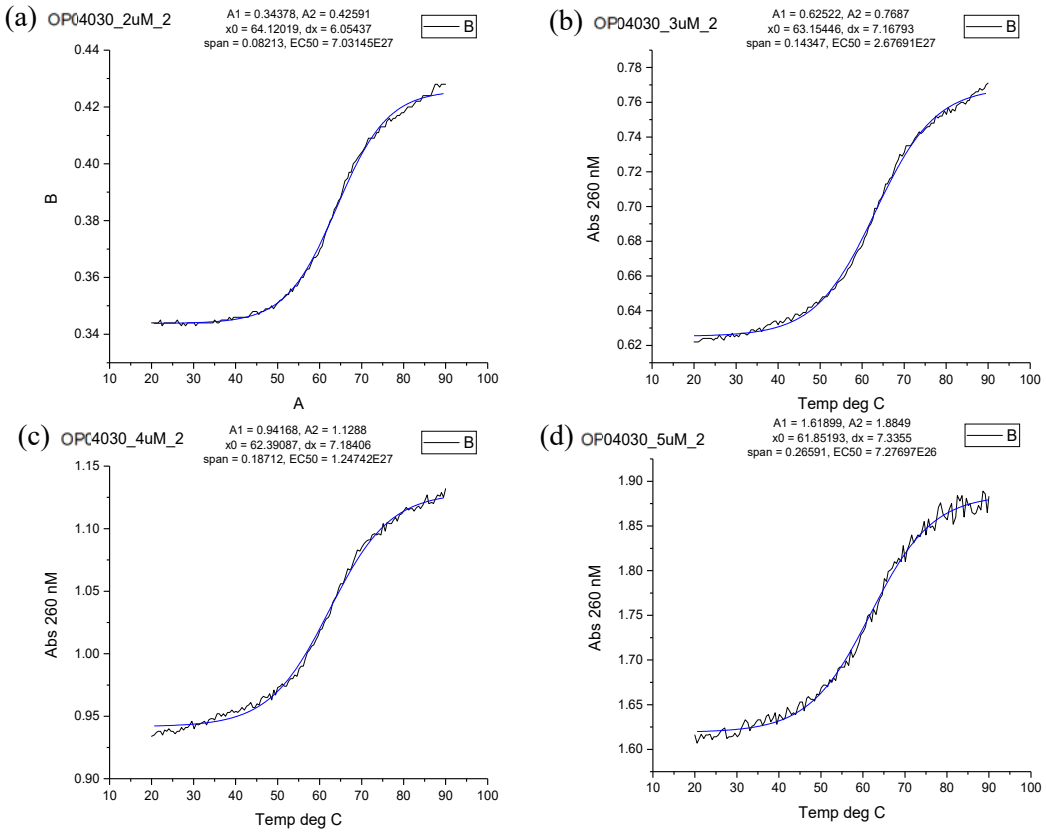

Figure 82. UV-vis melting profiles of (a) 2, (b) 3, (c) 4, and (d) 5 μM RNA. B = Boltzmann sigmoid fit.

As shown in Table 12, the T_m is consistent across the concentrations tested supporting the fact that unimolecular G4s are not concentration dependent. It was decided that for all subsequent experiments an RNA concentration of 2 μM would be used as this gave a suitable curve and used the least amount of RNA.

Table 12. Melting temperature of Q2 RNA at various [Q2_RNA]. N = number of replicates performed. Final value is an average of n. N/A = suitable results not achieved.

Entry	[Q2_RNA] (μM)	[K buffer] (mM)	[KCl] (mM)	T_m (°C)	N=
1	0.5	20	100	N/A	3
2	1	20	100	N/A	3
3	2	20	100	63.78	3
4	3	20	100	63.17	3
5	4	20	100	62.12	3
6	5	20	100	62.40	3
7	10	20	100	N/A	3
8	20	20	100	N/A	3

If the T_m of a G4 is very high, the upper baseline of the sigmoid curve will continue to slope upwards and not flatten out within the temperature range that the UV-melting experiment is carried out. This can lead to inaccuracies when trying to carry out accurate curve fitting to calculate the melting transition.[263] Changing the buffer conditions by either reducing the concentration of potassium ions or changing to a sodium buffer can negate these problems by destabilising the G4.[263] As the T_m of the Q2 RNA was already high, experimentation with buffer and buffer concentration was attempted to try and destabilise the G4. Initially the concentration of KCl was reduced and, as expected, a drop of ~13 °C was observed from 100 mM to 0 mM KCl. Next, a sodium phosphate buffer with NaCl salt was tested. A range of NaCl concentrations were examined and again a decrease in the T_m was observed with lower salt concentrations. Unexpectedly, Q2 RNA seems to be more stable in sodium buffer than potassium buffer prior to salt titration (Table 13, Entry 6 *vs* Table 14, Entry 6). This is unusual for G4s as potassium had been well documented to be the best cation for G4 stabilisation.[263]

Table 13. Melting temperature of Q2 RNA at various [KCl]. N = number of replicates performed. Final value is an average of n.

Entry	[Q2_RNA] μM	[K buffer] mM	[KCl] mM	T_m °C	N=
1	2	20	100	63.78	3
2	2	20	50	60.45	3
3	2	20	20	57.09	2
4	2	20	10	56.95	2
5	2	20	1	51.54	3
6	2	20	0	50.83	2

Table 14. Melting temperature of Q2 RNA at various [NaCl]. N = number of replicates performed. Final value is an average of n.

Entry	[Q2_RNA] µM	[Na buffer] mM	[NaCl] mM	T_m °C	N=
1	2	20	100	63.26	3
2	2	20	50	60.09	2
3	2	20	20	57.31	3
4	2	20	10	55.67	2
5	2	20	1	55.41	1
6	2	20	0	55.08	2

This could suggest a dynamic system where two different RNA structures are in equilibrium with each other and preferentially stabilised depending on which cation is used.[310,311]

15.2 Stabilisation of Q2 Bcl-x RNA by Ellipticine Derivatives

Firstly, the ellipticine derivative GQC-05 (**1.20**) was tested at a wide range of concentrations to determine the stability that this ligand could offer Q2 Bcl-x RNA. As the concentration of GQC-05 was increased, the T_m increased to a stabilisation of 9.11 °C with 40 µM GQC-05 (Table 15, Entry 5).

Table 15. Melting temperature of Q2 RNA at various [GQC-05]. N = number of replicates performed. Final value is an average of n.

Entry	[Q2_RNA] µM	[K buffer] mM	[KCl] mM	[GQC-05] µM	T_m °C	ΔT_m °C	N
1	2	20	100	0	63.78	N/A	3
2	2	20	100	5	65.43	1.65	3
3	2	20	100	10	66.49	2.72	2
4	2	20	100	20	71.05	7.27	3
5	2	20	100	40	72.88	9.11	3
6	2	20	100	60	76.80	13.02	3
7	2	20	100	80	N/A	N/A	3
8	2	20	100	100	N/A	N/A	3

T_m average over n number of runs

When the concentration of GQC-05 was increased to 60 µM, a double sigmodal curve was observed (Figure 83f). The T_m of the first inflection corresponded with the stabilisation at around 20 µM GQC-05 (69.7 °C). The second inflection exhibited a T_m of 81.2 °C. This suggests at high GQC-05 concentrations multiple RNA•ligand species are stabilised. Higher ligand concentrations (80 and 100 µM) did not give sigmoid curves.

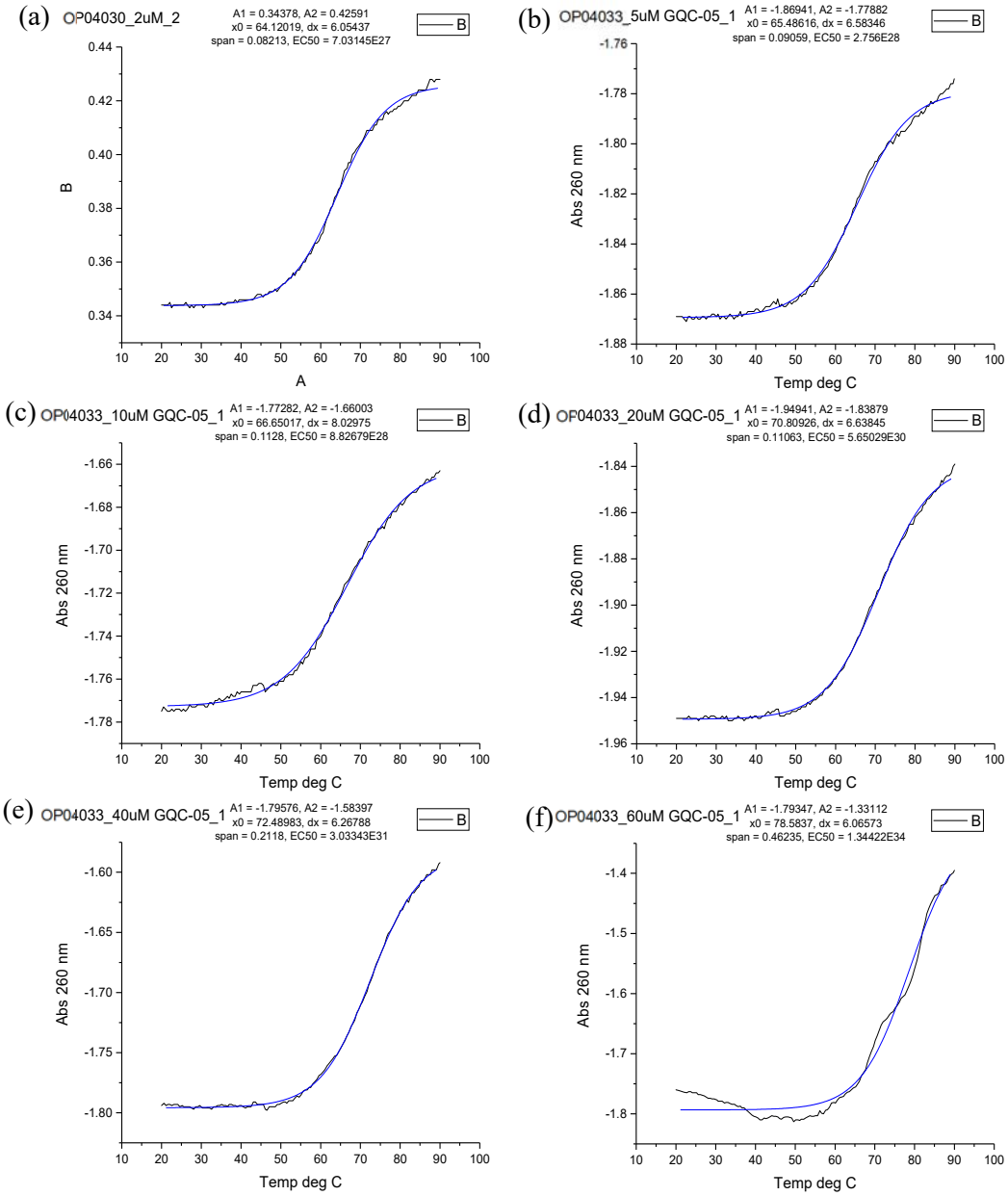

Figure 83. UV-vis melting profiles of (a) free Q2 RNA and with (b) 5, (c) 10, (d) 20, (e) 40, and (f) 60 μM GQC-05. B = Boltzmann sigmoid fit.

Next, six ellipticine derivatives (**3.62a-g**) were tested at 10, 40 and 60 μM. Solubility issues meant that compounds of type **3.80** were not examined.

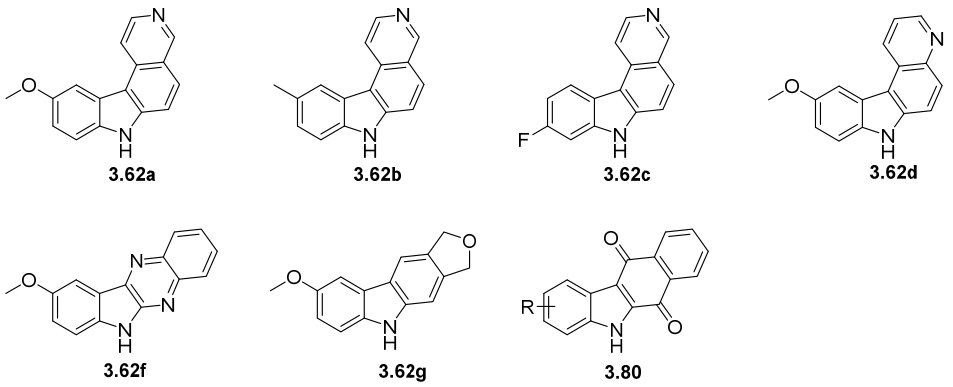

Figure 84. Structures of compounds tested in UV-melt analysis with Q2.

For compounds **3.62a** – **d** and **f** a dramatic loss in the 'S' shape of the sigmoidal curve was observed as the ligand concentration was increased (Figure 85a and b). Due to loss of the transition, an accurate T_m cannot be calculated which accounts for the drop in T_m values at 40 and 60 μM (e.g., Table 16, Entry 3 and 4). For compounds **3.62a**, **b**, **d**, and **f**, modest sigmoidal character is seen at 10 μM ligand. Only two compounds show any positive stabilisation at 10 μM, **3.62b** at 2.65 °C and ligand **3.62f** at 0.19 °C (Table 16, Entries 5 and 14, respectively).

Table 16. Melting temperature of Q2 RNA at various [ligand]. N = number of replicates performed. Final value is an average of n.

Entry	Ligand	[K buffer] mM	[KCl] mM	[Ligand] μM	T_m °C	ΔT_m °C	N=
1	None	20	100	0	63.78	N/A	3
2	**3.62a**	20	100	10	62.57	-	3
3		20	100	40	56.63	-	3
4		20	100	60	48.64	-	3
5	**3.62b**	20	100	10	66.43	2.65	3
6		20	100	40	73.33	*9.55*	3
7		20	100	60	63.55	-	3
8	**3.62c**	20	100	10	59.29	-	3
9		20	100	40	44.63	-	3
10		20	100	60	N/A	-	3
11	**3.62d**	20	100	10	62.71	-	2
12		20	100	40	61.42	-	3
13		20	100	60	57.69	-	3
14	**3.62f**	20	100	10	63.97	0.19	3
15		20	100	40	61.47	-	3
16		20	100	60	56.82	-	3
17	**3.62f**	20	100	10	62.94	-	3
18		20	100	40	63.05	-	3
19		20	100	60	63.22	-	3

3.62b also appears to show a 9.6 °C stabilisation at 40 μM, however the curve plotted from this data is nearly a straight line so as previously mentioned an accurate T_m is not possible. The melt stabilisation data and curve shape for compounds **3.62a** – **d** and **f** suggest that multiple RNA structures are formed once ligand is added. The only ligand that produces a strong sigmoid curve is **3.62g** (Figure 85c and d). However, as no stabilisation is seen as increasing concentrations of this ligand is added, it suggests that this ligand is not interacting at all with the RNA.

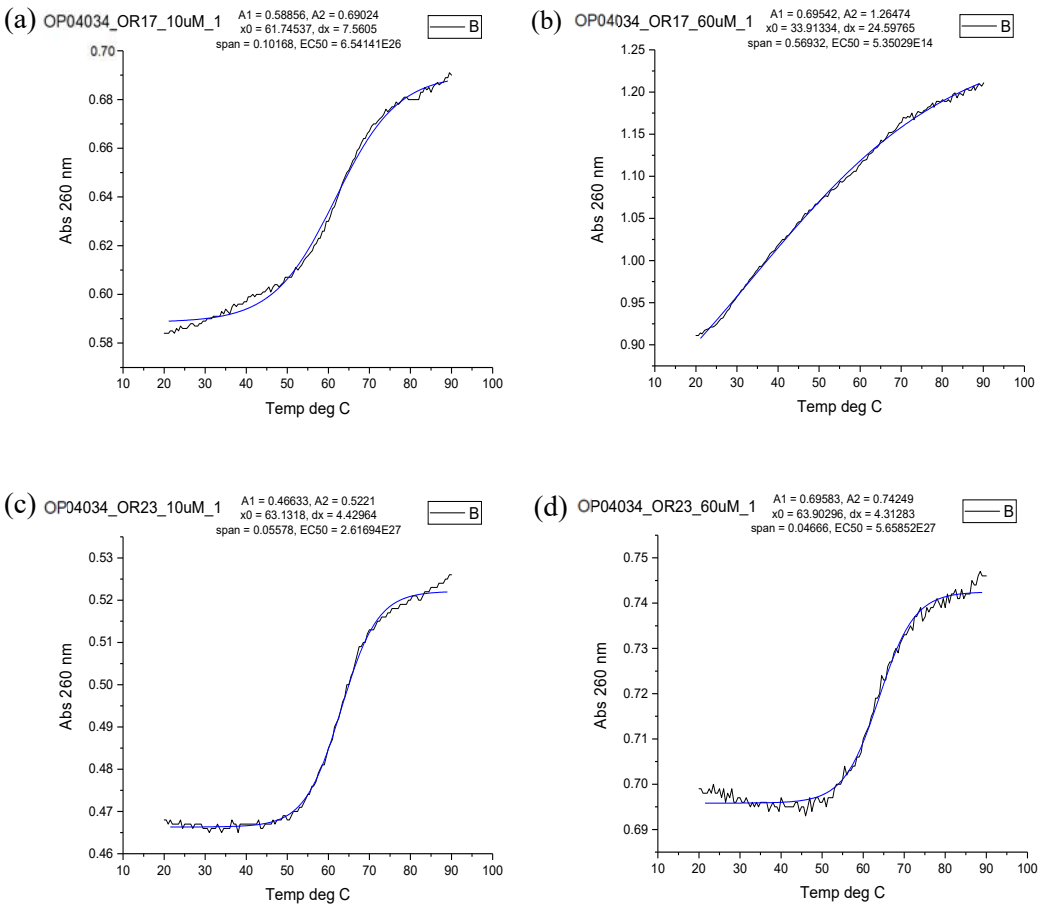

Figure 85. UV-vis melting profiles of (a) 10μM 3.62a, (b) 60μM 3.62a, (c) 10μM 3.62g, (d) 60μM 3.62g with Q2 RNA. B = Boltzmann sigmoid fit.

UV analysis of free- and ligand-complexed Bcl-x Q2 RNA suggests that a G4 structure could be forming in ligand free conditions, however once ligand is added the structure changes, with multiple structures present. Multiple structures may also be formed from the outset and the addition of ligand just alters the equilibrium between these multiple structures.

Previously CD results have suggested that the Q2 sequence demonstrated the characteristic peaks of a parallel G4 however, RNA footprinting of the overall Bcl-x-681 RNA suggests Q2 forms

part of an internal loop (Figure 86).[106] Although the results from the UV melting assays are not conclusive, they suggest that both a G4 and an internal loop could be formed.

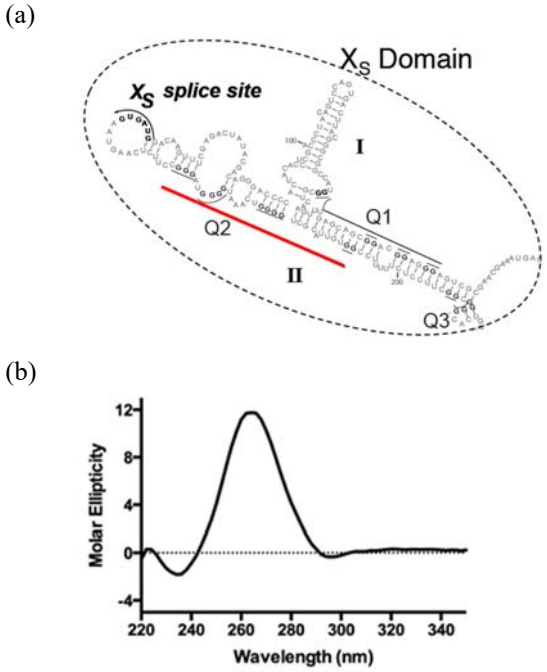

Figure 86. (a) Structure and sequence of Q2 as predicted by RNA footprinting and M-fold. (b) CD spectrum of Q2. Conditions of CD experiment were as follows: 20 mM potassium phosphate buffer at pH 7.0, 100 mM KCl with RNA diluted to a final concentration of 20 μM.[106]

15.3 Exploration of the DNA Binding Profiles of Ellipticines

It is important for small molecule binders to be specific for the oligonucleotide structure they are designed to target. To test the selectivity of the ellipticine derivatives of type **3.61** and **3.62** synthesised in Chapter 3, their ability to stabilise a range of DNA secondary structures was examined using a FRET based melting assay (Figure 87).

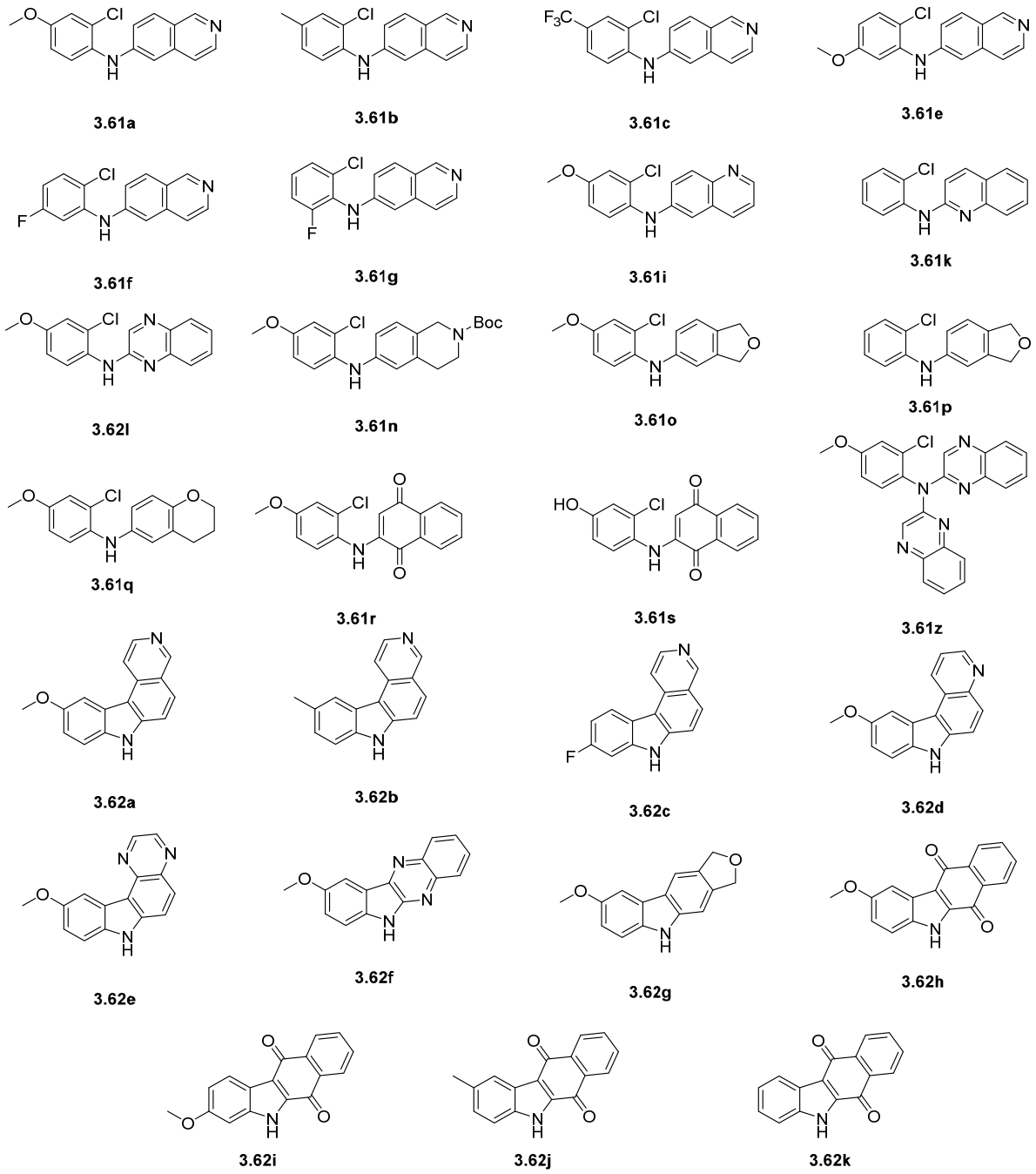

Figure 87. Structures of ellipticine derivatives investigated in this study.

Three different types of DNA structures were studied, including a double helix (dsDNA, pH 7.4), a DNA G4 (hTeloG), a folded (hTeloC pH 5.5) and unfolded (hTeloC pH 7.4) acidic i-motif and a second folded acidic i-motif (c-MycC pH 6.6).[274] Each DNA oligonucleotide was 5'-FAM labelled and 3'-TAMRA labelled to allow FRET analysis to be conducted. The ΔT_m measured for each DNA sequence when treated with 50 μM of ligand is shown in Figure 88.

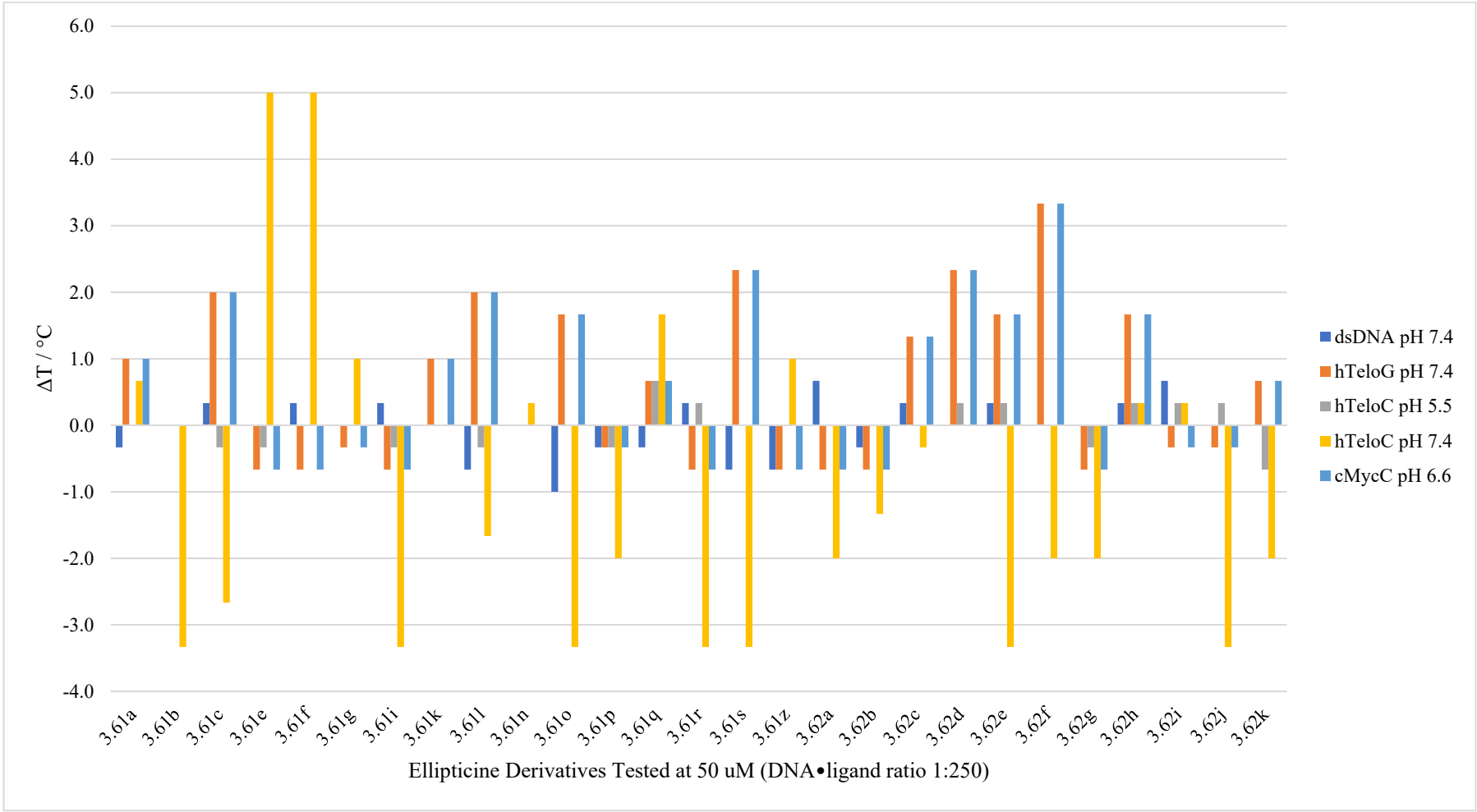

Figure 88. Plot of ΔT_m values for ellipticine derivatives of type **3.61** and **3.62** tested at 50 μM against a range of DNA structures. Experiments ran by Dr Elise P. Wright at the University of East Anglia.

The ellipticine derivatives **3.61** and **3.62** were tested at a higher concentration as it was expected that due to the lack of a cationic side chain, the interaction of these with the DNA structures would be lower. However, no strong secondary structure specific stabilisation was observed for any of the ellipticine derivatives tested (**3.61 – 3.62**), including the hTeloG G4. In contrast, compounds **3.61e** and **f** induced a 5 °C stabilisation on the hTeloC i-motif at pH 7.4. Although a 5 °C stabilisation is not particularly high, neutral i-motifs are rare due to the protonated cytosines that are generally required to form them.[274] These compounds could be candidates for further screening to see whether this stabilisation could be increased further. Although it was initially disappointing that none of the ligands exhibited a preference for G4 binding, the diarylamine compounds of type **3.62** exhibit a high degree of flexibility due to C-N bond rotation which means they lack a large aromatic surface area which is crucial for G4 binding. It is also known that the installation of cationic side chains to the core of the molecule should increase the G4 binding probability.[24] On the other hand, the lack of interaction of these small molecules with dsDNA and i-motif DNA is positive as this gives the option of trying to further optimise these ligands for selective G4 targeting.

Ellipticine (**2.5**), **1.41** and **1.42** (Figure 89) were subsequently tested against the different DNA structures to see whether the addition of cationic side chains increased the ligands affinity for any of the DNA structures (Table 17). This time the neutral i-motif HIF 1-alpha was also tested.

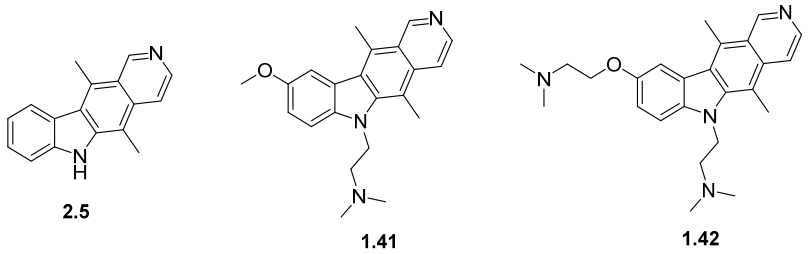

Figure 89. Structures of ellipticine (**2.5**) and two derivatives synthesised in Chapter 2 (**2.35** and **2.36**).

Table 17. ΔT_m values for three ellipticine compounds (10 μM) measured against a variety of DNA structures.

Compound	dsDNA pH 7.4	hTeloG pH 7.4	hTeloC pH 5.5	hTeloC pH 7.4	c-MycC pH 6.6	c-MycC pH 7.4	HIF 1-alpha pH 7.4
Ellipticine (2.5)	**3.7**	**7.2**	28.7	13.7	17.3	NT	NT
1.41	16.0	24.4	NT*	15.6	35.5	**23.5**	20.5
1.42	4.7	5.4	21.4	3.0	NT	5.4	12.0

*Values displaying NT were not tested. Notable results in bold.

Stabilisation was observed for all three compounds across the 7 DNA structures with little selectivity for one structure over another. Ligand **2.5** provided poor stabilisation to both dsDNA

and hTeloG which was unexpected as ellipticine has previously been shown to intercalate into dsDNA[136] and stabilise G4s.[140] Greater interaction could be seen for the folded and unfolded acidic i-motif structures hTeloC and c-MycC with ΔT_m values of 28.7 and 28.3 °C, respectively. Ligands **1.41** and **1.42** stabilise all structures fairly readily. Interestingly, a 23.5 °C stabilisation is recorded for the c-MycC:**1.41** complex at pH 7.4. Typically, this i-motif sequence would be unfolded at this pH therefore this result indicates that **1.41** is able to template the DNA to form the i-motif structure. The stabilisation of this i-motif at the neutral pH is significant due to the fact that there are few documented i-motif binders in the literature.[11]

15.4 Analysis of RNA and RNA•ligand Complexes by NMR

15.4.1 Analysis of Free Bcl-x Q2 RNA

The free RNA was initially analysed by ^{1}H NMR at 298 K with the RNA sample dissolved in a 90 % H_2O/10 % D_2O mixture. A concentration of 1 mM was used and the buffer conditions were consistent with those used in the UV-melt analysis (10 mM potassium phosphate, 100 mM KCl, pH 7.0). Analysing the overall structure (Figure A129), there is general line broadening which would suggest dynamic processes are at play. The imino region from the free Bcl-x Q2 RNA shows peaks ranging from 10.3 – 14.2 ppm (Figure 90). Around 7 peaks are visible in the G4 imino region and around 11 in the more downfield imino region. This would suggest that multiple RNA structures have been formed by the RNA in solution such as a G4 and an internal stem-loop.[106]

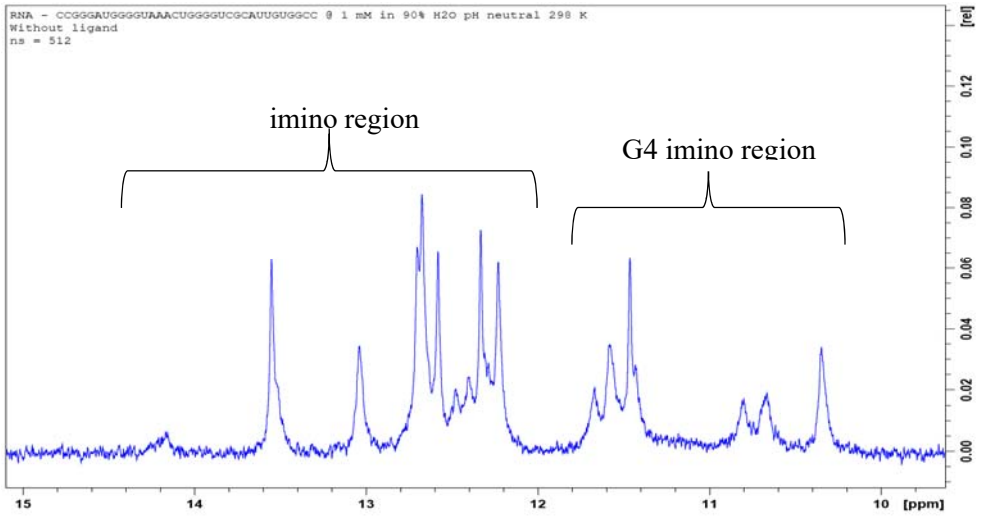

Figure 90. Imino region of free Bcl-x Q2 RNA.

GQC-05 (**1.20**) was titrated into the RNA solution at 0.2, 0.5, 1.0, 2.0, and 5.0 equivalents. Several key changes were observed during the titration experiment namely the disappearance of peaks within the imino region and the shifting and disappearance of peaks within the amino region.

15.4.2 Changes within the Imino and Amino Region of Bcl-x Q2 upon GQC-05 addition

The stacked plot Figure 91 clearly shows changes to the secondary RNA structure upon addition of **1.20**. The 7 peaks within the G4 imino region (10.0 – 12.0 ppm) diminish considerably to the point that three cannot be seen at all at 5.0 equivalents of **1.20**. This suggests that any potential G4 structures present in Q2 are lost on ligand addition.

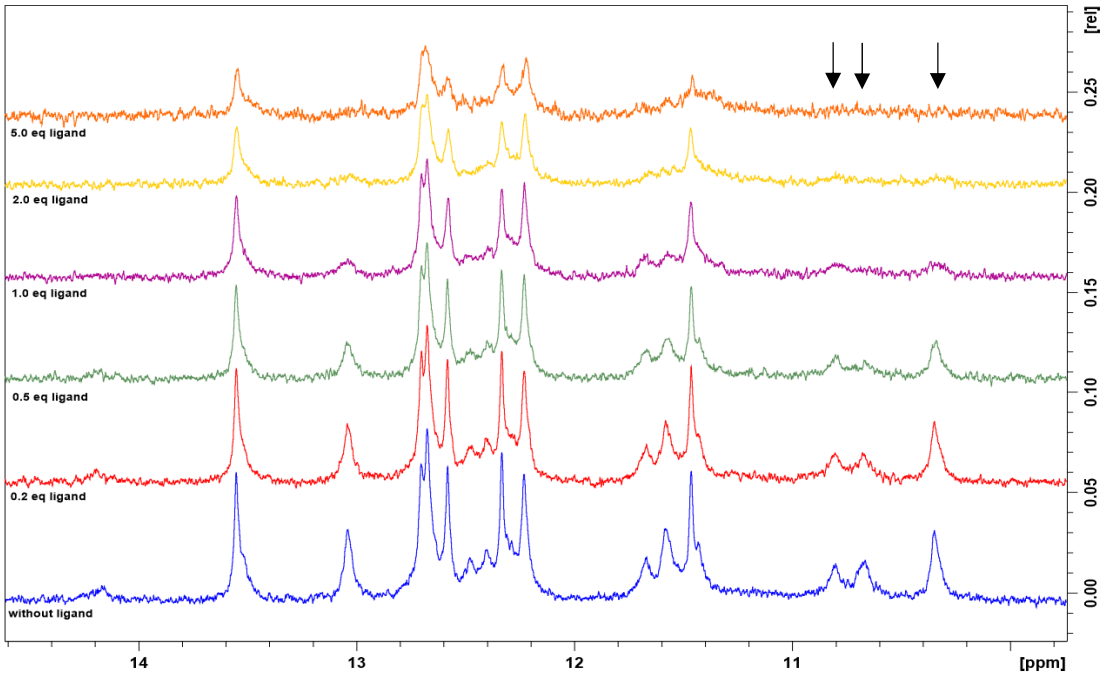

Figure 91. Stacked plot of imino region of free and complexed Bcl-x Q2 RNA. Black arrows mark missing peaks.

The remaining peaks between 12.0 – 14.2 ppm can also be seen to lose their intensity upon ligand titration. This overall reduced intensity could be characteristic of an intercalative binding mode of **1.20** to a hairpin or other duplex RNA structure with an intermediate exchange rate.[277] Overall line broadening and decreased signal intensity can also be observed in the amino region of the NMR (Figure 92). Several peaks were found to merge into one another or disappear as the equivalents of **1.20** was increased (Figure A130).

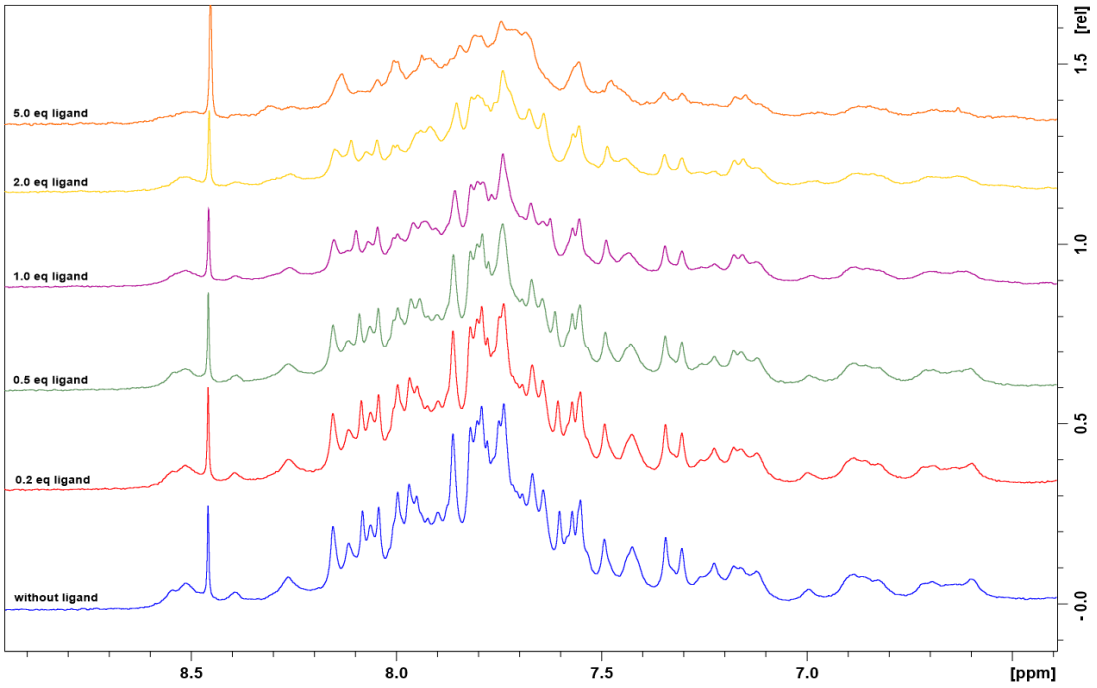

Figure 92. Stacked plot of amino region of free and complexed Bcl-x Q2 RNA.

Since NMR assignment could not be carried out, it is difficult to definitively state what these peak changes are associated with and what is happening to the overall structure on ligand addition.

15.4.3 NOESY NMR of Bcl-x•GQC-05 Complex

Ligand **1.20** has distinct signals in its proton spectra from the aromatic methyl groups and the amino methyl groups. It was thought that if these could be located in the ^{1}H NMR spectra when in complex with the RNA then it would be possible to pick out correlations within the 2D NOESY spectra. Unfortunately no nOe correlations between GQC-05 and RNA residues were identified

Probing the two key areas of the NOESY spectra for valuable G4 data (imino-imino region and imino-sugar region) shows no correlations indicative of a G4 structure (Figure A131, red and green boxes). This again suggests that the likelihood is another RNA secondary structure is forming preferentially when ligand is bound

15.5 *In Vitro* Splicing Assays of Ellipticine Derivatives

Although GQC-05 (**1.20**) was found to be the most potent splicing inducer, 9-hydroxyellipticine (**2.6**) was found to provide a sufficient alteration in the splicing ratio of Bcl-x by *in vitro* splicing assays (7-fold increase is xS/xL ratio).[111] The ellipticine derivatives synthesised in Chapter 3 were tested in Bcl-x *in vitro* splicing assays using the Bcl-x-681 transcript and HeLa nuclear extract. Although the dimethylamino tail was not installed on the ellipticine derivatives, they should give an indication of whether the core structure is able to produce any positive splicing results (compounds of type **3.62**). The biarylamine compounds of type **3.61** were also tested to see whether these flexible ligands were able to affect the splicing levels of Bcl-x. Unfortunately all of the compounds that were tested were inactive towards Bcl-x. An example of one of the *in vitro* splicing gels for compounds **1.41**, **1.20**, and **3.61b** is reported in Figure 93. Highlighted in red is where the clear loss of the xL band is seen on treatment of Bcl-x with 40 µM **1.20**. A darker band, suggesting more product, can be seen for the corresponding xS isoform at 40 µM. These changes cannot be seen in either **1.41**, which has previously shown to not affect Bcl-x splicing,[111] or **3.61b**. This suggests the inactivity of **3.61b** against Bcl-x.

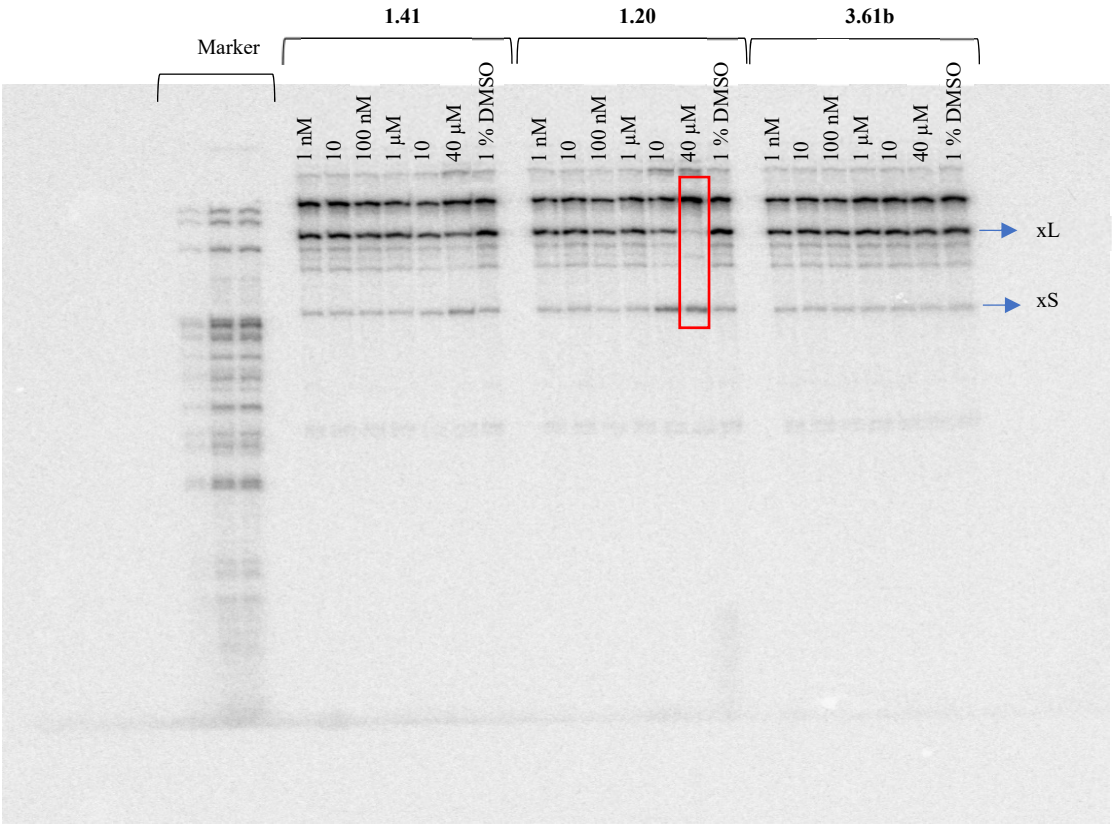

Figure 93. *In vitro* splicing assay as a function of increasing [ligand] for **1.41**, **1.20**, and **3.61b**. Experiments ran by Hatice Esenkaya at the University of Leicester.

16 Conclusions and Future Work

Previous work has shown that multiple regions within Bcl-x (681nt) wild type RNA have the possibility of forming G4 structures.[106] The Q2 region, which is downstream of the xS 5′ss, was chosen to be initially investigated using UV and FRET melting studies and NMR spectroscopy in the hope of understanding more about the structure upon ligand binding.

UV analysis demonstrated that the stabilisation of the Bcl-x Q2 region was 63.87 °C in a potassium buffer system. As expected for unimolecular G4s, stabilisation was not affected by concentration, however this is also true for other secondary RNA structures such as stem loops. It was found that at a higher stability was noted when the cation was changed to Na at lower salt concentrations (4.25 °C difference between K^+ and Na^+). This again is unusual for G4 structures as better stability is normally recorded in a potassium system.

When GQC-05 (**1.20**) was titrated into the RNA and UV analysis was performed a ΔT_m of 9.11 °C was recorded at 40 μM. When the concentration was increased to 60 μM a double sigmoidal curve was observed which suggested more than one structure was being stabilised. Unfortunately, when a palette of ellipticine derivatives were tested no stabilisation was seen for any of the compounds. In most cases the characteristic sigmoidal shape of the curve was lost. For future work it would be advantageous to test these compounds again with the dimethyl amino tail installed as this is expected to form important interactions with the RNA backbone which should encourage binding events. UV analysis of the Q2 region of Bcl-x RNA suggests that a G4 may form along with other secondary structures, however these are not stabilised on ligand addition.

FRET melting analysis was performed on a palette of DNA sequences, including dsDNA, i-motifs and G4s, to see whether the ellipticine derivatives **3.61** – **3.62** were able to induce a stabilisation of these structures. Overall no stabilisation was observed for both the diarylamine ligands **3.61** and the fully cross coupled ligands **3.62**. However, GQC-05 derivative **2.35** was also examined and showed a ΔT_m of 23.5 °C for the acidic i-motif c-MycC at neutral pH. Ligand **2.35** could therefore be developed as a ligand for the study of the formation of i-motifs in physiological conditions.

^{1}H NMR analysis of the free Bcl-x Q2 RNA suggests that at least two structures are present due to the spread of peaks across the imino region. These residues could correspond to both a G4 with two tetrads and another secondary structure, such as the internal loop that was predicted by RNA footprinting (Figure 94).

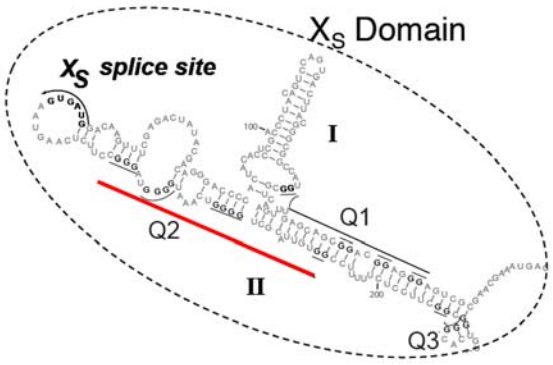

Figure 94. Predicted structure of Q2 section.

Upon addition of **1.20** there is loss of the suspected G4 imino protons and general definition and intensity loss across the remaining imino peaks. This could suggest that **1.20** is pushing the RNA towards another type of secondary structure such as an internal loop. If an internal loop is formed, for example, there could be intercalation of **1.20** between the bases pairs, which is known for ellipticine and derivatives in complex with dsDNA.[126,133] 2D NOESY analysis of the RNA•ligand complex at 2.0 equivalents **1.20** does not show any important G4 imino-imino or imino-aromatic interactions. It has also been impossible to pinpoint any correlations between ligand peaks and RNA peaks.

Overall the preliminary NMR data suggest that a G4 may be being formed in competition with another structure – most likely an internal loop as predicted by previous footprinting work.

To understand this dynamic system a high resolution NOESY will be needed of the free RNA and of the complexed structure. Due to the high degree of signal overlap seen in the NOESY that was acquired, it may be advantageous to use either labelled RNA or ligand to help pull apart the signals using complex NMR techniques. (Figure 95). Another popular technique often used in conjunction with G4 NMR work is ^{19}F labelling.[288] It is generally easier to label strands efficiently using this method as ^{19}F labels (e.g., 3,5 bis(trifluoromethyl)phenyl) can be coupled at the end of the RNA synthesis using traditional automated solid-phase phosphoramidite synthesis techniques.[312] Finally, a deuterium label could also be installed on the **1.20** backbone which would give a reference point in pinpointing nOe signals between ligand and RNA.

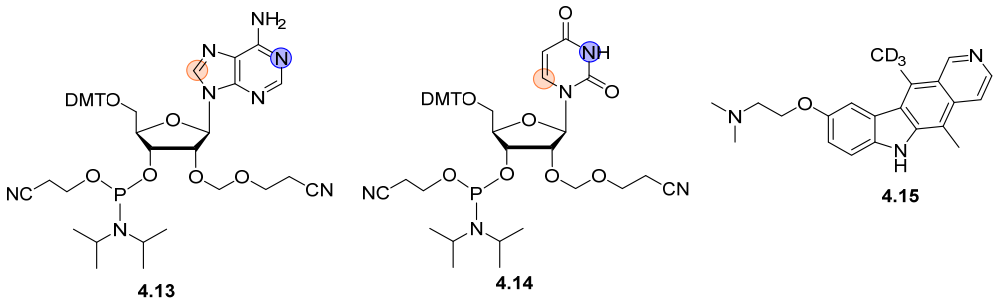

Figure 95. Possible ways to label RNA and ligand to simplify NMR assignment. (a) Phosphoramidites of A and U with ^{13}C labels coloured orange and ^{15}N labels coloured blue[313] (b) ^{2}H labelled GQC-05 (**4.15**).

Once the RNA or ligand is labelled, 2D filtered/edited NOESY experiments[314] could be recorded to pull apart the complex spectra and facilitate in the assignment of RNA structure and RNA•GQC-05 interactions.

In vitro Bcl-x splicing assays of the ellipticine derivatives **3.61** and **3.62** demonstrate that they are inactive towards modulation of the splicing preference of Bcl-x. This suggests that the compounds do not interact with the pre-mRNA of Bcl-x which is in agreement with the UV melting assays performed. This SAR data, along with the data previously published,[111] suggests:

(i) A basic tail extending from the main core of the molecule is important to increase the potency of the splicing modulator. Although previous results demonstrate 9-hydroxyellipticine to be active, GQC-05 is nearly 4 times more potent. The positioning of this tail around the ring may be important as structures tested with methoxy or methyl groups in different positions of the A-ring were not active. However, until a basic tail can be installed in these positions this hypothesis cannot be fully tested.

(ii) The loss of the methyl groups on the C-ring seems to have a detrimental effect on splicing.

(iii) The pyridine nitrogen in the D-ring may be important as when this was located in other positions around the D-ring the compounds were inactive.

(iv) The introduction of sp^3 character into the D-ring does not seem to enhance the production of Bcl-xS either. This could suggest that the planarity of the compound is important.

(v) The ellipticine regioisomers tested also had no effect on the splicing assay which suggest that the discrete structure of ellipticine is important.

From this work it seems like the core ellipticine structure is crucial to the splicing induction witnessed with GQC-05.

17 Experimental

17.1 General

Reagents and Solvents

All reagents and solvents were obtained from commercial suppliers and were used without further purification unless otherwise stated.

17.2 UV Melting Assays

Melting temperature analyses were performed on a Shimadzu UV spectrometer UV 1800 equipped with a thermocontrolled cell holder possessing a cell path length of 1 cm. An aqueous solution consisting of 20 mM potassium or sodium phosphate buffer, varying concentrations of both KCl and NaCl, at pH 7.0 was used as the analysis buffer. The concentration of both the RNA and ligand was varied depending on the experiments performed. Denaturating profiles were recorded at λ = 260 nm from 20 to 90 °C, with a heating rate of 0.5 °C/min. Analysis was carried out on OriginPro 2017 and a Boltzmann Sigmoidal fit was used. The reported melting temperatures were defined as averages of the maximum of first derivative plots of n = 2 or 3 independent denaturing profiles.

17.3 FRET Melting Assays

FRET melting assays were carried out by Dr Elise P. Wright under the supervision of Dr Zoë A. E. Waller in the University of East Anglia.

17.4 NMR

17.4.1 NMR sample preparation

RP-HPLC purified RNA CCGGGAUGGGGUAAACUGGGGUCGCAUUGUGGCC was purchased from TriLink. Each sample was dissolved in 222 µL of H_2O buffered with 20 mM potassium phosphate buffer and 100 mM KCl at pH 7.0 and containing 0.1 mM deuterated trimethylsilylpropionic acid sodium salt-d4 and freeze-dried to dryness. The samples were re-dissolved in 222 µL of 90 % H_2O with 10 % D_2O. The solution was transferred into a 3 mm high-precision NMR tube and used for RNA data acquisition. A concentrated solution of GQC-05 in 10 % d_6-DMSO in water was added in small aliquots. After each addition of GQC-05 to the

buffered solution containing RNA, a 1D ^{1}H NMR spectra was acquired until the end point of the titration was reached. 2D NOESY data was also acquired at certain points during the titration experiment.

17.4.2 NMR data acquisition

NMR data were typically acquired on a Bruker AVANCEII+ 600 NMR spectrometer operating at a magnetic field strength of 14.1 T (600.13 MHz for proton resonance) under TopSpin (version 3.5 patch level 5, Bruker, Reinstetten, Germany) running on a Hewlett Packard Z420 workstation under Windows Professional version 7 (Microsoft Inc.). A triple resonance probehead [TBI-z] equipped with actively shielded z-gradient coil for delivery of pulsed field gradients was manually tuned for proton resonance observation. The probe temperature was configured for both 298 K and 308 K. 1D ^{1}H NMR data were acquired using double pulsed field gradient spin-echo (pulse program zgesgp) to eliminate the residual solvent resonance. Data were typically acquired for 90 % H_2O samples with 512 transients into 65K data points (acquisition time: 2.18 s) over a frequency width equivalent to 25.0 ppm centred at $\delta^{1}H$ = 4.692 ppm for data acquired at 298 K, the offset being adjusted accordingly for elevated temperatures to maintain effective solvent suppression. Hard proton 90° pulses were typically calibrated at 9.6 W with an average value of 8.6 μs.

2D NOESY data were acquired with excitation sculpting for solvent suppression (pulse program: noesyesgpph) using State-TPPI for 1024 t1 increments and 2048 data points over F1 and F2 frequency widths equivalent to 25 ppm centred at the solvent frequency resonance. Data were acquired with 96 transients per t1 increment with a relaxation delay of 1.5 s between transients. The mixing time was defined as 150 ms. All data were processed according to established NMR data processing protocols under TopSpin (version 3.5 patch level 7, Bruker, Reinstetten, Germany).

17.5 *In Vitro* Splicing Assays

In vitro splicing assays were carried out by Hatice Esenkaya under the supervision of Professor Ian C. Eperon in the University of Leicester.

18 References

(1) Crick, F. Central Dogma of Molecular Biology. *Nature* **1970**, *227*, 561–563.

(2) Coffin, J. M.; Hughes, S. H.; Varmus, H. E. *Retroviruses*; Cold Spring Harbour Laboratory Press, 1997.

(3) O'Connor, C.; Adams, J. U.; Fairman, J. E. *Essentials of Cell Biology*; NPG Education, 2010.

(4) Boeger, H.; Bushnell, D. A.; Davis, R.; Griesenbeck, J.; Lorch, Y.; Strattan, J. S.; Westover, K. D.; Kornberg, R. D. Structural Basis of Eukaryotic Gene Transcription. *FEBS Lett.* **2005**, *579*, 899–903.

(5) Cheung, A. C. M.; Cramer, P. A Movie of RNA Polymerase II Transcription. *Cell* **2012**, *149*, 1431–1437.

(6) Blackburn, G, M.; Gait, M, J. *Nucleic Acids in Chemistry and Biology*, Second Edi.; Oxford University Press, 1996.

(7) Lee, T. I.; Young, R. A. Transcription of Eukaryotic Protein- Coding Genes. *Annu. Rev. Genet.* **2000**, *34*, 77–137.

(8) Kent, M. *Advanced Biology*; Oxford University Press, 2000.

(9) Rich, A. The Double Helix: A Tale of Two Puckers. *Nat. Struct. Biol.* **2003**, *10*, 247–249.

(10) Siddiqui-Jain, A.; Hurley, L. H. DNA Structure: Visualizing the Quadruplex. *Nat. Chem.* **2013**, *5*, 153–155.

(11) Day, H. A.; Pavlou, P.; Waller, Z. A. E. I-Motif DNA: Structure, Stability and Targeting with Ligands. *Bioorganic Med. Chem.* **2014**, *22*, 4407–4418.

(12) Alternative DNA structures: A-DNA, B-DNA and Z-DNA http://biotech.christopher-vidal.com/dnamolecule.htm (accessed Aug 17, 2015).

(13) Chen, Y.; Fender, J.; Legassie, J. D.; Jarstfer, M. B.; Bryan, T. M.; Varani, G. Structure of Stem-Loop IV of Tetrahymena Telomerase RNA. *EMBO J.* **2006**, *25*, 3156–3166.

(14) G-quadruplex nucleic acids http://www-leverhulme-bc.ch.cam.ac.uk/www-shankar/gquadnucleicacids.html (accessed Aug 18, 2015).

(15) Pandey, S.; Agarwala, P.; Maiti, S. Effect of Loops and G-Quartets on the Stability of RNA G-Quadruplexes. *J. Phys. Chem. B* **2013**, *117*, 6896–6905.

(16) Phan, A. T. Human Telomeric G-Quadruplex: Structures of DNA and RNA Sequences. *FEBS J.* **2010**, *277*, 1107–1117.

(17) Zhou, J.; Bourdoncle, A.; Rosu, F.; Gabelica, V.; Mergny, J. L. Tri-G-Quadruplex: Controlled Assembly of a G-Quadruplex Structure from Three G-Rich Strands. *Angew. Chemie - Int. Ed.* **2012**, *51*, 11002–11005.

(18) Moon, I. K.; Jarstfer, M. B. The Human Telomere and Its Relationship to Human Disease, Therapy, and Tissue Engineering. *Front. Biosci.* **2007**, *12*, 4595–4620.

(19) Huppert, J. L.; Balasubramanian, S. Prevalence of Quadruplexes in the Human Genome. *Nucleic Acids Res.* **2005**, *33*, 2908–2916.

(20) Millevoi, S.; Moine, H.; Vagner, S. G-Quadruplexes in RNA Biology. *Wiley Interdiscip. Rev. RNA* **2012**, *3*, 495–507.

(21) Joachimi, A.; Benz, A.; Hartig, J. S. A Comparison of DNA and RNA Quadruplex Structures and Stabilities. *Bioorg. Med. Chem.* **2009**, *17*, 6811–6815.

(22) Guo, J. U.; Bartel, D. P. RNA G-Quadruplexes Are Globally Unfolded in Eukaryotic Cells and Depleted in Bacteria. *Science (80-.).* **2016**, *353*, aaf5371.

(23) Neidle, S. Human Telomeric G-Quadruplex: The Current Status of Telomeric G-Quadruplexes as Therapeutic Targets in Human Cancer. *FEBS J.* **2010**, *277*, 1118–1125.

(24) Monchaud, D.; Teulade-Fichou, M.-P. A Hitchhiker's Guide to G-Quadruplex Ligands. *Org. Biomol. Chem.* **2008**, *6*, 627–636.

(25) Haider, S. M.; Neidle, S.; Parkinson, G. N. A Structural Analysis of G-Quadruplex/Ligand Interactions. *Biochimie* **2011**, *93*, 1239–1251.

(26) Parkinson, G. N.; Ghosh, R.; Neidle, S. Structural Basis for Binding of Porphyrin to Human Telomeres. *Biochemistry* **2007**, *46*, 2390–2397.

(27) Yao, X.; Song, D.; Qin, T.; Yang, C.; Yu, Z.; Li, X.; Liu, K.; Su, H. Interaction between G-Quadruplex and Zinc Cationic Porphyrin: The Role of the Axial Water. *Sci. Rep.* **2017**, *7*, 2–11.

(28) Collie, G. W.; Parkinson, G. N. The Application of DNA and RNA G-Quadruplexes to

Therapeutic Medicines. *Chem. Soc. Rev.* **2011**, *40*, 5867–5892.

(29) Rodriguez, R.; Müller, S.; Yeoman, J. A.; Trentesaux, C.; Riou, J. F.; Balasubramanian, S. A Novel Small Molecule That Alters Shelterin Integrity and Triggers a DNA-Damage Response at Telomeres. *J. Am. Chem. Soc.* **2008**, *130*, 15758–15759.

(30) Müller, S.; Sanders, D. A.; Di Antonio, M.; Matsis, S.; Riou, J.-F.; Rodriguez, R.; Balasubramanian, S. Pyridostatin Analogues Promote Telomere Dysfunction and Long-Term Growth Inhibition in Human Cancer Cells. *Org. Biomol. Chem.* **2012**, *10*, 6537–6546.

(31) Rodriguez, R.; Miller, K. M.; Forment, J. V; Bradshaw, C. R.; Nikan, M.; Britton, S.; Oelschlaegel, T.; Xhemalce, B.; Balasubramanian, S.; Jackson, S. P. Small Molecule-Induced DNA Damage Identifies Alternative DNA Structures in Human Genes. *Nat. Chem. Biol.* **2012**, *8*, 301–310.

(32) Granotier, C.; Pennarun, G.; Riou, L.; Hoffschir, F.; Gauthier, L. R.; De Cian, A.; Gomez, D.; Mandine, E.; Riou, J. F.; Mergny, J. L.; Mailliet, P.; Dutrillaux, B.; Boussin, F. D. Preferential Binding of a G-Quadruplex Ligand to Human Chromosome Ends. *Nucleic Acids Res.* **2005**, *33*, 4182–4190.

(33) De Cian, A.; De Lemos, E.; Mergny, J.-L.; Teulade-Fichou, M.-P.; Monchaud, D. Highly Efficient G-Quadruplex Recognition by Bisquinolinium Compounds. *J. Am. Chem. Soc.* **2007**, *129*, 1856–1857.

(34) Perry, P. J.; Read, M. A.; Davies, R. T.; Gowan, S. M.; Reszka, A. P.; Wood, A. A.; Kelland, L. R.; Neidle, S. 2,7-Disubstituted Amidofluorenone Derivatives as Inhibitors of Human Telomerase. *J. Med. Chem.* **1999**, *42*, 2679–2684.

(35) Read, M. A.; Wood, A. A.; Harrison, J. R.; Gowan, S. M.; Kelland, L. R.; Dosanjh, H. S.; Neidle, S. Molecular Modeling Studies on G-Quadruplex Complexes of Telomerase Inhibitors: Structure-Activity Relationships. *J. Med. Chem.* **1999**, *42*, 4538–4546.

(36) Haider, S. M.; Parkinson, G. N.; Neidle, S. Structure of a G-Quadruplex-Ligand Complex. *J. Mol. Biol.* **2003**, *326*, 117–125.

(37) Harrison, R. J.; Reszka, A. P.; Haider, S. M.; Romagnoli, B.; Morrell, J.; Read, M. A.; Gowan, S. M.; Incles, C. M.; Kelland, L. R.; Neidle, S. Evaluation of by Disubstituted Acridone Derivatives as Telomerase Inhibitors: The Importance of G-Quadruplex Binding. *Bioorganic Med. Chem. Lett.* **2004**, *14*, 5845–5849.

(38) Moore, M. J. B.; Schultes, C. M.; Cuesta, J.; Cuenca, F.; Gunaratnam, M.; Tanious, F. A.; Wilson, W. D.; Neidle, S. Trisubstituted Acridines as G-Quadruplex Telomere Targeting Agents. Effects of Extensions of the 3,6- and 9-Side Chains on Quadruplex Binding, Telomerase Activity, and Cell Proliferation. *J. Med. Chem.* **2006**, *49*, 582–599.

(39) Campbell, N. H.; Parkinson, G. N.; Reszka, A. P.; Neidle, S. Structural Basis of DNA Quadruplex Recognition by an Acridine Drug. *J. Am. Chem. Soc.* **2008**, *130*, 6722–6724.

(40) Burger, A. M.; Dai, F.; Schultes, C. M.; Reszka, A. P.; Moore, M. J.; Double, J. A.; Neidle, S. The G-Quadruplex-Interactive Molecule BRACO-19 Inhibits Tumor Growth, Consistent with Telomere Targeting and Interference with Telomerase Function. *Cancer Res.* **2005**, *65*, 1489–1496.

(41) Brown, R. V; Danford, F. L.; Gokhale, V.; Hurley, L. H.; Brooks, T. A. Demonstration That Drug-Targeted Down-Regulation of MYC in Non-Hodgkins Lymphoma Is Directly Mediated Through the Promoter G-Quadruplex. *J. Biol. Chem.* **2011**, *286*, 41018–41027.

(42) Grand, C. L.; Han, H.; Muñoz, R. M.; Weitman, S.; Von Hoff, D. D.; Hurley, L. H.; Bearss, D. J. The Cationic Porphyrin TMPyP4 Down-Regulates c-MYC and Human Telomerase Reverse Transcriptase Expression and Inhibits Tumor Growth in Vivo. *Mol. Cancer Ther.* **2002**, *1*, 565–573.

(43) Wei, C.; Jia, G.; Yuan, J.; Feng, Z.; Li, C. A Spectroscopic Study on the Interactions of Porphyrin with G-Quadruplex DNAs. *Biochemistry* **2006**, *45*, 6681–6691.

(44) Haq, I.; Trent, J. O.; Chowdhry, B. Z.; Jenkins, T. C. Intercalative G-Tetraplex Stabilization of Telomeric DNA by a Cationic Porphyrin. *J. Am. Chem. Soc.* **1999**, *121*, 1768–1779.

(45) Reed, J. E.; Arnal, A. A.; Neidle, S.; Vilar, R. Stabilization of G-Quadruplex DNA and Inhibition of Telomerase Activity by Square-Planar Nickel(II) Complexes. *J. Am. Chem. Soc.* **2006**, *128*, 5992–5993.

(46) Zhang, J.; Yu, Q.; Li, Q.; Yang, L.; Chen, L.; Zhou, Y.; Liu, J. A Ruthenium(II) Complex Capable of Inducing and Stabilizing Bcl-2 G-Quadruplex Formation as a Potential Cancer Inhibitor. *J. Inorg. Biochem.* **2014**, *134*, 1–11.

(47) Joachimi, A.; Benz, A.; Hartig, J. S. A Comparison of DNA and RNA Quadruplex Structures and Stabilities. *Bioorganic Med. Chem.* **2009**, *17*, 6811–6815.

(48) Gomez, D.; Guédin, A.; Mergny, J. L.; Salles, B.; Riou, J. F.; Teulade-Fichou, M. P.; Calsou, P. A G-Quadruplex Structure Within the 5′-UTR of TRF2 MRNA Represses Translation in Human Cells. *Nucleic Acids Res.* **2010**, *38*, 7187–7198.

(49) Nijjar, T.; Bassett, E.; Garbe, J.; Takenaka, Y.; Stampfer, M. R.; Gilley, D.; Yaswen, P. Accumulation and Altered Localization of Telomere-Associated Protein TRF2 in Immortally Transformed and Tumor-Derived Human Breast Cells. *Oncogene* **2005**, *24*, 3369–3376.

(50) Hsu, C. P.; Ko, J. L.; Shai, S. E.; Lee, L. W. Modulation of Telomere Shelterin by TFR1 and TRF2 Interacts with Telomerase to Maintain the Telomere Length in Non-Small Cell Lung Cancer. *Lung Cancer* **2007**, *58*, 310–316.

(51) Bugaut, A.; Rodriguez, R.; Kumari, S.; Hsu, S.-T. D.; Balasubramanian, S. Small Molecule-Mediated Inhibition of Translation by Targeting a Native RNA G-Quadruplex. *Org. Biomol. Chem.* **2010**, *8*, 2771–2776.

(52) Collie, G. W.; Sparapani, S.; Parkinson, G. N.; Neidle, S. Structural Basis of Telomeric RNA Quadruplex-Acridine Ligand Recognition. *J. Am. Chem. Soc.* **2011**, *133*, 2721–2728.

(53) Collie, G. W.; Haider, S. M.; Neidle, S.; Parkinson, G. N. A Crystallographic and Modelling Study of a Human Telomeric RNA (TERRA) Quadruplex. *Nucleic Acids Res.* **2010**, *38*, 5569–5580.

(54) Collie, G. W.; Parkinson, G. N.; Neidle, S. *Incomplete Structural Model of a Human Telomeric DNA Quadruplex-Acridine Complex. PDB Id 3QCR*; 2017.

(55) Elliott, D.; Ladomery, M. *Molecular Biology of RNA*; Oxford University Press, 2011.

(56) Berget, S. M.; Moore, C.; Sharp, P. A. Spliced Segments at the 5′ Terminus of Adenovirus 2 Late MRNA. *Proc. Natl. Acad. Sci.* **1977**, *74*, 3171–3175.

(57) Makarova, O. M. Spliceosome: The Unravelling Complexity. *Biochem. (Lond).* **2014**, 46–52.

(58) Matera, G.; Wang, Z. A Day in the Life of the Spliceosome. *Nat. Rev. Mol. Cell Biol.* **2014**, *15*, 108–121.

(59) Will, C. L.; Luhrmann, R. Spliceosome Structure and Function. *Cold Spring Harb Perspect Biol.* **2011**, *3*, a003707.

(60) Galej, W. P.; Wilkinson, M. E.; Fica, S. M.; Oubridge, C.; Newman, A. J.; Nagai, K. Cryo-EM Structure of the Spliceosome Immediately after Branching. *Nature* **2016**, *537*, 197–201.

(61) Wan, R.; Yan, C.; Bai, R.; Huang, G.; Shi, Y. Structure of a Yeast Catalytic Step I Spliceosome at 3.4 Å Resolution. *Science (80-.).* **2016**, *353*, 895–904.

(62) Hames, B. D.; Glover, D. M. *Transcription and Splicing*; IRL Press, 1988.

(63) Padgett, R. A. New Connections between Splicing and Human Disease. *Trends Genet.* **2012**, *28*, 147–154.

(64) De la Cruz, J.; Kressler, D.; Linder, P. Unwinding RNA in Saccharomyces Cerevisiae: DEAD-Box Proteins and Related Families. *Trends Biochem. Sci.* **1999**, *24*, 192–198.

(65) Rauhut, R.; Fabrizio, P.; Dybkov, O.; Hartmuth, K.; Pena, V.; Chari, A.; Kumar, V.; Lee, C.; Urlaub, H. Molecular Architechture of the Saccharomyces Cerevisiae Activated Spliceosome. *Science (80-.).* **2016**, *353*, 1399–1405.

(66) Chen, M.; Manley, J. L. Mechanisms of Alternative Splicing Regulation: Insights from Molecular and Genomics Approaches. *Nat. Rev. Mol. Cell Biol.* **2009**, *10*, 741–754.

(67) Pan, Q.; Shai, O.; Lee, L, J.; Frey, B, J.; Blencowe, B, J. Deep Surveying of Alternative Splicing Complexity in the Human Transcriptome by High-Throughput Sequencing. *Nat. Genet.* **2008**, *40*, 1413–1415.

(68) Wang, E. T.; Sandberg, R.; Luo, S.; Khrebtukova, I.; Zhang, L.; Mayr, C.; Kingsmore, Stephen, F.; Schroth, Gary, P.; Burge, Christopher, B. Alternative Isoform Regulation in Human Tissue Transcriptomes. *Nature* **2008**, *456*, 470–476.

(69) Jeanteur, P. *Alternative Splicing and Disease*; Springer-Verlag Berlin Heidelberg, 2006.

(70) Tazi, J.; Bakkour, N.; Stamm, S. Alternative Splicing and Disease. *Biochim. Biophys. Acta - Mol. Basis Dis.* **2009**, *1792*, 14–26.

(71) Scotti, M. M.; Swanson, M. S. RNA Mis-Splicing in Disease. *Nat. Rev. Genet.* **2016**, *17*, 19–32.

(72) Keren, H.; Lev-Maor, G.; Ast, G. Alternative Splicing and Evolution: Diversification, Exon Definition and Function. *Nat. Rev. Genet.* **2010**, *11*, 345–355.

(73) Krainer, A. R. *Eukaryotic MRNA Processing*; Oxford University Press, 2001.

(74) Eperon, I. C.; Makarova, O. V; Mayeda, A.; Munroe, S. H.; Hayward, D. G.; Krainer, A. R.; Ca, J. F. Selection of Alternative 5 J Splice Sites : Role of U1 SnRNP and Models for the Antagonistic Effects of SF2 / ASF and HnRNP A1. *Mol. Cell. Biol.* **2000**, *20*, 8303–8318.

(75) Long, J. C.; Caceres, J. F. The SR Protein Family of Splicing Factors : Master Regulators of Gene Expression. *Biochem. J.* **2009**, *419*, 15–27.

(76) Martinez-Contreras, R.; Cloutier, P.; Shkreta, L.; Fisette, J. F.; Revil, T.; Chabot, B. HnRNP Proteins and Splicing Control. *Adv. Exp. Med. Biol.* **2007**, *623*, 123–147.

(77) Kornblihtt, A. R.; Schor, I. E.; Alló, M.; Dujardin, G.; Petrillo, E.; Muñoz, M. J. Alternative Splicing: A Pivotal Step between Eukaryotic Transcription and Translation. *Nat. Rev. Mol. Cell Biol.* **2013**, *14*, 153–165.

(78) Burghes, A. H. M.; Beattie, C. E. Spinal Muscular Atrophy: Why Do Low Levels of Survival Motor Neuron Protein Make Motor Neurons Sick? *Nat. Rev. Neurosci.* **2009**, *10*, 597–609.

(79) Ferro, J. Facts About Spinal Muscular Atrophy. *Muscular Dystrophy Assoc.* **2009**.

(80) Mercuri, E.; Bertini, E.; Iannaccone, S. T. Childhood Spinal Muscular Atrophy: Controversies and Challenges. *Lancet Neurol.* **2012**, *11*, 443–452.

(81) Butchbach, M. E. R.; Burghes, A. H. M. Central Nervous System Perspectives on Models of Spinal Muscular Atrophy for Drug Discovery. **2004**, *1*, 151–156.

(82) Goodchild, J. *Therapeutic Oligonucleotides*; Humana Press, 2011.

(83) Brad Wan, W.; Seth, P. P. The Medicinal Chemistry of Therapeutic Oligonucleotides. *J. Med. Chem.* **2016**, *59*, 9645–9667.

(84) Commitee for Medicinal Product for Human Use. *Assessment Report Spinraza*; 2017; Vol. 44.

(85) Chiriboga, C. A.; Swoboda, K. J.; Darras, B. T.; Iannaccone, S. T.; Montes, J.; De Vivo, D. C.; Norris, D. A.; Bennett, C. F.; Bishop, K. M. Results from a Phase 1 Study of Nusinersen (ISIS-SMNRx) in Children with Spinal Muscular Atrophy. *Neurology* **2016**, *86*, 890–897.

(86) Wood, M. J. A.; Talbot, K.; Bowerman, M. Spinal Muscular Atrophy: Antisense Oligonucleotide Therapy Opens the Door to an Integrated Therapeutic Landscape. *Hum.*

Mol. Genet. **2017**, *26*, R151–R159.

(87) Calder, A. N.; Androphy, E. J.; Hodgetts, K. J. Small Molecules in Development for the Treatment of Spinal Muscular Atrophy. *J. Med. Chem.* **2016**, *59*, 10067–10083.

(88) Naryshkin, N. A.; Weetall, M.; Dakka, A.; Narasimhan, J.; Zhao, X.; Feng, Z.; Ling, K. K. Y.; Karp, G. M.; Qi, H.; Woll, M. G.; Chen, G.; Zhang, N.; Gabbeta, V.; Vazirani, P.; Bhattacharyya, A.; Furia, B.; Risher, N.; Sheedy, J.; Kong, R.; Ma, J.; Turpoff, A.; Lee, C.; Zhang, X.; Moon, Y.; Trifillis, P.; Welch, E. M.; Colacino, J. M.; Babiak, J.; Almstead, N. G.; Peltz, S. W.; Eng, L. A.; Chen, K. S.; Mull, J. L.; Lynes, M. S.; Rubin, L. L.; Fontoura, P.; Santarelli, L.; Haehnke, D.; Mccarthy, K. D.; Schmucki, R.; Ebeling, M.; Sivaramakrishnan, M.; Ko, C.; Paushkin, S. V; Ratni, H. SMN2 Splicing Modifiers Improve Motor Function and Longevity in Mice with Spinal Muscular Atrophy. *Science (80-.).* **2014**, *345*, 688–693.

(89) Feng, Z.; Ling, K. K. Y.; Zhao, X.; Zhou, C.; Karp, G.; Welch, E. M.; Naryshkin, N.; Ratni, H.; Chen, K. S.; Metzger, F.; Paushkin, S.; Weetall, M.; Ko, C. P. Pharmacologically Induced Mouse Model of Adult Spinal Muscular Atrophy to Evaluate Effectiveness of Therapeutics after Disease Onset. *Hum. Mol. Genet.* **2016**, *25*, 964–975.

(90) Zhao, X.; Feng, Z.; Ling, K. K. Y.; Mollin, A.; Sheedy, J.; Yeh, S.; Petruska, J.; Narasimhan, J.; Dakka, A.; Welch, E. M.; Karp, G.; Chen, K. S.; Metzger, F.; Ratni, H.; Lotti, F.; Tisdale, S.; Naryshkin, N. A.; Pellizzoni, L.; Paushkin, S.; Ko, C. P.; Weetall, M. Pharmacokinetics, Pharmacodynamics, and Efficacy of a Small-Molecule SMN2 Splicing Modifier in Mouse Models of Spinal Muscular Atrophy. *Hum. Mol. Genet.* **2016**, *25*, 1885–1899.

(91) Pinard, E.; Green, L.; Reutlinger, M.; Weetall, M.; Naryshkin, N. A.; Baird, J.; Chen, K. S.; Paushkin, S. V.; Metzger, F.; Ratni, H. Discovery of a Novel Class of Survival Motor Neuron 2 Splicing Modifiers for the Treatment of Spinal Muscular Atrophy. *J. Med. Chem.* **2017**, *60*, 4444–4457.

(92) Palacino, J.; Swalley, S. E.; Song, C.; Cheung, A. K.; Shu, L.; Zhang, X.; Van Hoosear, M.; Shin, Y.; Chin, D. N.; Keller, C. G.; Beibel, M.; Renaud, N. A.; Smith, T. M.; Salcius, M.; Shi, X.; Hild, M.; Servais, R.; Jain, M.; Deng, L.; Bullock, C.; McLellan, M.; Schuierer, S.; Murphy, L.; Blommers, M. J. J.; Blaustein, C.; Berenshteyn, F.; Lacoste, A.; Thomas, J. R.; Roma, G.; Michaud, G. A.; Tseng, B. S.; Porter, J. A.; Myer, V. E.; Tallarico, J. A.; Hamann, L. G.; Curtis, D.; Fishman, M. C.; Dietrich, W. F.; Dales, N. A.;

Sivasankaran, R. SMN2 Splice Modulators Enhance U1-Pre-MRNA Association and Rescue SMA Mice. *Nat. Chem. Biol.* **2015**, *11*, 511–517.

(93) U.S National Library of Medicine - ClinicalTrials.gov https://clinicaltrials.gov/ct2/show/NCT02908685 (Date Accessed: January 2018).

(94) U.S National Library of Medicine - ClinicalTrials.gov https://clinicaltrials.gov/ct2/show/NCT02913482 (Date Accessed: January 2018).

(95) U.S National Library of Medicine - ClinicalTrials.gov https://clinicaltrials.gov/ct2/show/NCT03032172 (Date Accessed: January 2018).

(96) U.S National Library of Medicine - ClinicalTrials.gov https://clinicaltrials.gov/ct2/show/NCT02268552 (Date Accessed: January 2018).

(97) Youle, R. J.; Strasser, A. The BCL-2 Protein Family : Opposing Activities That Mediate Cell Death. *Nat. Rev. Mol. Cell Biol.* **2008**, *9*, 47–59.

(98) Strasser, A. The Role of BH3-Only Proteins in the Immune System. *Nat. Rev. Immunol.* **2005**, *5*, 189–200.

(99) Czabotar, P. E.; Lessene, G.; Strasser, A.; Adams, J. M. Control of Apoptosis by the Bcl-2 Protein Family and Implications for Physiology and Therapy. *Nat. Rev. Mol. Cell Biol.* **2014**, *15*, 49–63.

(100) Mcilwain, D. R.; Berger, T.; Mak, T. W. Caspase Functions in Cell Death and Disease. *Cold Spring Harb Perspect Biol.* **2013**, *5*, a008656.

(101) Spierings, D.; McStay, G.; Saleh, M.; Bender, C.; Chipuk, J.; Maurer, U.; Green, D. R. Connected to Death: The (Unexpurgated) Mitochondrial Pathway of Apoptosis. *Science (80-.).* **2005**, *310*, 66–67.

(102) Kelekar, A.; Thompson, C. B. Bcl-2-Family Proteins: The Role of the BH3 Domain in Apoptosis. *Trends Cell Biol.* **1998**, *8*, 324–330.

(103) Mercatante, D. R.; Bortner, C. D.; Cidlowski, J. A.; Kole, R. Modification of Alternative Splicing of Bcl-x Pre-MRNA in Prostate and Breast Cancer Cells. Analysis of Apoptosis and Cell Death. *J. Biol. Chem.* **2001**, *276*, 16411–16417.

(104) Foreman, K. E.; Wrone-Smith, T.; Boise, L. H.; Thompson, C. B.; Polverinio, P. J.; Simonian, P. L.; Nunez, G.; Nickoloff, B. J. Kaposi's Sarcoma Tumor Cells Preferentially Express Bcl-XL. *Am. J. Pathol.* **1996**, *149*, 795–803.

(105) Taylor, J. K.; Zhang, Q. Q.; Wyatt, J. R.; Dean, N. M. Induction of Endogenous Bcl-XS through the Control of Bcl-x Pre-MRNA Splicing by Antisense Oligonucleotides. *Nat. Biotechnol.* **1999**, *17*, 1097–1100.

(106) Weldon, C.; Behm-Ansmant, I.; Hurley, L. H.; Burley, G. A.; Branlant, C.; Eperon, I. C.; Dominguez, C. Identification of G-Quadruplexes in Long Functional RNAs Using 7-Deazaguanine RNA. *Nat. Chem. Biol.* **2016**, *13*, 18–21.

(107) Kikin, O.; D'Antonio, L.; Bagga, P. S. QGRS Mapper: A Web-Based Server for Predicting G-Quadruplexes in Nucleotide Sequences. *Nucleic Acids Res.* **2006**, *34*, W676–W682.

(108) Murchie, A. I. H.; Lilley, D. M. J. Retinoblastoma Susceptibility Genes Contain 5' Sequences with a High Propensity to Form Guanine-Tetrad Structures. *Nucleic Acids Res.* **1992**, *20*, 49–53.

(109) McLuckie, K. I. E.; Di Antonio, M.; Zecchini, H.; Xian, J.; Caldas, C.; Krippendoff, B.; Tannahill, D.; Lowe, C.; Balasubramanian, S. G-Quadruplex DNA as a Molecular Target for Induced Synthetic Lethality in Cancer Cells. *J. Am. Chem. Soc.* **2013**, *135*, 9640–9643.

(110) Balasubramanian, S.; Hurley, L. H.; Neidle, S. Targeting G-Quadruplexes in Gene Promoters: A Novel Anticancer Strategy? *Nat. Rev. Drug Discov.* **2011**, *10*, 261–275.

(111) Weldon, C.; Dacanay, J. G.; Gokhale, V.; Boddupally, P. V. L.; Behm-Ansmant, I.; Burley, G. A.; Branlant, C.; Hurley, L. H.; Dominguez, C.; Eperon, I. C. Specific G-Quadruplex Ligands Modulate the Alternative Splicing of Bcl-X. *Nucleic Acids Res.* **2018**, *46*, 886–896.

(112) Boddupally, P. V. L.; Hahn, S.; Beman, C.; De, B.; Brooks, T. A.; Gokhale, V.; Hurley, L. H. Anticancer Activity and Cellular Repression of C-MYC by the G-Quadruplex-Stabilizing 11-Piperazinylquindoline Is Not Dependent on Direct Targeting of the G-Quadruplex in the c-MYC Promoter. *J. Med. Chem.* **2012**, *55*, 6076–6086.

(113) Kendrick, S.; Muranyi, A.; Gokhale, V.; Hurley, L. H.; Rimsza, L. M. Simultaneous Drug Targeting of the Promoter MYC G-Quadruplex. *J. Med. Chem.* **2017**, *60*, 6587–6597.

(114) Brown, R. V.; Wang, T.; Chappeta, Venkateshwar, R.; Wu, G.; Onel, B.; Chawla, R.; Quijada, H.; Camp, S. M.; Chiang, E. T.; Lassiter, Q. R.; Lee, C.; Phase, S.; Turnidge, M. A.; Zhao, P.; Garcia, J. G. N.; Gokhale, V.; Yang, D.; Hurley, L. H. The Consequences of Overlapping G-Quadruplexes and i-Motifs in the Platelet-Derived Growth Factor Receptor β Core Promoter Nuclease Hypersensitive Element Can Explain the Unexpected

Effects of Mutations and Provide Opportunities for Selective Targeting Of. *J. Am. Chem. Soc.* **2017**, *139*, 7456–7475.

(115) Weldon, C. Specific G-Quadruplex Molecules Regulate the Alternative Splicing of Bcl-X, PhD Thesis, University of Leicester, 2015.

(116) Miller, C. M.; McCarthy, F. O. Isolation, Biological Activity and Synthesis of the Natural Product Ellipticine and Related Pyridocarbazoles. *RSC Adv.* **2012**, *2*, 8883–8918.

(117) Woodward, R.; Schniutz, J. The Synthesis of Ellipticine. *J. Am. Chem. Soc.* **1959**, *81*, 4434–4435.

(118) May, C.; Moody, C. J. A New Precursor to 3,4-Didehydropyridine, and Its Use in the Synthesis of the Antitumour Alkaloid Ellipticine. *J. Chem. Soc. Perkin Trans. 1* **1988**, 247–250.

(119) Marsais, F.; Pineau, P.; Nivolliers, F.; Mallet, M.; Turck, A.; Godard, A.; Queguiner, G. A New Convergent Route to 1-Substituted Ellipticines. *J. Org. Chem.* **1992**, *57*, 565–573.

(120) Liu, C.-Y.; Knochel, P. Preparation of Polyfunctional Aryl Azides from Aryl Triazenes. A New Synthesis of Ellipticine, 9-Methoxyellipticine, Isoellipticine, and 7-Carbethoxyisoellipticine. *J. Org. Chem.* **2007**, *72*, 7106–7115.

(121) Dalton, L. K.; Demerac, S.; Elmes, B. C.; Lodger, J. W.; Swan, J. M.; Teitei, T. Synthesis of the Tumour Inhibitory Alkaloids, Ellipticine, 9-Methoxyellipticine and Related Pyrido[4,3-b]Carbazoles. *Austrlian J. Chem.* **1967**, *20*, 2715–2727.

(122) Larsen, A. K.; Paoletti, C. *New Experimental Modalities in the Control of Neoplasia*; Plenum Publishing Corporation, 1986.

(123) Ohashi, M.; Oki, T. Overview Oncologic , Endocrine & Metabolic Ellipticine and Related Anticancer Agents. *Expert Opin. Ther. Pat.* **1996**, *6*, 1285–1294.

(124) Paoletti, C.; Le Pecq, J. B.; Dat-Xuong, N.; Juret, P.; Garnier, H.; Amiel, J. L.; Rouesse, J. Antitumor Activity, Pharmacology, and Toxicity of Ellipticines, Ellipticinium, and 9-Hydroxy Derivatives: Preliminary Clinical Trials of 2-Methyl-9-Hydroxy Ellipticinium (NSC 264-137). *Recent Results Cancer Res.* **1980**, *74*, 107–123.

(125) Stiborová, M.; Poljaková, J.; Martínková, E.; Bořek-Dohalská, L.; Eckschlager, T.; Kizek, R.; Frei, E. Ellipticine Cytotoxicity to Cancer Cell Lines - A Comparative Study. *Interdiscip. Toxicol.* **2011**, *4*, 98–105.

(126) Sullivan, E. C. O.; Miller, C. M.; Deane, F. M.; McCarthy, F. O. Emerging Targets in the Bioactivity of Ellipticines and Derivatives. In *Studies in Natural Products Chemistry*; Elsevier B.V., 2013; Vol. 39, pp 189–232.

(127) Tse, W. C.; Boger, D. L. Sequence-Selective DNA Recognition: Natural Products and Nature's Lessons. *Chem. Biol.* **2004**, *11*, 1607–1617.

(128) Lerman, L. S. Structural Considerations in the Interaction of DNA and Acridines. *J. Mol. Biol.* **1961**, *3*, 18–30.

(129) Tewey, K. M.; Rowe, T. C.; Yang, L.; Halligan, B. D.; Liu, L. F. Adriamycin-Induced DNA Damage Mediated by Mammalian DNA Topoisomerase II. *Science (80-.).* **1983**, *226*, 466–468.

(130) Fuller, W.; Waring, M. J. A Molecular Model for the Interaction of Ethidium Bromide with Deoxyribonucleic Acid. *Berichte der Bunsengesellschaft für Phys. Chemie* **1964**, *68*, 805–808.

(131) Reinhardt, C. G.; Krugh, T. R. A Comparative Study of Ethidium Bromide Complexes with Dinucleotides and DNA: Direct Evidence for Intercalation and Nucleic Acid Sequence Preferences. *Biochemistry* **1978**, *17*, 4845–4854.

(132) Koch, H. P.; Czejka, M. J. Evidence for the Intercalation of Thalidomide into DNA: Clue to the Molecular Mechanism of Thalidomide Teratogenicity? *Zeitschrift fur Naturforsch. - Sect. C J. Biosci.* **1986**, *41*, 1057–1061.

(133) Kohn, K. W.; Waring, M. J.; Glaubiger, D.; Friedman, C. A. Intercalative Binding of Ellipticine to DNA. *Cancer Res.* **1975**, *35*, 71–76.

(134) Wang, J. C. The Degree of Unwinding of the DNA Helix by Ethidium. *J. Mol. Biol.* **1974**, *89*, 783–801.

(135) Liu, L. F.; Wang, J. C. On the Degree of Unwinding of the DNA Helix by Ethidium. II. Studies by Electron Microscopy. *Biochim. Biophys. Acta* **1975**, *395*, 405–412.

(136) Canals, A.; Purciolas, M.; Aymamí, J.; Coll, M. The Anticancer Agent Ellipticine Unwinds DNA by Intercalative Binding in an Orientation Parallel to Base Pairs. *Acta Crystallogr. Sect. D Biol. Crystallogr.* **2005**, *61*, 1009–1012.

(137) Baldwin, M.; Bachant, J. DNA Topoisomerases. *Annu. Rev. Biochem.* **1996**, *65*, 635–692.

(138) Nitiss, J. Targeting DNA Topoisomerase II in Cancer Chemotherapy. *Nat. Rev. Cancer*

2009, *9*, 338–350.

(139) Pommier, Y.; Leo, E.; Zhang, H.; Marchand, C. DNA Topoisomerases and Their Poisoning by Anticancer and Antibacterial Drugs. *Chem. Biol.* **2010**, *17*, 421–433.

(140) Ghosh, S.; Kar, A.; Chowdhury, S.; Dasgupta, D. Ellipticine Binds to a Human Telomere Sequence: An Additional Mode of Action as a Putative Anticancer Agent? *Biochemistry* **2013**, *52*, 4127–4137.

(141) Stiborová, M.; Černá, V.; Moserová, M.; Mrízová, I.; Arlt, V.; Frei, E. The Anticancer Drug Ellipticine Activated with Cytochrome P450 Mediates DNA Damage Determining Its Pharmacological Efficiencies: Studies with Rats, Hepatic Cytochrome P450 Reductase Null (HRN^{TM}) Mice and Pure Enzymes. *Int. J. Mol. Sci.* **2014**, *16*, 284–306.

(142) Stiborová, M.; Rupertova, M.; Schmeiser, H. H.; Frei, E. Molecular Mechanisms of Antineoplastic Action of an Anticancer Drug Ellipticine. *Biomed. Pap.* **2006**, *150*, 13–23.

(143) Stiborová, M.; Poljaková, J.; Ryšlavá, H.; Dračínský, M.; Eckschlager, T.; Frei, E. Mammalian Peroxidases Activate Anticancer Drug Ellipticine to Intermediates Forming Deoxyguanosine Adducts in DNA Identical to Those Found in Vivo and Generated from 12-Hydroxyellipticine and 13-Hydroxyellipticine. *Int. J. Cancer* **2007**, *120*, 243–251.

(144) Vendôme, J.; Letard, S.; Martin, F.; Svinarchuk, F.; Dubreuil, P.; Auclair, C.; Le Bret, M. Molecular Modeling of Wild-Type and D816V c-Kit Inhibition Based on ATP-Competitive Binding of Ellipticine Derivatives to Tyrosine Kinases. *J. Med. Chem.* **2005**, *48*, 6194–6201.

(145) Gribble, G. W.; Saulnier, M. G.; Obaza-Nutaitis, J. A.; Ketcha, D. M. A Versatile and Efficient Construction of the 6H-Pyrido[4,3-b]Carbazole Ring System. Syntheses of the Antitumor Alkaloids Ellipticine, 9-Met Hoxyellipticine, and Olivacine and Their Analogues. *J. Org. Chem.* **1992**, *57*, 5891–5899.

(146) Cranwell, P. A.; Saxton, J. E. A Synthesis of Ellipticine. *J. Chem. Soc.* **1962**, *683*, 3482–3487.

(147) Deane, F. M.; Miller, C. M.; Maguire, A. R.; McCarthy, F. O. Modifications to the Vilsmeier-Haack Formylation of 1,4-Dimethylcarbazole and Its Application to the Synthesis of Ellipticines. *J. Heterocycl. Chem.* **2011**, *48*, 814–823.

(148) Liu, Z.; Larock, R. C. Synthesis of Carbazoles and Dibenzofurans via Cross-Coupling of

o-Iodoanilines and o-Iodophenols with Silylaryl Triflates and Subsequent Pd-Catalyzed Cyclization. *Org. Lett.* **2004**, *6*, 3739–3741.

(149) Liu, Z.; Larock, R. C. Synthesis of Carbazoles and Dibenzofurans via Cross-Coupling of o-Iodoanilines and o-Iodophenols with Silylaryl Triflates and Subsequent Pd-Catalyzed Cyclization. *Tetrahedron* **2007**, *63*, 347–355.

(150) Jackson, B. A. H.; Jenkins, P. R.; Shannon, P. V. R. A New Approach to the Synthesis of Ellipticines. *J.S.C Perkin 1* **1975**, 1698–1704.

(151) Dračínský, M.; Sejbal, J.; Rygerová, B.; Stiborová, M. An Efficient Modification of Ellipticine Synthesis and Preparation of 13-Hydroxyellipticine. *Tetrahedron Lett.* **2007**, *48*, 6893–6895.

(152) Wang, Y.; Stretton, A. D.; Mcconnell, M. C.; Wood, P. A.; Parsons, S.; Henry, J. B.; Mount, A. R.; Galow, T. H. Flipping Twist by Guitia. *J. Am. Chem. Soc.* **2007**, *129*, 13193–13200.

(153) Rambabua, D.; Rajab, G.; Sreenivasa, B. Y.; Seerapua, G. P. K.; Kumar, K. L.; Deoraa, G. S.; Haldara, D.; Basaveswara Rao, M. V; Pal, M. Spiro Heterocycles as Potential Inhibitors of SIRT1: Pd/C-Mediated Synthesis of Novel N-Indolylmethyl Spiroindoline-3,2′-Quinazolines. *Bioorg. Med. Chem.* **2013**, *23*, 1351–1357.

(154) Wei-Jian, X.; Ya-Qiong, G.; Fang-Fang, G.; Hong-Zheng, L.; An-Xin, W. A Novel Self-Sequence Reaction Network Involving a Set of Six Reactions in One Pot: The Synthesis of Substituted Benzothiazoles from Aromatic Ketones and Anilines. *Org. Lett.* **2013**, *15*, 890–893.

(155) Luniewski, W.; Wietrzyk, J.; Godlewska, J.; Switalska, M.; Piskozub, M.; Peczynska-Czoch, W.; Kaczmarek, L. New Derivatives of 11-Methyl-6-[2-(Dimethylamino)Ethyl]-6H-Indolo[2,3-b]Quinoline as Cytotoxic DNA Topoisomerase II Inhibitors. *Bioorg. Med. Chem. Lett.* **2012**, *22*, 6103–6107.

(156) Armarego, E. L. F.; Chai, C. *In Purification of Laboratory Chemicals*; Butterworth-Heinemann, 2012.

(157) Kimball, D. B.; Weakley, T. J. R.; Haley, M. M. Cyclization of 1-(2-Alkynylphenyl)-3,3-Dialkyltriazenes: A Convenient,High-Yield Synthesis of Substituted Cinnolines and Isoindazoles. *J. Org. Chem.* **2002**, *67*, 6395–6405.

(158) Cope, A. C.; Burg, M. Sulfonic Acid Esters of Aminoalcohols. *J. Am. Chem. Soc.* **1952**, *74*, 611–614.

(159) Itoh, T.; Abe, T.; Choshi, T.; Nishiyama, T.; Yanada, R.; Ishikura, M. Concise Total Syntheses of Pyrido[4,3-b]Carbazole Alkaloids Using Copper-Mediated 6π-Electrocyclization. *European J. Org. Chem.* **2016**, *2016*, 2290–2299.

(160) Wu, X. F.; Anbarasan, P.; Neumann, H.; Beller, M. From Noble Metal to Nobel Prize: Palladium-Catalyzed Coupling Reactions as Key Methods in Organic Synthesis. *Angew. Chemie - Int. Ed.* **2010**, *49*, 9047–9050.

(161) Miyaura, N.; Suzuki, A. Palladium-Catalyzed Cross-Coupling Reactions of Organoboron Compounds. *Chem. Rev.* **1995**, *95*, 2457–2483.

(162) Negishi, E. Palladium- or Nickel-Catalyzed Cross Coupling. A New Selective Method for Carbon-Carbon Bond Formation. *Acc. Chem. Res.* **1982**, *15*, 340–348.

(163) Sonogashira, K. Development of Pd-Cu Catalyzed Cross-Coupling of Terminal Acetylenes with Sp2-Carbon Halides. *J. Organomet. Chem.* **2002**, *653*, 46–49.

(164) Heck, K. F.; Nolley, J. P. Palladium-Catalyzed Vinylic Hydrogen Substitution Reactions with Aryl, Benzyl, and Styryl Halides. *J. Org. Chem.* **1972**, *37*, 2320–2322.

(165) Guram, A. S.; Rennels, R. A.; Buchwald, S. L. A Simple Catalytic Method for the Conversion of Aryl Bromides to Arylamines. *Angew. Chemie - Int. Ed.* **1995**, *34*, 1348–1350.

(166) Torborg, C.; Beller, M. Recent Applications of Palladium-Catalyzed Coupling Reactions in the Pharmaceutical, Agrochemical, and Fine Chemical Industries. *Adv. Synth. Catal.* **2009**, *351*, 3027–3043.

(167) Louie, J.; Hartwig, J. F. Palladium-Catalyzed Synthesis of Arylamines from Aryl Halides. Mechanistic Studies Lead to Coupling in the Absence of Tin Reagents. *Tetrahedron Lett.* **1995**, *36*, 3609–3612.

(168) Shen, Q.; Hartwig, J. F. Palladium-Catalyzed Coupling of Ammonia and Lithium Amide with Aryl Halides. *J. Am. Chem. Soc.* **2006**, *128*, 10028–10029.

(169) Vo, G. D.; Hartwig, J. F. Palladium-Catalyzed Coupling of Ammonia with Aryl Chlorides, Bromides, Iodides, and Sulfonates: A General Method for the Preparation of Primary Arylamines. *J. Am. Chem. Soc.* **2009**, *131*, 11049–11061.

(170) Kosugi, M.; Kameyama, M.; Migita, T. Palladium-Catalyzed Aromatic Amination of Aryl Bromides with N,N-Diethylamino-Tributyltin. *Chem. Lett.* **1983**, *6*, 927–928.

(171) Kosugi, M.; Kameyama, M.; Sano, H.; Migita, T. Palladium-Catalyzed Aromatic Amination of Aryl Halides by Means of Aminotin Compounds. *Nippon Kagaku Kaishi* **1985**, *230*, 547–551.

(172) Driver, M. S.; Hartwig, J. F. A Second-Generation Catalyst for Aryl Halide Amination: Mixed Secondary Amines from Aryl Halides and Primary Amines Catalyzed by (DPPF)PdCl2. *J. Am. Chem. Soc.* **1996**, *118*, 7217–7218.

(173) Wolfe, J. P.; Wagaw, S.; Buchwald, S. L. An Improved Catalyst System for Aromatic Carbon-Nitrogen Bond Formation: The Possible Involvement of Bis(Phosphine) Palladium Complexes as Key Intermediates. *J. Am. Chem. Soc.* **1996**, *118*, 7215–7216.

(174) Lu, X. Control of the β-Hydride Elimination Making Palladium-Catalyzed Coupling Reactions More Diversified. *Top. Catal.* **2005**, *35*, 73–86.

(175) Old, D. W.; Wolfe, J. P.; Buchwald, S. L. A Highly Active Catalyst for Palladium-Catalyzed Cross-Coupling Reactions: Room-Temperature Suzuki Couplings and Amination of Unactivated Aryl Chlorides. *J. Am. Chem. Soc.* **1998**, *120*, 9722–9723.

(176) Aranyos, A.; Old, D. W.; Kiyomori, A.; Wolfe, J. P.; Sadighi, J. P.; Buchwald, S. L. Novel Electron-Rich Bulky Phosphine Ligands Facilitate the Palladium- Catalyzed Preparation of Diaryl Ethers. *J. Am. Chem. Soc.* **1999**, *121*, 4369–4378.

(177) Hartwig, J. F.; Richards, S.; Barañano, D.; Paul, F. Influences on the Relative Rates for C−N Bond-Forming Reductive Elimination and β-Hydrogen Elimination of Amides. A Case Study on the Origins of Competing Reduction in the Palladium-Catalyzed Amination of Aryl Halides. *J. Am. Chem. Soc.* **1996**, *118*, 3626–3633.

(178) Birkholz (née Gensow), M.-N.; Freixa, Z.; van Leeuwen, P. W. N. M. Bite Angle Effects of Diphosphines in C–C and C–X Bond Forming Cross Coupling Reactions. *Chem. Soc. Rev.* **2009**, *38*, 1099–1118.

(179) Wolfe, J. P.; Buchwald, S. L. A Highly Active Catalyst for the Room-Temperature Amination and Suzuki Coupling of Aryl Chlorides. *Angew. Chemie - Int. Ed.* **1999**, *38*, 2413–2416.

(180) Surry, D. S.; Buchwald, S. L. Biaryl Phosphane Ligands in Palladium-Catalyzed

Amination. *Angew. Chemie - Int. Ed.* **2008**, *47*, 6338–6361.

(181) Surry, D. S.; Buchwald, S. L. Dialkylbiaryl Phosphines in Pd-Catalyzed Amination: A User's Guide. *Chem. Sci.* **2011**, *2*, 27–50.

(182) Marion, N.; Navarro, O.; Mei, J.; Stevens, E. D.; Scott, N. M.; Nolan, S. P. Modified (NHC)Pd(Allyl)Cl (NHC = N-Heterocyclic Carbene) Complexes for Room-Temperature Suzuki-Miyaura and Buchwald-Hartwig Reactions. *J. Am. Chem. Soc.* **2006**, *128*, 4101–4111.

(183) Navarro, O.; Marion, N.; Mei, J.; Nolan, S. P. Rapid Room Temperature Buchwald-Hartwig and Suzuki-Miyaura Couplings of Heteroaromatic Compounds Employing Low Catalyst Loadings. *Chem. - A Eur. J.* **2006**, *12*, 5142–5148.

(184) Cawley, M. J.; Cloke, F. G. N.; Fitzmaurice, R. J.; Pearson, S. E.; Scott, J. S.; Caddick, S. Development of a Practical Buchwald-Hartwig Amine Arylation Protocol Using a Conveniently Prepared (NHC)Pd(R-Allyl)Cl Catalyst. *Org. Biomol. Chem.* **2008**, *6*, 2820–2825.

(185) Le Duc, G.; Meiries, S.; Nolan, S. P. Effect of Electronic Enrichment of NHCs on the Catalytic Activity of [Pd(NHC)(Acac)Cl] in Buchwald−Hartwig Coupling. *Organometallics* **2013**, *32*, 7547–7551.

(186) Kantchev, E. A. B.; O'Brien, C. J.; Organ, M. G. *Palladium Complexes of N-Heterocyclic Carbenes as Catalysts for Cross-Coupling Reactions - A Synthetic Chemist's Perspective*; 2007; Vol. 46.

(187) Clavier, H.; Nolan, S. P. Percent Buried Volume for Phosphine and N-Heterocyclic Carbene Ligands: Steric Properties in Organometallic Chemistry. *Chem. Commun.* **2010**, *46*, 841-.

(188) Fortman, G. C.; Nolan, S. P. N-Heterocyclic Carbene (NHC) Ligands and Palladium in Homogeneous Cross-Coupling Catalysis: A Perfect Union. *Chem. Soc. Rev.* **2011**, *40*, 5151–5169.

(189) Chemler, S. R.; Trauner, D.; Danishefsky, S. J. The B-Alkyl Suzuki-Miyaura Cross-Coupling Reaction: Development, Mechanistic Study, and Applications in Natural Product Synthesis. *Angew. Chemie - Int. Ed.* **2001**, *40*, 4544–4568.

(190) Leadbeater, N. E.; Marco, M. Ligand-Free Palladium Catalysis of the Suzuki Reaction in

Water Using Microwave Heating. *Org. Lett.* **2002**, *4*, 2973–2976.

(191) Narayanan, R.; El-Sayed, M. A. Effect of Catalysis on the Stability of Metallic Nanoparticles: Suzuki Reaction Catalyzed by PVP-Palladium Nanoparticles. *J. Am. Chem. Soc.* **2003**, *125*, 8340–8347.

(192) Park, J.; Kang, E.; Son, S. U.; Park, H. M.; Lee, M. K.; Kim, J.; Kim, K. W.; Noh, H. J.; Park, J. H.; Bae, C. J.; Park, J. G.; Hyeon, T. Monodisperse Nanoparticles of Ni and NiO: Synthesis, Characterization, Self-Assembled Superlattices, and Catalytic Applications in the Suzuki Coupling Reaction. *Adv. Mater.* **2005**, *17*, 429–434.

(193) Organ, M. G.; Avola, S.; Dubovyk, I.; Hadei, N.; Kantchev, E. A. B.; O'Brien, C. J.; Valente, G. A User-Friendly, All-Purpose Pd-NHC (NHC = N-Heterocyclic Carbene) Precatalyst for the Negishi Reaction: A Step Towards a Universal Cross-Coupling Catalyst. *Chem. - A Eur. J.* **2006**, *12*, 4749–4755.

(194) Johansson Seechurn, C. C. C.; Kitching, M. O.; Colacot, T. J.; Snieckus, V. Palladium-Catalyzed Cross-Coupling: A Historical Contextual Perspective to the 2010 Nobel Prize. *Angew. Chemie - Int. Ed.* **2012**, *51*, 5062–5085.

(195) McGlacken, G. P.; Bateman, L. M. Recent Advances in Aryl–aryl Bond Formation by Direct Arylation. *Chem. Soc. Rev.* **2009**, *38*, 2447–2464.

(196) Ackermann, L.; Vicente, R.; Kapdi, A. R. Transition-Metal-Catalyzed Direct Arylation of (Hetero)Arenes by C-H Bond Cleavage. *Angew. Chemie - Int. Ed.* **2009**, *48*, 9792–9826.

(197) Alberico, D.; Scott, M. E.; Lautens, M. Aryl−Aryl Bond Formation by Transition-Metal-Catalyzed Direct Arylation. *Chem. Rev.* **2007**, *107*, 174–238.

(198) Catellani, M.; Chiusoli, G. P. Palladacycle Formation by Electrophilic Aromatic Substitution, as Monitored by 1H NMR Spectroscopy. *J. Organomet. Chem.* **1992**, *425*, 151–154.

(199) Martín-Matute, B.; Mateo, C.; Cárdenas, D. J.; Echavarren, A. M. Intramolecular C-H Activation by Alkylpalladium(II) Complexes: Insights into the Mechanism of the Palladium-Catalyzed Arylation Reaction. *Chem. - A Eur. J.* **2001**, *7*, 2341–2348.

(200) Hughes, C. C.; Trauner, D. Concise Total Synthesis of (-)-Frondosin B Using a Novel Palladium-Catalyzed Cyclization. *Angew. Chemie - Int. Ed.* **2002**, *41*, 1569–1572.

(201) Park, C. H.; Ryabova, V.; Seregin, I. V.; Sromek, A. W.; Gevorgyan, V. Palladium-

Catalyzed Arylation and Heteroarylation of Indolizines. *Org. Lett.* **2004**, *6*, 1159–1162.

(202) Lane, B. S.; Brown, M. A.; Sames, D. Direct Palladium-Catalyzed C-2 and C-3 Arylation of Indoles: A Mechanistic Rationale for Regioselectivity. *J. Am. Chem. Soc.* **2005**, *127*, 8050–8057.

(203) Mota, A. J.; Dedieu, A.; Bour, C.; Suffert, J. Cyclocarbopalladation Involving an Unusual 1,5-Palladium Vinyl to Aryl Shift as Termination Step: Theoretical Study of the Mechanism. *J. Am. Chem. Soc.* **2005**, *127*, 7171–7182.

(204) Fairlamb, I. J. S. Regioselective (Site-Selective) Functionalisation of Unsaturated Halogenated Nitrogen, Oxygen and Sulfur Heterocycles by Pd-Catalysed Cross-Couplings and Direct Arylation Processes. *Chem. Soc. Rev.* **2007**, *36*, 1036–1045.

(205) Gorelsky, S. I.; Lapointe, D.; Fagnou, K.; Lilly, E.; Zeneca, A. Analysis of the Concerted Metalation-Deprotonation Mechanism in Palladium-Catalyzed Direct Arylation Across a Broad Range of Aromatic Substrates. *J. Am. Chem. Soc.* **2008**, *130*, 10848–10849.

(206) Westheimer, F. H. The Magnitude of the Primary Kinetic Isotope Effect for Compounds of Hydrogen and Deuterium. *Chem. Rev.* **1961**, *61*, 265–273.

(207) Zollinger, H. Hydrogen Isotope Effects in Aromatic Substitution Reactions. *Adv. Phys. Org. Chem.* **1964**, *2*, 163–200.

(208) Sharma, U.; Modak, A.; Maity, S.; Arun, M.; Maiti, D. Direct Arylation Via C – H Bonds Activation. In *New Trends in Cross-Coupling: Theory and Applications*; Colacot, T. J., Ed.; The Royal Society of Chemistry, 2014; pp 551–609.

(209) García-Cuadrado, D.; Braga, A. A. C.; Maseras, F.; Echavarren, A. M. Proton Abstraction Mechanism for the Palladium-Catalyzed Intramolecular Arylation. *J. Am. Chem. Soc.* **2006**, *128*, 1066–1067.

(210) García-Cuadrado, D.; De Mendoza, P.; Braga, A. A. C.; Maseras, F.; Echavarren, A. M. Proton-Abstraction Mechanism in the Palladium-Catalyzed Intramolecular Arylation: Substituent Effects. *J. Am. Chem. Soc.* **2007**, *129*, 6880–6886.

(211) Campeau, L. C.; Parisien, M.; Leblanc, M.; Fagnou, K. Biaryl Synthesis via Direct Arylation: Establishment of an Efficient Catalyst for Intramolecular Processes. *J. Am. Chem. Soc.* **2004**, *126*, 9186–9187.

(212) Campeau, L. C.; Thansandote, P.; Fagnou, K. High-Yielding Intramolecular Direct

Arylation Reactions with Aryl Chlorides. *Org. Lett.* **2005**, *7*, 1857–1860.

(213) Campeau, L.; Parisien, M.; Jean, A.; Fagnou, K. Intramolecular Direct Arylation with Aryl Chlorides, Bromides and Iodides: Developments Leading to New Intermolecular Processes. *J. Am. Chem. Soc.* **2006**, *128*, 581–590.

(214) Lie, B.; Lee, D.; Huestis, M. P.; Stuart, D. R.; Fagnou, K. Intramolecular Pd (II) -Catalyzed Oxidative Biaryl Synthesis Under Air : Reaction Development and Scope Intramolecular Pd (II) -Catalyzed Oxidative Biaryl Synthesis Under Air : Reaction Development and Scope Benoît Lie. *J. Org. Chem.* **2008**, *73*, 5022–5028.

(215) Liégault, B.; Lapointe, D.; Caron, L.; Vlassova, A.; Fagnou, K. Establishment of Broadly Applicable Reaction Conditions for the Palladium-Catalyzed Direct Arylation of Heteroatom-Containing Aromatic Compounds. *J. Org. Chem.* **2009**, *74*, 1826–1834.

(216) Lafrance, M.; Lapointe, D.; Fagnou, K. Mild and Efficient Palladium-Catalyzed Intramolecular Direct Arylation Reactions. *Tetrahedron* **2008**, *64*, 6015–6020.

(217) Knolker, H.-J.; Reddy, K. R. Isolation and Synthesis of Biologically Active Carbazole Alkaloids. *Chem. Rev.* **2002**, *102*, 4303–4427.

(218) Borsche, W. Ueber Tetra-Und Hexahydrocarbazolverbindungen Und Eine Neue Carbazolsynthese.(Mitbearbeitet von. A. Witte Und W. Bothe.). *Justus Liebigs Ann. Chem.* **1908**, *69*, 49–80.

(219) Drechsel, E. Ueber Elektrolyse Des Phenols Mit Wechselströmen. *J. Prakt. Chem.* **1888**, *38*, 65–74.

(220) Jordan-Hore, J. A.; Johansson, C. C. C.; Gulias, M.; Beck, E. M.; Gaunt, M. J. Oxidative Pd(II)-Catalyzed C-H Bond Amination to Carbazole at Ambient Temperature. *J. Am. Chem. Soc.* **2008**, *130*, 16184–16186.

(221) Suzuki, C.; Hirano, K.; Satoh, T.; Miura, M. Direct Synthesis of N -H Carbazoles via Iridium(III)-Catalyzed Intramolecular C–H Amination. *Org. Lett.* **2015**, *17*, 1597–1600.

(222) James, M. J.; Clubley, R. E.; Palate, Kleopas, Y.; Procter, T. J.; Wyton, A. C.; O'Brien, P.; Taylor, R. J. K.; Unsworth, W. P. Silver(I)-Catalyzed Dearomatization of Alkyne-Tethered Indoles: Divergent Synthesis of Spirocyclic Indolenines and Carbazoles. *Org. Lett.* **2015**, *17*, 4372–4375.

(223) Liddon, J. T. R.; James, M. J.; Clarke, A. K.; O'Brien, P.; Taylor, R. J. K.; Unsworth, W.

P. Catalyst-Driven Scaffold Diversity: Selective Synthesis of Spirocycles, Carbazoles and Quinolines from Indolyl Ynones. *Chem. - A Eur. J.* **2016**, *22*, 8777–8780.

(224) Chen, S.; Li, Y.; Ni, P.; Huang, H.; Deng, G.-J. Indole-to-Carbazole Strategy for the Synthesis of Substituted Carbazoles under Metal-Free Conditions. *Org. Lett.* **2016**, *18*, 5384–5387.

(225) Ackermann, L.; Althammer, A. Domino N-H / C-H Bond Activation : Palladium-Catalyzed Synthesis of Annulated Heterocycles Using Dichloro(Hetero)Arenes. *Angew. Chemie - Int. Ed.* **2007**, *46*, 1627–1629.

(226) Ackermann, L.; Althammer, A.; Mayer, P. Palladium-Catalysed Direct Arylatio-Based Domino Synthesis of Annulated N-Heterocycles Using Alkenyl or (Hetro)Aryl 1,2-Dihalides. *Synthesis (Stuttg).* **2009**, *20*, 3493–3503.

(227) Bedford, R. B.; Cazin, C. S. J. A Novel Catalytic One-Pot Synthesis of Carbazoles via Consecutive Amination and C – H Activation. *Chem. Commun.* **2002**, *2*, 2310–2311.

(228) Bedford, R. B.; Betham, M. N-H Carbazole Synthesis from 2-Chloroanilines via Consecutive Amination and C-H Activation. *J. Org. Chem.* **2006**, *71*, 9403–9410.

(229) Bedford, R. B.; Betham, M.; Charmant, J. P. H.; Weeks, A. L. Intramolecular Direct Arylation in the Synthesis of Fluorinated Carbazoles. *Tetrahedron* **2008**, *64*, 6038–6050.

(230) Tsvelikhovsky, D.; Buchwald, S. L. Synthesis of Heterocycles via Pd-Ligand Controlled Cyclization of 2-Chloro-N-(2-Vinyl)Aniline: Preparation of Carbazoles, Indoles, Dibenzazepines, and Acridines. *J. Am. Chem. Soc.* **2010**, *132*, 14048–14051.

(231) Ackermann, L.; Althammer, A.; Mayer, P. Palladium-Catalyzed Direct Arylation-Based Domino Synthesis of Annulated N-Heterocycles Using Alkenyl or (Hetero)Aryl 1,2-Dihalides. *Synthesis (Stuttg).* **2009**, *20*, 3493–3503.

(232) Fors, B. P.; Watson, D. A.; Biscoe, M. R.; Buchwald, S. L. A Highly Active Catalyst for Pd-Catalyzed Amination Reactions: Cross-Coupling Reactions Using Aryl Mesylates and the Highly Selective Monoarylation of Primary Amines Using Aryl Chlorides. *J. Am. Chem. Soc.* **2008**, *3*, 3–5.

(233) Yang, Y.; Mustard, T. J. L.; Cheong, P. H. Y.; Buchwald, S. L. Palladium-Catalyzed Completely Linear-Selective Negishi Cross-Coupling of Allylzinc Halides with Aryl and Vinyl Electrophiles. *Angew. Chemie - Int. Ed.* **2013**, *52*, 14098–14102.

(234) Bressel, U.; Katritzky, R. Kinetics and Mechanism of Electrophilic Substitution of Hetero-Aromatic Compounds. Part XXIII. Acid-Catalysed Hydrogen Exchange of Quinoline, Isoquinoline, and Their N-Oxides. *J. Chem. Soc. B* **1971**, *0*, 4–10.

(235) Hall, R.; Dharmasena, P.; Merchant, J.; Oliveira-Campos, A.-M.; Queiroz, M.-J.; Raposo, M.; Shannon, P. A Flexible Approach to Pyrido[4,3-b]Carbazoles. The Syntheses of 8,10-Dimethoxy-5-Methyl-,5,11 -Dimethoxy-7,1 O-Dimethyl- and 9-Fluoro-5,11 -Dimethylpyrido[4,3-b]Carbazoles by Variations of the "Type D" Route. *J. Chem. Soc. Perkin Trans. I* **1993**, 1879–1889.

(236) Taylor, D. A.; Joule, J. A. Short, Flexible Synthesis of Ellipticine. *J. Chem. Soc. Chem. Commun.* **1979**, *318*, 642–643.

(237) Watanabe, M.; Snieckus, V. Tandem Directed Metalation Reactions. Short Syntheses of Polycyclic Aromatic Hydrocarbons and Ellipticine Alkaloids. *J. Am. Chem. Soc.* **1980**, *102*, 1457–1460.

(238) Bennasar, M. L.; Roca, T.; Ferrando, F. Regioselective Intramolecular Reactions of 2-Indolylacyl Radicals with Pyridines: A Direct Synthetic Entry to Ellipticine Quinones. *J. Org. Chem.* **2005**, *70*, 9077–9080.

(239) Miller, R. B.; Moock, T. A General Synthesis of 6-H-Pyrido[4,3-b]Carbazole Alkaloids. *Tetrahedron* **1980**, *21*, 3319–3322.

(240) Kürti, L.; Czakó, B. *Strategic Applications of Named Reactions in Organic Synthesis*; Elsevier Inc., 2005.

(241) Abdelwahab, A. B.; Shaaban, M.; Ismail, M. A. H.; Abouzid, K. A. M.; Hanna, A. G. Synthesis and Cytotoxicity Studies of Some New Amino Isoquinolin-5,8-Dione and Quinolin-5,8-Dione Derivatives. *Indian J. Chem.* **2014**, *53*, 1098–1109.

(242) Choi, H. Y.; Chi, D. Y. Simple Preparation of 7-Alkylamino-2-Methylquinoline-5,8-Diones: Regiochemistry in Nucleophilic Substitution Reactions of the 6- or 7-Bromo-2-Methylquinoline-5, 8-Dione with Amines. *Tetrahedron* **2004**, *60*, 4945–4951.

(243) Van Leeuwen, P. W. N. M. Decomposition Pathways of Homogeneous Catalysts. *Appl. Catal. A Gen.* **2001**, *212*, 61–81.

(244) Iwasawa, T.; Tokunaga, M.; Obora, Y.; Tsuji, Y. Homogeneous Palladium Catalyst Suppressing Pd Black Formation in Air Oxidation of Alcohols. *J. Am. Chem. Soc.* **2004**,

126, 6554–6555.

(245) Ahond, A.; Poupat, C.; Potier, P. Etude Par RM13C D'Alcaloides a Squelette Acridinone 9(10H) et Pyrido(4,3b)Carbazole(6H). *Tetrahedron* **1978**, *34*, 2385–2388.

(246) Morales-Rios, M. S.; Espineira, J.; Joseph-Nathan, P. 13C NMR Spectroscopy of Indole Derivatives. *Magn. Reson. Chem.* **1987**, *25*, 377–395.

(247) Dowlatabadi, R.; Khalaj, A.; Rahimian, S.; Montazeri, M.; Amini, M.; Shahverdi, A.; Mahjub, E. Impact of Substituents on the Isatin Ring on the Reaction Between Isatins with Ortho-Phenylenediamine. *Synth. Commun.* **2011**, *41*, 1650–1658.

(248) Sieveking, I.; Thomas, P.; Estévez, J. C.; Quiñones, N.; Cuéllar, M. A.; Villena, J.; Espinosa-Bustos, C.; Fierro, A.; Tapia, R. A.; Maya, J. D.; López-Muñoz, R.; Cassels, B. K.; Estévez, R. J.; Salas, C. O. 2-Phenylaminonaphthoquinones and Related Compounds: Synthesis, Trypanocidal and Cytotoxic Activities. *Bioorganic Med. Chem.* **2014**, *22*, 4609–4620.

(249) Sridharan, V.; Antonia Martín, M.; Carlos Menéndez, J. Acid-Free Synthesis of Carbazoles and Carbazolequinones by Intramolecular Pd-Catalyzed, Microwave-Assisted Oxidative Biaryl Coupling Reactions Efficient Syntheses of Murrayafoline A, 2-Methoxy-3-Methylcarbazole, and Glycozolidine. *European J. Org. Chem.* **2009**, *27*, 4614–4621.

(250) Guo, J.; Kiran, I. N. C.; Reddy, R. S.; Gao, J.; Tang, M.; Liu, Y.; He, Y. Synthesis of Carbazolequinones by Formal [3 + 2] Cycloaddition of Arynes and 2-Aminoquinones. *Org. Lett.* **2016**, *18*, 2499–2502.

(251) Miller, C. M.; O'Sullivan, E. C.; Devine, K. J.; McCarthy, F. O. Synthesis and Biological Evaluation of Novel Isoellipticine Derivatives and Salts. *Org. Biomol. Chem.* **2012**, *10*, 7912–7921.

(252) Boberg, F.; Deters, K.; Schulz, J.; Torges, K.-F. Alkyl-10,11-Dihydrodiindeno-[1,2-b:2′,1′-d]Thiophene. *Phosphorus. Sulfur. Silicon Relat. Elem.* **1994**, *91*, 69–80.

(253) Nagao, Y.; Hirota, K.; Tokumaru, M.; Kozawa, K. Synthesis of 7-Substituted Derivatives of 5,8-Dimethylisoquinoline. *Heterocycles* **2007**, *73*, 593–602.

(254) Frim, R.; Rabinovitz, M.; Bodwellb, G.; Raulfs, F. W.; Hopf, H. [2.2]Indenophane Mono- and Dianions: PReparation and Nuclear Magnetic Resonance Spectra. *Chem. Ber.* **1989**, *122*, 737–744.

(255) Raposo, M.; Pereira, A.; Oliveira-Campos, A.; Shannon, P. V. R. Studies on 5-Bromo-4,7-Dimethylindene, an Intermediate in the Synthesis of 6-Bromo-5,8-Dimethylisoquinoline. *J. Chem. Res.* **1999**, *S*, 466–467.

(256) Nishiyama, T.; Hatae, N.; Mizutani, M.; Yoshimura, T.; Kitamura, T.; Miyano, M.; Fujii, M.; Satsuki, N.; Ishikura, M.; Hibino, S.; Choshi, T. Concise Synthesis and Antiproliferative Activity Evaluation of Ellipticine Quinone and Its Analogs. *Eur. J. Med. Chem.* **2017**, *136*, 1–13.

(257) Murat, P.; Singh, Y.; Defrancq, E. Methods for Investigating G-Quadruplex DNA/Ligand Interactions. *Chem. Soc. Rev.* **2011**, *40*, 5293–5307.

(258) Rachwal, P. A.; Fox, K. R. Quadruplex Melting. *Methods* **2007**, *43*, 291–301.

(259) Dumas, P.; Ennifar, E.; Disdier, F.; Walter, P. UV Melting Studies with RNA. In *Handbook of RNA Biochemistry: Second, Completely Revised and Enlarged Edition*; Wiley-VCH Verlag GmbH & Co. KGaA, 2014; pp 445–480.

(260) Arora, N.; Jayaram, B. Energetics of Base Pairs in B-DNA in Solution: An Appraisal of Potential Functions and Dielectric Treatments. *J Phys Chem B* **1998**, *102*, 6139–6144.

(261) Khandelwal, G.; Bhyravabhotla, J. A Phenomenological Model for Predicting Melting Temperatures of DNA Sequences. *PLoS One* **2010**, *5*, 1–9.

(262) Wilson, W. D.; Tanious, F. A.; Fernandez-Saiz, M.; Rigl, T. C. Evaluation of Drug-Nucleic Acid Interactions by Thermal Melting Curves. In *Drug'DNA Interaction Protocols*; Humana Press, 1997; pp 219–240.

(263) Mergny, J. L.; Lacroix, L. UV Melting of G-Quadruplexes. *Curr. Protoc. Nucleic Acid Chem.* **2009**, *37*, 1–15.

(264) Mergny, J. L.; De Cian, A.; Ghelab, A.; Saccà, B.; Lacroix, L. Kinetics of Tetramolecular Quadruplexes. *Nucleic Acids Res.* **2005**, *33*, 81–94.

(265) Than, P. L. T.; De Cian, A.; Gros, J.; Moriyama, R.; Mergny, J.-L. Tetramolecular Quadruplex Stability and Assembly. In *Topics in Current Chemistry*; Springer, 2012; pp 243–273.

(266) Forster, T. Energiewanderung Und Fluoreszenz. *Naturwissenschaften* **1946**, *33*, 166–175.

(267) Főrster, T. Delocalized Excitation and Excitation Transfer. *U.S. Stomic Energy Comm.* **1965**, *18*, 1–66.

(268) Broussard, J. A.; Rappaz, B.; Webb, D. J.; Brown, C. M. Fluorescence Resonance Energy Transfer Microscopy as Demonstrated by Measuring the Activation of the Serine/Threonine Kinase Akt. *Nat. Protoc.* **2013**, *8*, 265–281.

(269) Selvin, P. R. The Renaissance of Fluorescence Resonance Energy Transfer. *Nat. Struct. Biol.* **2000**, *7*, 730–734.

(270) Sapsford, K. E.; Berti, L.; Medintz, I. L. Materials for Fluorescence Resonance Energy Transfer Analysis: Beyond Traditional Donor-Acceptor Combinations. *Angew. Chemie - Int. Ed.* **2006**, *45*, 4562–4588.

(271) Jares-Erijman, E. A.; Jovin, T. M. FRET Imaging. *Nat. Biotechnol.* **2003**, *21*, 1387–1395.

(272) Xie, Y.; Dix, A. V.; Tor, Y. FRET Enabled Real Time Detection of RNA-Small Molecule Binding. *J. Am. Chem. Soc.* **2009**, *131*, 17605–17614.

(273) El-Sagheer, A. H.; Brown, T. New Strategy for the Synthesis of Chemically Modified RNA Constructs Exemplified by Hairpin and Hammerhead Ribozymes. *Proc. Natl. Acad. Sci.* **2010**, *107*, 15329–15334.

(274) Wright, E. P.; Day, H. A.; Ibrahim, A. M.; Kumar, J.; Boswell, L. J. E.; Huguin, C.; Stevenson, C. E. M.; Pors, K.; Waller, Z. A. E. Mitoxantrone and Analogues Bind and Stabilize I-Motif Forming DNA Sequences. *Sci. Rep.* **2016**, *6*, 4–10.

(275) Simonsson, T.; Sjöback, R. DNA Tetraplex Formation Studied with Fluorescence Resonance Energy Transfer. *J. Biol. Chem.* **1999**, *274*, 17379–17383.

(276) De Rache, A.; Mergny, J. L. Assessment of Selectivity of G-Quadruplex Ligands via an Optimised FRET Melting Assay. *Biochimie* **2015**, *115*, 194–202.

(277) Parkinson, J. A. Selected Applications of NMR Spectroscopy: Nucleic Acids. In *Modern NMR Techniques for Synthetic Chemistry*; Taylor and Francis, 2014; pp 298–330.

(278) Bessi, I.; Wirmer-bartoschek, J.; Dash, J.; Schwalbe, H. Targeting G-Quadruplex with Small Molecules: An NMR View. In *Modern Magnetic Resonance*; Springer International Publishing, 2017; pp 1–22.

(279) Rippe, K. Analysis of Protein-DNA Binding at Equilibrium. *BIF Futur.* **1997**, *12*, 20–26.

(280) Bloomfield, V. A.; Crothers, D. M.; Tinoco, I. *Nucleic Acids: Structures, Properties and Functions*, 1st ed.; University Science Books, 1999.

(281) Fürtig, B.; Richter, C.; Wöhnert, J.; Schwalbe, H. NMR Spectroscopy of RNA. *ChemBioChem* **2003**, *4*, 936–962.

(282) Weldon, C.; Eperon, I. C.; Dominguez, C. Do We Know Whether Potential G-Quadruplexes Actually Form in Long Functional RNA Molecules? *Biochem. Soc. Trans.* **2016**, *44*, 1761–1768.

(283) Adrian, M.; Heddi, B.; Phan, A. T. NMR Spectroscopy of G-Quadruplexes. *Methods* **2012**, *57*, 11–24.

(284) Lu, K.; Miyazaki, Y.; Summers, M. F. Isotope Labeling Strategies for NMR Studies of RNA. *J. Biomol. NMR* **2010**, *46*, 113–125.

(285) Paredes, E.; Evans, M.; Das, S. R. RNA Labeling, Conjugation and Ligation. *Methods* **2011**, *54*, 251–259.

(286) Liu, Y.; Sousa, R.; Wang, Y. X. Specific Labeling: An Effective Tool to Explore the RNA World. *BioEssays* **2016**, *38*, 192–200.

(287) Davis, J. H.; Tonelli, M.; Scott, L. G.; Jaeger, L.; Williamson, J. R.; Butcher, S. E. RNA Helical Packing in Solution: NMR Structure of a 30 KDa GAAA Tetraloop-Receptor Complex. *J. Mol. Biol.* **2005**, *351*, 371–382.

(288) Bao, H. L.; Ishizuka, T.; Sakamoto, T.; Fujimoto, K.; Uechi, T.; Kenmochi, N.; Xu, Y. Characterization of Human Telomere RNA G-Quadruplex Structures in Vitro and in Living Cells Using 19F NMR Spectroscopy. *Nucleic Acids Res.* **2017**, *45*, 5501–5511.

(289) Dalvit, C.; Mongelli, N.; Papeo, G.; Giordano, P.; Veronesi, M.; Moskau, D.; Kümmerle, R. Sensitivity Improvement in 19F NMR-Based Screening Experiments: Theoretical Considerations and Experimental Applications. *J. Am. Chem. Soc.* **2005**, *127*, 13380–13385.

(290) Bao, H. L.; Ishizuka, T.; Iwanami, A.; Oyoshi, T.; Xu, Y. A Simple and Sensitive19F NMR Approach for Studying the Interaction of RNA G-Quadruplex with Ligand Molecule and Protein. *ChemistrySelect* **2017**, *2*, 4170–4175.

(291) Marshall, W. S.; Kaiser, R. J. Recent Advances in the High-Speed Solid Phase Synthesis of RNA. *Curr. Opin. Chem. Biol.* **2004**, *8*, 222–229.

(292) Juen, M. A.; Wunderlich, C. H.; Nussbaumer, F.; Tollinger, M.; Kontaxis, G.; Konrat, R.; Hansen, D. F.; Kreutz, C. Excited States of Nucleic Acids Probed by Proton Relaxation

Dispersion NMR Spectroscopy. *Angew. Chemie - Int. Ed.* **2016**, *55*, 12008–12012.

(293) Wunderlich, C. H.; Spitzer, R.; Santner, T.; Fauster, K.; Tollinger, M.; Kreutz, C. Synthesis of (6-13C)Pyrimidine Nucleotides as Spin-Labels for RNA Dynamics. *J. Am. Chem. Soc.* **2012**, *134*, 7558–7569.

(294) Conn, G. L. *Recombinant and In Vitro RNA Synthesis: Methods and Protocols*; Humana Press, 2009.

(295) Stark, M. R.; Pleiss, J. A.; Deras, M.; Scaringe, S. A.; Rader, S. D. An RNA Ligase-Mediated Method for the Efficient Creation of Large, Synthetic RNAs. *RNA* **2006**, *12*, 2014–2019.

(296) Liu, Y.; Holmstrom, E.; Zhang, J.; Yu, P.; Wang, J.; Dyba, M. A.; Chen, D.; Ying, J.; Lockett, S.; Nesbitt, D. J.; Ferré-D'Amaré, A. R.; Sousa, R.; Stagno, J. R.; Wang, Y. X. Synthesis and Applications of RNAs with Position-Selective Labelling and Mosaic Composition. *Nature* **2015**, *522*, 368–372.

(297) Martadinata, H.; Tua, A. Structure of Propeller-Type Parallel-Stranded RNA G-Quadruplexes , Formed by Human Telomeric RNA Sequences in K+ Solution Structure of Propeller-Type Parallel-Stranded RNA G-Quadruplexes , Formed by Human Telomeric RNA Sequences in K + Solution. *Structure* **2009**, *131*, 2570–2578.

(298) Liu, H.; Matsugami, A.; Katahira, M.; Uesugi, S. A Dimeric RNA Quadruplex Architecture Comprised of Two G:G(:A):G:G(:A) Hexads, G:G:G:G Tetrads and UUUU Loops. *J. Mol. Biol.* **2002**, *322*, 955–970.

(299) Martadinata, H.; Phan, A. T. Structure of Human Telomeric RNA (TERRA): Stacking of Two G-Quadruplex Blocks in K+ Solution. *Biochemistry* **2013**, *52*, 2176–2183.

(300) Berman, H. M.; Westbrook, J.; Feng, Z.; Gilliland, G.; Bhat, T. N.; Weissig, H.; Shindyalov, I. N.; Bourne, P. E. The Protein Data Bank. *Nucleic Acids Res.* **2000**, *28*, 235–242.

(301) Davis, J. H.; Szostak, J. W. Isolation of High-Affinity GTP Aptamers from Partially Structured RNA Libraries. *Proc. Natl. Acad. Sci. U. S. A.* **2002**, *99*, 11616–11621.

(302) Carothers, J. M.; Oestreich, S. C.; Davis, J. H.; Szostak, J. W. Informational Complexity and Functional Activity of RNA Structures. *J. Am. Chem. Soc.* **2004**, *126*, 5130–5137.

(303) Nasiri, A. H.; Wurm, J. P.; Immer, C.; Weickhmann, A. K.; Wöhnert, J. An Intermolecular

G-Quadruplex as the Basis for GTP Recognition in the Class V–GTP Aptamer. *RNA* **2016**, *22*, 1750–1759.

(304) Mayeda, A.; Krainer, A. R. Mammalian In Vitro Splicing Assays. In *RNA-Protein Interaction Protocols*; Humana Press, 1999; pp 315–321.

(305) Mueller, W. F.; Hertel, K. J. Kinetic Analysis of In Vitro Pre-MRNA Splicing in HeLa Nuclear Extract. In *Spliceosomal Pre-mRNA Splicing*; Humana Press, 2014; pp 161–168.

(306) O'Brien, K.; Matlin, A. J.; Lowell, A. M.; Moore, M. J. The Biflavonoid Isoginkgetin Is a General Inhibitor of Pre-MRNA Splicing. *J. Biol. Chem.* **2008**, *283*, 33147–33154.

(307) Berg, M. G.; Wan, L.; Younis, I.; Diem, M. D.; Soo, M.; Wang, C.; Dreyfuss, G. A Quantitative High-Throughput In Vitro Splicing Assay Identifies Inhibitors of Spliceosome Catalysis. *Mol. Cell. Biol.* **2012**, *32*, 1271–1283.

(308) Salton, M.; Misteli, T. Small Molecule Modulators of Pre-MRNA Splicing in Cancer Therapy. *Trends Mol. Med.* **2016**, *22*, 28–37.

(309) Mayeda, A.; Hayase, Y.; Inoue, H.; Ohtsuka, E.; Ohshima, Y. Surveying Cis-Acting Sequences of Pre-MRNA by Adding Antisense 2'-O-Methyl Oligoribonucleotides to a Splicing Reaction. *J. Biochem.* **1990**, *108*, 399–405.

(310) Wang, Y.; Patel, D. J. Solution Structure of the Human Telomeric Repeat d[AG3(T2AG3)3] G-Tetraplex. *Structure* **1993**, *1*, 263–282.

(311) Parkinson, G. N.; Lee, M. P. H.; Neidle, S. Crystal Structure of Parallel Quadruplexes from Human Telomeric DNA. *Nature* **2002**, *417*, 876–880.

(312) Reese, C. B. Oligo- and Poly-Nucleotides: 50 Years of Chemical Synthesis. *Org. Biomol. Chem.* **2005**, *3*, 3851–3868.

(313) Kremser, J.; Strebitzer, E.; Plangger, R.; Juen, M. A.; Nußbaumer, F.; Glasner, H.; Breuker, K.; Kreutz, C. Chemical Synthesis and NMR Spectroscopy of Long Stable Isotope Labelled RNA. *Chem. Commun.* **2017**, *53*, 12938–12941.

(314) Peterson, R. D.; Theimer, C. A.; Wu, H.; Feigon, J. New Applications of 2D Filtered/Edited NOESY for Assignment and Structure Elucidation of RNA and RNA-Protein Complexes. *J. Biomol. NMR* **2004**, *28*, 59–67.